

The University of Nottingham

UNITED KINGDOM · CHINA · MALAYSIA

Time-Resolved Spectroscopic Studies of Reactive Intermediates

Thomas Stephen Murphy MSci

Thesis submitted to the University of Nottingham
for the degree of Doctor of Philosophy

December 2015

Declaration

I hereby declare that this Thesis and the work presented in it are my own, unless acknowledged otherwise.

Thomas Murphy

December 2015

Abstract

Chapter 1. Introduction

An introduction to the detection of reactive intermediates by various spectroscopic techniques is given, as well as a brief introduction to perfluorinated solvents, which are used throughout the work presented in Chapters 2 to 4.

Chapter 2. Time-Resolved Studies of Spin-Forbidden Reactions of Transition Metal Carbonyls with Weak Ligands

The photolysis of a series of first-row transition metal carbonyl compounds which have been previously reported to form 16-electron coordinatively unsaturated intermediates was examined in a series of perfluorinated solvents using $TR^{M}PS$ (time-resolved multiple probe spectroscopy) and TRIR (time-resolved infrared) spectroscopy. In the case of $Fe(CO)_5$, $CpMn(CO)_3$, $(MeCp)Mn(CO)_3$ and $CpV(CO)_4$, the rate of reaction of the 16-electron intermediate with the perfluorinated solvent was found to be slower than that previously reported for weakly coordinating solvents (e.g. alkanes). Addition of cyclopentane, CO_2, Xe and C_2H_6 to a solution of $CpMn(CO)_3$ in perfluoro(methylcyclohexane) was shown to change the rate of this spin-forbidden reaction, as well as the ν(CO) band positions of the resulting $^1CpMn(CO)_2X$ (X = solvent or dopant) complex. Other perfluorinated materials (perfluoro(hexanes) and perfluoro(triethylamine)) are also shown to allow formation of such weakly-coordinated alkane and noble gas complexes in room-temperature liquid solution.

Chapter 3. Further Time-Resolved Studies of Alkane and Noble Gas Complexes in Room Temperature Perfluoroalkane Solutions

The photochemistry of various model transition metal compounds in perfluoroalkane solutions was examined with $TR^{M}PS$ and TRIR spectroscopy. 266 nm photolysis of $CpRe(CO)_3$, $Cp^*Re(CO)_3$ and $CpRe(CO)_2(N_2)$ in perfluoro-(methylcyclohexane) solution was found to result in the formation of two distinct dicarbonyl species of the form $CpRe(CO)_2X$, the first of which decay completely

on the nanosecond timescale to form the second. The rate of formation, rate of decay and ν(CO) band positions of this second dicarbonyl species were found to be dependent on the nature of the the solvents or dopants including Xe or cyclopentane present in solution. Similar results were observed for complexes of the form $M(CO)_6$ (M = Cr, Mo, W). DFT calculations were used in conjunction with spectroscopic studies to attempt to confirm the structure of the initially formed species following photolysis of $CpRe(CO)_3$ and $M(CO)_6$ in PFMCH solution. Good agreement was observed between the calculated ν(CO) band positions of coordinatively unsaturated species and the unknown initially formed CO loss species. Doping of CH_4 or C_2H_6 into a solution of $CpRe(CO)_3$ or $Cp^*Re(CO)_3$ resulted in observation of a C-H activated alkyl hydride complex, with the amount of observed C-H activation vaying in the order: $CpRe(CO)_3$ with ethane < $Cp^*Re(CO)_3$ with ethane < $CpRe(CO)_3$ with methane < $Cp^*Re(CO)_3$ with methane. Photolysis of $CpRh(CO)_2$ in perfluoroalkane solvents was shown to lead to formation of a monocarbonyl solvent complex, followed by the dimeric species $Cp_2Rh_2(CO)_3$, as well as another species, very tentatively assigned to a C-F activated oxidative addition product. Addition of Xe to the above solution was shown to slow formation of the dimeric species, with no evidence of C-F activation observed, indicating formation of CpRh(CO)Xe in room temperature solution.

Chapter 4. Time-Resolved Spectroscopic Studies of Organometallic Triethylsilane Complexes

TR^MPS studies of $CpMn(CO)_3$, $CpRe(CO)_3$ and $Cp^*Re(CO)_3$ were undertaken in neat $HSiEt_3$ solvent. Photolysis of $CpMn(CO)_3$ resulted in initial formation of $^3CpMn(CO)_2$, following by both direct and indirect formation of the Si-H activated species $CpMn(CO)_2(H\text{---}SiEt_3)$ on the picosecond and nanosecond timescales, respectively. Photolysis of $CpRe(CO)_3$ and $Cp^*Re(CO)_3$ was shown to result in formation of a σ-complex, followed by Si-H activation on the microsecond timescale. Doping of a small amount of $HSiEt_3$ into solutions of $CpMn(CO)_3$ and $CpRe(CO)_3$ in perfluoro(methylcyclohexane) was found to result in alteration of the reaction rates, while the final product was still found to be the Si-H activated species in both cases. Photolysis of $W(CO)_6$ was found to result in initial formation of the ethyl-bound $W(CO)_5(EtSiHEt_2)$, which interconverted to

form the Si-H-bound species $W(CO)_5(H{-}SiEt_3)$. Preliminary time-resolved x-ray absorption fine structure spectroscopic studies are also presented. Photolysis of $W(CO)_6$ and $CpRe(CO)_3$ in neat $HSiEt_3$ was observed to cause subtle changes in the absorption edge compared to ground state XAFS spectra, indicating possible formation of transient species in both cases.

Chapter 5. Experimental

The experimental techniques utilised in this Thesis are described.

Acknowledgements

At the very beginning of my PhD it quickly became obvious that although a single name appears on the cover of a doctoral Thesis, nothing is possible without the support, patience and cooperation of a large group of people. Firstly, I'd like to thank my supervisor Prof. Mike George, without whose advice and experience none of this work would have been possible. I would also like to extend thanks to Prof. Sir Martyn Poliakoff, whose input was invaluable towards the start of this project.

A research group is at its most effective if everyone involved is willing to share their knowledge. With this in mind, I'm grateful to Drs. Raphael Horvath, Xue-Zhong Sun, James Calladine, Michelle Hamilton, Charlotte Clark, Andrew Davies, Al Wriglesworth and Magnus Hanson-Heine. Additional thanks go out to Magnus for offering advice regarding DFT calculations, as well as for performing some of the calculations presented in this Thesis. I'd also like to thank Prof. Jeremy Harvey and Dr. Zhen Liu of KU Leuven for additional computational studies and helpful discussion.

Much of this work was undertaken at the Central Laser Facility at the Rutherford Appleton Laboratory. I'd like to thank the Lasers for Science Facility and the Science and Technology Facilities Council for use of the ULTRA system, and give personal thanks to Prof. Mike Towrie, Dr. Ian Clark and Dr. Greg Greetham for their vital assistance in performing these experiments. Additionally, I'd like to thank Prof. John Evans and Dr. Stuart Bartlett of the DySS consortium, and Dr. Sofia Diaz-Moreno and Dr. Andy Dent of Diamond Light Source for helpful discussion and guidance, particularly regarding XAFS studies. For their assistance during X-ray beamtime, I'd like to thank Drs. Maarten Nachtegaal and Grigory Smolentsev of the SLS, and Drs. Xiaoyi Zhang and Qingyu Kong and Mr. Rick Spence of the APS.

When things aren't going to plan it's good to have a group of people who are willing to sympathise, but also willing to tell you that you're wrong when you need it. With this in mind I'd like to thank the other members of the George Group, past and present, for their friendship and honesty. Whether a late night, coffee run, lunchtime chat, beamtime or traffic jam on the A34, it's been a pleasure to be able to spend so much time with you all.

Finally, I'd like to thank my friends and family for their support, and Leanna for her love and understanding.

Contents

Declaration iii

Abstract v

Acknowledgements viii

Abbreviations xii

1 Introduction 1
- 1.1 Generation and Study of Reactive Intermediates . . . 2
- 1.2 Time-Resolved Spectroscopy . . . 4
  - 1.2.1 Time-Resolved Infrared Spectroscopy . . . 5
    - 1.2.1.1 Ultrafast Time-Resolved Infrared Spectroscopy . . . 7
- 1.3 Other Techniques Used To Study Reactive Intermediates . . . 9
  - 1.3.1 Low Temperature Solution Studies . . . 9
  - 1.3.2 Matrix Isolation . . . 10
- 1.4 Perfluorinated Solvents . . . 11

2 Time-Resolved Studies of Spin-Forbidden Reactions of Transition Metal Carbonyls with Weak Ligands 15
- 2.1 Introduction . . . 15
  - 2.1.1 Organometallic Alkane and Noble Gas Complexes . . . 16
  - 2.1.2 The Photochemistry of $Fe(CO)_5$ . . . 18
    - 2.1.2.1 Low Temperature Characterisation of $^3Fe(CO)_4$ and $^3Fe(CO)_3$ . . . 18
    - 2.1.2.2 Time-Resolved Spectroscopic Studies of $Fe(CO)_5$ in the Gas Phase . . . 22
    - 2.1.2.3 Time-Resolved Spectroscopic Studies of $Fe(CO)_5$ in the Solution Phase . . . 26
  - 2.1.3 Additional Studies of Spin-Forbidden Reactions of Transition Metal Carbonyl Species . . . 35
    - 2.1.3.1 IR Spectroscopic Studies of $^3CpMn(CO)_2$ . . . 35
    - 2.1.3.2 TRIR Spectroscopic Studies of $CpCo(CO)_2$ and $CpV(CO)_4$ 41
  - 2.1.4 Aims . . . 45
- 2.2 Results and Discussion . . . 47

2.2.1 TRIR of $Fe(CO)_5$ in Perfluoro(methylcyclohexane) 47
2.2.2 Picosecond TRIR of $CpMn(CO)_3$ in *n*-heptane 58
2.2.3 Picosecond and Nanosecond TRIR of $CpMn(CO)_3$ in Perfluoro-(methylcyclohexane) 65
2.2.4 Density Functional Theory Study of the Geometry and Spin-State of $^3CpMn(CO)_2$ 70
2.2.5 Picosecond TRIR of $CpMn(CO)_3$ in Perfluoro(methylcyclohexane) with a Liquid Alkane Dopant 74
2.2.6 TRIR of $CpMn(CO)_3$ in Perfluoro(methylcyclohexane) with Gaseous Dopants 80
2.2.6.1 TRIR of $CpMn(CO)_3$ in Xenon Doped Perfluoro(methylcyclohexane) 80
2.2.6.2 TRIR of $CpMn(CO)_3$ in CO_2 Doped Perfluoro(methylcyclohexane) 84
2.2.6.3 TRIR of $CpMn(CO)_3$ in CH_4 and C_2H_6 Doped Perfluoro(methylcyclohexane) 86
2.2.6.4 TRIR Spectroscopy of $CpMn(CO)_3$ in Perfluoro(hexanes) and Perfluoro(triethylamine) 89
2.2.6.5 TRIR Spectroscopy of $(MeCp)Mn(CO)_3$ in Perfluoro-(methylcyclohexane) 106
2.2.7 Discussion of the Reaction Mechanism Following Photolysis of $CpMn(CO)_3$ 115
2.2.8 TR^MPS of $CpCo(CO)_2$ and $CpV(CO)_4$ in Perfluoroalkanes . . . 120
2.3 Conclusions 132

3 Further Time-Resolved Studies of Alkane and Noble Gas Complexes in Room Temperature Perfluoroalkane Solutions 135
3.1 Introduction 135
3.1.1 Organometallic Alkane Complexes 137
3.1.2 Organometallic Noble Gas Complexes Complexes 145
3.1.3 Aims 152
3.2 Results and Discussion 152
3.2.1 TRIR Studies of $CpRe(CO)_3$ in Perfluoroalkane Solvents 153
3.2.2 TRIR Studies of $CpRe(CO)_3$ in Perfluoroalkane Solvents with Noble Gas and Liquid Alkane Dopants 162
3.2.3 TRIR Studies of $CpRe(CO)_3$ Derivatives in Perfluoroalkane Solvents 168
3.2.4 DFT Studies of Transient Species Produced Following Photolysis of $CpRe(CO)_3$ 175
3.2.5 TRIR Studies of C-H Activation at Re in Perfluoro(methylcyclohexane) 178
3.2.5.1 Characterisation of $CpRe(CO)_2$(alkane) (Alkane = Methane, Ethane) in Room Temperature Perfluoroalkane Solution 179
3.2.5.2 Characterisation of $Cp^*Re(CO)_2$(alkane) (Alkane = Methane, Ethane) in Room Temperature Perfluoroalkane Solution 185
3.2.6 TRIR Studies of $CpRh(CO)_2$ in Perfluoroalkane Solvents 189

3.2.7 Spectroscopic Studies of $M(CO)_6$ (M = Cr, Mo, W) in Perfluoroalkane Solvents . . . 200
3.2.8 DFT Studies of Transient Species Produced Following Photolysis of $M(CO)_6$ (M = Cr, Mo, W) . . . 212
3.3 Conclusions . . . 215

4 Time-Resolved Spectroscopic Studies of Organometallic Triethylsilane Complexes 221
4.1 Introduction . . . 221
4.1.1 IR Spectroscopy of Transition Metal Hydrosilane Complexes . . 223
4.1.2 Aims . . . 228
4.2 Results and Discussion . . . 229
4.2.1 TR^MPS Studies of $CpMn(CO)_3$ in Neat Triethylsilane . . . 230
4.2.2 TR^MPS Studies of $CpRe(CO)_3$ and $Cp^*Re(CO)_3$ in Neat Triethylsilane . . . 236
4.2.3 TR^MPS Studies of $CpMn(CO)_3$ and $CpRe(CO)_3$ in Triethylsilane-Doped Perfluoro(methylcyclohexane) . . . 240
4.2.4 TR^MPS Studies of $W(CO)_6$ in Neat Triethylsilane . . . 250
4.2.5 Preliminary TR-XAFS Studies of $CpRe(CO)_3$ and $W(CO)_6$ in Neat $HSiEt_3$ . . . 254
4.2.5.1 TR-XAFS Spectroscopy of $CpRe(CO)_3$ in Neat $HSiEt_3$ 254
4.2.5.2 TR-XAFS Spectroscopy of $W(CO)_6$ in Neat $HSiEt_3$ . . 256
4.3 Conclusions and Future Outlook . . . 258

5 Experimental 263
5.1 Time-Resolved Spectroscopic Measurements . . . 263
5.1.1 Nottingham TRIR Apparatus . . . 264
5.1.2 TRIR Apparatus at the Rutherford Appleton Laboratory . . . 265
5.1.3 TR^MPS Apparatus at the Rutherford Appleton Laboratory . . . 266
5.1.4 Transient Absorption Apparatus at the Rutherford Appleton Laboratory . . . 267
5.1.5 TRIR, TR^MPS and TA Data Analysis . . . 267
5.1.6 Time-Resolved XAFS Spectroscopy at the Swiss Light Source . . 268
5.1.7 Time-Resolved XAFS Spectroscopy at the Advanced Photon Source 269
5.2 Other Spectroscopic Measurements . . . 269
5.2.1 FTIR and UV-visible Spectroscopy . . . 269
5.3 Sample Preparation . . . 270
5.3.1 Solution Phase Sample Preparation . . . 270
5.4 Materials . . . 271
5.4.1 Materials Used in Chapter 2 . . . 271
5.4.2 Materials Used in Chapter 3 . . . 271
5.4.3 Materials Used in Chapter 4 . . . 272

References 273

Abbreviations

Abs	Absorbance
APD	Avalanche photodiode
Cp	η^5-cyclopentadienyl
Cp*	η^5-pentamethylcyclopentadienyl
cw	Continuous wave
DFT	Density functional theory
EXAFS	Extended x-ray absorption fine structure
FTIR	Fourier transform infrared
fwhm	Full-width at half maximum
IR	Infrared
$\boldsymbol{k_{obs}}$	Observed rate constant
Liq	Liquid
MCD	Magnetic circular dichroism
MCT	Mercury cadmium telluride
MeCp	η^5-methylcyclopentadienyl
MECP	Minimum energy crossing point
NMR	Nuclear magnetic resonance
OPA	Optical parametric amplifier
PAC	Photoacoustic calorimetry
PFH	Perfluoro(hexanes)
PFMCH	Perfluoro(methylcyclohexane)
PFTEA	Perfluoro(triethylamine)
QCL	Quantum cascade laser

RECP	Relativistic effective core potential
sc	Supercritical
TA	Transient absorption
THF	Tetrahydrofuran
TRIR	Time-resolved infrared
TR$^{\mathbf{M}}$PS	Time-resolved multiple probe spectroscopy
TR-XAFS	Time-resolved x-ray absorption fine structure
UV	Ultraviolet
WLC	White light continuum
XAFS	X-ray absorption fine structure
$\mathbf{\Delta Abs}$	Change in absorbance
$\lambda_{\mathbf{max}}$	Wavelength at absorbance maximum
ν**(CO)**	Carbonyl stretching frequency
τ	Lifetime

Chapter 1

Introduction

The reactions of the transition metals and their compounds are of great interest across many fields of study including, but not limited to, catalysis,[1–6] solar energy production,[7–10] CO_2 capture and storage[11–14] and pharmaceuticals.[15–18] Determining the nature and subsequent reactivity of any intermediates produced during the course of a chemical reaction is key to understanding the reaction itself. Information pertaining to the rates and mechanisms of chemical reactions can be elucidated using a variety of spectroscopic techniques.

In this Thesis, time-resolved spectroscopies have been used to examine a variety of different photochemical and photophysical processes. In particular, the work can be divided into three areas (i) the spin-forbidden reactions that occur following photoinduced carbonyl loss from a series of first row transition metal compounds, and subsequent formation of noble gas and alkane complexes; (ii) the formation and stability of organometallic alkane and noble gas complexes at room temperature; (iii)

the formation of hydrosilane complexes and subsequent activation of Si-H bonds by a series of transition metal carbonyl species following photoinduced ligand loss. Since each Chapter begins with its own introduction, only a brief outline of the generation and study of reactive intermediates is given in this Introduction.

Although the majority of the work presented within this Thesis contains time-resolved infrared spectroscopic measurements, the original aim was that such experiments would underpin development of time-resolved x-ray absorption studies of short-lived organometallic species, including alkane and noble gas complexes. These x-ray studies would be used in conjunction with IR studies to provide a structural probe of any reactive intermediates formed, and provide additional detail regarding the formation and reactivity of such transient species.

1.1 Generation and Study of Reactive Intermediates

Even a seemingly simple chemical reaction can proceed through a complex mechanism. The work in this Thesis largely concerns the possible reaction of a metal carbonyl complexes with a coordinating solvent, which can include many reactive intermediates, a possible example of which is shown in Scheme 1.1.

$$[\mathrm{M}]{-}\mathrm{CO} \xrightarrow{\mathrm{h}\nu} ([\mathrm{M}]{-}\mathrm{CO})^{*} \xrightarrow{\text{-CO}} [\mathrm{M}] \xrightarrow{\text{+Sol}} [\mathrm{M}]{-}\mathrm{Sol}$$

Scheme 1.1: Example reaction scheme for the photochemical ligand exchange of a transition metal carbonyl $[\mathrm{M}]{-}\mathrm{CO}$ with solvent 'Sol'. This solvent complex can go on to react with additional solvent, dopant or parent molecules, or undergo isomerism, rearrangement, oxidative addition or elimination.

The study of these transient species using conventional analytical techniques raises an interesting problem. Reactive intermediates tend to have very short lifetimes due to their high reactivity, and are therefore often present in very low concentrations within the reaction mixture. The study of reactive intermediates therefore requires the use of techniques that can either extend the lifetime of the transient species by cooling the reaction down such that these species can be studied with conventional spectroscopic techniques, e.g., matrix isolation, or allow rapid observation of the intermediates before they decay as in time-resolved spectroscopies.

The work described in this Thesis involves the generation of reactive intermediates by photochemical means. In the work presented within this Thesis, ultraviolet light is used to photolyse metal carbonyl complexes, causing the loss of a carbonyl or nitrogen ligand. This results in the formation of coordinatively unsaturated 16-electron complexes. While these intermediates would normally react very rapidly with the solvent,[19,20] the unusual solvent environment utilised in Chapters 2 and 3 extends the lifetime of these species. In all of the cases that are investigated in this Thesis, the wavelength of UV or visible light used to excite the sample is tuned to selectively initiate the reaction or process of interest. This selectivity is a major advantage of photochemical initiation. The use of ultrafast laser pulses is also advantageous, allowing extremely rapid generation of the intermediates of interest. In all of these cases, an IR reporter ligand is utilised to probe the reaction mechanism or monitor the kinetics.

1.2 Time-Resolved Spectroscopy

Many time-resolved spectroscopies make use of a "pump-probe" approach, originally based on the flash photolysis experiments developed by Norrish and Porter.[21] These "pump-probe" techniques utilise the basic principle of flash photolysis, generating reactive intermediates with a short pulse while also using fast detection to observe these intermediates in "real-time". Early experiments used UV flash lamps to both pump and probe the sample of interest,[22,23] allowing mechanistic details of reactions occurring on the millisecond timescale to be elucidated. In subsequent years, spectrometers have been developed which can monitor chemical reactions on the femtosecond timescale.[24] A simple schematic of a "pump-probe" experiment is shown in Figure 1.1.

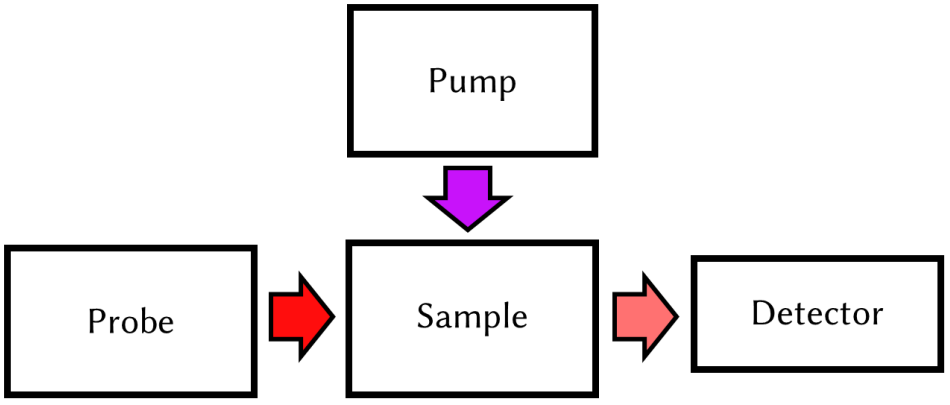


FIGURE 1.1: Schematic of the pump-probe technique. In the context of this Thesis, UV or visible light acts as the pump, while an IR, UV, visible light or x-ray source acts as the probe.

Time-resolved spectroscopy can be used to monitor the concentrations of the species involved in a chemical reaction, including parent, intermediate and product compounds giving information on chemical structure and reaction kinetics. Spectra can be recorded for a series of time delays, and by observing how the absorbance of the

signature absorption bands of each species changes with time, mechanistic details can be determined.

1.2.1 Time-Resolved Infrared Spectroscopy

Time-resolved infrared (TRIR) spectroscopy has proven to be an incredibly powerful technique for studying chemical reactions, not only for transition metal complexes, but organic and biological species as well.[25–29] Time-resolved UV/visible flash photolysis is a powerful approach, but in the condensed phase absorbance bands are broad and featureless. Time-resolved vibrational spectroscopies offer a structurally sensitive alternative to a UV/visible approach. Time-resolved infrared spectroscopy involves photolysis of the sample of interest using a UV or visible pulse, followed by fast detection of intermediates using an IR pulse. In its earliest incarnations, TRIR spectroscopy utilised an adapted dispersive IR spectrometer to probe intermediates on a millisecond timescale. These early experiments are reported in detail in the literature,[30] and will not be discussed further here. However, these early experiments do bear some resemblance to more modern TRIR spectroscopy techniques. Rapid-scan Fourier transform infrared (FTIR) spectroscopy is capable of achieving time resolutions on the millisecond timescale, limited by the amount of time required to move the mirror of the Michelson interferometer. Step-scan FTIR (s^2-FTIR) is a related technique, which allows a much better time resolution of 1 ns to be achieved, limited by the rise-time of the detector.[31]

While the above techniques utilise a broadband IR source, point-by-point TRIR spectroscopy uses a single wavelength to probe the sample. The change in IR absorbance

with time at that specific frequency, following UV or visible irradiation of the sample, yields kinetic data. This process can then be repeated for a series of IR wavelengths, and the spectrum can be built up "point-by-point", as outlined in Figure 1.2.

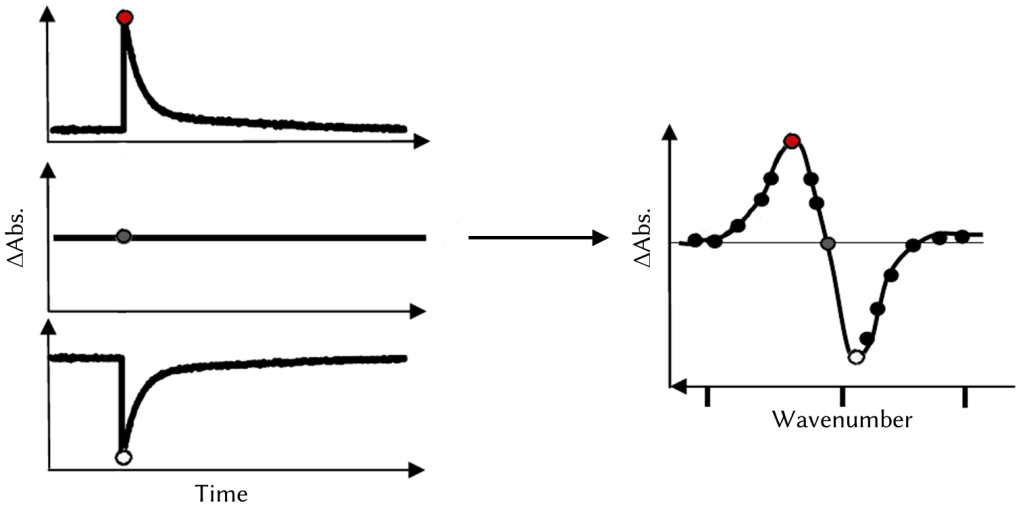


FIGURE 1.2: Illustration of the data outputted by a point-by-point TRIR system, showing how difference spectra can be built up from a series of single-wavenumber kinetic traces.

The time resolution of a point-by-point TRIR experiment is determined by the rise-time of the IR detector, and the length of the UV or visible excitation pulse. The use of a fast mercury-cadmium-telluride (MCT) detector allows for the detection of reactive intermediates on a nanosecond timescale. Various different cw (continuous wave) IR lasers have been utilised for this purpose.[32,33] However, in recent years advances in semiconductor manufacture have allowed for the development of external cavity Quantum Cascade lasers, which offer many advantages over other mid-IR laser sources, used for TRIR experiments.[34,35]

1.2.1.1 Ultrafast Time-Resolved Infrared Spectroscopy

In a point-by-point TRIR experiment the rise-time of the MCT detector is still a limiting factor, and the time resolution is generally 1-10 ns. Measurements on a sub-nanosecond timescale require a different approach. In such experiments, the pump and probe pulses are separated in time using an optical delay line, with the pump pulse arriving either before or after the probe pulse, depending on the length of the path each beam travels.[24] The two beams meet at the sample position, after which the IR pulse is dispersed onto a linear MCT array detector. In the experiments described in this Thesis, every second pump pulse is removed by an optical chopper, and a difference spectrum is produced by subtracting the pump-off signal from the pump-on signal at each time delay. This technique has allowed chemical reactions on the picosecond timescale to be studied.[36,37] The ultrafast TRIR apparatus used in this Thesis is described in detail in Chapter 5.[24,38] Figure 1.3 shows a schematic of a modern ultrafast TRIR system.

Ultrafast TRIR systems generally rely on the output of a Ti:Sapphire laser, which emits at 800 nm. Pulsewidths are often very short. This initial seed pulse is used to generate both the UV/visible and IR pulses through the use of optical parametric amplifiers (OPA). These ultra-short pulses are synchronised and tunable. Very high repetition (1-10 kHz) rates allow for very low concentrations of transient species to be observed.[24] However, this repeated excitation of the sample may lead to sample heating or degradation, which may involve the build-up of product species on spectroscopic cell windows. This problem can be minimised by rastering the sample cell, and by flowing the sample in order to constantly refresh it.

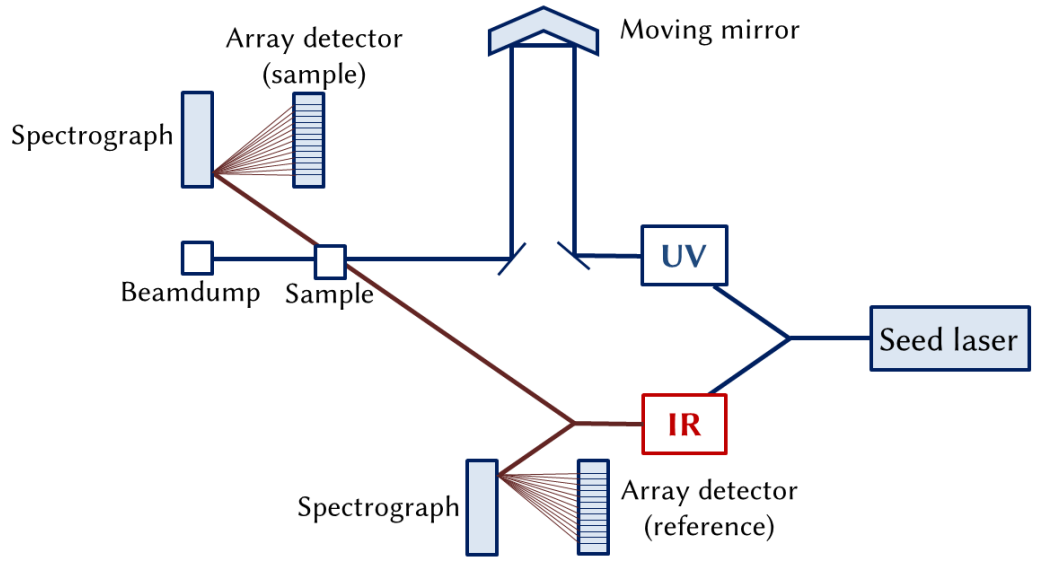


FIGURE 1.3: Schematic of a modern broadband picosecond TRIR spectrometer, utilising a UV pump and a mid-IR probe.

A recent development in the area of TRIR is time-resolved multiple probe spectroscopy ($TR^{M}PS$) at the Rutherford Appleton Laboratory that has allowed for the collection of difference spectra at many different time delays for each pump pulse.[39] This is achieved by using a different repetition rate for the pump and probe beams. This system allows for chemistry occurring on the fs to ms timescales to be studied during a single experiment. Figure 1.4 shows a schematic of a $TR^{M}PS$ experiment in the sample is pumped by a 1 kHz UV pulse and probed by successive 10 kHz IR pulses.

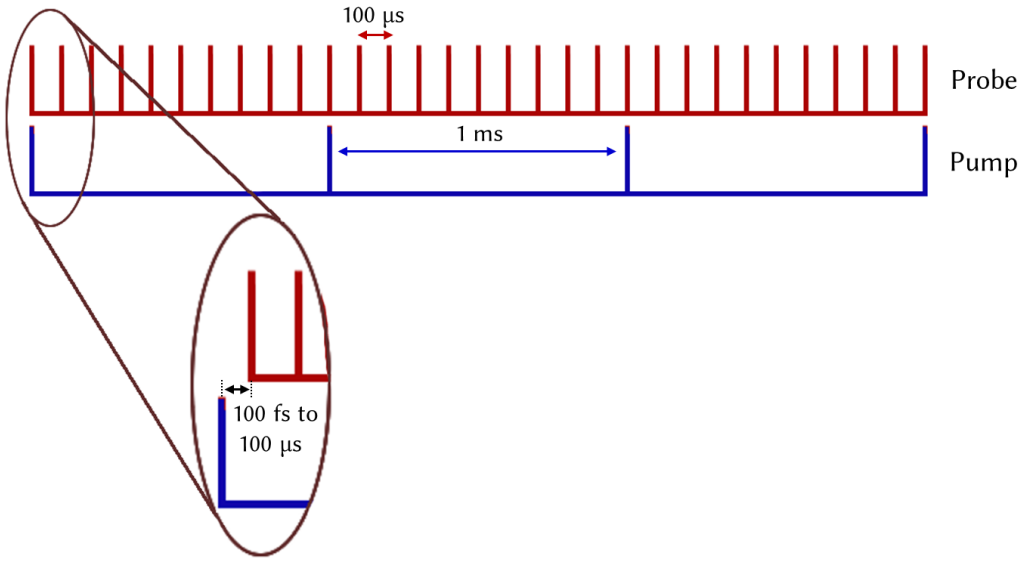


FIGURE 1.4: Model of a TR^{M}PS experiment, showing how time delays from 100 fs to 1 ms can be achieved in the same experiment.

1.3 Other Techniques Used To Study Reactive Intermediates

1.3.1 Low Temperature Solution Studies

Cooling a solution to low temperature can extend the lifetime of reactive intermediates allowing them to be studied with conventional spectroscopic techniques. This approach offers an important advantage, in that it allows the lifetimes of reactive species to be prolonged while still allowing diffusion of intermediates within the solution. Standard analytical techniques such as NMR[40–47] and FTIR spectroscopies[41–43,46–48] can be used to characterise the species of interest. Common solvents for these studies include alkanes and liquefied noble gases (e.g., Xe, Kr).[42,49,50] The noble gases in particular possess an advantage in that they have no IR absorption bands of their own.

1.3.2 Matrix Isolation

Matrix isolation can also be used to extend the lifetimes of reactive intermediates, again allowing them to be characterised by conventional spectroscopic techniques.[51] Unlike low temperature solution studies described above, matrix isolation involves the containment of reactive intermediates within a solid medium. An inert matrix material is doped with the molecule of interest. The molecule of interest is irradiated, and any reactive intermediates produced are contained within the matrix material. These reactive species are isolated from other species by the matrix, and are unable to diffuse through the matrix in order to undergo further reaction, e.g., recombination or intermolecular electron transfer. During the experiment, the matrix material is often kept at low temperature leaving any transient species with little energy to undergo chemical reactions. Many different matrix materials have been reported, including frozen noble gases,[52–54] organic solvents[55,56] and polymers.[57,58]

Matrix isolation is an extremely powerful technique for the study of reactive species which are short-lived at ambient temperatures. However, the technique does have several disadvantages. For example, the matrix material may have its own strong IR absorbance bands, which may obscure the absorbance bands of the molecule of interest, making spectra more difficult to interpret. This is particularly relevant when organic solvent or polymer matrices are used, though the impact of the matrix on the spectrum can be minimised through the use of a noble gas matrix. The melting point of the matrix material may limit the temperature range at which the intermediates of interest can be studied. In extreme cases this may impede the study of the intermediate of interest entirely. Finally, the transient species of interest may interact with the matrix

itself, altering the mechanism of the reaction and the structure of the intermediates being studied. This phenomenon is known as the "matrix effect".[59]

1.4 Perfluorinated Solvents

A large part of the work presented in this Thesis utilises perfluorinated solvents as the reaction medium. A brief introduction to this interesting class of materials is given here. While perfluoroalkane polymers are well known and are widely utilised in various chemical applications as well as in everyday life, small molecule perfluorinated materials which are liquid at room temperature have seen comparatively limited use. First synthesised over 70 years ago,[60] perfluoroalkanes have found limited use in industrial applications as inert fluids, coolants, etchants, oxygen carriers and non-toxic surgical fluids.[61,62]

The chemistry of perfluoroalkanes is unusual and limited, and largely dictated by the very strong carbon-fluorine bond. Fluorine is known to form the strongest single bond to carbon, with a potential bond dissociation enthalpy of *ca.* 500 kJ/mol. Perfluoroalkanes are known to be extremely stable, with very low intermolecular attracting forces leading to low boiling points and high volatilities compared to alkanes of similar length, despite large differences in molecular weight.[63] Perfluorinated alkanes are non-toxic, non-flammable and extremely non-polar. This extreme lack of polarity does not lend itself to use as a solvent, with many organic and organometallic compounds exhibiting little to no solubility in perfluoroalkanes. Despite this, perfluoroalkanes have been observed to have the ability to dissolve large quantities of gases, which has led to

their use as solvents in oxidation and epoxidation processes.[64–66] Interest in the use of perfluoroalkanes as solvents in synthetic chemistry has been buoyed by the need for solvents which do not deplete the ozone layer, and do not produce any toxic byproducts upon decomposition. Additionally, perfluorinated solvents can be easily recovered and recycled. Along with the growth of the use of such media as ionic liquids[67] and supercritical fluids[68] as solvents in synthetic chemistry, perfluoroalkane solvents have so far been utilised in various synthetic procedures, including polymerisations[69] and Friedel-Crafts reactions.[70] In cases where the solvent is simply used to allow the mixing of reagents and transfer of heat to or from the reaction, perfluoroalkane fluids can offer a non-toxic and recyclable alternative to traditionally used volatile organic and chlorinated solvents. Many of the reactions which have utilised perfluorous fluids as solvents have made use of their unusual solubility characteristics in a biphasic solvent system.[71]

While perfluorinated liquids are generally regarded as chemically inert, they do exhibit some chemistry of their own. Interest in development of reaction routes to synthesis of perfluorinated building blocks has led to research into transition metal mediated activation of C-F bonds.[72,73] Several different transition metals have exhibited the ability to activate C-F bonds through oxidative addition of the C-F moiety across the metal, including platinum,[74] palladium,[75] nickel[76] and most notably rhodium.[73,75]

Chapters 2, 3 and 4 of this Thesis involve the use of perfluorinated fluids as solvents for photolysis of transition metal carbonyl species. Such perfluorous solvents have found use in this field previously,[77] most notable by Kelly and co-workers.[78,79] It has been found that the inert, non-coordinating nature of these materials allows access

to some unusual chemistry. Previous photochemical studies in perfluorinated solvents will be described in greater detail in Chapters 2 and 3. As stated above, each Chapter of this Thesis will include its own Introduction, with a detailed overview of relevant literature and theory provided in each case.

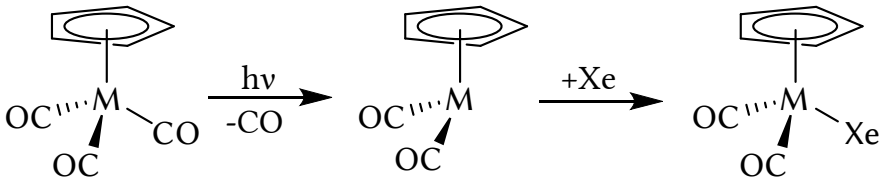
Chapter 2

Time-Resolved Studies of Spin-Forbidden Reactions of Transition Metal Carbonyls with Weak Ligands

2.1 Introduction

As stated in Chapter 1, the initial aim of the work described in this Chapter was to undertake time-resolved infrared (TRIR) spectroscopy and TR^{M}PS (time-resolved multiple probe spectroscopy) measurements to determine the viability of studying short-lived organometallic intermediates using time-resolved x-ray absorption fine structure (TR-XAFS) spectroscopy.

One particular class of reactive intermediates of interest for future TR-XAFS studies is organometallic noble gas complexes, particularly complexes involving a metal-xenon bond. An example of the formation of an organometallic xenon complex is shown in Scheme 2.1.[34]



SCHEME 2.1: Example reaction scheme showing photolysis of a metal carbonyl complex to yield a coordinatively unsaturated intermediate, which reacts with xenon, forming a metal-noble gas bond.

Organometallic Xe complexes have never been isolated, though they have been known for more than 40 years. Much of their chemistry is related to that of organometallic alkane complexes.

2.1.1 Organometallic Alkane and Noble Gas Complexes

Organometallic alkane and noble gas complexes were first observed by Perutz and Turner, using a combination of UV-visible spectroscopy and IR spectroscopy following photolysis in low temperature matrices.[80] Expanding on earlier matrix isolation experiments by Turner and co-workers,[59] $M(CO)_6$ (M = Cr, Mo, W) was confined within a series of matrices at 12 K, including noble gases, alkanes and perfluorinated materials. Upon photolysis, the highly reactive $M(CO)_5$ intermediate was produced, which was shown to be coordinated to the matrix itself to form a complex of the form $M(CO)_5X$, where 'X' is the matrix material. The evidence for the formation of such complexes came from an observed shift in the UV-vis absorption maxima (λ_{max}) and a shift in the IR ν(CO)

bands of the photoproduct. The magnitude of these shifts, for example the λ_{max} of the photoproduct observed following photolysis of $Cr(CO)_6$ in a Ne matrix (624 nm) compared to that observed in a CH_4 matrix (489 nm), indicated an interaction between the matrix and the $Cr(CO)_5$ fragment, which is highly dependent on the nature of the matrix material.

These studies are of particular interest considering the work described within this Chapter in that CF_4 was used as a matrix material during this study, and was found to be very weakly coordinating. In these studies, λ_{max} was found to be a good measure of the strength of coordination to the metal centre. The position of λ_{max} for the photoproduct formed upon photolysis of $Cr(CO)_6$ in a CF_4 matrix was shown to be 547 nm, indicating that the observed interaction with the empty coordination site of $Cr(CO)_5$ is of similar strength to that of Ar (533 nm), and weaker than that observed for CH_4 (489 nm) and Xe (492 nm).

Kelly and Long reported one of the first observations of an organometallic alkane complex in cyclohexane solution.[81] In later work, they demonstrated that a perfluorinated alkane bound to the metal much more weakly than cyclohexane resulting in preferential formation of a cyclohexane complex, suggesting very weak binding of the perfluoroalkane solvent compared to the doped alkane.[78,79]

A more detailed introduction to organometallic noble gas and alkane complexes will be given in Chapter 3, while the remainder of this Introduction will deal with studies of spin-forbidden reactions in metal carbonyl complexes, and its relevance to the formation of short-lived and weakly-bound organometallic species.

2.1.2 The Photochemistry of $Fe(CO)_5$

As will be seen later in this Chapter, the spin-state of the coordinatively unsaturated metal carbonyl fragments produced following photolysis plays an important role in any subsequent interaction with the solvent or dopant ligand. The photochemistry of $Fe(CO)_5$ has been widely studied as a model system for investigation of spin-forbidden reactions.[82] $Fe(CO)_5$ has been reported to undergo complex chemistry following photolysis including the loss of one or more CO ligands, and its small size allows for increasingly complex theoretical calculations to be carried out on its structure and reactivity.[83] The photochemistry of $Fe(CO)_5$ has been studied in the gas and solution phases, as well as at low temperatures.[82] Aside from its interesting photochemistry, $Fe(CO)_5$ has found widespread use in many catalytic applications including alkene hydrogenation[84,85] and isomerisation,[86] and hydrosilation reactions.[87]

The photochemistry of $Fe(CO)_5$ has been the subject of numerous extensive reviews.[82,88–90] This section contains a summary of studies $Fe(CO)_5$, with a particular focus on IR spectroscopic studies of the resulting reactive intermediates $^3Fe(CO)_4$ and $^3Fe(CO)_3$. Subsequent studies of other metal carbonyl species which have been shown, or are suspected, to undergo spin-forbidden chemical reactions following photolysis will also be summarised.

2.1.2.1 Low Temperature Characterisation of $^3Fe(CO)_4$ and $^3Fe(CO)_3$

Low temperature matrix isolation has proven to be a powerful technique for the study of reactive intermediates of metal carbonyl complexes, and studies of $Fe(CO)_5$

following UV photolysis have proven enlightening. Initial studies carried out by Sheline *et al.* first identified a series of coordinatively unsaturated iron carbonyl complexes following photolysis of $Fe(CO)_5$ in hydrocarbon matrices at 77 K.[91] Similar results were subsequently obtained in noble gas matrices.[92] It was observed that upon doping an Ar matrix with alkenes or alkynes, the hydrocarbon dopant could be observed to coordinate to the unsaturated $^3Fe(CO)_4$ fragment.[93] An extensive study was carried out by Poliakoff and Turner, in which $Fe(CO)_5$ was photolysed in a series of low temperature matrices, including noble gases, methane, tetrafluoromethane and sulfur hexafluoride.[94] The resulting tetracarbonyl intermediate $^3Fe(CO)_4$ was thought to possess a C_{3v} structure, however following similar matrix isolation photolysis experiments on isotopically enriched $Fe(CO)_5$, also performed by Poliakoff and Turner, $^3Fe(CO)_4$ was determined to have a C_{2v} structure in its triplet ground state.[95]

At around this time, the first discussion of the spin-state of ground state $^3Fe(CO)_4$ was initiated by Burdett, whose molecular orbital method calculations concluded that this unsaturated carbonyl fragment would be a triplet in its ground state C_{2v} geometry.[96] This assignment was later confirmed by magnetic circular dichroism (MCD) studies undertaken by Barton.[97] During these studies, it was observed that MCD spectra were temperature independent before photolysis when only $Fe(CO)_5$ was present in the Ar matrix. However following photolysis the MCD spectra were found to be temperature dependent indicating the paramagnetic nature of $^3Fe(CO)_4$. The assignment of the geometry and spin-state of $^3Fe(CO)_4$ has since been further supported by *ab initio* calculations.[98] UV irradiation of $^3Fe(CO)_4$ was shown to lead to loss of another CO ligand to produce $^3Fe(CO)_3$. Due to the observation of 2 ν(CO) bands for $^3Fe(CO)_3$, a

planar D_{3h} geometry could be eliminated. Distortion to a pyramidal C_{3v} geometry was confirmed by ^{13}CO enrichment.[95,99] This complex was also predicted by Burdett to be a triplet in its ground state.[96] Further *ab initio* studies have since corroborated this assignment.[100] The structures and electronic configurations of $Fe(CO)_5$, $^3Fe(CO)_4$ and $^3Fe(CO)_3$ are shown in Figure 2.1.

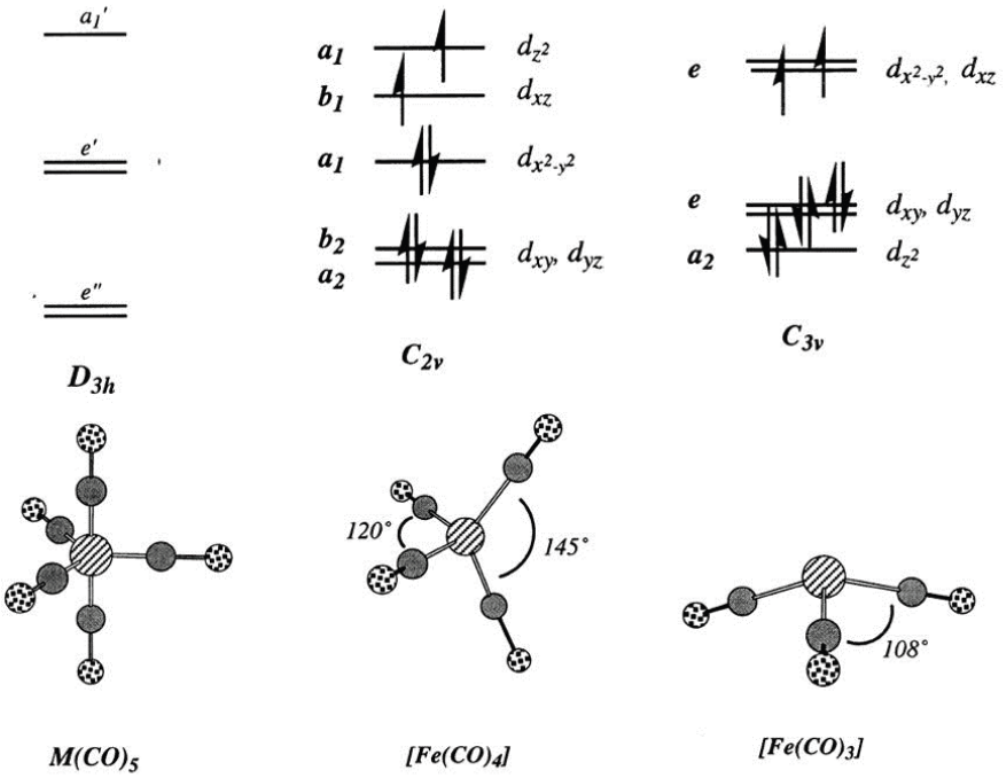
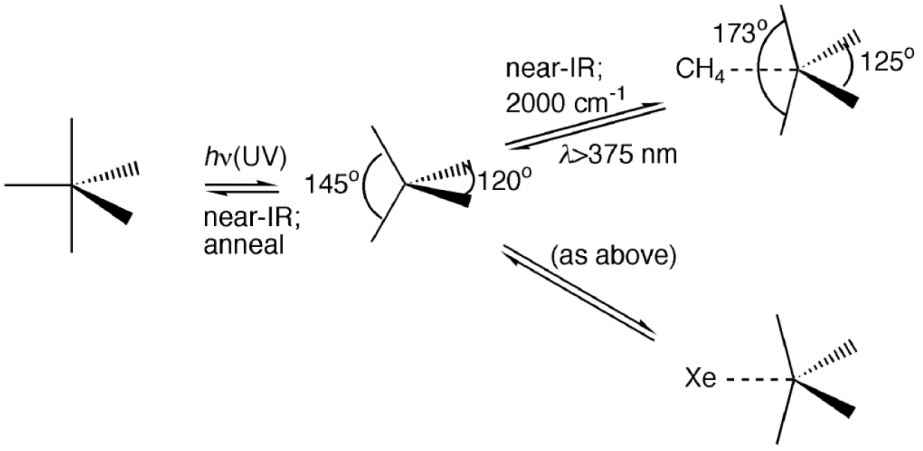


FIGURE 2.1: Structures and orbitals of $Fe(CO)_5$, $^3Fe(CO)_4$ and $^3Fe(CO)_3$. Adapted from ref 82.

Low temperature matrix studies carried out in Ne and Ar matrices demonstrated that upon irradiation of the unsaturated intermediate $^3Fe(CO)_4$ with near-IR light, partial reformation of the parent $Fe(CO)_5$ could be induced.[95] This is in contrast to results obtained in N_2, methane and xenon matrices. During these experiments, irradiation with IR light yielded a new species, $^1Fe(CO)_4X$ (X = matrix material),

which could then be photolysed with UV light to yield the unsaturated $^3Fe(CO)_4$. This result indicated formation of a more stable species upon binding of the matrix material to the metal centre, and represents the first characterisation of noble gas and methane complexes of $^3Fe(CO)_4$. Further to this work, studies carried out in frozen hydrocarbon matrices at 77 K showed only the formation of $^1Fe(CO)_4X$ (X = matrix material), with no detection of the unsaturated $^3Fe(CO)_4$. It is interesting to note that throughout all of the studies described above, no evidence of an unsaturated singlet complex $^1Fe(CO)_4$ was observed, indicating that a spin-forbidden reaction of $^3Fe(CO)_4$ to form the singlet may require a reaction with an incoming ligand. A proposed reaction scheme based on low temperature matrix experiments is outlined in Scheme 2.2.



Scheme 2.2: Reaction scheme for photolysis of $Fe(CO)_5$ in a methane of xenon matrix at low temperature, showing formation of $^3Fe(CO)_4$ following photolysis, and subsequent addition of the matrix material as a ligand. Adapted from ref 89.

Low temperature matrix isolation studies have also been used to identify various dimeric iron carbonyl species, including both bridged and unbridged structures of

$Fe_2(CO)_8$, as well as $Fe_2(CO)_9$,[101,102] which are often observed as additional photoproducts following photolysis of $Fe(CO)_5$.[103]

2.1.2.2 Time-Resolved Spectroscopic Studies of $Fe(CO)_5$ in the Gas Phase

$^3Fe(CO)_4$, due to its coordinatively unsaturated nature was expected to be short-lived in the gas phase, due to the lack of stabilisation afforded by confinement within a matrix. Because of this, the conventional spectroscopic techniques applied to the matrix isolation studies presented above could not be used. $Fe(CO)_5$ has been widely studied in the gas phase using TRIR spectroscopy, which has proven itself to be a powerful technique for the study of reactive intermediates,[104] including those produced following photolysis of $Fe(CO)_5$. A comparison of gas phase TRIR and low temperature matrix FTIR spectra of $Fe(CO)_5$ is shown in Figure 2.2.

Initial experiments involved 248 nm photolysis of $Fe(CO)_5$ in an Ar buffer gas.[105,106] The authors of these studies reported the formation of a series of transient spectral features in the gas phase. These features were assigned to the previously observed coordinatively unsaturated complexes $^3Fe(CO)_4$ and $^3Fe(CO)_3$, as well as further products of additional carbonyl loss. Experiments performed under a CO atmosphere showed that $^3Fe(CO)_3$ rapidly decays to reform $^3Fe(CO)_4$, while reformation of the parent $Fe(CO)_5$ was not observed. Due to the similarity of spectral features observed in the gas phase with those observed during matrix isolation experiments, $^3Fe(CO)_4$ was concluded to exhibit C_{2v} geometry in the gas phase.

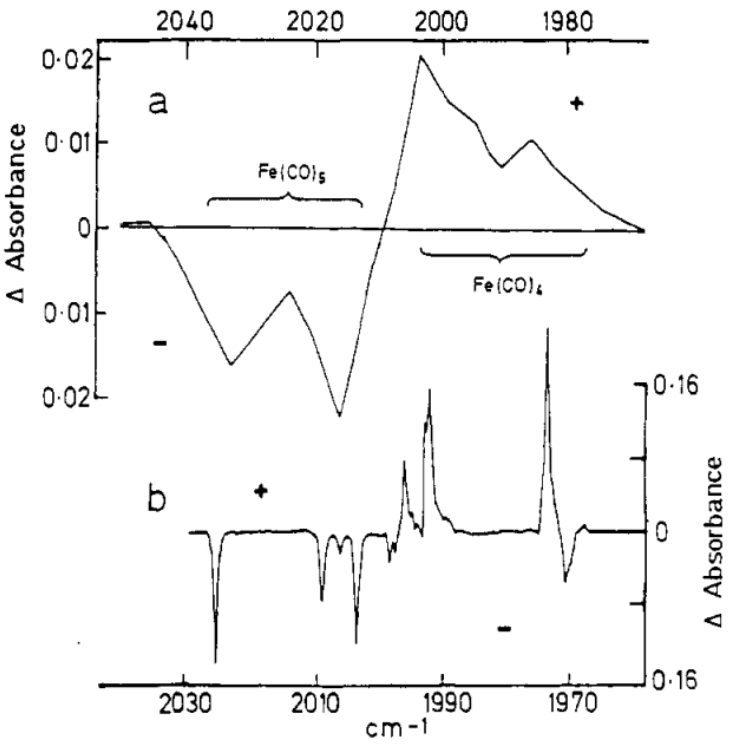


FIGURE 2.2: IR spectra in a) Gas phase TRIR and b) low temperature Ar matrix FTIR spectra of $Fe(CO)_5$ and $^3Fe(CO)_4$. Reproduced from ref 88.

Further studies concluded that the yield of products of multiple carbonyl ligand loss following photolysis of $Fe(CO)_5$ is not dependent on the laser power, indicating the absence of two-photon effects. However, the relative yields of these various unsaturated species were found to be sensitive to the energy of the incident UV photon, as shown in Figure 2.3.[107] Variable excitation wavelength studies were carried out to examine the dissociation of varying numbers of carbonyl ligands following photolysis of $Fe(CO)_5$.[108,109] Photolysis with a XeF excimer laser at 351 nm yielded only $^3Fe(CO)_4$ and $^3Fe(CO)_3$, however an increase in laser energy to 248 nm (KrF) yields $^3Fe(CO)_3$ and $^3Fe(CO)_2$, and a further increase to 193 nm (ArF) yielded $^3Fe(CO)_2$ and Fe(CO). These products were determined to be formed following absorption of a single photon by the parent $Fe(CO)_5$. The difference in behaviour between matrix isolated and

gas phase $Fe(CO)_5$ was proposed to be due to the difference in rate of vibrational relaxation. Following initial photolysis and loss of CO, the resulting $^3Fe(CO)_4$ would be expected to be vibrationally "hot", with enough energy to expel the next CO ligand to form $^3Fe(CO)_3$. Under gas phase conditions intramolecular pathways for energy redistributions would be expected to be faster than any intermolecular pathways. This conclusion is in agreement with the observation of vibrationally hot fragments in the gas phase.[107] Photoelectron spectroscopy of $Fe(CO)_5$ in the gas phase reported dissociation energies for loss of successive carbonyl ligands to be 55, 5, 32 and 23 kcal/mol, for loss of 1, 2, 3 and 4 carbonyl ligands, respectively.[110]

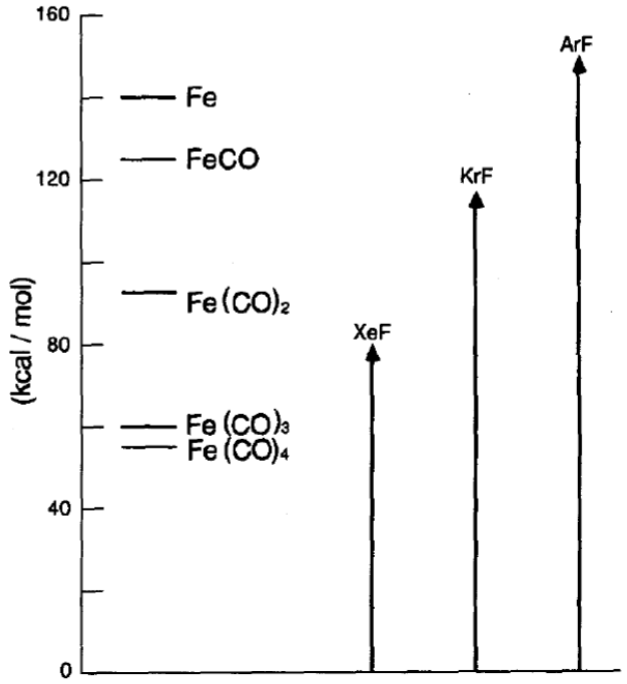


FIGURE 2.3: Calculated dissociative energies of successive CO ligands from $Fe(CO)_5$ at different excitation wavelengths provided by different Excimer laser sources. Adapted from ref 107.

The loss of multiple carbonyl ligands has been determined to occur in a stepwise

manner.[107–109], as previously indicated by chemical trapping studies.[111,112] Two possible mechanisms have been proposed for the loss a carbonyl ligand following photolysis of $Fe(CO)_5$.[98,107,113,114] The first of these mechanisms, often designated as the 'triplet mechanism' involves initial excitation of $Fe(CO)_5$, followed by spin-crossover to triplet $Fe(CO)_5$, which loses a carbonyl to form $^3Fe(CO)_4$. The second mechanism, designated the singlet mechanism, involves excitation of $Fe(CO)_5$, followed by loss of a carbonyl to form $^1Fe(CO)_4$, which undergoes a spin-change to yield $^3Fe(CO)_4$. Previously, neither $^3Fe(CO)_5$*, nor $^1Fe(CO)_4$ had been observed spectroscopically.

The first observation of coordinatively unsaturated $^3Fe(CO)_4$ by gas phase TRIR experiments was reported by Ryther and Weitz.[108] By varying the pressure of the buffer gas, it is possible to alter the rate of relaxation of the initially formed transient species. By repeating experiments described above utilising 248 nm and 351 nm excitation at lower buffer gas pressure, the authors observed two new species, which had not previously been reported. However, both of these transients were short-lived. These new species were assigned as singlet states of $^3Fe(CO)_4$ and $^3Fe(CO)_3$. This observation of $^1Fe(CO)_4$ in the gas phase provided evidence for formation of $^3Fe(CO)_4$ through the "singlet" mechanism described above. Further evidence to support this mechanism comes from Trushin and co-workers, who describe the femtosecond reaction dynamics of CO loss following photolysis of $Fe(CO)_5$. The authors determined that at low pressures, the initial CO dissociation occurs on a fast femtosecond timescale (*ca.* 30 fs), resulting in the initial formation of $^1Fe(CO)_4$, in an excited singlet state. This species then relaxed to the ground singlet state (*ca.* 50 fs), before undergoing a spin-change to form $^3Fe(CO)_4$. This spin-change was not observed in these experiments however, indicating

that under these conditions of low pressure the spin-forbidden reaction takes place on a timescale outside of the capabilities of the instrument used (>500 ps). Later work by Ihee *et al.* utilised ultrafast electron diffraction spectroscopy also observed the singlet state $^{1}Fe(CO)_4$ following two-photon excitation at 620 nm.[115] However, once again no evidence of a spin-forbidden reaction to form $^{3}Fe(CO)_4$ was observed on the timescale of this experiment. Interestingly, comparison of electron diffraction data for $^{1}Fe(CO)_4$ and data obtained from low temperature matrix isolation studies[95] show very little difference in the structure of coordinated and non-coordinated $^{1}Fe(CO)_4$. OC-Fe-CO bond angles were found to be very similar; 169 (±2)° and 125 (±2)° for gas phase studies, 173° and 125° for CH_4 matrix studies. This leads to the conclusions that there is very little deformation in the geometry of $^{3}Fe(CO)_4$ following the coordination of methane.

2.1.2.3 Time-Resolved Spectroscopic Studies of $Fe(CO)_5$ in the Solution Phase

While low temperature matrix isolation studies and gas phase TRIR studies may offer a fantastic insight into the nature of reactive intermediates, the majority of preparative chemistry occurs in the solution phase. Understanding the mechanism of chemical reactions in the solution phase is therefore key to understanding the process involved in chemical synthesis and catalysis. For solution phase studies, TRIR still offers a powerful insight into these reaction mechanisms through study of photolytically produced intermediates.

The first solution phase TRIR spectroscopic studies of $Fe(CO)_5$ were undertaken by Church and co-workers.[116] Following photolysis of $Fe(CO)_5$ with UV light in benzene-d_6, the authors reported observation of transient IR bands which were assigned to the solvent complex $^1Fe(CO)_4(C_6D_6)$. These bands were assigned by comparison with experiments undertaken in low temperature methane matrices. Further TRIR spectroscopic studies were carried out, this time on a solution of $Fe(CO)_5$ in cyclohexane.[117] Once again, the product formed following photolysis was assigned as a singlet complex with the solvent by comparison to previous studies in hydrocarbon matrices. In a solution saturated with CO, this transient was observed to decay on a fast microsecond timescale, forming the dimeric species $Fe_2(CO)_8$ and $Fe_2(CO)_9$, while a small amount would go on to react with CO to reform the parent $Fe(CO)_5$. No evidence of formation of the triplet species $^3Fe(CO)_4$ was observed during these studies, indicating that the spin-forbidden reaction in cyclohexane solution was likely to take place on a timescale faster than that measurable by their instrument (<1 μs). These observations represent the first example of a $^1Fe(CO)_4$(alkane) complex characterised in a room temperature solution. It would require an instrument capable of recording transient IR spectra on a picosecond timescale before triplet intermediates would be detected in a room temperature solution.

The first of these studies was carried out by Harris and group.[118] Following 295 nm photolysis of $Fe(CO)_5$ in n-heptane solution, the authors observed two initial transient ν(CO) bands, which were assigned to the triplet state $^3Fe(CO)_4$ by reference to earlier matrix isolation experiments. These spectra are shown in Figure 2.4. In this case, $^3Fe(CO)_4$ was found to be stable past the end of the experiment, 660 ps after photolysis.

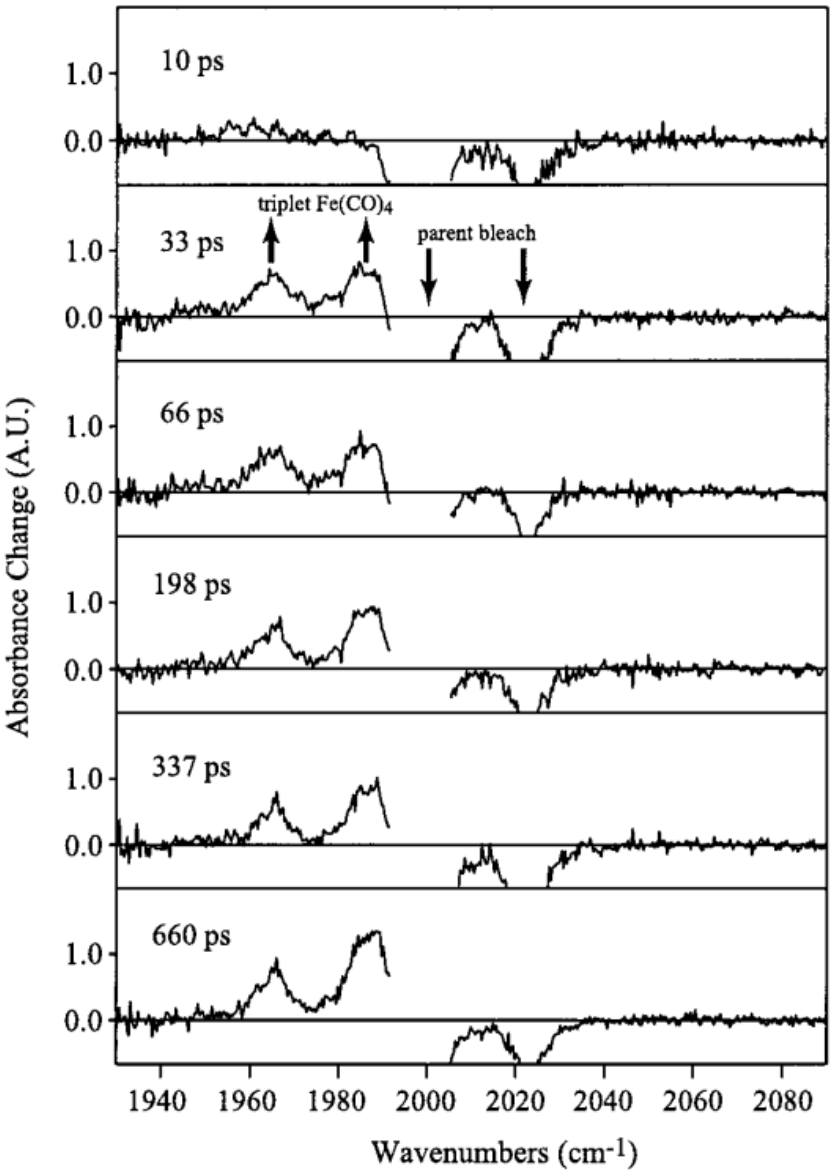


FIGURE 2.4: TRIR difference spectra of $Fe(CO)_5$ in *n*-heptane recorded following 295 nm photolysis. Reproduced from ref 118

Contrasting results were obtained following photolysis of $Fe(CO)_5$ in triethylsilane, however. $^3Fe(CO)_4$ was observed in triethylsilane as the initial photoproduct, however it was found to be unstable on the picosecond timescale, decaying to form the Si-H activated complex $^1Fe(CO)_4H(SiEt_3)$.

In contrast to gas phase measurements described above, no evidence for formation

of $^{3}Fe(CO)_3$ was observed during these first solution phase measurements. Earlier photolytic ligand substitution studies were performed by Wrighton *et al.*, in which photolysis of $Fe(CO)_5$ in the presence of PPh_3 showed evidence of formation of *trans*-$Fe(CO)_3(PPh_3)_2$ in solution, which was proposed to form via a single-photon pathway.[84] Further studies of the behaviour of $Fe(CO)_5$ following photolysis in the presence of phosphines were performed by Burkey and group, who once again reported formation of $Fe(CO)_3(PEt_3)_2$ phosphine complex through a single-photon process.[119,120] In addition to these studies, $Fe(CO)_5$ was photolysed in the presence of cyclooctene, yielding evidence for formation of $Fe(CO)_3(cyclooctene)_2$.[121]

The earliest TRIR spectroscopic identification of $Fe(CO)_3(Sol)$ or $Fe(CO)_3(Sol)_2$ (Sol = solvent) was reported by Snee *et al.*, who studied photolysis of a solution of $Fe(CO)_5$ in alcohols and PEt_3.[122] Experiments undertaken in alcohol solvent showed initial formation of $^{3}Fe(CO)_4$, following by coordination of the alcohol solvent. Formation of alcohol complexes was found to occur on the picosecond timescale (*ca.* 40 ps), indicating a strong interaction between the solvent and the metal centre. This result was an indication of the control the incoming ligand has on the rate of the spin-forbidden reaction. Results obtained following photolysis of $Fe(CO)_5$ in triethylphosphine show very different behaviour from those observed in alcohol solution. No evidence for the formation of $^{3}Fe(CO)_4$ is observed, while $^{1}Fe(CO)_4(PEt_3)$ was observed to form within 50 ps. Further transient bands were observed, which were assigned to the tricarbonyl phosphine adducts $Fe(CO)_3(PEt_3)$ and $Fe(CO)_3(PEt_3)_2$. The former was observed within 10 ps of photolysis, while the latter was observed to form through reaction of $Fe(CO)_3(PEt_3)$ with a further solvent molecule. As part of the same study, DFT

calculations were used to examine the spin-states of both of these phosphine adducts. The singly solvated species was found to have a triplet ground state, in agreement with previous theoretical predictions,[96] while the doubly solvated species was found to be a singlet in its ground state. A subsequent study examining the photochemistry of $Fe(CO)_5$ in cyclohexane solution was carried out.[123] This study once again demonstrated that $Fe(CO)_3(Sol)$ forms through a one-photon process representing the first identification of an iron tricarbonyl alkane complex in room temperature solution.

Recently, an in depth study of the formation and behaviour of iron tricarbonyl complexes in room temperature solution was reported.[124] The authors describe an interesting difference between the observed dynamics of $^3Fe(CO)_3$ in alcohol and alkane solutions. In alkanes, the band at 1926 cm^{-1} remains at the same frequency until *ca.* 500 ns, indicating increased relative stability of the unsolvated $^3Fe(CO)_3$ compared to its solvated analogue. In alcohol solution, however, evidence of coordination of hydroxyl groups to the tricarbonyl complex is observed within tens of picoseconds after photolysis. The triplet spin-state of the unsolvated complex was reported to be maintained upon coordination of the solvent. This result is in contrast to the observations in alkanes discussed above,[123] as well as others presented later in this section.[103,125]

While reactions of $^3Fe(CO)_3$ with a solvent require no change in spin-state as shown above,[124] reactions of $^3Fe(CO)_4$ to form $^1Fe(CO)_4X$ are spin-forbidden and require a change of spin-state. In previous TRIR studies described above, this process has not been directly observed, and the rate of this process has therefore not been measured. The first direct observation of this process was reported during a TRIR study which reported difference spectra recorded across the picosecond, nanosecond and microsecond

timescales,[103] rather than the more limited timescales used in previous studies.[116,118,122] Photolysis of $Fe(CO)_5$ was carried out in a variety of solvents during this study, including liquid *n*-heptane, supercritical noble gases Ar and Xe, and supercritical methane. Following photolysis in all cases, fast formation of $^3Fe(CO)_4$ was observed. In *n*-heptane, *sc*Xe and *sc*CH_4, decay of $^3Fe(CO)_4$ was observed to occur on this nanosecond timescale, concurrently with growth of new features in the spectrum assigned to $^1Fe(CO)_4$(Sol). Example spectra are shown in Figure 2.5. The rate of this spin-forbidden reaction with the solvent from $^3Fe(CO)_4$ to form $^1Fe(CO)_4$(Sol) appeared to be dependent on the solvent, with the alkanes giving the fastest rates, while *sc*Xe gave the slowest rate. Interestingly, no evidence of formation of $^1Fe(CO)_4$(Sol) was observed in *sc*Ar. In this case $^3Fe(CO)_4$ was observed to be stable into the microsecond timescale. The double carbonyl loss product $^3Fe(CO)_3$ was also observed during these studies and was found to form within the risetime of the experiment (<20 ps). The concentration of $^3Fe(CO)_3$ was observed to be dependent on the concentration of $Fe(CO)_5$ in the initial solution, as well as the concentration of CO. This dependence on CO concentration indicated a possible reaction to form $^3Fe(CO)_4$ or $^1Fe(CO)_4$, or a reaction with the parent complex to form the dimer $Fe_2(CO)_8$. A reaction scheme is presented in Scheme 2.3.

A further study published in 2009 expands upon the work described above.[125] Combined experimental and computational techniques were used to examine both the structures and rates of reaction of the various intermediates produced following photolysis of $Fe(CO)_5$ in various solvents. Experiments recorded in alkane and noble gas solvents were found to agree with previously published results. As part of this study, the temperature dependence of the rates of the spin-forbidden reaction of *n*-heptane

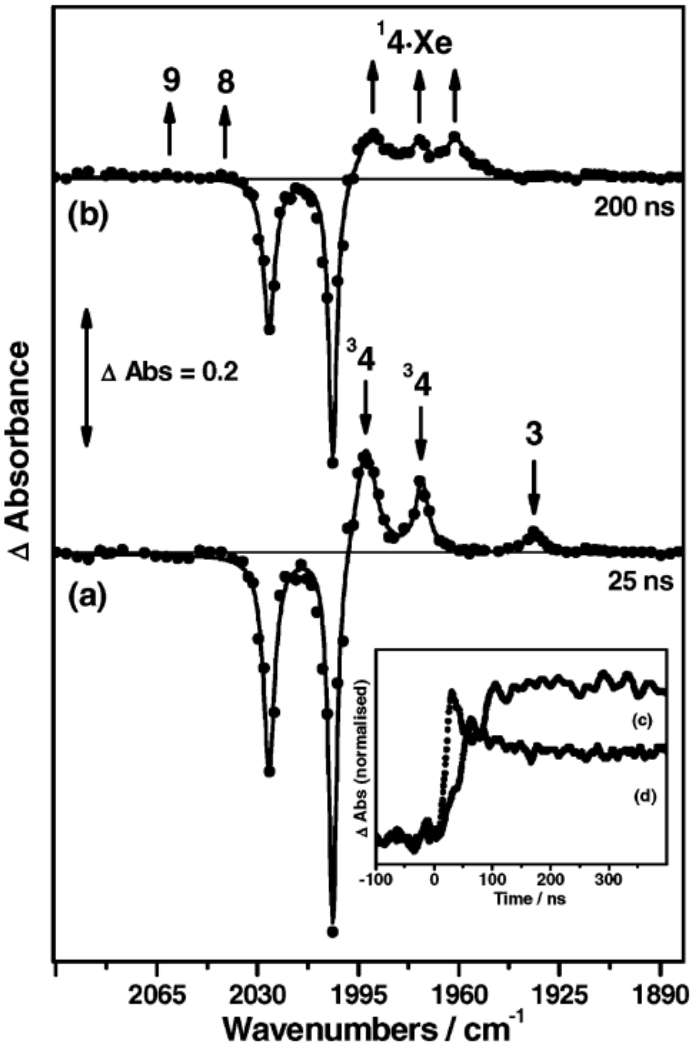
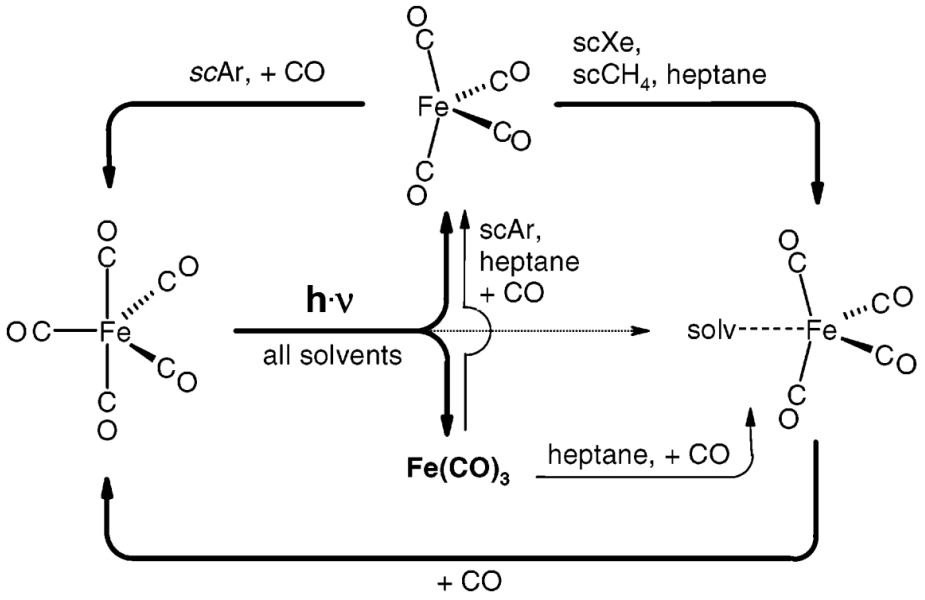


FIGURE 2.5: TRIR difference spectra of $Fe(CO)_5$ in *sc*Xe doped with CO, showing the spectra recorded a) 25 ns following photolysis and b) 200 ns following photolysis. The decay of $^3Fe(CO)_4$ (^{3}4) and $^3Fe(CO)_3$ (3) can be seen, along with formation of $^1Fe(CO)_4Xe$ (^{1}4•Xe). Reproduced from ref 103

or Xe with $^3Fe(CO)_4$ were measured, in order to calculate the activation energy for these processes. In both cases, a significant activation energy barrier was determined. Photolysis of $Fe(CO)_5$ in *sc*Ar doped with H_2 was found to result in formation of $^3Fe(CO)_4$, which reacts with H_2 on a nanosecond timescale.

Additional insight into the reaction mechanism following photolysis of $Fe(CO)_5$



SCHEME 2.3: Proposed reaction scheme following UV photolysis of $Fe(CO)_5$ in *n*-heptane, *sc*CH_4, *sc*Xe and *sc*Ar. Adapted from ref 103.

was obtained through extensive computational studies. Theoretical studies such as these have previously been used to provide insight into spin-crossover processes.[126–131] However, calculations of the minimum energy crossing points (MECPs) between the two potential energy surfaces of different spins which have proven to be most useful.[132–134] Harvey and co-workers have published a variety of studies which examine reactivity in systems that require a spin-crossover.[135–137] They have also shown the ability to calculate rate coefficients for these processes.[83,138] Accurate DFT studies of the singlet and triplet potential energy surfaces for $^3Fe(CO)_4$ and its reaction products, along with their intersections are provided along with experimental details described above.[125] Calculations for addition of CO to $^3Fe(CO)_4$ yield good agreement with experimental results, predicting a direct mechanism of addition in which ligand addition and spin-crossover occur in a single step. Poorer agreement with experimental results was obtained for addition of Xe or H_2 to $^3Fe(CO)_4$ when a similar mechanism of addition

was assumed. Addition of these ligand was proposed to occur through initial spin-crossover from $^3Fe(CO)_4$ to $^1Fe(CO)_4$, followed by barrierless addition of the ligand. Despite the lack of experimental observation of $^1Fe(CO)_4$, the above mechanism is in good agreement with the measured activation energy for addition of H_2 at the concentrations used in gas and solution phase experiments. This scheme is shown in Figure 2.6.

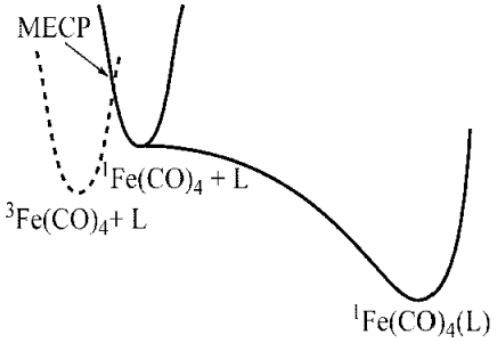


FIGURE 2.6: Proposed potential energy surfaces, including MECP, for the reaction of $Fe(CO)_5$ with ligand L. Adapted from ref 139.

Very recently, Wernet *et al.* published a study utilising femtosecond x-ray spectroscopy to probe the frontier orbital interactions and reaction dynamics following photolysis of $Fe(CO)_5$.[140] The authors report the first direct observation of an excited singlet state of $^1Fe(CO)_4$. This singlet state then goes on to either convert to $^3Fe(CO)_4$, or combine with CO or a solvent molecule to form a pentacoordinated species on a sub-picosecond timescale. This finding lends more evidence for the formation of $^3Fe(CO)_4$ through the "singlet pathway".[98,107,114,141] Despite the vast array of studies on the nature of $Fe(CO)_5$ and its reactive intermediates, application of new and evolving techniques such as fast x-ray spectroscopies can still yield exciting discoveries.

2.1.3 Additional Studies of Spin-Forbidden Reactions of Transition Metal Carbonyl Species

While the coordinatively unsaturated metal carbonyl species produced following photolysis of $Fe(CO)_5$ may be the most widely studied, they are by no means the only recorded cases of such a phenomenon. Cyclopentadienyl complexes $CpCo(CO)_2$,[142–146] $CpV(CO)_4$[147–149] and $CpMn(CO)_3$[53,122,150–152] have been shown to form metastable 16-electron complexes following photolysis, as have $Fe(dmpe)_2$[153,154] (dmpe = $Me_2PCH_2CH_2PMe_2$) and (PNP)Co(CO) (PNP = $[(^tBu_2PCH_2SiMe_2)_2N]^-$),[155,156] as well as various Fe(PNP) complexes.[157] The remainder of this introduction will focus on the photochemistry of cyclopentadienyl metal carbonyl complexes and their coordinatively unsaturated reactive intermediates.

2.1.3.1 IR Spectroscopic Studies of $^3CpMn(CO)_2$

Coordinatively unsaturated species produced following the photolysis of $CpMn(CO)_3$ have been widely studied with both experimental[55,149,158–163] and theoretical techniques.[164–166] Many of these experimental studies utilised low temperature matrix isolation. However, $^1CpMn(CO)_2$ has also been characterised in a Nujol mull,[167] and in a polyethylene thin film.[168] Akin to $Fe(CO)_5$, $CpMn(CO)_3$ itself has been shown to be an important model system for probing excited state and reaction dynamics.[169–172] $CpMn(CO)_2$ has been observed by TRIR in the solution phase, however in most of these studies it appears as $^1CpMn(CO)_2X$ (X = solvent or dopant), not in its unsaturated form, but with a donor ligand.[46,149,162,163,173–181] This is also the case when the solvent is a noble gas, leading to formation of a weakly-bound noble gas complex.[177,182–185]

The first room temperature gas phase observation of an unsaturated cyclopentadienyl manganese carbonyl fragment came in 1992, by Zheng and co-workers.[152] Upon UV photolysis of $CpMn(CO)_3$ in the gas phase using Ar as a buffer gas, the authors noted formation of a series of photoproducts, which were found to vary with the excitation wavelength. Upon photolysis at 266 nm, a single intermediate was observed, with a single ν(CO) band at 1948 cm^{-1}, shown Figure 2.7. However, upon 355 nm photolysis a second, additional intermediate was observed, with two ν(CO) bands at 1874 and 2021 cm^{-1}. These two species were assigned to the double and single carbonyl loss product respectively. However, the ν(CO) band positions of the single carbonyl loss species were found to be in disagreement with previously reported results in the condensed phase.[149,162]

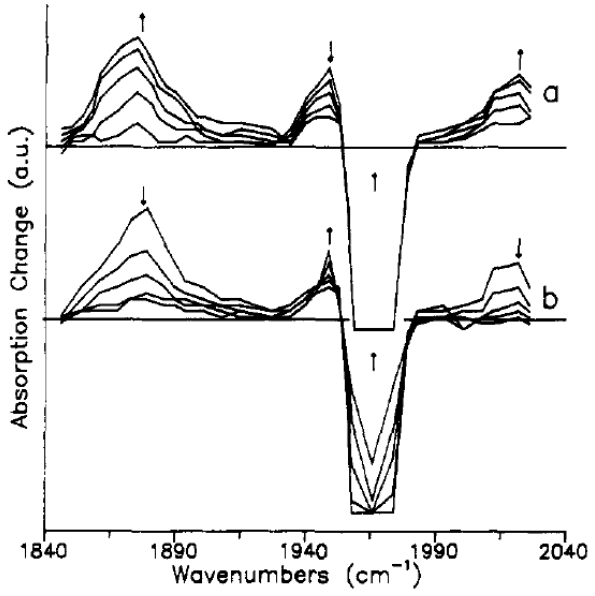


FIGURE 2.7: TRIR difference spectra recorded following 266 nm photolysis of $CpMn(CO)_3$ under CO in the gas phase, showing a) Spectra recorded at 1 μs intervals and b) Spectra recorded at 11 μs intervals. Initial increase of $^3CpMn(CO)_2$ followed by its subsequent decay can be seen. Reproduced from ref 152.

It was found that over time, the monocarbonyl species $CpMn(CO)$ combined with added CO to form $CpMn(CO)_2$, which itself eventually decays to reform the parent $CpMn(CO)_3$. The rate constant of the reaction of $CpMn(CO)$ with CO was measured, and found to be on the same order of magnitude as those of other spin-allowed reactions, while the reaction with $CpMn(CO)_2$ was found to be much slower. Conversely, the reaction of $CpMn(CO)_2$ with O_2 was found to be fast, indicating that the spin-state of $CpMn(CO)_2$ may be a factor in such reactions. This study includes the first discussion of the possibility of a triplet spin-state for unsaturated $CpMn(CO)_2$. The authors reported an additional study of reactivity of these unsaturated manganese carbonyl intermediates with small molecules, and again found significant differences in reaction rates, again suggesting that spin-allowed and disallowed processes are at play, controlling these rates.

Harris and group used TRIR spectroscopy to study the behaviour of $CpMn(CO)_3$ in triethylsilane solution.[186] In this case, two transient species were reported, which were assigned to the silane σ-complex $CpMn(CO)_2(EtSiHEt_2)$, and the unsaturated 16-electron intermediate $CpMn(CO)_2$. Only a single $\nu(CO)$ band of this intermediate was observed however, while the other, lower energy band observed previously by Zheng *et al.* lay outside of the spectroscopic window of the instrument. Later studies by the same group attempted to give further insight into the mechanism of Si-H bond activation at manganese carbonyl centres using a combination of TRIR spectroscopic studies and theoretical calculations. Spin-crossover from the triplet to the solvated singlet state in this case was found to occur on the picosecond timescale (*ca.* 100 ps).[150,187]

A further study also examined the behaviour of $CpMn(CO)_3$ following photolysis in an alkane solution.[118] It was found that in contrast to the long lifetimes observed for $^3Fe(CO)_4$, $^3CpCo(CO)$ and $^3CpV(CO)_3$ in alkane solution, $^3CpMn(CO)_2$ decays with a lifetime on the picosecond timescale (119 ps), along with corresponding increases in the ν(CO) bands of the alkane solvated dicarbonyl complex. This difference in rate of the spin-forbidden reaction is attributed to the large spin-orbit coupling present in $CpMn(CO)_3$, as well as the relatively low triplet/singlet energy gap.

Despite these interesting findings, no in-depth time-resolved spectroscopic studies of the spin-forbidden reaction of $^3CpMn(CO)_2$ to form $^1CpMn(CO)_2X$ in the solution phase have been published to date. However, in 2012 Kemnitz *et al.* produced an extensive study of the structure and photochemistry or $CpMn(CO)_3$, its Cp ring-substituted derivatives and their many reactive intermediates and photoproducts.[53] This study involved the use of matrix isolation techniques as well as IR spectroscopy and DFT calculations. Upon photolysis of $CpMn(CO)_3$ in an Ar matrix at 10 K, the authors reported observation of a number of different photoproducts assigned to coordinatively unsaturated species. These species were characterised as triplet and singlet $CpMn(CO)_2$. Spectra taken from this study are shown in Figure 2.8. Over time, the ν(CO) bands of $^3CpMn(CO)_2$ were observed to decrease, concomitantly with an increase in intensity of the ν(CO) bands of $^1CpMn(CO)_2$.

Photolysis of $CpMn(CO)_3$ in other matrix media yielded similar results, with a shift in the ν(CO) band positions of the observed photoproduct bands consistent with the changing matrix environment. Photolysis in a methylcyclohexane glass yielded only the solvated singlet state, with no observation of $^3CpMn(CO)_2$ reported. As part of this

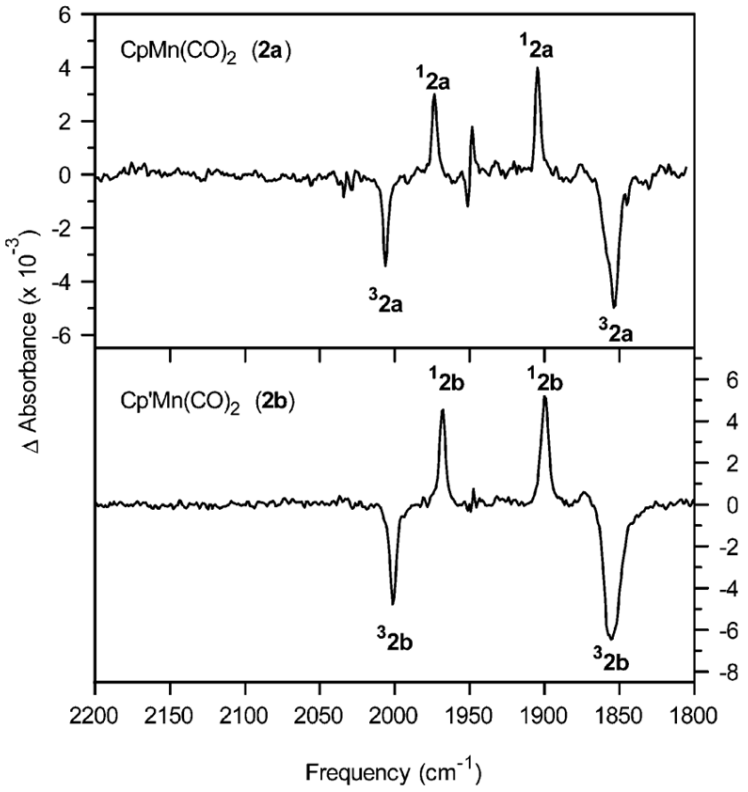


FIGURE 2.8: IR difference spectra recorded following photolysis of $CpMn(CO)_3$ and $(MeCp)Mn(CO)_3$ in Ar matrix at 10 K, showing the 16-electron triplet (^{3}2a and ^{3}2b) and the singlet species (^{1}2a and ^{1}2b). Adapted from ref 53.

study, the authors examined the structures and energies of the various photoproducts as well as the parent complex. Computed structures for singlet dicarbonyl species showed good agreement with previous work,[150] and structures of the parent showed good agreement with experimental values.[188] Discussion of the structure and energy of the triplet state however was more complex and involved. Upon calculation of the geometry of the triplet dicarbonyl species, two minima were found on the potential energy surface, indicating two geometries which are very close in energy. One of these species is planar at manganese, while the other has a bent pyramidal structure, as shown in Figure 2.9. The authors interpret this result as evidence of a flat potential energy surface in the region of these two structures. Examination of the computed IR spectra

for these two structures clearly indicates that the bent structure of $CpMn(CO)_2$ is the most likely candidate, giving the best agreement with observed experimental results. An interesting observation made by the authors is the remarkably large interaction between the two carbonyl ligands of the triplet species, leading to an unusually large calculated difference between the two ν(CO) bands of $^3CpMn(CO)_2$ of *ca.* 150 cm^{-1}.

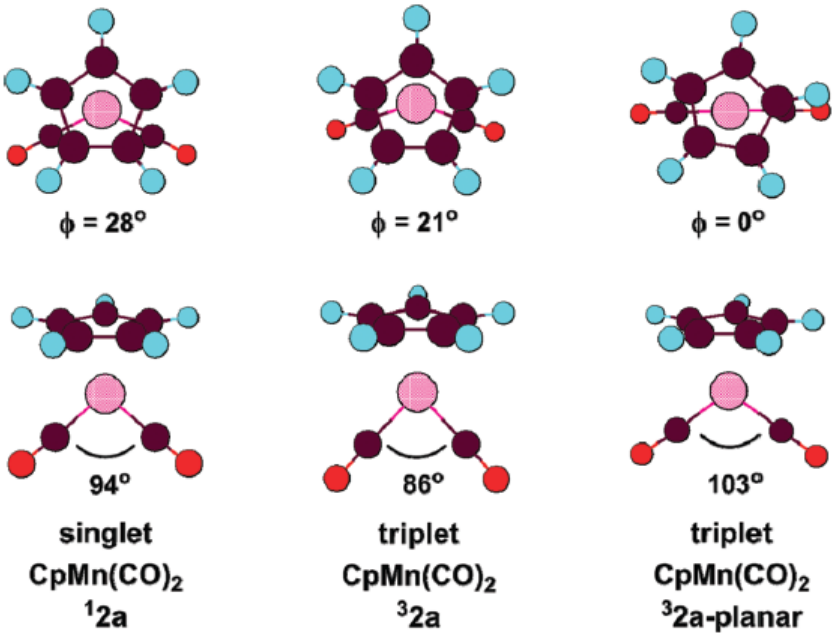


FIGURE 2.9: Computed, none ring-slipped structures considered as candidates for assignment of $CpMn(CO)_2$ (B3LYP/LANL2DZ). ϕ is used here as a measure of 'pyramidality'. Adapted from ref 53.

Calculations of the singlet-triplet energy gap were found to be highly dependent on the computational method used, in accordance with previous results.[189] The authors consider the a η^3 ring-slipped species as a further candidate for the structure of the triplet species, due to good agreement of its computed IR spectrum with experimental results. However, this is deemed unlikely, and the final assignment of the triplet intermediate is the bent pyramidal $^3CpMn(CO)_2$.

2.1.3.2 TRIR Spectroscopic Studies of $CpCo(CO)_2$ and $CpV(CO)_4$

In all of the above studies, the reaction dynamics of the singlet and triplet species have been largely the same, with the unsaturated 16-electron triplet species showing little or no interactions with the solvent, while the singlet species is strongly solvated. The spin-forbidden reaction in these cases appears to be facilitated by the incoming solvent in some way. However, an exception to this rule comes in the case of $CpCo(CO)_2$. Lomont, Nguyen and Harris summarise the photochemistry of this species in their recent review.[190] A short introduction to the behaviour of triplet $^3CpCo(CO)$ will be given here.

Harris and co-workers have shown the ability of the 16-electron triplet form of $^3CpCo(CO)$ to bind to ligands which contain an oxygen lone-pair, e.g., THF and alcohols,[145] as shown in Figure 2.10. In these studies, $CpCo(CO)_2$ was photolysed with UV light, using the ligand of interest as the solvent. Following photolysis, solvated forms of both the singlet and triplet monocarbonyl photoproducts were observed. DFT calculations performed as part of this study confirmed that coordination of the solvent to the unsaturated triplet in this case does indeed yield a favourable interaction. Further DFT studies concluded that in the gas phase the triplet state is highly favoured over the singlet, by 13-26 kcal/mol. This difference is much larger than that calculated for the equivalent energy gap in $Fe(CO)_5$.[144] Because of this increased stability, no singlet alkane complex has ever been reported following photolysis of $CpCo(CO)_2$ in solution.[191] Harris *et al.* note the irony of the exceptional nature of $^3CpCo(CO)$ regarding its ability to coordinate solvent in its triplet state. $^3CpCo(CO)$ was in fact

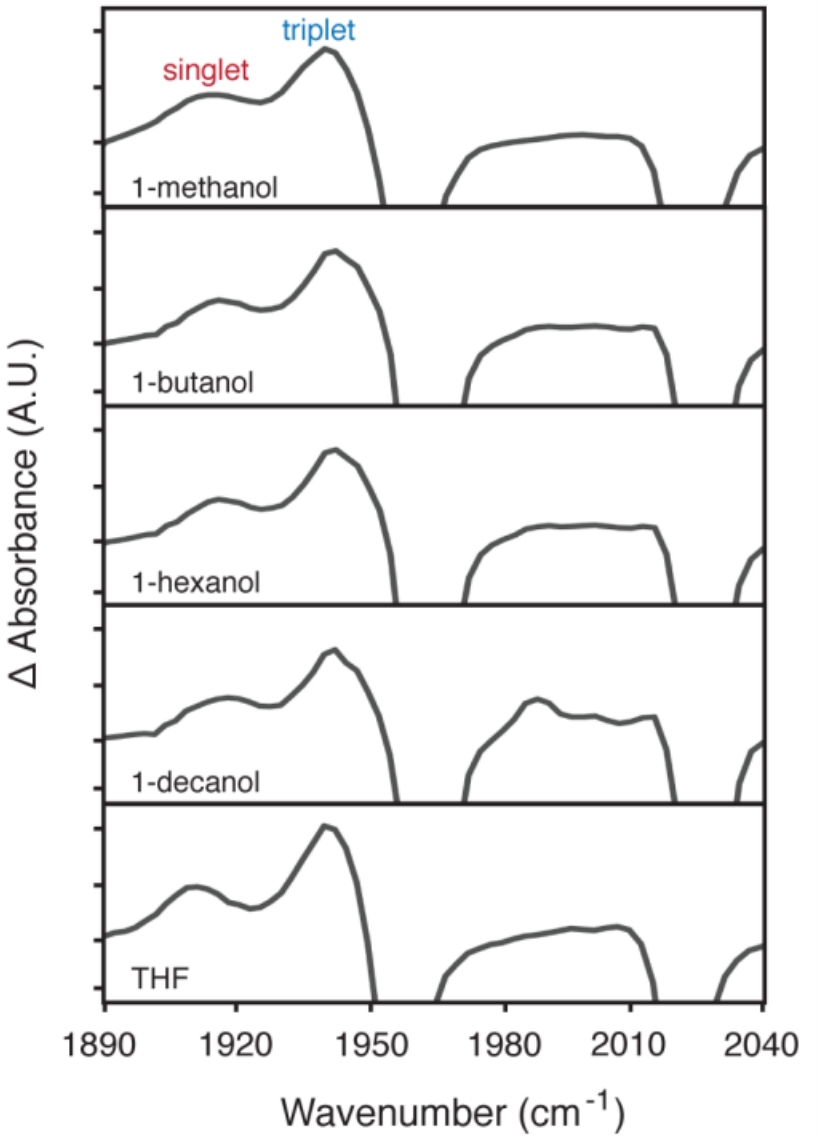


FIGURE 2.10: TRIR difference spectra recorded following photolysis of $CpCo(CO)_2$ in a series of alcohol solvent, as well as THF. ν(CO) bands indicating coordination of the solvent to both $^3CpCo(CO)$ and $^1CpCo(CO)$ can be seen. Adapted from ref 190.

the first unsaturated triplet species which was shown not to coordinate solvents in its triplet ground state. Earlier experiments in liquid noble gases,[142] and cyclohexane[191] showed no evidence of formation of a singlet solvent complex. In both of these cases, the triplet $^3CpCo(CO)$ undergoes reaction with the parent to form $Cp_2Co_2(CO)_3$ (and in the case of the *liq*Kr experiment, $Cp_2Co_2(CO)_2$). The rate of formation of this dimer

species was found to be diffusion limited, and dependent on the concentration of the parent complex.

Harris and group have subsequently studied the photochemistry and reactivity of $CpCo(CO)_2$ in neat alkene and alkyne solutions.[146] It was discovered that the unsaturated species first binds the alkyne or alkene in its triplet state, before undergoing a spin-forbidden reaction on the picosecond timescale (*ca.* 30 ps) to the singlet solvent complex. Both of these complexes were found to be bound in an η^2 fashion, through the π bond of the ligand in question. The authors note that this timescale is similar to that of vibrational cooling of the initial photoproducts, and hypothesise that the initial hot state of these intermediates may aid the spin-change process. Recently, DFT[192] and experimental studies[144] have described the ability of $^3CpCo(CO)$ to activate silane Si-H bonds without having to pass through the silane solvated singlet complex.

The least well studied of the 16-electron intermediates described within this Chapter is $^3CpV(CO)_3$. This intermediate was first proposed following UV irradiation of $CpV(CO)_4$ in low temperature matrices.[54,193] Various photolytic ligand substitution studies have been carried out on $CpV(CO)_4$ in various liquid solvents at room temperature.[194–197] All of these studies have proposed that upon photolysis, $CpV(CO)_4$ loses a carbonyl ligand, which is first replaced by the solvent and subsequently reacts with the ligand of interest to produce $^1CpV(CO)_3X$. None of these studies reported observation of a metastable 16-electron unsaturated species.

Snee *et al.* published the first ultrafast TRIR spectroscopic study of the photolysis of $CpV(CO)_4$ in 1999.[147] In this study, the mechanism of silicon-hydrogen bond activation was examined, in a similar way to previous studies of $CpMn(CO)_3$.[150,186,187]

Photolysis of $CpV(CO)_4$ in *n*-heptane was carried out for subsequent comparison with studies in triethylsilane. Upon UV irradiation, several intermediates were produced. The first of which, exhibiting a single ν(CO) band at 2020 cm^{-1}, which was assigned to the triplet species $^3CpV(CO)_3$. This species was shown to exhibit a decay of *ca.* 15 % of its initial value, concurrent with formation of two new ν(CO) bands at 1990 and 1895 cm^{-1}. These new bands were assigned to the *n*-heptane complex $^1CpV(CO)_3(C_7H_{16})$. Unusually, the triplet species was not observed to fully decay within the timescale of the experiment (660 ps), instead it remains following the formation of the solvated singlet complex.

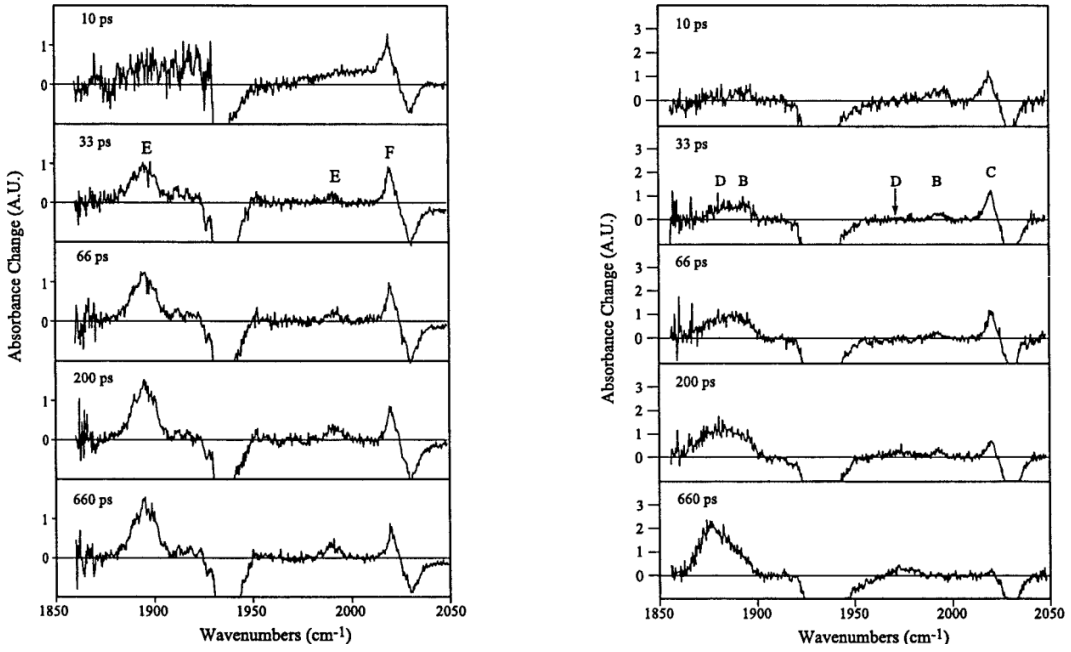


FIGURE 2.11: TRIR difference spectra recorded following photolysis of $CpV(CO)_4$ in *n*-heptane (left) showing formation of $^3CpV(CO)_3$ (F) and $^1CpV(CO)_3(C_7H_{16})$ (E), and triethylsilane (right) showing formation of $^3CpV(CO)_3$ (C) and the silane solvent complex in its ethyl-bound (B) and silyl-bound (D) forms. Adapted from ref 147.

Photolysis of $CpV(CO)_4$ in triethylsilane yielded different results. Formation of the triplet $^3CpV(CO)_3$ was still observed, however in this case it was seen to decay

fully, concurrent with formation of the singlet solvent complex, which is observed in two forms. The first of these was assigned to be bound through an ethyl moiety of triethylsilane, and the second bound though the Si-H bond. A ring-slipped intermediate was initially considered as a candidate for assignment of the ν(CO) band at 2020 cm^{-1}, however due to the fast reaction of this species with solvents in question, as well as the difference in reaction rate between the two solvents, this assignment was deemed unlikely. DFT and MP2 calculations concerning the geometries and energies of these intermediates were also performed as part of this study. A lower energy was predicted for the triplet state of $^3CpV(CO)_3$ than its singlet analogue. A concerted spin-change reaction mechanism is proposed to explain the additional of ligands to $^3CpV(CO)_3$. More recent studies have further bolstered the assignment of these intermediates as $^3CpV(CO)_3$.[118,144]

2.1.4 Aims

The aim of the work presented in this Chapter is to examined to formation of organometallic alkane and noble gas complexes in room temperature solution, particularly complexes of Xe. The main reason for targeting such organometallic Xe complexes is the large change that should be observed in the resulting EXAFS (extended x-ray absorption fine structure) region of the XAFS spectrum upon changing from a metal-carbon bond to metal-xenon bond following photolysis in the presence of xenon. This large change should give us the best chance of observing such weakly coordinated organometallic systems. Previous work has utilised supercritical noble gas solvents to form noble gas complexes at room temperatures, however studies of this nature require

high pressure conditions, necessitating bulky sample cells with small windows which are not conducive to the full range of fast spectroscopic techniques available for potential characterisation of such species.

It was hypothesised that perfluorinated solvents would allow access to a large range of weakly-bound complexes at room temperature and ambient pressure, by doping the ligand of interest into the perfluoroalkane. It was proposed that in addition to binding liquid alkanes this may allow for the observation of organometallic complexes of ligands which are gaseous at room temperature, including the noble gas; xenon, and alkanes; methane and ethane. While examining the photochemistry of a series of model metal carbonyl complexes in perfluoro(methylcyclohexane) solvent with TRIR spectroscopy, it became apparent that this solvent, and others like it, have an effect on the stability of short-lived intermediates. Due to the non-coordinating nature of these solvents, as described by Kelly and Long,[78] they can be utilised to extend the lifetimes of coordinatively unsaturated species. Observation of the long-lived 16-electron complex $^3Fe(CO)_4$ in perfluorinated alkane solution spurred us to investigate this effect further, leading to the studies of various coordinatively unsaturated 16-electron intermediates described in this Chapter. It was hoped that by examining the rates of reaction of these intermediates with the solvent using TRIR, and comparing this rate to that observed following addition of a weakly-binding ligand dopant to the solution, the affinity of the first row transition metals for noble gas and alkane ligands in conventional room temperature solution could be examined. This insight would allow us to develop a methodology for producing these weakly-bound coordination complexes in room temperature solution, allowing future studies of these complexes using more structurally

diagnostic techniques e.g., EXAFS, or nuclear magnetic resonance (NMR) spectroscopy to be carried out more readily.

2.2 Results and Discussion

2.2.1 TRIR of $Fe(CO)_5$ in Perfluoro(methylcyclohexane)

As described above and in the introduction to Chapter 3, a number of organometallic Xe complexes have been previously characterised following irradiation of metal carbonyl complexes in supercritical Xe solution at room temperature, or liquified Xe at cryogenic temperatures. Initially, one of the main aims for the work presented below was to observe organometallic xenon complexes in conventional liquid solution at room temperature, removing the pressure and temperature constraints required for formation and study of such complexes in supercritical or liquid xenon. $Fe(CO)_5$ was initially selected as the transition metal complex for these studies due to the extensive literature describing its photochemistry in a wide range of liquid and supercritical solvents, and solid matrices.[58,89,94,95,99,103,108,124,125,198–201] $Fe(CO)_5$ is a liquid at room temperature and was also found to have high miscibility with the a wide range of solvents discussed in this Chapter. This property allows access to a wide range of solution concentrations, which will be fundamental to developing future TR-XAFS experiments. The photochemistry of $Fe(CO)_5$ in perfluoro(methylcyclohexane) (PFMCH) is described below.

Selected spectra from the picosecond TRIR of $Fe(CO)_5$ in PFMCH following excitation at 266 nm under an Ar atmosphere are shown in Figure 2.12. Upon excitation, the two ν(CO) bands of the parent $Fe(CO)_5$ are depleted. Within 1 ps of excitation, a

new transient is observed with vibrationally hot ν(CO) bands to lower energy compared to those of the parent. These ν(CO) bands narrow and blue-shift over the first 30 ps of the experiment, consistent with cooling of the initially formed transient, to yield two distinct ν(CO) bands at 1996 and 1977 cm^{-1}. By comparison with previous TRIR studies, these bands can be assigned to the coordinatively unsaturated 16-electron triplet species, $^3Fe(CO)_4$.[94,95,103,122,125,202]

A further, weak band is observed around 1935 cm^{-1} and is assigned to the double carbonyl loss product $^3Fe(CO)_3$.[103,108] As mentioned previously, the spin-state of the tetracarbonyl intermediate $^3Fe(CO)_4$ has been confirmed by MCD studies.[97] Although no MCD experiments have been carried out to confirm the spin-state of the tricarbonyl intermediate, *ab initio* and molecular orbital calculations have predicted that $^3Fe(CO)_3$ is a triplet in its ground state.[96,100,122] The formation of this 14-electron tricarbonyl complex is reported to occur through a single photon process, resulting in the loss of two carbonyl ligands from the parent complex upon excitation.[103,124] Recent work by Harris and co-workers has shown that while more strongly coordinating solvents such as alcohols interact directly with the metal centre on a picosecond timescale, alkane solvents do not show any significant interaction.[124] From this, the tricarbonyl complex formed during our experiments is assigned as the bare, coordinatively unsaturated $^3Fe(CO)_3$. It is clear from the TRIR difference spectrum obtained 500 ps following excitation that the ν(CO) bands of both $^3Fe(CO)_4$ and $^3Fe(CO)_3$ transient species are still present on this timescale, while no reformation of the parent complex is observed between 1 and 500 ps. Table 2.1 shows the ν(CO) band positions for all parent, transient and product complexes observed in this study, as well as selected data from

the literature for comparison.

TABLE 2.1: Infrared ν(CO) bands of iron carbonyl species in various liquid and supercritical solvents, as well as in the vapour phase.

Compound	**Solvent**	**ν(CO) (cm^{-1})**	**Reference**
$Fe(CO)_5$	None (vapour)	2032, 2018	108
	n-heptane	2023, 2002	103
	*sc*Xe	2025, 2004	103
	PFMCH	2028, 2006	This work
$^3Fe(CO)_4$	None (vapour)	2000, 1984	103
	n-heptane	1988, 1967	103
	*sc*Xe	1993, 1972	103
	PFMCH	1996, 1977	This work
$^3Fe(CO)_3$	*n*-heptane	1926	103
	*sc*Xe	1931	103
	PFMCH	1935	This work
$^1Fe(CO)_4$(Sol)	*n*-heptane	2083, 1989, 1973, 1953	103
	*sc*Xe	2085, 1990, 1974, 1961	103
	PFMCH	2073, 1976, 1961, 1945	This work
$Fe_2(CO)_8$	None (vapour)	2046, 2016, 1982	108
	n-heptane	2035	103
	*sc*Xe	2043	103
	PFMCH	2034, 2100	This work

Table 2.2 shows a comparison of the ratio of $^3Fe(CO)_3$:$^3Fe(CO)_4$ formed in a series of solvents, estimated by taking the heights of the ν(CO) bands for each complex and assuming similar IR extinction coefficients. This should be considered an approximation of the real ratio, as the real extinction coefficients of these species are likely to differ. This assumption may introduce significant error dependent on the real extinction coefficient values for $^3Fe(CO)_3$ and $^3Fe(CO)_4$. However, it is expected that the extinction coefficients of these species should not change significantly in different solvents, thereby allowing us to draw a useful comparison between various solvents.

From this point of view, an interesting comparison of this ratio in various solvents

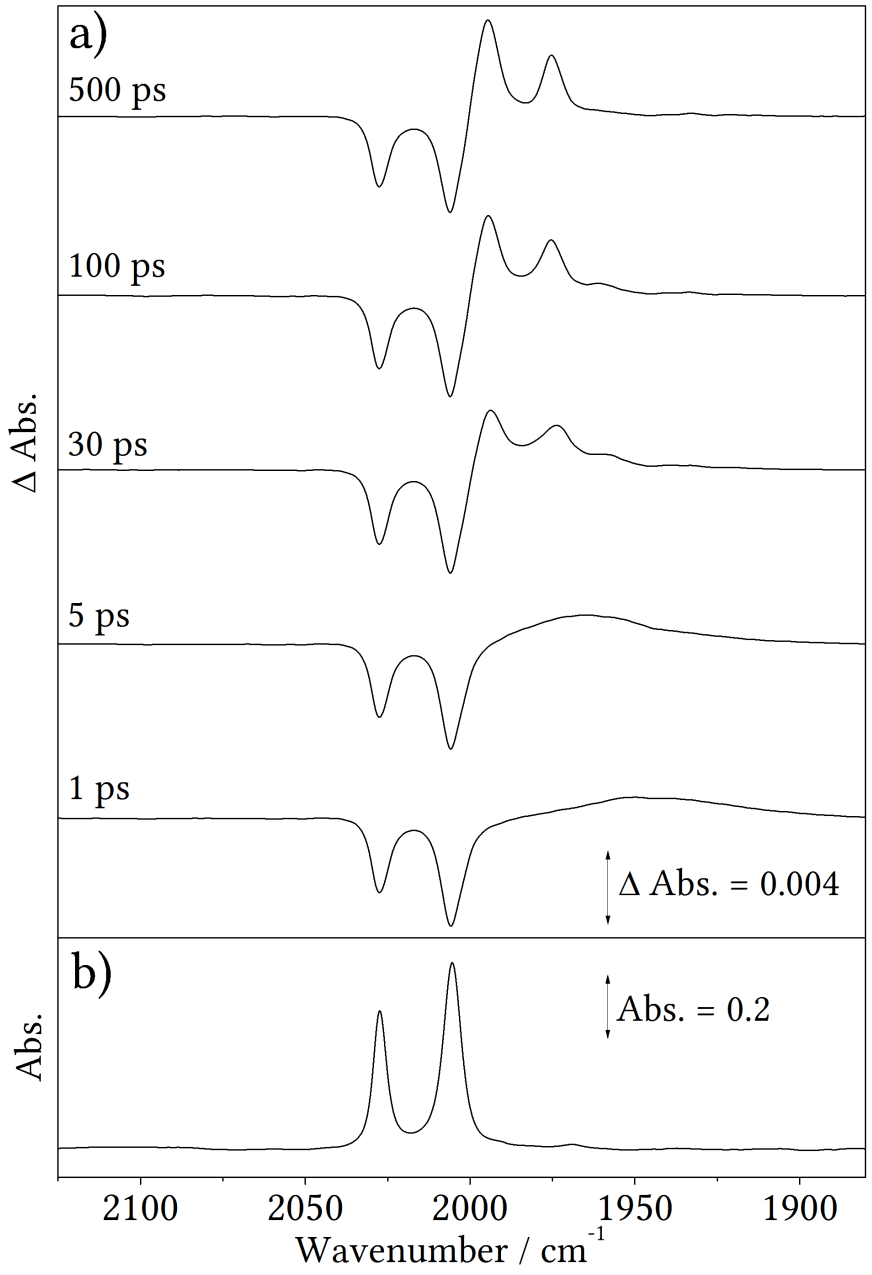


FIGURE 2.12: a) Selected picosecond TRIR spectra obtained at 1, 5, 30, 100 and 500 ps following 266 nm irradiation of $Fe(CO)_5$ in PFMCH under argon, showing the formation of $^3Fe(CO)_4$ in solution. b) FTIR of same solution before photolysis.

can be drawn. From the assumed non-coordinating nature of the PFMCH solvent, this ratio might be expected to lie closer to that observed for *sc*Xe and *sc*Ar solvents than the ratio observed in *n*-heptane, suggesting the perfluoroalkane may have an effect more

TABLE 2.2: Ratio of $^3Fe(CO)_3$:$^3Fe(CO)_4$ observed by TRIR in a series of solvents. The ratio is calculated from the area of the ν(CO) band of $^3Fe(CO)_3$ and the sum of the areas of the two ν(CO) bands of $^3Fe(CO)_4$.

Solvent	**$^3Fe(CO)_3$:$^3Fe(CO)_4$ Ratio**	**Reference**
PFMCH	01:50	This work
n-heptane	01:17	103
*sc*Xe	01:05	103
*sc*Ar	01:03	103

akin to a supercritical noble gas than a conventional alkane solvent. However, only a very small amount of $^3Fe(CO)_3$ is observed in PFMCH solution. While, as stated above, formation of $^3Fe(CO)_3$ in solution is suggested to occur by a single-photon process, a two-photon mechanism has been previously observed, and as such cannot be ruled out.[99] This may explain this unexpected behaviour in the perfluorinated solvent. Furthermore, it has been suggested that the formation of $^3Fe(CO)_3$ may be related to the rate of vibrational relaxation of the tetracarbonyl intermediate, with experiments in *sc*Xe showing a slower relaxation rate than those performed in *n*-heptane;[103] however, no detailed studies of this process have been reported, and further work will be required to fully examine this effect.

Figure 2.13 shows a series of selected difference spectra from nanosecond TRIR experiments following 266 nm photolysis of $Fe(CO)_5$ in PFMCH solvent under an Ar atmosphere. The spectrum recorded 1 ns following excitation clearly shows the presence of the two ν(CO) bands of the triplet $^3Fe(CO)_4$ (1996 and 1977 cm^{-1}) as observed in the picosecond spectra reported in Figure 2.12. The ν(CO) band of the tricarbonyl species $^3Fe(CO)_3$ is still present on this timescale, however only a small amount appears to remain in solution after this time. The two bands of $^3Fe(CO)_4$ decay

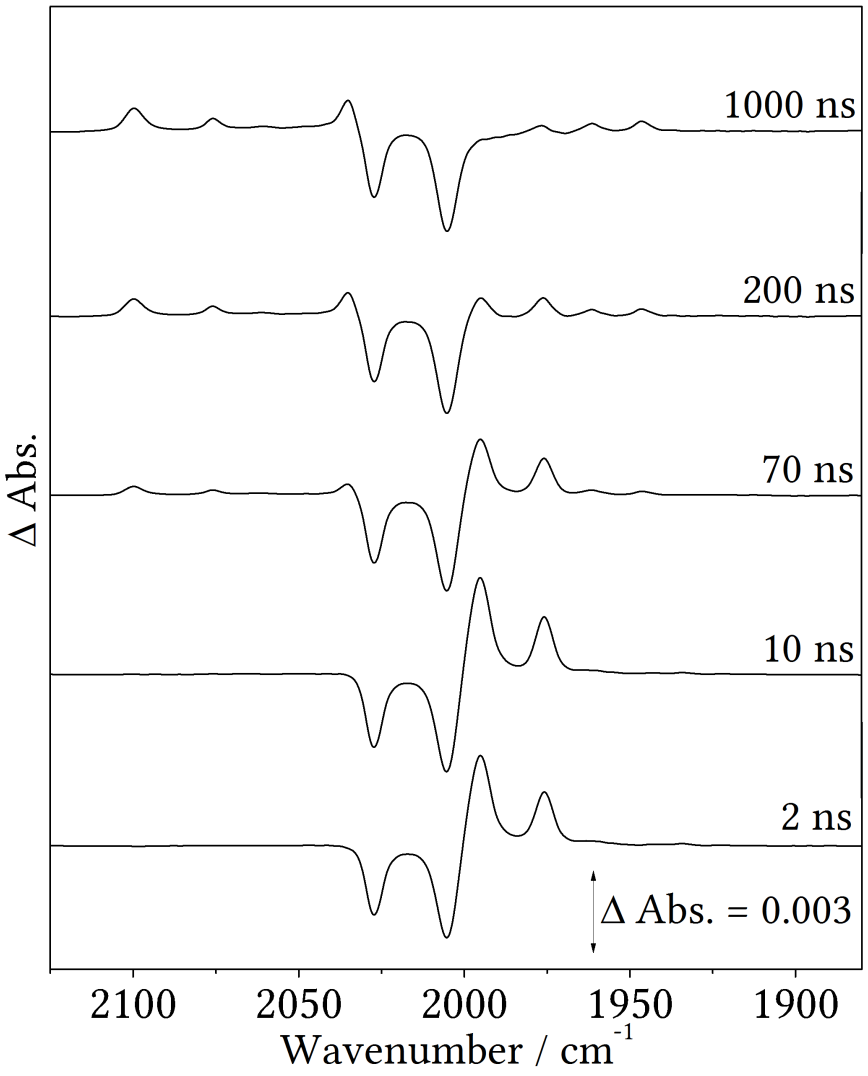


FIGURE 2.13: a) Selected nanosecond TRIR spectra obtained at 2, 10, 70, 200 and 1000 ns following 266 nm irradiation of $Fe(CO)_5$ in PFMCH under argon, showing the decay of $^3Fe(CO)_4$, and formation of $^1Fe(CO)_4(C_7F_{14})$ and $Fe_2(CO)_8$ in solution.

(τ = 140 ($\pm$10) ns) concurrently with the formation of six new ν(CO) bands. Three of these bands lie to lower energy compared to the parent ν(CO) bands (1976, 1961 and 1945 cm^{-1}) are assigned to the singlet solvent complex $^1Fe(CO)_4(C_7F_{14})$ by comparison with previous TRIR studies.[103,125] A fourth band, which grows in at 2073 cm^{-1}, is also assigned to this singlet solvent complex.[95,103,125] The decay of the triplet species $^3Fe(CO)_4$ and the growth of the singlet solvent complex $^1Fe(CO)_4(C_7F_{14})$ occur at the

same rate (k_{obs} = 7.0 (±0.8) x 10^6 s^{-1}), shown in Figure 2.14, suggesting formation of $^1Fe(CO)_4(C_7F_{14})$ directly from $^3Fe(CO)_4$. A summary of observed rate constants for the processes observed following photolysis of $Fe(CO)_5$ in PFMCH is presented in Table 2.3.

TABLE 2.3: Observed rate constants for the processes observed following photolysis of $Fe(CO)_5$ in perfluoro(methylcyclohexane) solution at 298 K.

ν(CO) (cm^{-1})	**Assignment**	**k_{obs} (s^{-1})**
1996	$^3Fe(CO)_4$	7.1 (±0.7) x 10^6
1977	$^3Fe(CO)_4$	7.0 (±0.7) x 10^6
2073	$^1Fe(CO)_4(C_7F_{14})$	6.9 (±0.6) x 10^6
1976	$^1Fe(CO)_4(C_7F_{14})$	6.9 (±0.7) x 10^6
1961	$^1Fe(CO)_4(C_7F_{14})$	7.0 (±0.8) x 10^6
1945	$^1Fe(CO)_4(C_7F_{14})$	7.0 (±0.7) x 10^6
1935	$^3Fe(CO)_3$	1.2 (±0.3) x 10^7
2100	$Fe_2(CO)_8$	8.3 (±0.8) x 10^6
2034	$Fe_2(CO)_8$	8.2 (±0.7) x 10^6

The fifth and sixth new ν(CO) bands at 2034 and 2100 cm^{-1}, respectively, grow in on a nanosecond timescale. These bands are assigned to the iron carbonyl dimer species $Fe_2(CO)_8$. The lower energy band assigned to this complex has been previously reported in both supercritical and liquid solvents, as well as matrix isolation studies, however the higher energy band at 2100 cm^{-1} has not been previously observed.[101–103,123] Previous matrix isolation studies have reported observation of ν(CO) bands for both the bridged and unbridged isomers of $Fe_2(CO)_8$ at *ca.* 2040 cm^{-1},[101,102] raising the possibility of the formation of both of these isomers following photolysis of $Fe(CO)_5$ in PFMCH.

The rate of growth of the ν(CO) band at 2100 cm^{-1} (τ = 122 (±5) ns) is within error of the rate of growth of the lower energy band at 2034 cm^{-1} (τ = 120 (±4) ns) suggesting that these two bands are due to the same species. It is possible that

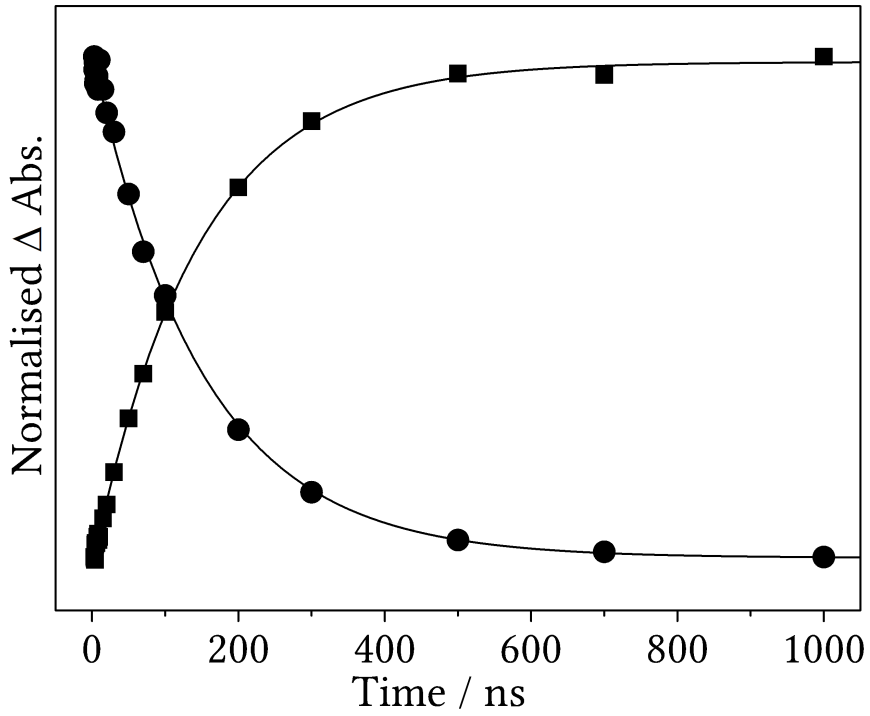


FIGURE 2.14: Normalised, single-point kinetic traces from TRIR spectra obtained following 266 nm photolysis of $Fe(CO)_5$ in PFMCH under Ar. Decay of $^3Fe(CO)_4$ at 1996 cm^{-1} (circles) and growth of $^1Fe(CO)_4(C_7F_{14})$ at 1946 cm^{-1}(squares) are shown. Solid lines are mono-exponential fits.

formation of this octacarbonyl dimer species is also a decay pathway for the small concentration of the tricarbonyl $^3Fe(CO)_3$ produced during these experiments.[108]

The decay of $^3Fe(CO)_3$, shown in Figure 2.16, occurs at a similar rate to the growth of $Fe_2(CO)_8$ (k_{obs} = 1.2 (±0.3) x 10^7 s^{-1} and 8.3 (±0.8) x 10^6 s^{-1}, respectively), but they are not identical. These two processes occur on a similar timescale, and a reaction between $^3Fe(CO)_3$ and the parent $Fe(CO)_5$ would exhibit pseudo first-order kinetics, which is expected from the observed growth of the ν(CO) bands of $Fe_2(CO)_8$ shown in Figure 2.15. However, the quality of the kinetic data obtained from the TRIR spectra presented above is not sufficient to definitively unravel the role of pseudo first- and second-order processes which may be occurring on this timescale, leading to the

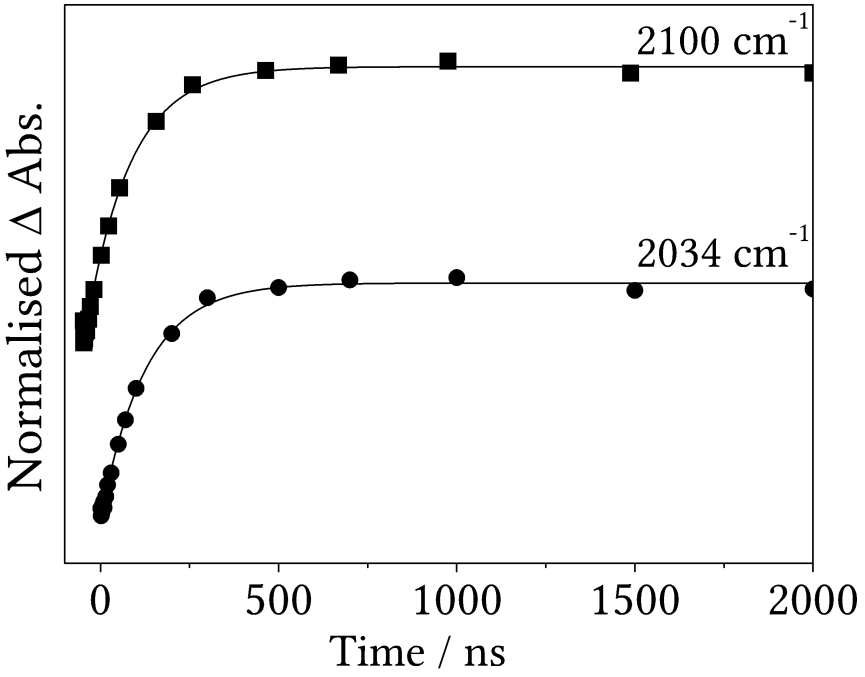


FIGURE 2.15: Normalised, single-point kinetic traces from TRIR spectra recorded following photolysis of $Fe(CO)_5$ in PFMCH under Ar, showing matching rates of growth for the ν(CO) bands at 2100 and 2034 cm^{-1}. These bands are assigned to the dimer $Fe_2(CO)_8$.

formation of $Fe_2(CO)_8$. It is possible that dimerisation of $^3Fe(CO)_4$ to form $Fe_2(CO)_8$ is a competing pathway. If this were the case, formation of the dimer would be expected to be to be a second-order kinetic process, highly dependent on the concentration of $^3Fe(CO)_4$. The two proposed pathways for formation of this $Fe_2(CO)_8$ dimer are shown in Scheme 2.4.

$$^3Fe(CO)_3 + Fe(CO)_5 \longrightarrow Fe_2(CO)_8 \quad (2.1)$$

$$^3Fe(CO)_4 + {}^3Fe(CO)_4 \longrightarrow Fe_2(CO)_8 \quad (2.2)$$

SCHEME 2.4: Proposed reaction pathways for the formation of $Fe_2(CO)_8$ following 266 nm photolysis of $Fe(CO)_5$ in PFMCH solution under Ar.

Further studies are required to fully elucidate the kinetics of these processes,

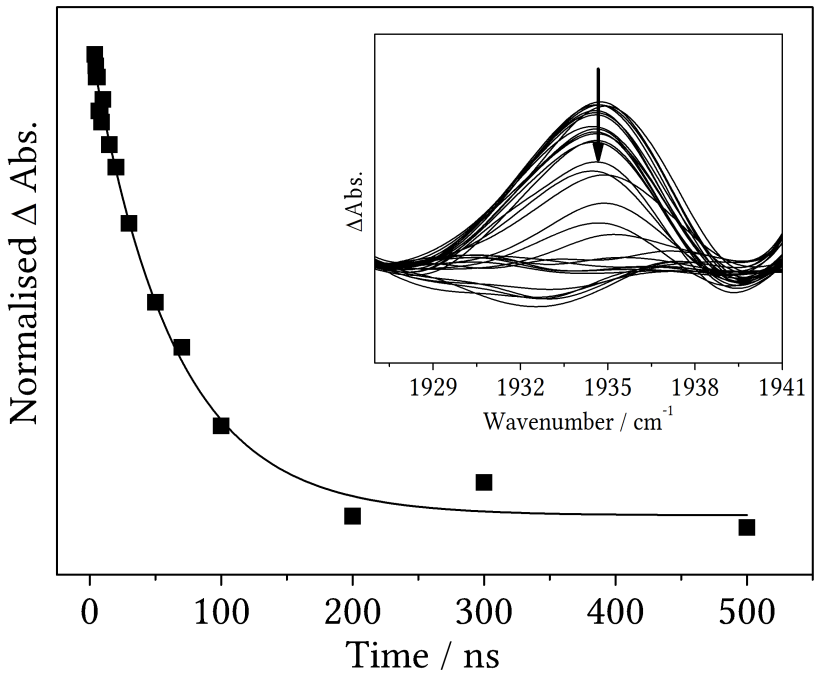


FIGURE 2.16: Normalised, single-point kinetic trace from TRIR spectra recorded following photolysis of $Fe(CO)_5$ in PFMCH under Ar, showing decay for the ν(CO) bands 1935 cm^{-1}, assigned to $^3Fe(CO)_3$. Inset: Series of TRIR difference spectra showing the decay of the ν(CO) band of $^3Fe(CO)_3$ at 1935 cm^{-1} on the nanosecond timescale.

but under these conditions it appears that the dominant process for the formation of $Fe_2(CO)_8$ is a reaction between $^3Fe(CO)_3$ and the parent $Fe(CO)_5$. Previous solution phase studies have also reported the formation of small amounts of $Fe_2(CO)_9$.[103,108] No ν(CO) bands corresponding to this nonacarbonyl dimer are observed following photolysis in PFMCH. Formation of this dimer species has only previously been observed in experiments performed under a pressure of CO, and the CO molecule may have a role in the reaction required to form $Fe_2(CO)_9$ from $^3Fe(CO)_4$ and other intermediates.[108] The experiments described in this Chapter are all performed under an Ar atmosphere, reducing the likelihood the possibility of a reaction involving CO.

It is interesting to note the low intensity of the observed ν(CO) bands of the

solvent complex, compared with those of the observed dimer complex, $Fe_2(CO)_8$. As stated above, previous experiments performed in *sc*Ar[103] and *sc*Kr[202] solvent showed no evidence of the formation of a singlet solvent complex, $^1Fe(CO)_4(Sol)$ (Sol = solvent), due to the very weakly interacting nature of the noble gas solvents. The low concentration of $^1Fe(CO)_4(C_7F_{14})$ produced following photolysis in PFMCH suggests a weak interaction between metal and solvent, possibly leading to increased formation of the dimer from $^3Fe(CO)_4$ when compared with similar experiments in *n*-heptane, though a change in extinction coefficient may play a role in this observed effect.

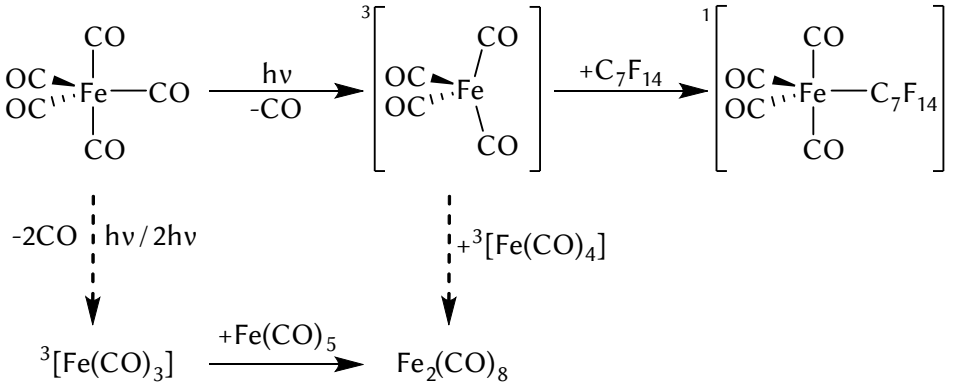
TABLE 2.4: Lifetimes (in ns) for the spin-forbidden reaction of $^3Fe(CO)_4$ to form $^1Fe(CO)_4(Sol)$ following photolysis of $Fe(CO)_5$ in a series of supercritical and liquid solvents (all data recorded at 298 K).

Solvent	**τ (ns)**	**Reference**
PFMCH	140 (±10)	This work
*sc*Ar	N/A	103
*sc*Kr	N/A	198
*sc*Xe	60 (±7)	103
scCH_4	200 (±50)	103
n-heptane	13.1 (±0.2)	103
c-pentane	12.0 (±1.6)	198
CH_2Cl_2	3.8 (±0.6)	198
CH_3OH	0.05 (±0.01)	198

Table 2.4 shows a comparison of lifetimes for the decay of $^3Fe(CO)_4$ and the formation of $^1Fe(CO)_4(Sol)$ in various supercritical and liquid solvents. This reaction with the solvent is much slower in PFMCH than in other weakly coordinating solvents such as *n*-heptane and xenon. The rate of decay of the triplet $^3Fe(CO)_4$ in PFMCH solvent is faster than that reported in *sc*Ar. However unlike PFMCH, *sc*Ar does not appear to interact with the metal centre to form a singlet complex, as no new ν(CO) bands were observed to form concurrently with decay of the triplet bands.[103] The slow

rate for this process observed in PFMCH suggests a very weak interaction between the solvent and the metal centre compared with other liquid solvents, and is the slowest reported for this process in a conventional room temperature liquid solution.

The weak interaction between Fe and PFMCH may also explain the relatively large amount of $Fe_2(CO)_8$, and small amount of $^1Fe(CO)_4(C_7F_{14})$ formed during the experiment. Scheme 2.5 shows the proposed photochemical reaction which takes place following 266 nm photolysis of $Fe(CO)_5$ in PFMCH.



SCHEME 2.5: Proposed reaction pathways following irradiation of $Fe(CO)_5$ in PFMCH solvent, showing initial formation of the triplet intermediates $^3Fe(CO)_3$ and $^3Fe(CO)_4$, leading to formation of the solvent complex $^1Fe(CO)_4(C_7F_{14})$, and the dimer $Fe_2(CO)_8$. Dashed arrows show minor pathways.

2.2.2 Picosecond TRIR of $CpMn(CO)_3$ in *n*-heptane

Given the dramatic effect of perfluorinated solvents on the rate of triplet to singlet interconversion shown in the above experiments, this study was extended to examine the photochemistry of $CpMn(CO)_3$ (Cp = η^5-cyclopentadienyl) in several perfluorinated solvents.

Harris and co-workers identified the short-lived coordinatively unsaturated triplet intermediate $^{3}CpMn(CO)_2$ during ps-TRIR experiments on $CpMn(CO)_3$ performed in *n*-heptane and triethylsilane solvents. This triplet intermediate was shown to decay to form the singlet solvent complex $^{1}CpMn(CO)_2(Sol)$ (Sol = solvent).[118] Before examining the effect of perfluorinated solvents on this spin-state interconversion, the experiment reported by Harris and co-workers in an alkane solvent was repeated.

Several TRIR difference spectra recorded on the picosecond timescale following excitation at 266 nm of $CpMn(CO)_3$ in *n*-heptane under an Ar atmosphere are shown in Figure 2.17. 1 ps following excitation the two ν(CO) bands of the parent molecule are clearly depleted, and two new broad ν(CO) bands appear, centred at 2000 and 1846 cm^{-1}. These new ν(CO) bands sharpen and blue-shift over the first 5 ps following excitation, yielding final band positions of 2004 and 1849 cm^{-1}, consistent with vibrational cooling of the CO ligands.[203–205] From the work of Harris and co-workers, these bands are assigned as being due to the coordinatively unsaturated triplet complex $^{3}CpMn(CO)_2$.[118] A summary of ν(CO) band positions for all Mn complexes is given in Table 2.5.

The previous studies reported in triethylsilane have also observed a further ν(CO) band at approximately 1883 cm^{-1}, with no data recorded below 1860 cm^{-1}.[150] The authors attribute this additional band to a short-lived triplet species. No evidence of this band was observed in our experiments. Our assignment of the unsaturated triplet complex $^{3}CpMn(CO)_2$ is also supported by low temperature matrix isolation studies of $CpMn(CO)_3$ and derivatives.[53] The authors of this study also suggest an explanation for the unusually large $\Delta\nu$ between the two observed carbonyl stretching modes of the triplet species. Natural bond order population analyses showed an orbital symmetry

TABLE 2.5: ν(CO) absorption band frequencies of $CpMn(CO)_3$ and intermediates produced following photolysis of $CpMn(CO)_3$, recorded in various pure solvents at 298 K and an Ar matrix at 10 K.

Compound	**Solvent/Matrix**	**ν(CO) (cm^{-1})**	**Reference**
$CpMn(CO)_3$	*n*-heptane	2028, 1946	This work
	c-pentane	2027, 1946	This work
	PFMCH	2033, 1952	This work
	PFH	2033, 1956	This work
	PFTEA	2034, 1954	This work
	Triethylsilane	2028, 1947	118
	Ar matrix	2032, 1948	53
$^3CpMn(CO)_2$	*n*-heptane	2004, 1849	This work
	c-pentane	2000, 1844	This work
	PFMCH	2008, 1850	This work
	PFH	2006, 1860	This work
	PFTEA	2006, 1855	This work
	Triethylsilane	2002, 1883	118
	Ar matrix	2006, 1853	53
$^1CpMn(CO)_2$(Sol)	*n*-heptane	1960, 1897	This work
	c-pentane	1959, 1891	This work
	PFMCH	1965, 1898	This work
	PFH	1968, 1903	This work
	PFTEA	1965, 1899	This work
	Triethylsilane	1960, 1892	118
	Ar matrix	1973, 1904	53

favourable for interaction between the highest energy singly occupied orbital of the triplet and the antibonding orbitals of the carbonyl ligands. This stabilisation energy was observed to be much greater than that seen in the singlet species, reflecting the comparatively strong interaction between the two carbonyl ligands of the unsaturated triplet.

The two ν(CO) bands of $^3CpMn(CO)_2$ decay concomitantly with the formation of two new bands at 1960 and 1897 cm^{-1}, which are assigned to the dicarbonyl solvent complex $^1CpMn(CO)_2(C_7H_{16})$.

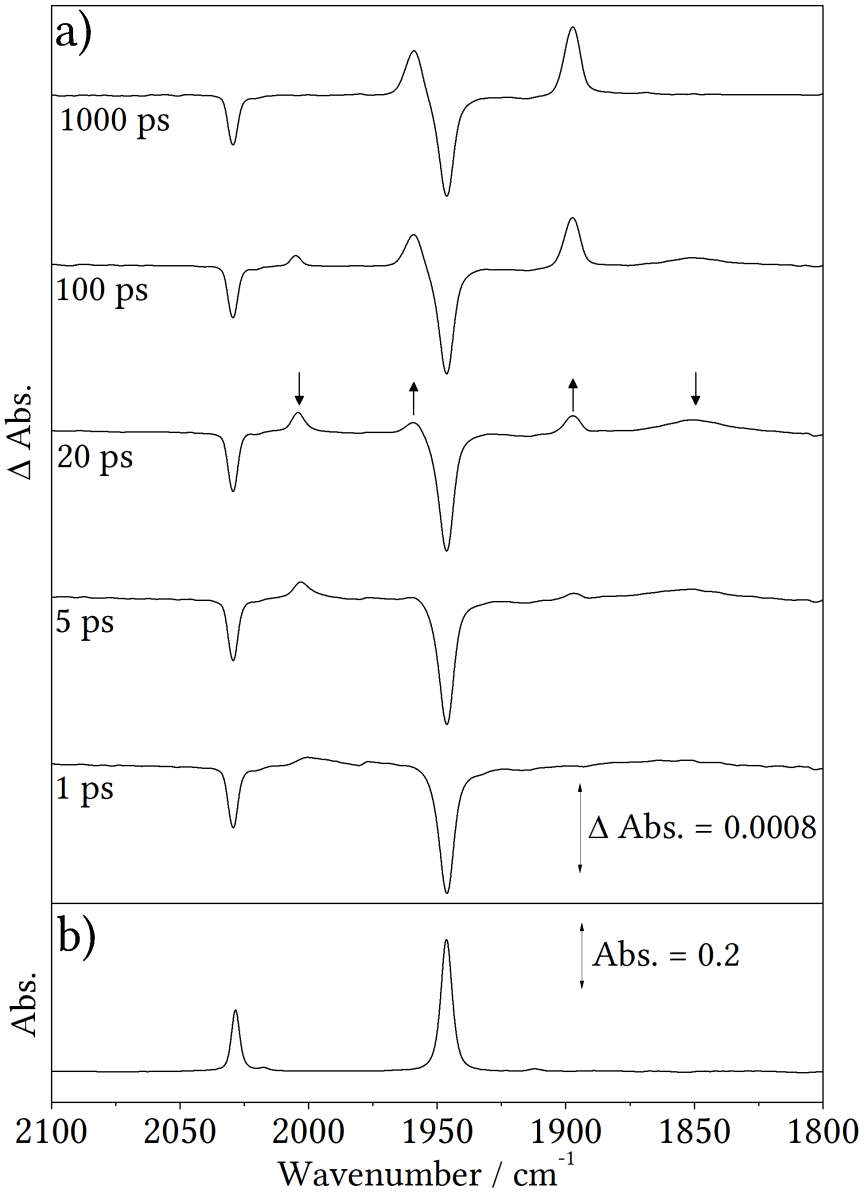


FIGURE 2.17: a) Selected picosecond TRIR difference spectra recorded at a series of time delays following 266 nm photolysis of a solution of $CpMn(CO)_3$ in *n*-heptane. Decay of the ν(CO) bands of $^3CpMn(CO)_2$ and growth of those corresponding to $^1CpMn(CO)_2(C_7H_{16})$ can be clearly seen. b) FTIR spectrum of the same solution.

Observed rate constants for the processes observed following the photolysis of $CpMn(CO)_3$ in *n*-heptane are shown in Table 2.6. The rates of the decay of $^3CpMn(CO)_2$ (τ = 0.11 ($\pm$0.02) ns) and formation of $^1CpMn(CO)_2(C_7H_{16})$ (τ = 0.10 ($\pm$0.01) ns) are consistent with direct formation of $^1CpMn(CO)_2(C_7H_{16})$ directly from

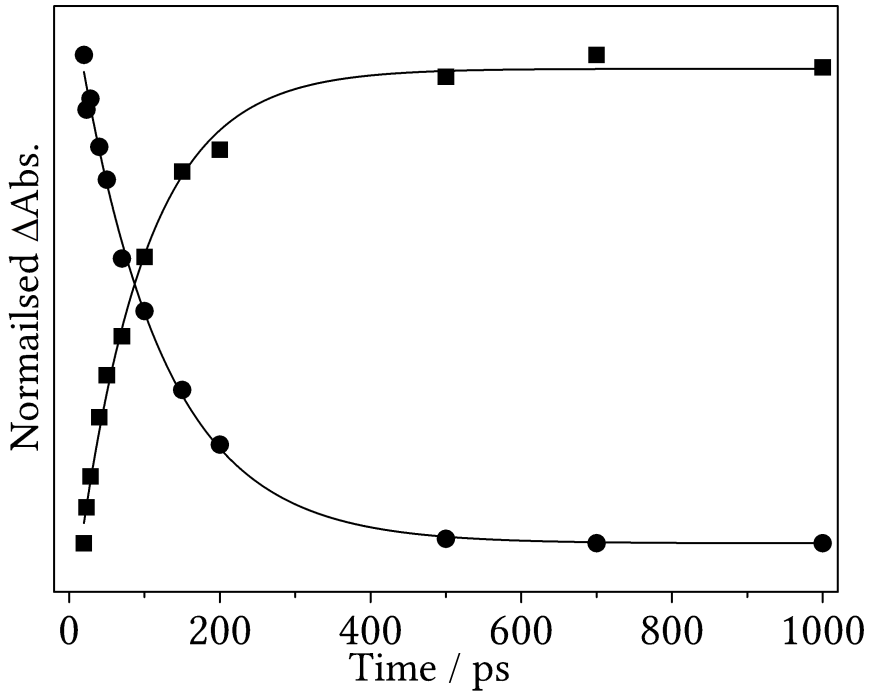


FIGURE 2.18: Kinetic traces from TRIR spectra recorded following 266 nm irradiation of $CpMn(CO)_3$ in *n*-heptane solution. Showing matching rates for the decay of $^3CpMn(CO)_2$ at 2004 cm^{-1} (circles) and growth of $^1CpMn(CO)_2(C_7H_{16})$ at 1897 cm^{-1} (squares). Solid lines are mono-exponential fits.

TABLE 2.6: Observed rate constants for the processes observed following 266 nm photolysis of $CpMn(CO)_3$ in *n*-heptane solution at 298 K.

ν**(CO) (cm^{-1})**	**Assignment**	k_{obs} **(s^{-1})**
2004	$^3CpMn(CO)_2$	9.1 ($\pm$0.5) x 10^9
1849	$^3CpMn(CO)_2$	8.9 ($\pm$0.4) x 10^9
1960	$^1CpMn(CO)_2(C_7H_{16})$	9.0 ($\pm$0.4) x 10^9
1897	$^1CpMn(CO)_2(C_7H_{16})$	9.1 ($\pm$0.3) x 10^9

$^3CpMn(CO)_2$. Kinetic traces for these processes are shown in Figure 2.18, and lifetimes in all solvents are summarised in Table 2.7. The spectrum recorded 1000 ps after excitation shows only the bands of $^1CpMn(CO)_2(C_7H_{16})$, which do not decay on the timescale of this experiment.

For comparison with results obtained for photolysis of $CpMn(CO)_3$ in pure

TABLE 2.7: Lifetimes (in ns) for the spin-forbidden reaction of $^3CpMn(CO)_2$ to form $^1CpMn(CO)_2(Sol)$ following photolysis of $CpMn(CO)_3$ in a series of pure liquid solvents (all data recorded at 298 K).

Solvent	**Lifetime τ (ns)**	**Reference**
n-heptane	0.11 (±0.02)	This work
c-pentane	0.09 (±0.01)	This work
PFMCH	18 (±2)	This work
PFH	90 (±30)	This work
PFTEA	36 (±4)	This work
Triethylsilane	0.105	118

n-heptane presented above, as well as those in the mixed solvent system PFMCH:*c*-pentane presented later in this Chapter, photolysis of $CpMn(CO)_3$ was also examined in pure *c*-pentane. The results obtained for this experiment were similar to those described above following photolysis in *n*-heptane. 1 ps after photolysis, the two parent ν(CO) bands of $CpMn(CO)_3$ (2027 and 1946 cm^{-1}) were bleached, and two new, broad ν(CO) bands were present. These bands were observed to sharpen and blue-shift on a picosecond timescale to yield absorbance bands at 2000 and 1844 cm^{-1}, assigned to the 16-electron triplet species $^3CpMn(CO)_2$, as expected from TRIR studies of $CpMn(CO)_3$ in *n*-heptane reported above. This vibrational cooling process occurs over the first 5 ps following photolysis, matching the rate of the cooling process observed in *n*-heptane. These bands appear to approximately 4 cm^{-1} lower in energy than those observed for the same 16-electron species following photolysis in *n*-heptane. It is possible that this change is simply due to the difference in solvent environment between the two alkanes, however this change in band position is larger than the change in energy for the parent $CpMn(CO)_3$ ν(CO) bands.

As above in *n*-heptane, the 16-electron triplet species decays concomitantly with

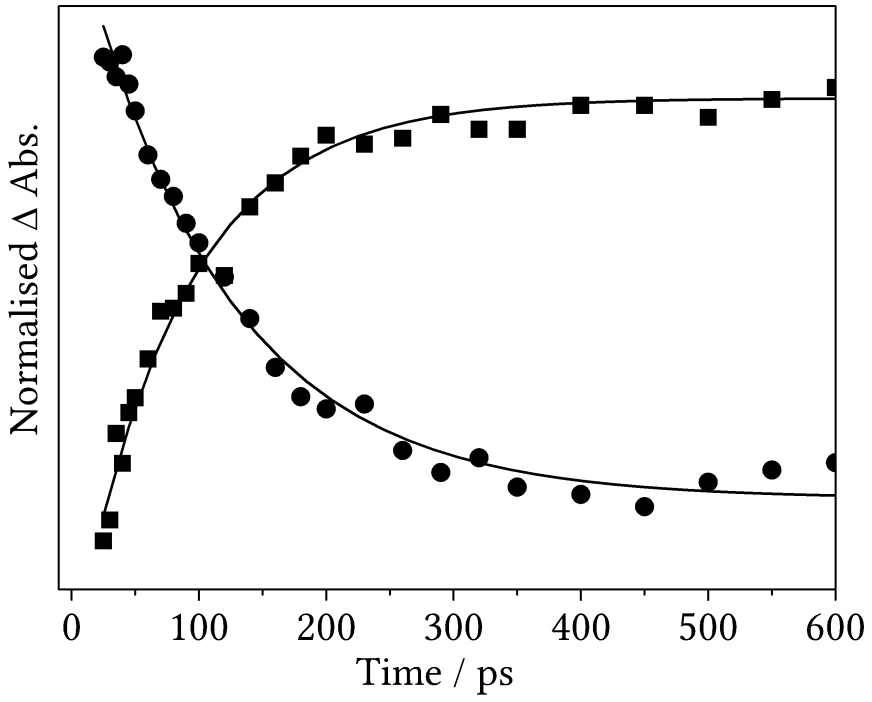


FIGURE 2.19: Kinetic traces from TRIR spectra recorded following 266 nm irradiation of $CpMn(CO)_3$ in *c*-pentane solution, showing matching rates for the decay of $^3CpMn(CO)_2$ at 2000 cm^{-1} (circles) and growth of $^1CpMn(CO)_2(C_5H_{10})$ at 1891 cm^{-1} (squares). Solid lines are mono-exponential fits.

the growth of two new ν(CO) bands at 1959 and 1891 cm^{-1}, which are assigned to the solvent complex $^1CpMn(CO)_2(C_5H_{10})$. Once again, these bands appear at lower energy compared to those of the corresponding *n*-heptane complex, suggesting a possible difference in interaction between these two solvents and the metal centre. However, the decay of $^3CpMn(CO)_2$ and formation of $^1CpMn(CO)_2(C_5H_{10})$ in this case (τ = 0.09 ($\pm$0.01) ns) is only slightly faster than that observed in *n*-heptane, suggesting a similar interaction between the solvent ligand and metal centre for these two alkanes. It is possible that these changes in band positions are simply a result of the differing solvent environment, however other factors may be at play (e.g., sterics), which may change the strength of the interaction between solvent and metal, or the geometry of the resulting organometallic alkane complex. Observed rate constants for processes

involved in the spin-forbidden reaction following 266 nm photolysis of $CpMn(CO)_3$ in cyclopentane solution are shown in Table 2.8.

TABLE 2.8: Observed rate constants for the processes observed following 266 nm photolysis of $CpMn(CO)_3$ in *c*-pentane solution at 298 K.

ν(CO) (cm^{-1})	Assignment	k_{obs} (s^{-1})
2004	$^3CpMn(CO)_2$	1.1 (±0.1) x 10^{10}
1849	$^3CpMn(CO)_2$	1.1 (±0.1) x 10^{10}
1959	$^1CpMn(CO)_2(C_5H_{10})$	1.0 (±0.1) x 10^{10}
1891	$^1CpMn(CO)_2(C_5H_{10})$	1.1 (±0.2) x 10^{10}

It has previously been shown that cyclic alkanes give rise to more stable organometallic alkane complexes than linear alkanes.[48,206,207] The results reported above appear to agree with this trend, with the cyclic solvent cyclopentane exhibiting a slightly faster reaction rate and band positions suggesting greater donation of electron density from solvent to metal than experiments performed in *n*-heptane. It is also possible that the changing viscosity of the solvent plays a role in changing the rate of this spin-forbidden reaction by altering the rate of diffusion.

2.2.3 Picosecond and Nanosecond TRIR of $CpMn(CO)_3$ in Perfluoro(methylcyclohexane)

Following on from the experiments in pure alkane solvents described above, the photochemistry of $CpMn(CO)_3$ in perfluoro(methylcyclohexane) was investigated. Figure 2.20 shows a series of TRIR difference spectra recorded following 266 nm excitation of $CpMn(CO)_3$ in PFMCH, under an Ar atmosphere.

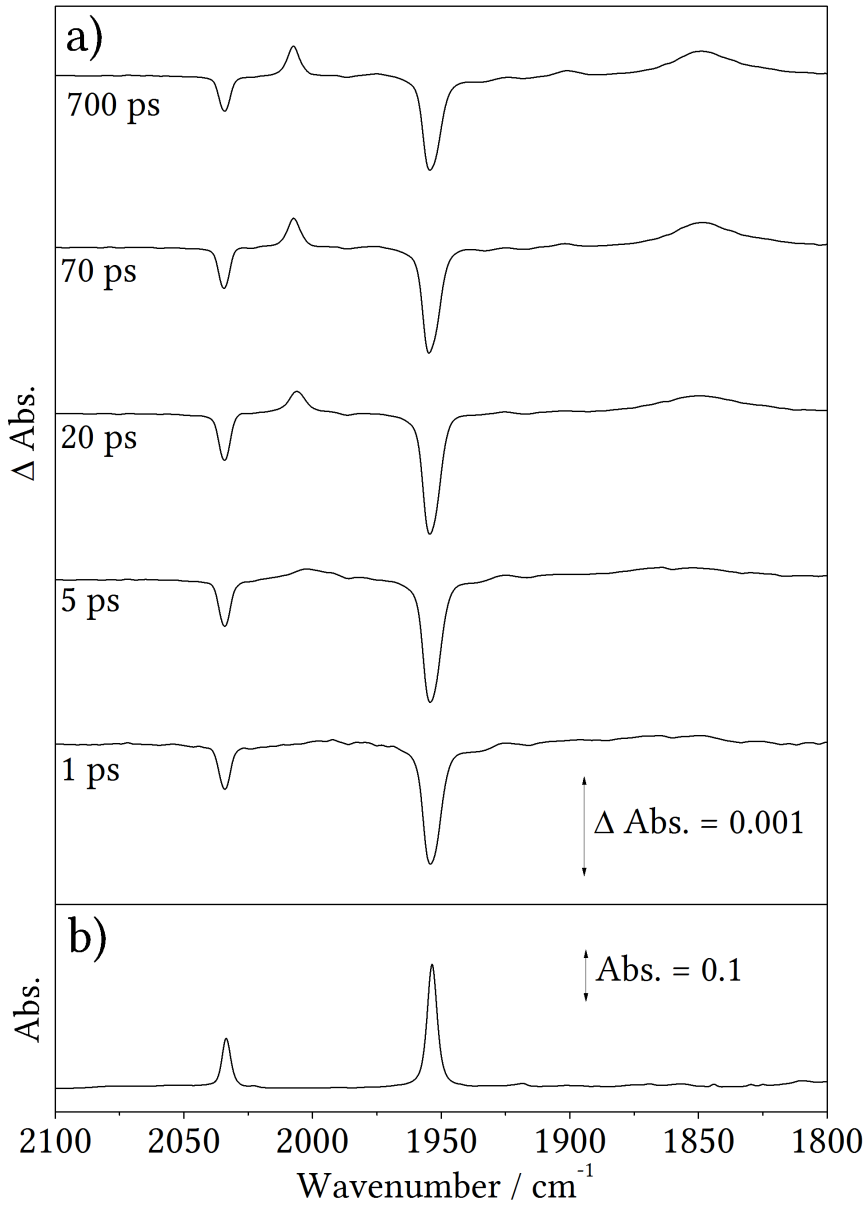


FIGURE 2.20: a) Selected picosecond TRIR difference spectra recorded at a series of time delays following 266 nm photolysis of a solution of $CpMn(CO)_3$ in PFMCH. Depletion of the ν(CO) bands of the parent molecule, and subsequent growth and cooling of the ν(CO) bands of $^3CpMn(CO)_2$ can be seen. b) FTIR spectrum of the same solution.

The two ν(CO) bands corresponding to the parent complex (2034 and 1954 cm^{-1}) are depleted within 1 ps of photolysis, yielding two new, broad ν(CO) bands. These bands appear vibrationally hot, and cool over *ca.* 30 ps to yield band positions of 2007

and 1848 cm^{-1}, again showing a large $\Delta\nu$ as observed following photolysis in *n*-heptane. This cooling process is much slower than that observed for the corresponding ν(CO) bands in *n*-heptane. From previous TRIR experiments, these two ν(CO) bands can be assigned to the unsaturated 16-electron triplet species, $^3CpMn(CO)_2$, as above.[53,118] Interestingly, the triplet complex is stable after 700 ps in PFMCH, much longer than experiments performed in *n*-heptane solvent. This effect appears shows agreement with observations made following photolysis of $Fe(CO)_5$ in perfluoro(methylcyclohexane), in which the lifetime of the unsaturated intermediate $^3Fe(CO)_4$ was extended greatly compared photolysis experiments in alkane solvent.

The ν(CO) absorbance bands of both the parent complex and the unsaturated triplet intermediate all appear at higher energy in PFMCH solution relative to the corresponding bands observed in *n*-heptane solution. This shift is consistent with a weaker, less stabilising interaction between the solvent and the highly polar carbonyl ligands due to the low polarity of the perfluoroalkane compared to the alkane.[208]

Following the observation of a long-lived, coordinatively unsaturated intermediate during picosecond TRIR studies, a nanosecond TRIR study was carried out in an attempt to determine whether $^3CpMn(CO)_2$ decays to form a solvent complex in PFMCH and to examine the lifetime of this and any other processes occurring following excitation. Figure 2.21 shows selected TRIR difference spectra recorded at a series of nanosecond time delays following 266 nm photolysis of $CpMn(CO)_3$ in PFMCH under an Ar atmosphere.

The two ν(CO) bands of $^3CpMn(CO)_2$, as assigned above, can be seen clearly

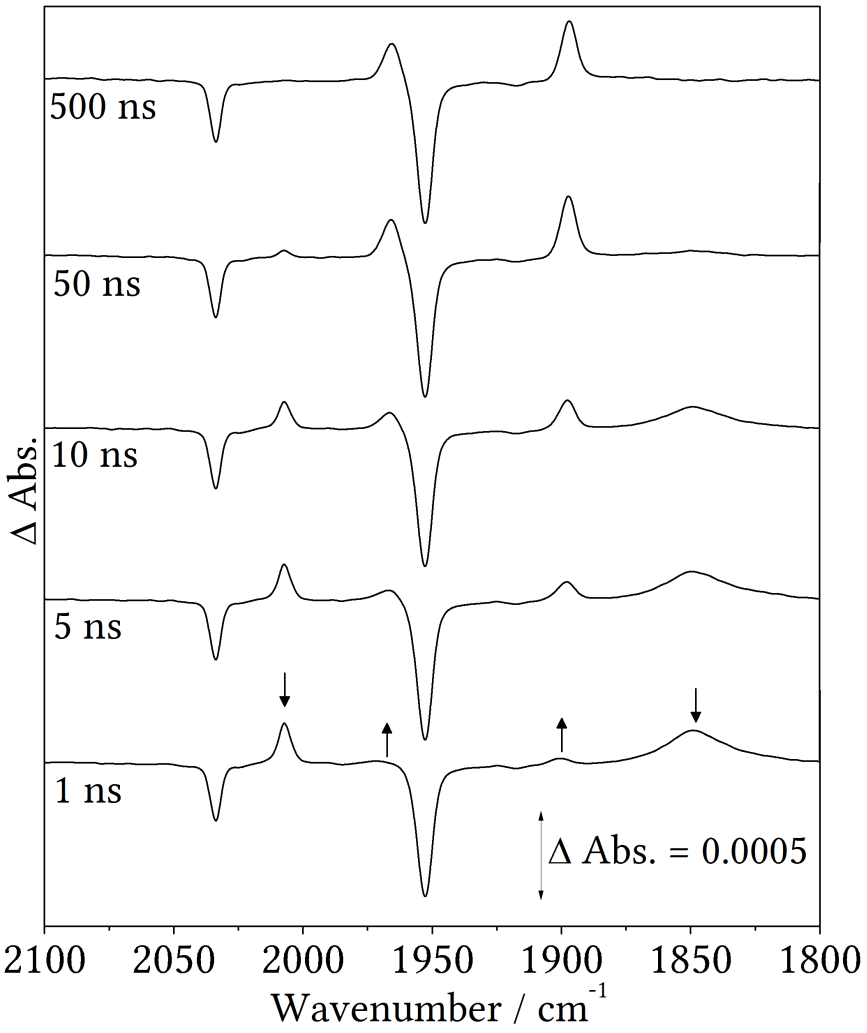


FIGURE 2.21: Selected nanosecond TRIR difference spectra recorded at a series of time delays following 266 nm photolysis of a solution of $CpMn(CO)_3$ in PFMCH. Decay of the ν(CO) bands of $^3CpMn(CO)_2$ and growth of those corresponding to $^1CpMn(CO)_2(C_7F_{14})$ can be clearly seen.

in the 1 ns spectrum. A further two weak ν(CO) bands are also observed at 1966 and 1898 cm^{-1} in the 1 ns spectrum, which are assigned to the singlet solvent complex $^1CpMn(CO)_2(C_7F_{14})$. These bands appear at slightly higher energy compared to those of the *n*-heptane complex $^1CpMn(CO)_2(C_7H_{16})$. The observed rate constants for the spin-forbidden reaction which occurs following photolysis of $CpMn(CO)_3$ in PFMCH are shown in Table 2.9. The continued formation of this solvent complex occurs concurrently

with the decay of the triplet $^3CpMn(CO)_2$, indicating that $^1CpMn(CO)_2(C_7F_{14})$ is formed directly from $^3CpMn(CO)_2$, as expected.

TABLE 2.9: Observed rate constants for the processes observed following 266 nm photolysis of $CpMn(CO)_3$ in perfluoro(methylcyclohexane) solution at 298 K.

ν(CO) (cm^{-1})	Assignment	k_{obs} (s^{-1})
2008	$^3CpMn(CO)_2$	5.6 (±0.3) x 10^7
1850	$^3CpMn(CO)_2$	5.6 (±0.2) x 10^7
1965	$^1CpMn(CO)_2(C_7F_{14})$	5.8 (±0.3) x 10^7
1898	$^1CpMn(CO)_2(C_7F_{14})$	5.8 (±0.3) x 10^7

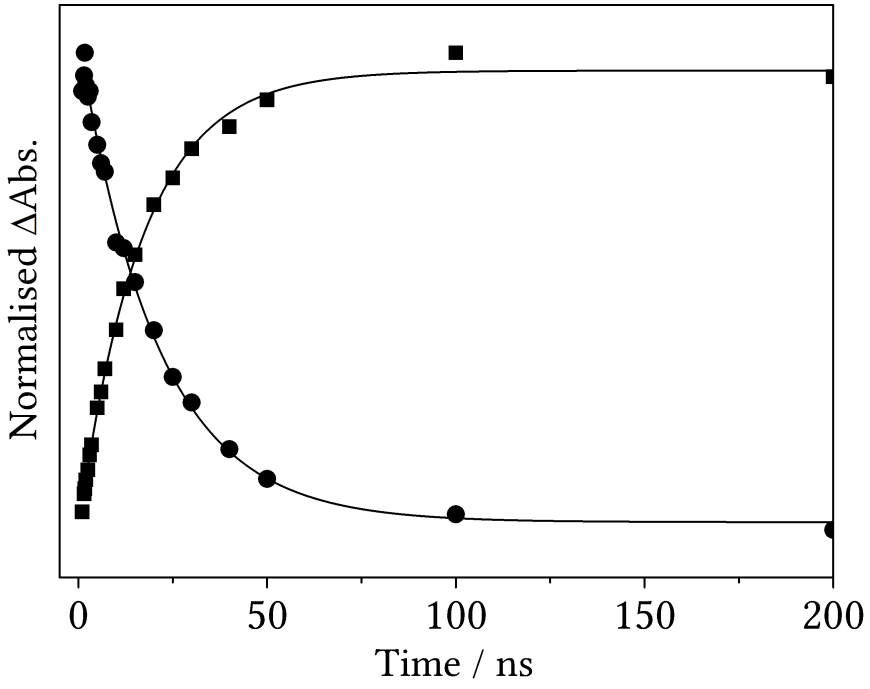


FIGURE 2.22: Nanosecond kinetic traces from TRIR spectra recorded following 266 nm irradiation of $CpMn(CO)_3$ in PFMCH solution, showing matching rates for the decay of $^3CpMn(CO)_2$ at 2007 cm^{-1} (circles) and growth of $^1CpMn(CO)_2(C_7F_{14})$ at 1898 cm^{-1} (squares). Solid lines are mono-exponential fits.

The TRIR kinetic traces for the decay of $^3CpMn(CO)_2$ (τ = 18 (±2) ns) and formation of $^1CpMn(CO)_2(C_7F_{14})$ (τ = 17 (±2) ns) are shown in Figure 2.22. The rates for these processes are an order of magnitude slower than those observed in *n*-heptane solution, possibly due to a weaker interaction between the PFMCH solvent and the Mn

centre, though the precise reason for this dramatic difference will be discussed later in this Chapter. The weak interaction leads to a vastly increased lifetime of the highly reactive coordinatively unsaturated 16-electron intermediate, consistent with results reported above for photolysis of $Fe(CO)_5$ in PFMCH. The spectrum recorded 700 ns following excitation shows only the ν(CO) bands of the singlet solvent complex.

2.2.4 Density Functional Theory Study of the Geometry and Spin-State of $^3CpMn(CO)_2$

Following observation of the 16-electron unsaturated intermediate $^3CpMn(CO)_2$ described above, investigations to determine the geometry and confirm the spin-state of this unusual intermediate were undertaken.

Optimised geometries and harmonic vibrational frequencies were calculated by Dr. Magnus Hanson-Heine at the University of Nottingham using density functional theory (DFT) at the M06 level of theory[209] within the Q-Chem quantum chemical software package.[210] Calculations were converged using the triple-ζ 6-311G(d,p) basis set for C, O and H atoms and quasi-relativistic SRSC pseudo-potential and basis set for Mn, together with an EML-(75,302) integration grid.[211] Initial molecular structures were optimised without constraint to minimum energy geometries, confirmed by the absence of imaginary frequencies. The resulting harmonic frequencies were scaled by a uniform factor of 0.95.[212]

The structures of $^3CpMn(CO)_2$ which were considered are shown in Figure 2.23. Two triplet species were considered, one with a bent structure and C_s symmetry, and

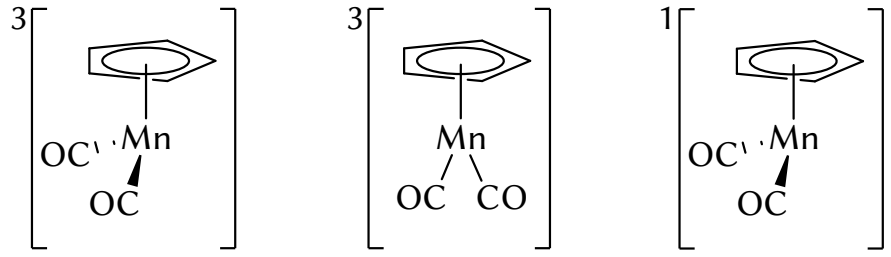


FIGURE 2.23: Structures considered as possible candidates for the unsaturated intermediate observed unsaturated intermediate following photolysis of $CpMn(CO)_3$ in solution.

another with planar geometry and C_{2v} symmetry. A further singlet structure was also calculated, with a bent structure and C_s symmetry. For comparison, the vibrational frequencies of the parent $CpMn(CO)_3$ complex were also calculated. Previous DFT studies have also considered the possibility of a coordinatively unsaturated ring-slipped intermediate,[53] many of which have been observed spectroscopically.[54,186,193,213–215] However, in the interest of simplicity only η^5 structures have been considered in this study. Figure 2.24 shows the ν(CO) vibrational frequencies for all calculated structures, as well as an experimental TRIR difference spectrum showing ν(CO) bands of the parent complex and 16-electron intermediate.

Calculated vibrational frequencies for the parent complex $CpMn(CO)_3$ at 2026 and 1961 cm^{-1} are in reasonable agreement with those observed experimentally by TRIR spectroscopy (2033 and 1953 cm^{-1}). Comparison of the calculated vibrational frequencies of the various structures of the 16-electron intermediate with a TRIR difference spectrum recorded 1 ns after photolysis of a solution of $CpMn(CO)_3$ in PFMCH shows a very good match between the experimental ν(CO) band positions of $^3CpMn(CO)_2$ (2007 and 1849 cm^{-1}) with those of the calculated bent triplet structure (2003 and 1847 cm^{-1}). Calculated frequencies for this bent triplet structure exhibit an

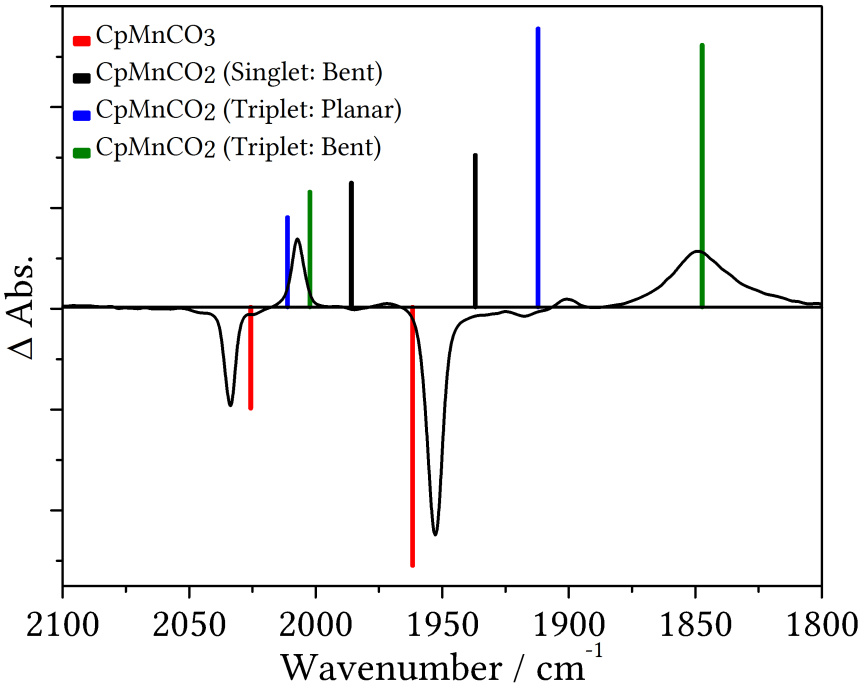


FIGURE 2.24: Calculated vibrational frequencies for a series of possible structures of a coordinatively unsaturated cyclopentadienyl manganese dicarbonyl complex, and calculated vibrational frequencies of $CpMn(CO)_3$, overlaid with a single TRIR difference spectrum recorded 1 ns following photolysis of $CpMn(CO)_3$ in PFMCH solution. Calculated absorption bands of ν(CO) have been made negative in order to mimic the presented difference spectrum.

unusually large $\Delta\nu$ (156 cm^{-1}) which matches well with experimental observations ($\Delta\nu$ = 158 cm^{-1}). The planar triplet structure shows good agreement for the higher energy of the two ν(CO) bands of the intermediate, while the bent singlet structure shows poor agreement with the experimental spectrum for all ν(CO) band frequencies. A summary of all calculated and experimentally obtained ν(CO) vibrational frequencies for $CpMn(CO)_3$ and various structures of the unsaturated intermediate are shown in Table 2.10

The very good agreement between the calculated vibrational frequencies of the triplet bent structure of $^3CpMn(CO)_2$ and the experimentally observed frequencies of the intermediate formed following photolysis of $CpMn(CO)_3$ in solution adds to the

TABLE 2.10: Experimentally obtained ν(CO) absorption band frequencies of $CpMn(CO)_3$ and $^3CpMn(CO)_2$, and calculated ν(CO) frequencies for $CpMn(CO)_3$ and a series of possible structures of a 16-electron, coordinatively unsaturated intermediate produced following photolysis of $CpMn(CO)_3$ in solution.

Source	**Compound**	**ν(CO) (cm^{-1})**	**Geometry**
Experimental	$CpMn(CO)_3$	2033, 1953	
	$^3CpMn(CO)_2$	2007, 1849	
Calculated	$CpMn(CO)_3$	2026, 1961	
	$^3CpMn(CO)_2$	2003, 1847	Bent
	$^3CpMn(CO)_2$	2011, 1912	Planar
	$^1CpMn(CO)_2$	1986, 1937	Bent

evidence for the triplet spin-state of this intermediate. These results are somewhat in agreement with those of Kemnitz and co-workers, who found a significant match between experimentally observed ν(CO) bands calculated bands for a bent geometry of $^3CpMn(CO)_2$. The authors also considered a planar geometry, which showed poorer agreement with experimental data.[53] In addition to these two η^5 species, the authors also calculated the vibrational spectra of a ring-slipped η^3 triplet species, and found good agreement with observed experimental data for the triplet state, identifying a distortion in the direction of the ring-slipped intermediate in their calculated geometry of $^3CpMn(CO)_2$, which may go some may to explaining the similar calculated ν(CO) absorption frequencies. While no ring-slipped species were considered during this study, it is interesting to note that no such distortion is observed in our calculated geometry for the bent triplet $^3CpMn(CO)_2$, but a good match between calculated and experimental spectra is still observed.

2.2.5 Picosecond TRIR of $CpMn(CO)_3$ in Perfluoro(methylcyclohexane) with a Liquid Alkane Dopant

Following observation of the dramatic effect the perfluorinated solvent PFMCH had on the rate of the spin-forbidden reaction of $^3CpMn(CO)_2$ to form $^1CpMn(CO)_2(C_7F_{14})$ compared to those observed in alkane solvents, experiments using mixed solvent systems were undertaken. TRIR spectra presented earlier in this Chapter following photolysis of $CpMn(CO)_3$ or $Fe(CO)_5$ in PFMCH show that PFMCH is a very weakly coordinating solvent, which should allow the selective binding of more strongly coordinating ligands (e.g., alkanes). By doping a small amount of alkane into the perfluoroalkane solvent, a change in the rate of formation of the singlet complex $^1CpMn(CO)_2X$ (X = solvent or dopant), as well as its ν(CO) band positions, should be observed. These changes, if observed, would indicate formation of a different species from the solvent complex observed following irradiation in pure PFMCH.

During these experiments, a small amount of an alkane solvent (*c*-pentane) was doped into a solution of $CpMn(CO)_3$ in perfluoro(methylcyclohexane) to give a 0.5 M concentration of the alkane. This ratio was shown by FTIR spectroscopy to preserve the ν(CO) band positions of the $CpMn(CO)_3$ parent complex observed in pure PFMCH, suggesting that the parent complex is predominantly solvated by the perfluoroalkane. Following on from the work of Kelly and co-workers described earlier,[78] in which an interaction between the transition metal and alkane was observed following photolysis of $M(CO)_6$ (M = Cr, Mo, W) in a perfluorinated solvent, and more recent work by Rábay *et al.* in which perfluoro(methylcyclohexane) was used as the solvent for C−H activation of alkanes at an iridium centre,[77] we hoped to observe preferential formation

of an alkane complex in perfluoroalkane solvent. Cyclopentane was selected as the initial alkane dopant of interest due to its reported formation of long-lived organometallic alkane complexes with both $CpMn(CO)_3$ and $CpRe(CO)_3$,[48] and its miscibility with perfluoro(methylcyclohexane).

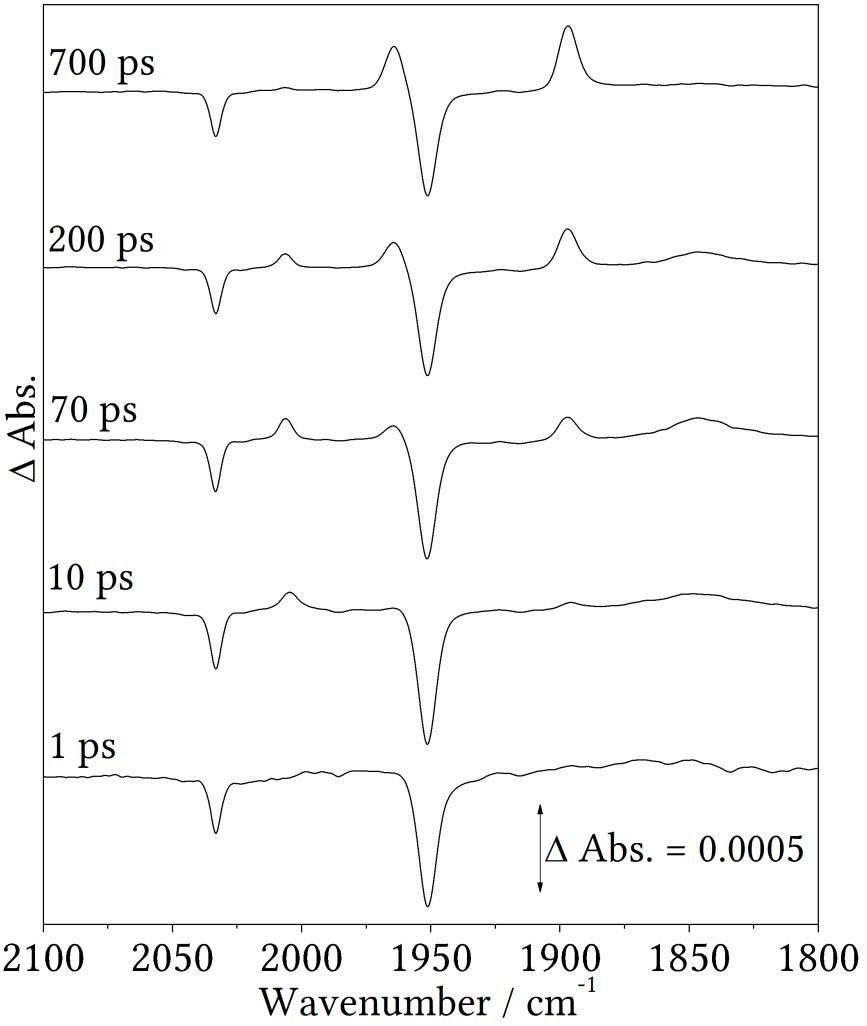


FIGURE 2.25: Selected ps-TRIR difference spectra recorded at 1, 10, 70, 200 and 700 ps following 266 nm photolysis of $CpMn(CO)_3$ in PFMCH doped with 0.5 M *c*-pentane under Ar, showing the formation and subsequent decay of $^3CpMn(CO)_2$ to form the alkane complex $^1CpMn(CO)_2(C_5H_{10})$.

A selection of picosecond TRIR difference spectra recorded following photolysis at 266 nm of $CpMn(CO)_3$ in PFMCH doped with 0.5 M *c*-pentane under an Ar atmosphere

are shown in Figure 2.25. After 1 ps following photolysis, the two ν(CO) bands of the $CpMn(CO)_3$ parent complex at 2033 and 1952 cm^{-1} are bleached, and two broad ν(CO) transient bands appear at lower energy relative to the bleached parent bands. These two bands sharpen and blue-shift over approximately 30 ps, consistent with the vibrational cooling process observed in the pure perfluorinated solvent above, to yield two transient ν(CO) bands at 2008 and 1850 cm^{-1}, with a similarly large $\Delta\nu$ observed above (158 cm^{-1}). A summary of the ν(CO) band positions of $CpMn(CO)_3$ and all intermediates produced following 266 nm photolysis in a series of weak ligand doped PFMCH solutions, some of which will be discussed in later sections, is given in Table 2.11. Similarly to the experiments in pure alkane and perfluoroalkane solvent described above, these two bands are assigned to the 16-electron triplet species $^3CpMn(CO)_2$. The observed energy of the ν(CO) bands of $^3CpMn(CO)_2$ appear to be unaffected by the addition of *c*-pentane to the perfluorinated solvent, suggesting a minimal interaction between the alkane or perfluoroalkane and the metal centre for this triplet species.

The spectrum recorded 10 ps after photolysis shows some evidence of two more ν(CO) bands. The two bands assigned to $^3CpMn(CO)_2$ begin to decay on a picosecond timescale, concurrently with continued formation of these additional ν(CO) bands at 1963 and 1896 cm^{-1} (k_{obs} = 3.7 ($\pm$0.4) x 10^9 s^{-1}). A summary of observed rate constants for all processes observed following photolysis of $CpMn(CO)_3$ in *c*-pentane doped PFMCH is shown in Table 2.12. The observed rate at which the triplet $^3CpMn(CO)_2$ undergoes the spin-forbidden reaction to form the solvent complex $^1CpMn(CO)_2X$ in the mixed solvent system is much faster than the rate observed in pure perfluoroalkane, suggesting that a different, more favourable interaction between metal and solvent is

TABLE 2.11: ν(CO) absorption band frequencies of $CpMn(CO)_3$ and intermediates produced following photolysis of $CpMn(CO)_3$ in pure PFMCH or PFMCH doped with *c*-pentane, Xe, CO_2, CH_4 or C_2H_6.

Compound	**Dopant**	**ν(CO) (cm^{-1})**
$CpMn(CO)_3$		2033, 1952
	c-pentane	2033, 1952
	Xe	2033, 1952
	CO_2	2033, 1952
	CH_4	2033, 1952
	C_2H_6	2033, 1952
$^3CpMn(CO)_2$		2008, 1850
	c-pentane	2008, 1850
	Xe	2008, 1849
	CO_2	2008, 1850
	CH_4	2008, 1850
	C_2H_6	2008, 1849
$^1CpMn(CO)_2X$		1965, 1897
	c-pentane	1963, 1896
	Xe	1967, 1898
	CO_2	1964, 1896
	CH_4	1965, 1897
	C_2H_6	1964, 1896

TABLE 2.12: Observed rate constants for the processes observed following 266 nm photolysis of $CpMn(CO)_3$ in PFMCH solution doped with 0.5 M *c*-pentane at 298 K.

ν(CO) (cm^{-1})	**Assignment**	**k_{obs} (s^{-1})**
2008	$^3CpMn(CO)_2$	3.7 ($\pm$0.4) x 10^9
1850	$^3CpMn(CO)_2$	3.6 ($\pm$0.4) x 10^9
1963	$^1CpMn(CO)_2(C_5H_{10})$	3.6 ($\pm$0.3) x 10^9
1896	$^1CpMn(CO)_2(C_5H_{10})$	3.7 ($\pm$0.3) x 10^9

present in this case. TRIR kinetic traces for this reaction are shown in Figure 2.26, while the lifetimes for this process in a series of PFMCH solutions doped with weak ligands is presented in Table 2.13. The ν(CO) bands of $^1CpMn(CO)_2X$ are slightly shifted to lower energy relative to those observed in PFMCH alone, while the ν(CO) bands of the parent $CpMn(CO)_3$ and triplet intermediate $^3CpMn(CO)_2$ do not exhibit any change in position. While it is possible that this is due to preferential solvation

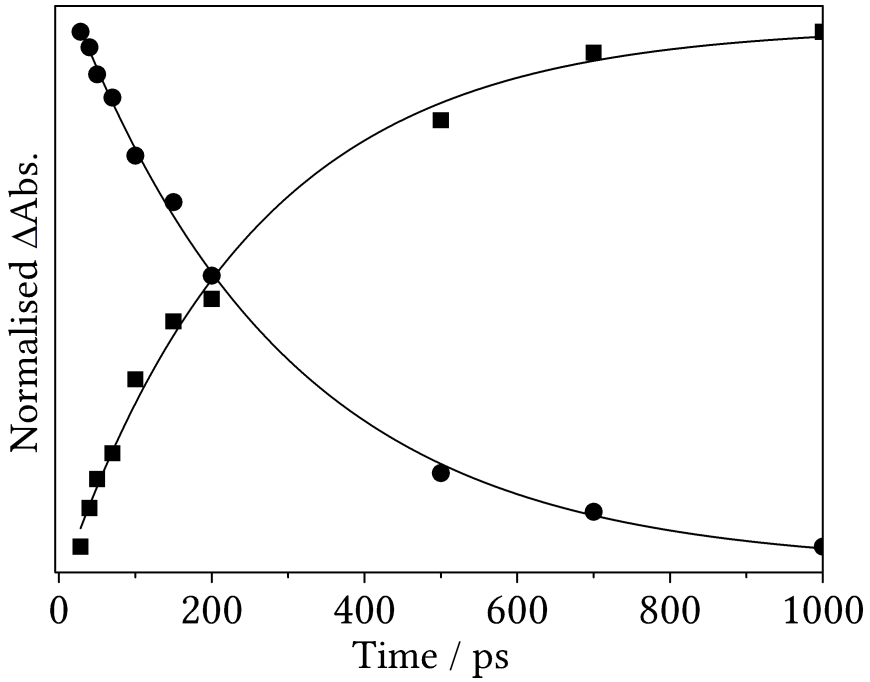


FIGURE 2.26: Picosecond kinetic traces from TRIR spectra recorded following 266 nm irradiation of $CpMn(CO)_3$ in PFMCH solution doped with 0.5 M *c*-pentane, showing matching rates for the decay of $^3CpMn(CO)_2$ at 2008 cm^{-1} (circles) and growth of $^1CpMn(CO)_2(C_5H_{10})$ at 1896 cm^{-1} (squares). Solid lines are mono-exponential fits.

of the singlet solvent complex by *c*-pentane, based on the change in spin-forbidden reaction rate compared to experiments in pure PFMCH, this change is attributed to a direct interaction between the alkane dopant and metal to form $^1CpMn(CO)_2(C_5H_{10})$. This direct interaction increases the amount of electron donation from the solvent ligand to the metal centre when compared with PFMCH, increasing back-bonding from the metal to the remaining carbonyl ligands, lowering the energy of the carbonyl ligand vibrations. The rate of this spin-forbidden reaction is indeed more akin to that observed above in pure alkane than in pure PFMCH. However, the rate of reaction in this doped system is *ca.* 3 times slower than the rate of the corresponding reaction to form the solvent complex in pure cyclopentane. It is possible that the rate of this reaction is limited by the need for $^3CpMn(CO)_2$ and *c*-pentane to diffuse towards each

other before a reaction can occur, due to the low concentration of these two species in solution. The diffusion limited rate constant (k_d) for a reaction such as this can be estimated using the expression:

$$k_d = 4\pi R^*(D_A + D_B)N_A 10^3$$

Where R^* is the critical reaction radius, and D_A and D_B are the diffusion coefficients of reactants A and B respectively, given by the Stokes-Einstein equation:

$$D = \frac{k_B T}{6\pi\eta a}$$

Where η is the viscosity of the solvent, and a is the effective radius of the solvated species. Assuming that the two reactants are of similar size, and assuming that the contact distance at which the reaction occurs $R^* = 2a$, the equation can be simplified to:

$$k_d = \frac{8k_B T}{3\eta} N_A 10^3$$

Using this equation, k_d for this reaction is estimated to be *ca.* 4 x 10^9 $M^{-1}s^{-1}$. This is consistent with the experimentally obtained rate constant for reaction of $^3CpMn(CO)_2$ with *c*-pentane in PFMCH, however the approximations made during calculation of this theoretical diffusion controlled rate make this comparison far from conclusive. The effect of addition of *c*-pentane on the rate of reaction of $^3CpMn(CO)_2$ to form $^1CpMn(CO)_2X$, and the change in the ν(CO) band positions of $^1CpMn(CO)_2X$ are clear however. This leads to the conclusion that in a mixed solvent system of PFMCH

and 0.5 M cyclopentane, $^3CpMn(CO)_2$ reacts preferentially with the alkane to form $^1CpMn(CO)_2(C_5H_{10})$. This alkane complex is stable on the nanosecond timescale.

TABLE 2.13: Lifetimes (in ns) for the spin-forbidden reaction of $^3CpMn(CO)_2$ to form $^1CpMn(CO)_2X$ (X = solvent or dopant) following photolysis of $CpMn(CO)_3$ in a series of solvent/dopant systems (all data recorded at 298 K). *In the case of methane, no evidence for formation of $^1CpMn(CO)_2(CH_4)$ is observed, the singlet complex formed is assigned as $^1CpMn(CO)_2(C_7F_{14})$.

Dopant	**Lifetime τ (ns)**
None	18 (±2)
c-pentane	0.27 (±0.04)
Xe	3.9 (±0.4)
CO_2	4.7 (±0.5)
CH_4	19 (±4)*
C_2H_6	1.9 (±0.2)

2.2.6 TRIR of $CpMn(CO)_3$ in Perfluoro(methylcyclohexane) with Gaseous Dopants

2.2.6.1 TRIR of $CpMn(CO)_3$ in Xenon Doped Perfluoro(methylcyclohexane)

The experiments presented earlier in this Chapter show successful formation of an organometallic alkane complex in perfluoroalkane solution. This was achieved by doping the liquid solvent of choice into PFMCH to form a mixture of a known ratio. Following on from these experiments, solutions incorporating various gaseous dopants were prepared. Previously, solutions incorporating liquid alkane dopants were prepared under an Ar atmosphere, then held under 1.5 bar Ar for the duration of the experiment. In the case of gaseous dopants however, solvents were first degassed to remove dissolved argon. Solutions were prepared under an atmosphere of the gaseous dopant of interest, then pressurised to 1.5 bar and agitated under pressure to ensure saturation.

The first gaseous dopant that was selected for study in perfluorinated solvent was Xe. While $^{1}CpMn(CO)_2Xe$ has been previously characterised by IR spectroscopy in supercritical Xe solution,[185] it has never been observed in liquid solution at room temperature. Xenon has been shown to form the most stable organometallic complexes, compared to the other noble gases.[48,183,185,216]

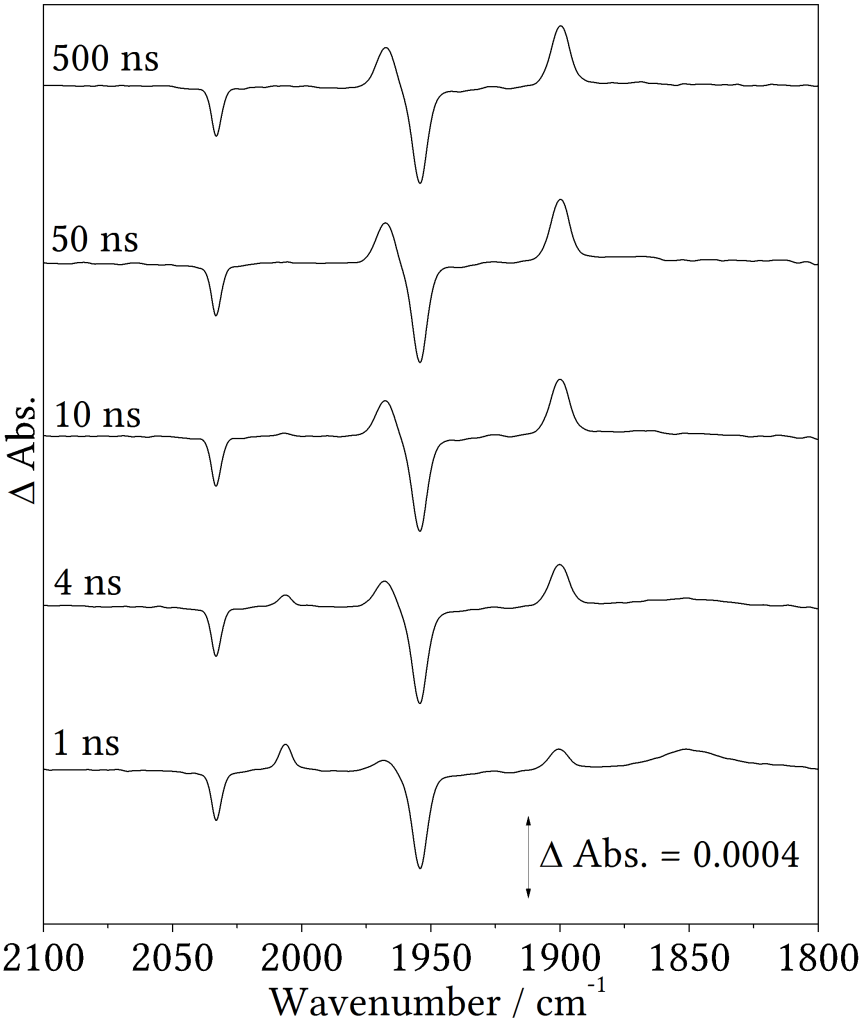


FIGURE 2.27: Selected ns-TRIR difference spectra recorded at 1, 4, 10, 50 and 500 ns following 266 nm photolysis of $CpMn(CO)_3$ in a Xe saturated PFMCH solution at 1.5 bar, showing the formation and subsequent decay of $^{3}CpMn(CO)_2$ to form $^{1}CpMn(CO)_2Xe$.

TRIR spectra recorded on the picosecond timescale show bleaching of the two

parent bands, followed by the subsequent formation of a vibrationally hot transient assigned to $^{3}CpMn(CO)_2$, with ν(CO) bands at 2008 and 1949 cm^{-1}. This species undergoes vibrational cooling over *ca.* 30 ps matching experiments performed in pure PFMCH, as well as those in the mixed alkane and perfluoroalkane solvent system described above. The triplet dicarbonyl species is stable after 500 ps.

Figure 2.27 shows a series of selected ns-TRIR difference spectra recorded following photolysis at 266 nm of $CpMn(CO)_3$ in a Xe saturated PFMCH solution at a pressure of 1.5 bar. The spectrum recorded 1 ns following irradiation shows the two ν(CO) bands assigned previously to $^{3}CpMn(CO)_2$. Two more ν(CO) bands are also present 1 ns after irradiation at 1966 and 1898 cm^{-1}, similar to the band positions of the various $^{1}CpMn(CO)_2X$ (X = solvent or dopant) complexes characterised above. The ν(CO) bands of $^{3}CpMn(CO)_2$ decay on the nanosecond timescale (τ = 3.9 ($\pm$0.4) ns) at the same rate as continued formation of $^{1}CpMn(CO)_2X$. The TRIR kinetic traces for this process are shown in Figure 2.28 and observed rate constants for the growth and decay of all ν(CO) bands involved in this process are summarised in Table 2.14.

The rate of the spin-forbidden reaction in this case is faster than that observed in pure PFMCH solution by approximately a factor of 4, but is slower than than that observed in the mixed solvent system of PFMCH and 0.5 M cyclopentane by an order of magnitude. This change in reaction rate upon addition of Xe to the PFMCH solution suggests formation of a different, more stable complex than $^{1}CpMn(CO)_2(C_7F_{14})$. The singlet dicarbonyl complex formed in this case is therefore assigned as the Xe complex $^{1}CpMn(CO)_2Xe$. In addition to the change in reaction rate from $^{3}CpMn(CO)_2$ to form $^{1}CpMn(CO)_2Xe$, the ν(CO) band positions are also very similar (within 2 cm^{-1}) of

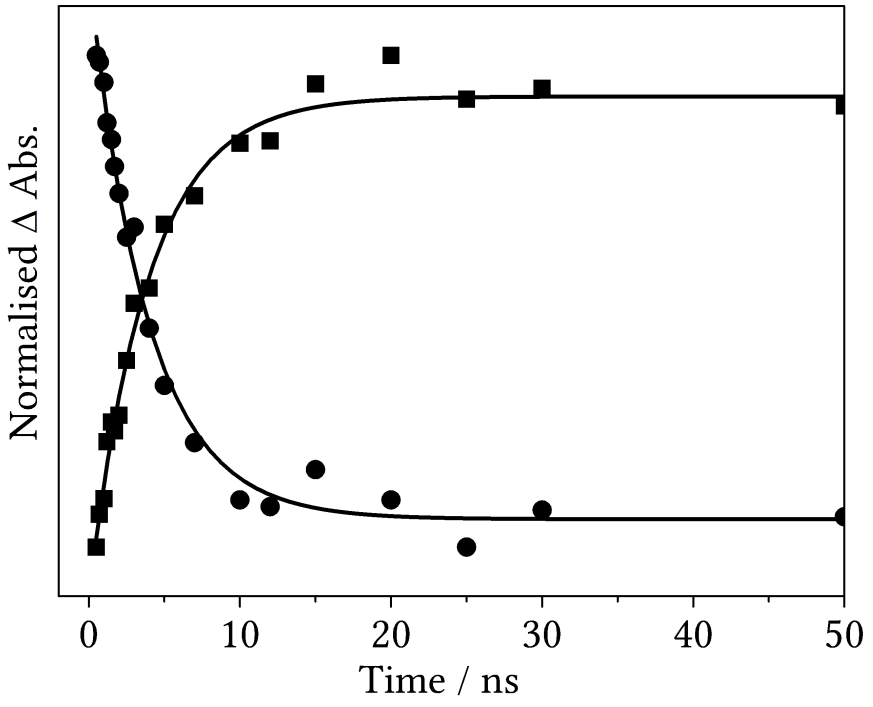


FIGURE 2.28: Nanosecond kinetic traces from TRIR spectra recorded following 266 nm irradiation of $CpMn(CO)_3$ in Xe doped PFMCH solution, under 1.5 bar Xe, showing matching rates for the decay of $^3CpMn(CO)_2$ at 2008 cm^{-1} (circles) and formation of $^1CpMn(CO)_2Xe$ at 1897 cm^{-1} (squares). Solid lines are mono-exponential fits.

those of $^1CpMn(CO)_2(C_7F_{14})$, suggesting that the xenon is donating a similar amount of electron density to the metal centre as the PFMCH solvent upon binding. While this may be unexpected considering the faster spin-forbidden reaction rate upon addition of Xe, the nature of the interaction between the perfluorinated solvent and metal centre is still unknown, and it is likely that other factors (e.g., sterics) may play a role in determining which ligand will bind preferentially.

TABLE 2.14: Observed rate constants for the processes observed following 266 nm photolysis of $CpMn(CO)_3$ in a Xe saturated PFMCH solution, at 1.5 bar and 298 K.

ν(CO) (cm^{-1})	Assignment	k_{obs} (s^{-1})
2008	$^3CpMn(CO)_2$	2.6 (±0.3) x 10^8
1850	$^3CpMn(CO)_2$	2.7 (±0.2) x 10^8
1966	$^1CpMn(CO)_2Xe$	2.5 (±0.2) x 10^8
1898	$^1CpMn(CO)_2Xe$	2.6 (±0.3) x 10^8

2.2.6.2 TRIR of $CpMn(CO)_3$ in CO_2 Doped Perfluoro(methylcyclohexane)

After successful observation of $^1CpMn(CO)_2Xe$ in room temperature liquid solution, the investigation was expanded to incorporate other weakly binding ligands which are gaseous at room temperature. One such ligand of interest is CO_2, which has been previously shown to coordinate to $CpM(CO)_3$ (M = Mn, Re) to form $CpM(CO)_2(CO_2)$ in both liquid and *sc*CO_2 solutions, as well as CO_2 doped *sc*Kr solution. The stability of the resulting $^1CpMn(CO)_2(CO_2)$ complex was shown to be similar to that of $^1CpMn(CO)_2Xe$.[173,216]

As above, a solution of $CpMn(CO)_3$ in PFMCH was prepared under an atmosphere of CO_2, agitated to ensure saturation with the dopant gas, and held at 1.5 bar pressure of CO_2 during the experiment. The resulting solution was irradiated at 266 nm and a series of TRIR difference spectra on the picosecond and nanosecond timescales were recorded. 1 ps after photolysis, the ν(CO) parent bands (2033 and 1952 cm^{-1}) were bleached, and two new ν(CO) bands were formed. These bands were observed to sharpen and blue-shift over *ca.* 30 ps, to yield the two ν(CO) bands (2008 and 1850 cm^{-1}) previously assigned to the triplet 16-electron complex $^3CpMn(CO)_2$. As reported above for experiments in pure PFMCH, and Xe-doped PFMCH, the triplet species was observed to be stable on the picosecond timescale, and the TRIR difference spectrum recorded 500 ps after photolysis shows only the bands of $^3CpMn(CO)_2$. In this case, as observed previously in Xe-doped PFMCH, the spin-forbidden reaction to form the singlet complex $^1CpMn(CO)_2X$ occurs on the fast nanosecond timescale. The difference spectrum recorded 1 ns after photolysis shows evidence for two new ν(CO) bands at 1964 and 1896 cm^{-1}, which grow at the same rate as the decay of those assigned

to $^3CpMn(CO)_2$ (lifetime τ = 4.7 (±0.5)), suggesting a similar spin-change reaction pathway to those reported above. In this case, the product of the reaction is assigned as $^1CpMn(CO)_2(CO_2)$.

TABLE 2.15: Observed rate constants for the processes observed following 266 nm photolysis of $CpMn(CO)_3$ in a CO_2 doped PFMCH solution at 1.5 bar and 298 K.

ν(CO) (cm^{-1})	Assignment	k_{obs} (s^{-1})
2008	$^3CpMn(CO)_2$	2.1 (±0.2) x 10^8
1850	$^3CpMn(CO)_2$	2.1 (±0.2) x 10^8
1964	$^1CpMn(CO)_2(CO_2)$	2.0 (±0.3) x 10^8
1896	$^1CpMn(CO)_2(CO_2)$	2.1 (±0.2) x 10^8

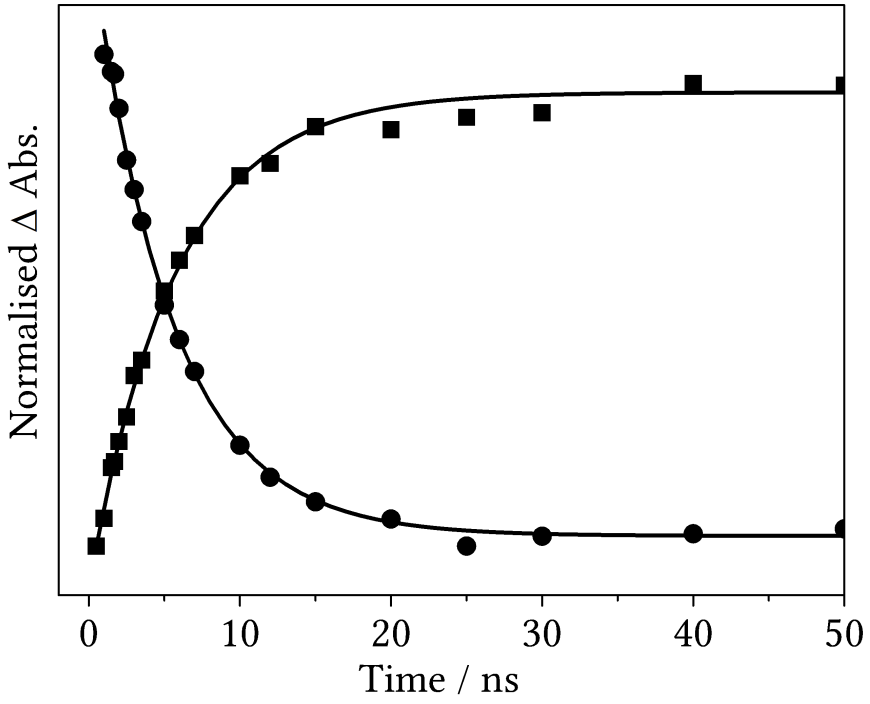


FIGURE 2.29: Nanosecond kinetic traces from TRIR spectra recorded following 266 nm irradiation of $CpMn(CO)_3$ in CO_2 doped PFMCH solution, under 1.5 bar CO_2, showing matching rates for the decay of $^3CpMn(CO)_2$ at 2008 cm^{-1} (circles) and formation of $^1CpMn(CO)_2(CO_2)$ at 1896 cm^{-1} (squares). Solid lines are mono-exponential fits.

The observed lifetime for the formation of $^1CpMn(CO)_2(CO_2)$ is within error of that observed for the spin-forbidden reaction to form $^1CpMn(CO)_2Xe$ in PFMCH

solution, suggesting a similar binding strength for these two ligands. This observation is in agreement with previously reported comparisons of the similar reaction rates of $^1CpMn(CO)_2Xe$ and $^1CpMn(CO)_2(CO_2)$ with CO to reform $CpMn(CO)_3$ in solution.[173] TRIR kinetic traces for this process are shown in Figure 2.29, and observed rate constants for the growth and decay of the ν(CO) bands of both species involved in this reaction are summarised in Table 2.15.

Comparison of the ν(CO) band positions for a series of $^1CpMn(CO)_2X$ species (Table 2.11) shows that in this case the ν(CO) bands of $^1CpMn(CO)_2X$ appear at similar but slightly lower energies compared to those assigned to $^1CpMn(CO)_2(C_7F_{14})$ and $^1CpMn(CO)_2Xe$, but to slightly higher energies compared to those assigned to $^1CpMn(CO)_2(C_5H_{10})$. This trend roughly follows that observed for the rate of the spin-forbidden reaction with the solvent or dopant, from fastest to slowest; *c*-pentane $>$ Xe $\approx$ CO_2 $>$ PFMCH. This suggests a weak binding mode for CO_2, consistent with the η^1-O end-on binding mode reported by Yang and co-workers.[173]

2.2.6.3 TRIR of $CpMn(CO)_3$ in CH_4 and C_2H_6 Doped Perfluoro(methylcyclohexane)

Along with noble gas and CO_2 complexes mentioned previously, an ethane complex has also been observed following photolysis of $CpMn(CO)_3$ in liquid ethane solution at room temperature by TRIR[34,47] and NMR,[47] while methane complexes of $CpMn(CO)_3$ have so far only been characterised by infrared spectroscopy in liquid and supercritical methane solutions.[34]

Photolysis of a CH_4 saturated solution of $CpMn(CO)_3$ in PFMCH yielded no significant evidence for formation of $^1CpMn(CO)_2(CH_4)$. The observed rate of the spin-forbidden reaction of $^3CpMn(CO)_2$ to $^1CpMn(CO)_2X$ (lifetime τ = 19 ($\pm$4)), as well as the ν(CO) band positions of the product of this reaction (1965 and 1898 cm^{-1}) were within error of those observed in pure PFMCH. From this it is concluded that $^1CpMn(CO)_2(CH_4)$ was not formed following photolysis, and the product of the spin-forbidden reaction is assigned as the solvent complex $^1CpMn(CO)_2(C_7F_{14})$. This result appears consistent with rate constants for the reaction of $^1CpMn(CO)_2(CH_4)$ with CO to reform the parent $CpMn(CO)_3$ reported by Calladine *et al.*[34] The authors reported the reaction rate of this methane complex with CO to be orders of magnitude faster than analogous manganese *n*-heptane, xenon or *c*-pentane complexes.

Organometallic complexes of ethane, however, exhibit high stability compared to their methane analogues. In order to attempt characterisation of an organometallic ethane complex following photolysis of $CpMn(CO)_3$, a solution of $CpMn(CO)_3$ in PFMCH was prepared under ethane, and held under 1.5 bar of ethane throughout TRIR experiments, as described above for other gaseous dopants. Within 1 ps of irradiation at 266 nm the two parent bands of $CpMn(CO)_3$ are depleted, giving way to two vibrationally hot ν(CO) bands which undergo cooling over *ca.* 30 ps to yield bands at 2008 and 1849 cm^{-1}. These bands are assigned to $^3CpMn(CO)_2$, as above.

The 16-electron triplet species was observed to be stable 500 ps after photolysis. The difference spectrum recorded 700 ps following photolysis shows two additional ν(CO) bands at 1964 and 1896 cm^{-1}. These two bands continue to form as those of $^3CpMn(CO)_2$ decay, indicating a spin-forbidden reaction with the solvent or dopant.

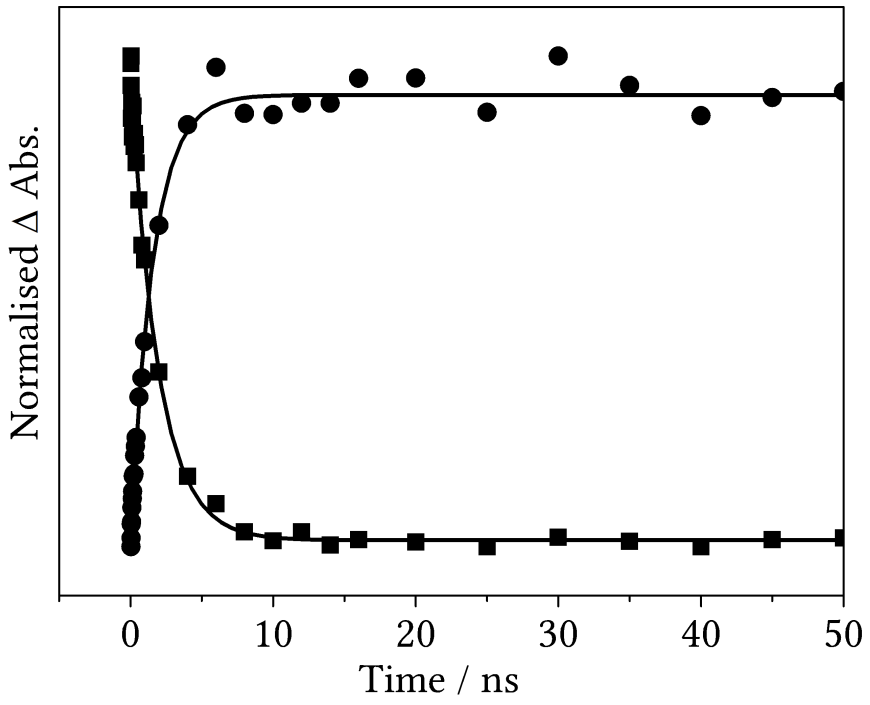


FIGURE 2.30: Nanosecond kinetic traces from TRIR spectra recorded following 266 nm irradiation of $CpMn(CO)_3$ in C_2H_6 doped PFMCH solution, under 1.5 bar C_2H_6, showing matching rates for the decay of $^3CpMn(CO)_2$ at 2008 cm^{-1} (squares) and formation of $^1CpMn(CO)_2(C_2H_6)$ at 1896 cm^{-1} (circles). Solid lines are mono-exponential fits.

Observed rate constants for all spectral changes which occur as a result of this reaction are reported in Table 2.16. The rate of reaction (τ = 1.9 ±0.2 ns) in this case was observed to be *ca.* 2 times faster than observed in Xe or CO_2 doped PFMCH solutions, but slower than the rate observed in PFMCH doped with cyclopentane reported earlier in this Chapter. From this, the $^1CpMn(CO)_2X$ complex formed in this case is assigned as $^1CpMn(CO)_2(C_2H_6)$. This trend mirrors that reported for the recombination reaction of $^1CpMn(CO)_2X$ with CO in a series of liquid and supercritical alkanes and noble gases.[34]

The observed trend for the spin-forbidden reaction rate follows closely that reported for the rate of the recombination reactions of $^1CpMn(CO)_2X$ with CO in a

TABLE 2.16: Observed rate constants for the processes observed following 266 nm photolysis of $CpMn(CO)_3$ in a C_2H_6 doped PFMCH solution at 1.5 bar and 298 K.

ν(CO) (cm^{-1})	Assignment	k_{obs} (s^{-1})
2008	$^3CpMn(CO)_2$	5.3 ($\pm$0.5) x 10^8
1850	$^3CpMn(CO)_2$	5.2 ($\pm$0.4) x 10^8
1965	$^1CpMn(CO)_2(C_2H_6)$	5.3 ($\pm$0.5) x 10^8
1898	$^1CpMn(CO)_2(C_2H_6)$	5.3 ($\pm$0.4) x 10^8

series of pure liquid and supercritical alkanes and noble gases.[34] The overall trend for spin-forbidden reaction rate in the series of doped solutions studied above is as follows: *c*-pentane > C_2H_6 > Xe $\approx$ CO_2 > PFMCH. These observations suggest that PFMCH is a powerful solvent for facilitating the formation of weakly-bound organometallic complexes in room temperature solutions at near-ambient pressure. Very weakly binding solvents have been previously exploited to characterise short-lived organometallic complexes,[173] including use of *sc*Kr doped with Xe to facilitate formation of an organometallic xenon complex.[103,174] However, the work presented above represents the first time this has been achieved using a conventional liquid solvent at room temperature.

2.2.6.4 TRIR Spectroscopy of $CpMn(CO)_3$ in Perfluoro(hexanes) and Perfluoro(triethylamine)

In the experiments described above perfluoro(methylcyclohexane) has been shown to be a powerful solvent for allowing observation of unusual weakly-bound organometallic complexes in room temperature liquid solutions. While PFMCH is the most widely available of the perfluorinated alkanes, other perfluorinated materials could potentially offer more favourable properties such greater ability to dissolve species of interest, or slower reactivity with transition metals leading to slower rates for spin-forbidden

reactions. Investigations into the use of two additional perfluorinated materials, perfluoro(hexanes) (PFH) and perfluoro(triethylamine) (PFTEA), as solvents for TRIR and TRMPS spectroscopic studies of $CpMn(CO)_3$ are described below.

A solution of $CpMn(CO)_3$ in PFH was prepared under an Ar atmosphere and photolysed at 266 nm. A series of TR^MPS difference spectra recorded at a series of ps and ns time delays following photolysis are presented in Figure 2.31. Immediately following photolysis, the two parent ν(CO) bands (2032 and 1956 cm^{-1}) have bleached and two new broad ν(CO) bands can be observed, both of which blue-shift and sharpen over the first 60 ps of the experiment to yield ν(CO) bands at 2006 and 1860 cm^{-1}. The rate of this cooling process is *ca.* half as fast as in PFMCH, suggesting a weaker interaction between solvent and solute during this process in PFH.

The ν(CO) bands at 2006 and 1860 cm^{-1} share the same large $\Delta\nu$ and similar band positions with those observed above for the 16-electron triplet species $^3CpMn(CO)_2$, therefore these two bands are assigned to this species. This species is stable after 10 ns. The TRIR difference spectrum recorded 100 ns after photolysis shows two additional ν(CO) bands at 1968 and 1903 cm^{-1}, similar to those assigned to $^1CpMn(CO)_2X$ previously. Unlike experiments in various doped and pure solvent systems reported above however, this new species is not stable on a nanosecond timescale. This species is assigned as $^1CpMn(CO)_2(C_6F_{14})$.

The continued decay of $^3CpMn(CO)_2$, as well as the decay of $^1CpMn(CO)_2(C_6F_{14})$, is accompanied by growth of four new ν(CO) bands, at 2046, 2002, 1988 and 1937 cm^{-1}. Previous work has shown that dinuclear species can form following photolysis

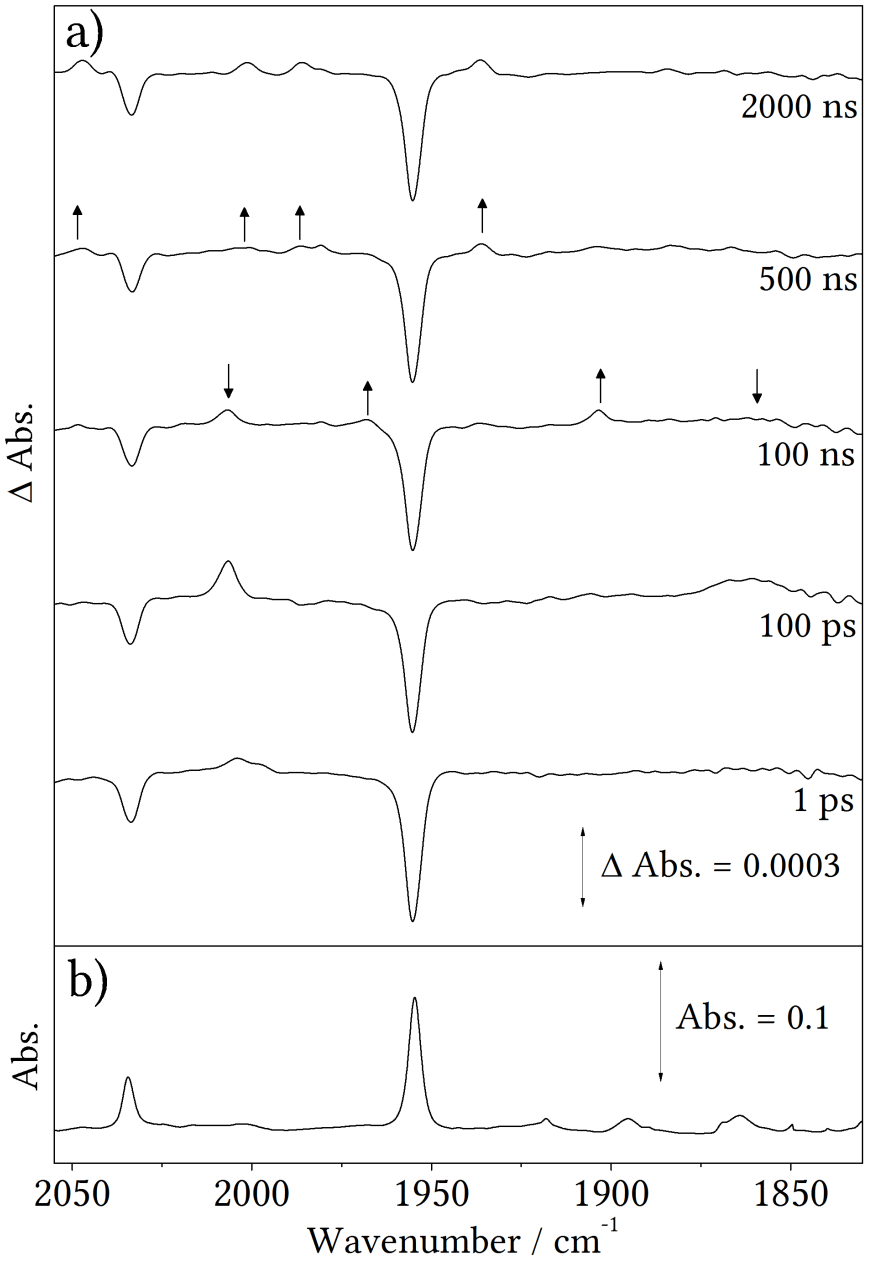


FIGURE 2.31: Selected nanosecond TRIR difference spectra recorded at a series of time delays following 266 nm photolysis of a solution of $CpMn(CO)_3$ in PFH. ν(CO) bands assigned to $^3CpMn(CO)_2$ can be seen to sharpen and blue-shift indicating vibrational cooling. Subsequent decay of the ν(CO) bands of $^3CpMn(CO)_2$ and growth of those corresponding to $^1CpMn(CO)_2(C_6F_{14})$ can be clearly seen. These bands go on to decay concurrently with formation of ν(CO) bands which remain unassigned.

of $CpMn(CO)_3$ in solution,[162] and in nujol mull at 77 K.[167] Creaven *et al.* reported terminal ν(CO) band positions for the dimeric species $Cp_2Mn_2(CO)_5$ at 1993, 1955,

1934, 1907 cm^{-1}, with bridging ν(CO) bands at 1777 and 1740 cm^{-1} in *n*-heptane solution. During experiments reported as part of this study, no data were recorded below 1825 cm^{-1}, making it impossible to observe any bridging ν(CO) bands. The two ν(CO) bands observed in these experiments at 2046 and 2002 cm^{-1} also cannot be matched to those reported by Creaven *et al.*, as they reported no data above 2000 cm^{-1}. The band reported by the authors at 1955 cm^{-1}, may be present in our spectra, however this band is likely to overlap with the ν(CO) band of the parent $CpMn(CO)_3$. The two remaining bands reported by the authors at 1993 and 1934 cm^{-1} are somewhat consistent with two ν(CO) bands observed in this study at 1988 and 1937 cm^{-1}. The difference in ν(CO) band positions for this species are potentially accounted for by the differing interaction with the perfluoroalkane solvent, compared to the alkane. This change in ν(CO) band positions is reflected in the change in position of the parent bands in these two solvents; 2028 and 1946 cm^{-1}, and 2033 and 1956 cm^{-1}, for *n*-heptane and PFH respectively. Formation of $Cp_2Mn_2(CO)_5$ is reported to occur through a reaction between $^1CpMn(CO)_2X$ and the parent $CpMn(CO)_3$.[162] While the decay of $^1CpMn(CO)_2X$ and formation of this unassigned species appear to occur on the same timescale in this study, no increased consumption of the parent complex is observed on this timescale. The low concentration of the parent complex present during this experiment, due to the low solubility of $CpMn(CO)_3$ in PFH, would also limit the formation of $Cp_2Mn_2(CO)_5$. Based on the lack of evidence for bridging carbonyl ligands, and the lack of increased consumption of the parent complex on the timescale of formation of this final photoproduct, the ν(CO) bands of this complex can not be conclusively assigned from the available data. It is possible that these bands correspond to one or more breakdown products of the weakly-bound Mn-PFH complex, or that

$^1CpMn(CO)_2(C_6F_{14})$ reacts with a trace impurity present in the solvent. Further studies would be required to conclusively determine the structure of this photoproduct, and such studies are beyond the scope of the work presented here.

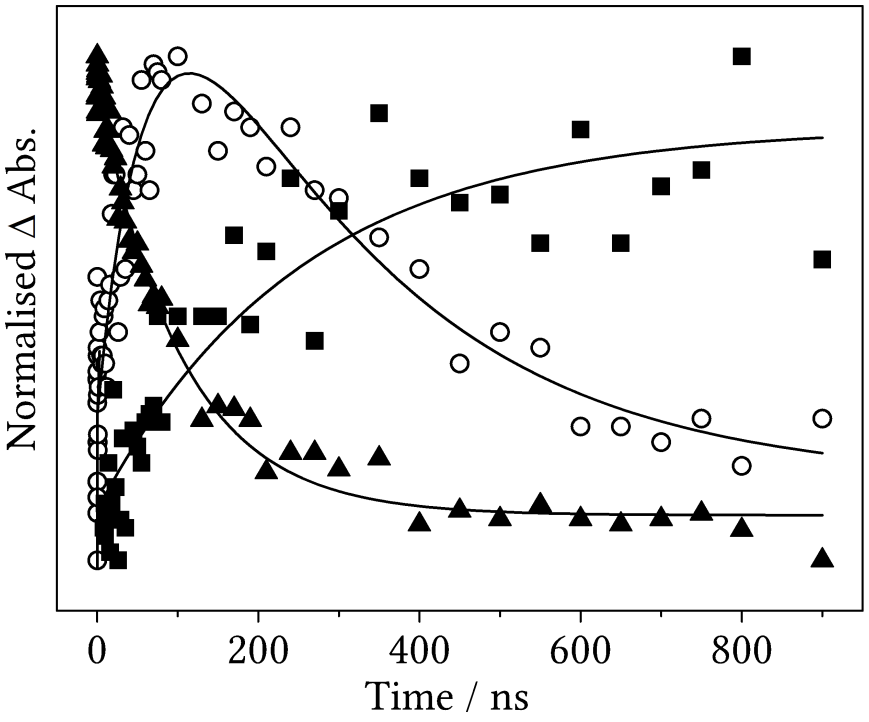


FIGURE 2.32: Nanosecond kinetic traces from TRIR spectra recorded following 266 nm irradiation of $CpMn(CO)_3$ in PFH solution, under Ar, showing the decay of $^3CpMn(CO)_2$ at 2006 cm^{-1} (triangles), formation and decay of $^1CpMn(CO)_2(C_6F_{14})$ at 1903 cm^{-1} (open circles) and formation of the final photoproduct at 1937 cm^{-1} (squares). Solid lines are exponential fits.

TRIR kinetic traces for the decay of $^3CpMn(CO)_2$, the growth and subsequent decay of $^1CpMn(CO)_2(C_6F_{14})$ and the growth of the final photoproduct are shown in Figure 2.32. The lifetime for the decay of the 16-electron intermediate $^3CpMn(CO)_2$ (τ = 105 ±15 ns) is within error of that for the initial growth of the solvent complex (τ = 85 ±20 ns). Additionally, the lifetime for the subsequent decay of $^1CpMn(CO)_2(C_6F_{14})$ (τ = 267 ±40 ns) is observed to be within error of that for the growth of the final photoproduct (τ = 240 ±60 ns). Due to the fact that these processes occur on very

similar timescales, and ν(CO) bands of $^3CpMn(CO)_2$ are still present in the spectra during formation of the final photoproduct, formation of this photoproduct directly from $^3CpMn(CO)_2$ can not be completely ruled out. Observed rate constants for all processes reported following photolysis of $CpMn(CO)_3$ in PFH are given in Table 2.17. Decay of $^1CpMn(CO)_2(C_6F_{14})$ on a nanosecond timescale suggests that this complex is much less stable than its PFMCH analogue. This observation is in agreement with the rate of spin-forbidden reaction of $^3CpMn(CO)_2$ with the solvent, which is *ca.* 4x faster in PFMCH, as well as the energy of ν(CO) bands assigned to $^1CpMn(CO)_2(C_6F_{14})$ (1968 and 1903 cm^{-1}) which appear to higher energy than those of $^1CpMn(CO)_2(C_7F_{14})$ (1965 and 1898 cm^{-1}). All of these observations suggest a very weak interaction between solvent and metal in the case of PFH, even weaker than observed in PFMCH.

Following experiments performed in pure PFH described above, in which PFH was shown to significantly slow the reaction rate of $^3CpMn(CO)_2$ to form $^1CpMn(CO)_2(C_6F_{14})$ when compared to the equivalent reaction in PFMCH, experiments using doped PFH solvent systems were carried out. The two dopants chosen for initial studies in this case were a liquid alkane (*n*-heptane) and the noble gas, Xe.

As in the case of experiments described earlier in this Chapter that utilised PFMCH as a solvent, a solution of $CpMn(CO)_3$ in PFH was prepared under an Ar atmosphere and doped with *n*-heptane (0.5 M). This ratio was selected due to the low miscibility of *n*-heptane in PFH, and was observed to preserve the ν(CO) band positions of the parent complex in pure PFH. The solution was irradiated at 266 nm, and a series of TR^MPS difference spectra were recorded across the picosecond and nanosecond timescales.

TABLE 2.17: Observed rate constants for the processes observed following 266 nm photolysis of $CpMn(CO)_3$ in pure PFH under Ar, PFH with 0.5 M *n*-heptane under Ar, and Xe-doped PFH solution at 1.5 bar and 298 K.

ν(CO) (cm^{-1})	Assignment	k_{obs} (s^{-1})
2006	$^3CpMn(CO)_2$	9.7 (±0.8) x 10^6
1860	$^3CpMn(CO)_2$	9.5 (±0.7) x 10^6
1968	$^1CpMn(CO)_2(C_6F_{14})$	1.3 (±0.2) x 10^7
		3.8 (±0.5) x 10^6
1903	$^1CpMn(CO)_2(C_6F_{14})$	1.5 (±0.2) x 10^7
		3.6 (±0.6) x 10^6
2046	final photoproduct	4.4 (±0.8) x 10^6
2002	final photoproduct	4.3 (±0.7) x 10^6
1987	final photoproduct	4.0 (±0.8) x 10^6
1937	final photoproduct	4.2 (±0.8) x 10^6
2006	$^3CpMn(CO)_2$	9.1 (±0.8) x 10^8
1859	$^3CpMn(CO)_2$	9.0 (±1.0) x 10^8
1965	$^1CpMn(CO)_2(C_7H_{16})$	9.2 (±0.8) x 10^8
1899	$^1CpMn(CO)_2(C_7H_{16})$	9.2 (±0.7) x 10^8
2006	$^3CpMn(CO)_2$	2.6 (±0.3) x 10^8
1859	$^3CpMn(CO)_2$	2.7 (±0.4) x 10^8
1967	$^1CpMn(CO)_2Xe$	2.6 (±0.3) x 10^8
1902	$^1CpMn(CO)_2Xe$	2.7 (±0.2) x 10^8

1 ps following photolysis the two parent ν(CO) bands of $CpMn(CO)_3$ (2033 and 1956 cm^{-1}) were observed to bleach, and two broad ν(CO) bands were present. These two new bands were observed to sharpen and blue-shift over *ca.* 40 ps to yield two ν(CO) bands at 2006 and 1860 cm^{-1}. These bands are assigned to $^3CpMn(CO)_2$. The rate of vibrational cooling in this case appears to be faster than observed in pure PFH, indicating the possibility of some interaction between the vibrationally hot $^3CpMn(CO)_2$ and the alkane dopant. The two ν(CO) bands of $^3CpMn(CO)_2$ were shown to decay concomitantly with formation of two new ν(CO) bands at 1965 and 1899 cm^{-1}, at lower energy compared to those of the PFH solvent complex $^1CpMn(CO)_2(C_6F_{14})$. The rate

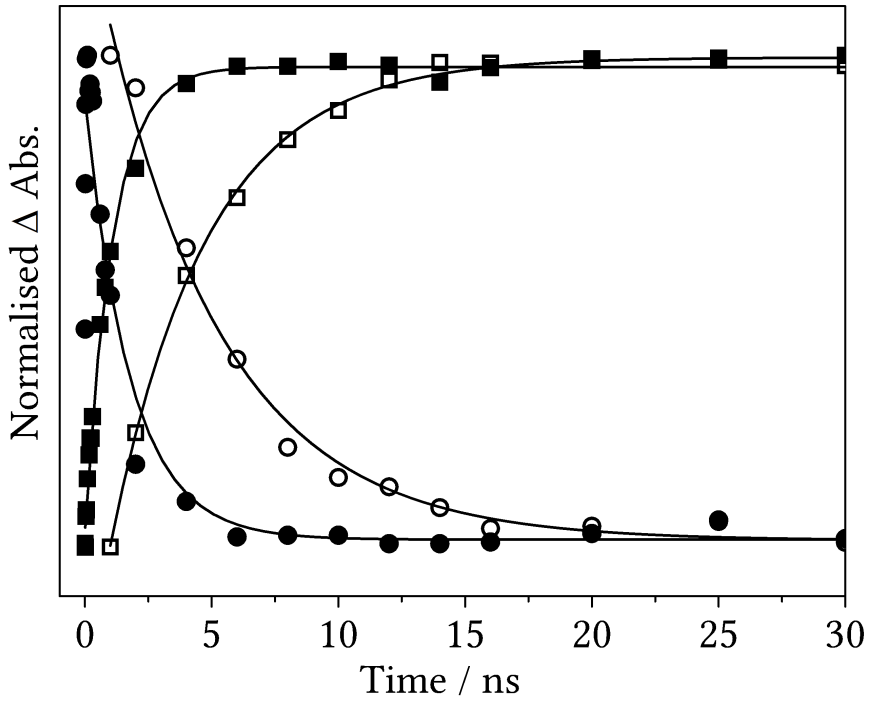


FIGURE 2.33: Kinetic traces from $TR^{M}PS$ spectra recorded following 266 nm irradiation of $CpMn(CO)_3$ in PFH doped with *n*-heptane (0.5 M) under 1.5 bar Ar showing matching rates for the decay of $^{3}CpMn(CO)_2$ at 2006 cm^{-1} (closed circles) and formation of $^{1}CpMn(CO)_2(C_7H_{16})$ at 1899 cm^{-1} (closed squares). Nanosecond kinetic traces from $TR^{M}PS$ spectra recorded following 266 nm irradiation of $CpMn(CO)_3$ in Xe saturated PFH solution, under 1.5 bar Xe. Matching rates for the decay of $^{3}CpMn(CO)_2$ at 2006 cm^{-1} (open circles) and formation of $^{1}CpMn(CO)_2Xe$ at 1902 cm^{-1} (open squares) can be seen. Solid lines are mono-exponential fits.

of reaction to form this new species is much faster than in pure PFH, with a lifetime of $\tau = 1.1$ (± 0.1) ns, compared to $\tau = 90$ (± 30) ns for the pure perfluoroalkane. As observed previously for mixed solvent systems, doping a small amount of *n*-heptane into PFH causes a dramatic change in spin-forbidden reaction rate, and alters the ν(CO) band positions of the resulting $^{1}CpMn(CO)_2X$ complex. From this, the product of the reaction in this case is assigned to the alkane complex $^{1}CpMn(CO)_2(C_7H_{16})$. TRIR kinetic traces for the decay of $^{3}CpMn(CO)_2$ and growth of $^{1}CpMn(CO)_2(C_7H_{16})$ are shown in Figure 2.33 and observed rate constants for this process are given in Table 2.17. While the rate of reaction with the *n*-heptane dopant in this system is much faster than

observed in pure PFH, it is *ca.* 10x faster in pure *n*-heptane. A comparison of lifetimes for the formation of $^{1}CpMn(CO)_2X$ in doped and pure PFH and PFTEA solvents is given in Table 2.18. It is proposed, as above in mixed PFMCH/alkane solvent, that the low concentrations of both alkane and $CpMn(CO)_3$ in solution cause this rate to be limited by diffusion, and hence slower than the rate observed in pure *n*-heptane. Unlike $^{1}CpMn(CO)_2(C_6F_{14})$, the *n*-heptane complex formed in this study does not decay on the nanosecond timescale, indicating higher stability than the perfluoroalkane complex.

TABLE 2.18: Lifetimes (in ns) for the spin-forbidden reaction of $^{3}CpMn(CO)_2$ to form $^{1}CpMn(CO)_2X$ (X = solvent or dopant) following photolysis of $CpMn(CO)_3$ in a series of solvent/dopant systems (all data recorded at 298 K).

Solvent	**Dopant**	**Lifetime τ (ns)**
PFH		90 (±30)
	n-heptane	1.1 (±0.1)
	Xe	3.8 (±0.3)
PFTEA		36 (±5)
	n-heptane	1.0 (±0.1)
	Xe	4.1 (±0.4)

The effect of addition of Xe to a solution of $CpMn(CO)_3$ in PFH was also investigated. As above, the solvent was first degassed, the solution was prepared under Xe and then held under 1.5 bar Xe throughout the measurement. TRIR difference spectra recorded on the picosecond timescale following photolysis at 266 nm show the same vibrational cooling behaviour of the $^{3}CpMn(CO)_2$ ν(CO) bands observed in the pure solvent PFH, with cooling taking place over *ca.* 60 ps. This is in contrast to the change in this rate observed upon addition of alkane, and suggests a lack of any additional interaction between Xe and $^{3}CpMn(CO)_2$ which would facilitate cooling. The ν(CO) band positions were observed to be consistent with those observed previously in PFH (2006 and 1859 cm^{-1}). The rate of spin-forbidden reaction in this case (lifetime

τ = 3.8 (±0.3) ns) was observed to be *ca.* 20x faster than in the pure solvent, but slower than in PFH doped with *n*-heptane. This rate is within error of that observed for analogous studies in Xenon-doped PFMCH solution. ν(CO) band positions for the product of the spin-forbidden reaction in this case appear to higher energy than those of the previously observed $^1CpMn(CO)_2(C_7H_{16})$ in PFH, indicating less donation of electron density from ligand to metal in this case. From this it is concluded that the product of the spin-forbidden reaction is $^1CpMn(CO)_2Xe$. As observed previously in PFMCH solution, $^1CpMn(CO)_2Xe$ is stable on a nanosecond timescale, finally decaying with a lifetime of *ca.* 10 μs.

TABLE 2.19: ν(CO) absorption band frequencies of $CpMn(CO)_3$ and intermediates produced following photolysis of $CpMn(CO)_3$ in pure PFH as well as *n*-heptane and Xe doped PFH, and pure PFTEA as well as *n*-heptane and Xe doped PFTEA.

Compound	**Solvent**	**Dopant**	**ν(CO) (cm^{-1})**
$CpMn(CO)_3$	PFH		2033, 1956
		n-heptane	2033, 1956
		Xe	2033, 1956
	PFTEA		2034, 1954
		n-heptane	2034, 1954
		Xe	2034, 1954
$^3CpMn(CO)_2$	PFH		2006, 1860
		n-heptane	2006, 1860
		Xe	2006, 1859
	PFTEA		2006, 1855
		n-heptane	2005, 1855
		Xe	2006, 1855
$^1CpMn(CO)_2X$	PFH		1968, 1903
		n-heptane	1965, 1899
		Xe	1967, 1902
	PFTEA		1965, 1899
		n-heptane	1963, 1897
		Xe	1965, 1898
Final Photoproduct	PFH		2046, 2002, 1987, 1937

While the results observed in PFH solution appear promising for observation of

weakly-bound organometallic complexes in room temperature solution, the solubility and miscibility of compounds and dopants of interest is very limited. The very low concentrations of transition metal complexes achievable in this solvent (*ca.* 0.5 mM) would be unsuitable for further study using XAFS spectroscopy. A solvent which allows formation of more highly concentrated solutions, while still retaining the non-coordinating nature of PFH would allow a wider array of alkane and noble complexes to be characterised in conventional room temperature solution.

In addition to the perfluoroalkanes, two of which have been examined as potential solvents so far in this Chapter, other perfluorinated materials may also offer favourable properties for observation of weakly-bound organometallic complexes at room temperature. One such class of compounds is the perfluorinated amines, of which perfluoro(triethylamine) (PFTEA, $N(C_2F_5)_3$) is of particular interest. Gaensslen *et al.* produced an in-depth study of the structure and properties of this unusual material.[217] The authors reported a near-planar geometry, with a C−N−C bond angle of 119.3(4)°. The basicity of the perfluoroamine was found to be vastly reduced in comparison to its tertiary amine analogue, due to the strong electron withdrawing effect of the perfluorinated groups, leading to delocalisation of the lone pair across the perfluoroethyl groups bound to the central N atom. Modelling of the van der Waals radii of PFTEA showed that the central N atom is almost completely obscured by the terminal CF_3 groups on one side of the molecule, and partially obscured by the CF_2 groups on the other. It was hoped that the delocalisation of the lone pair, as well as the fact that the N atom and its lone pair are obscured by the inert CF_2 and CF_3 groups may facilitate the use of PFTEA as a non-coordinating solvent.

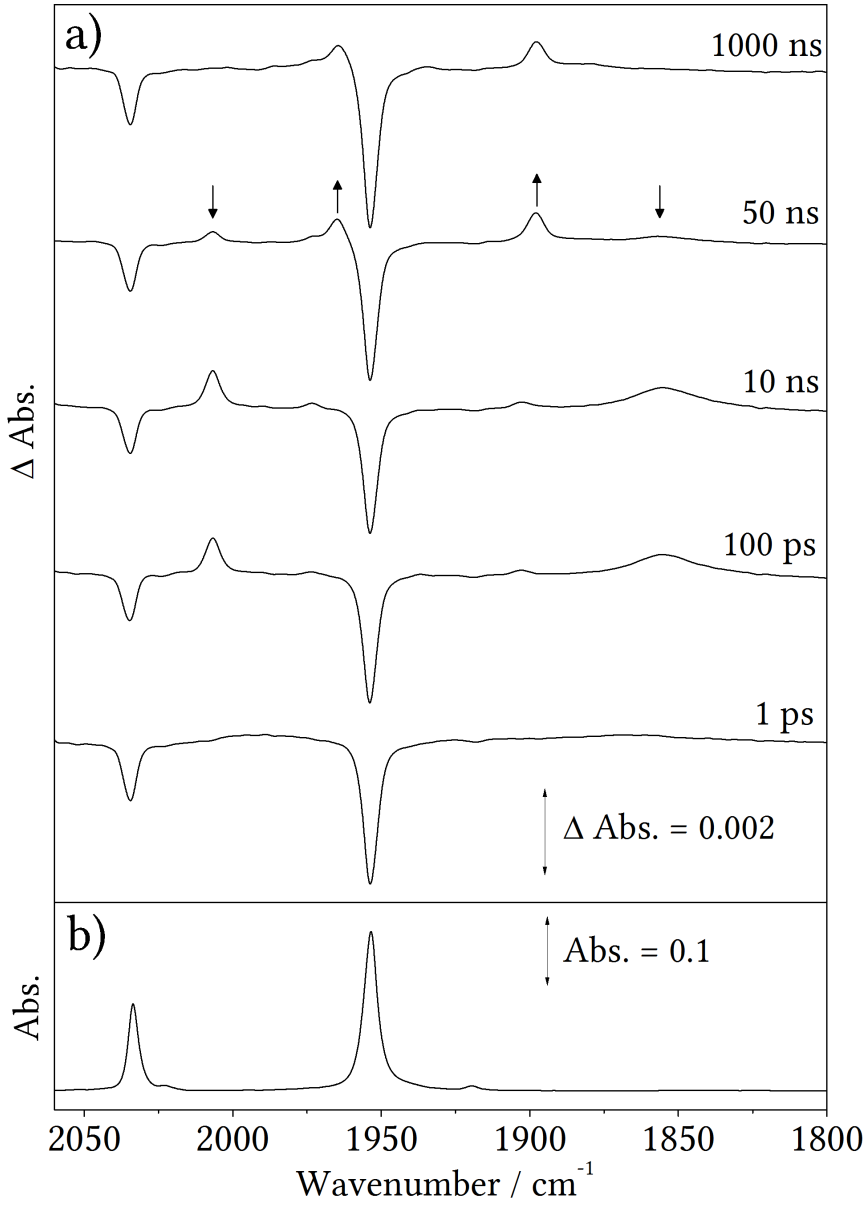


FIGURE 2.34: Selected picosecond and nanosecond TR^{M}PS difference spectra recorded at a series of time delays following 266 nm photolysis of a solution of $CpMn(CO)_3$ in PFTEA. Decay of the ν(CO) bands of $^{3}CpMn(CO)_2$ and growth of those corresponding to $^{1}CpMn(CO)_2(N(C_2F_5)_3)$ can be seen.

In order to investigate if this was the case, a solution of $CpMn(CO)_3$ in PFTEA was prepared as above, and a series of TR^{M}PS difference spectra were recorded following 266 nm irradiation. A selection of these difference spectra, as well as the FTIR spectrum of $CpMn(CO)_3$ in PFTEA is shown in Figure 2.34. The spectrum recorded 1 ps after

photolysis clearly shows that the two ν(CO) bands of $CpMn(CO)_3$ (2034 and 1954 cm^{-1}) have bleached, and two broad features are present at lower energy relative to the parent bands. These broad features sharpen and blue-shift over the first *ca.* 40 ps to yield two new ν(CO) bands at (2006 and 1855 cm^{-1}) with the characteristically large $\Delta\nu$ of the 16-electron triplet $^3CpMn(CO)_2$. 100 ps after photolysis, two new features can be observed in the difference spectrum. These two small bands occur at 1973 and 1904 cm^{-1}, and are suggestive of fast formation of $^1CpMn(CO)_2X$, however these bands appear very high in energy relative to the parents bands compared to previous experiments in PFMCH and PFH. This high energy is suggestive of a very weak mode of coordination to the metal centre, or possibly a complete lack of coordination of the solvent to the metal centre. These two bands appear stable on a nanosecond timescale, and do not continue to grow as the two ν(CO) bands of $^3CpMn(CO)_2$ decay. A species with ν(CO) bands that exactly match those observed here was reported by Kemnitz *et al.* following photolysis of $CpMn(CO)_3$ in an Ar matrix at 12 K.[53] The authors assign this complex as the coordinatively unsaturated singlet species $^1CpMn(CO)_2$, by reference to previous photolysis studies, as well as their own calculated vibrational spectra.[55,158–161,165,167,168,218] The authors acknowledge the possibility of a weak interaction between the unsaturated singlet species and the matrix material, in this case Ar, anticipating an interaction energy of no greater that 2-3 kcal/mol. Gas phase studies undertaken by Zheng *et al.* yielded similar ν(CO) bands following photolysis of $CpMn(CO)_3$ in an Ar atmopshere, which the authors go on to assign as evidence of a favourable Mn-Ar interaction.[151,152] In PFTEA solution however, coordination of Ar to the metal centre seems unlikely. In previous matrix isolation studies under steady-state low intensity illumination, $^1CpMn(CO)_2$ has

been noted as the primary photoproduct of $CpMn(CO)_3$.[53] In contrast, experiments utilising short, high intensity laser pulses have noted $^3CpMn(CO)_2$ as the primary photoproduct,[150,186,187] in agreement with the spectra presented here. While the final identity of this complex cannot be determined from these results, two possibilities present themselves. It is possible that this complex is a coordinatively unsaturated 16-electron singlet complex $^1CpMn(CO)_2$. Alternatively, it is also possible that the PFTEA solvent may be coordinating to the metal at early time, possibly through a different coordination mode to the longer lived $^1CpMn(CO)_2(N(C_2F_5)_3)$ complex. Neither of these explanations satisfactorily account for the fact that this phenomenon has not been observed previously in either PFH or PFMCH. It is possible that PFTEA may present a coordination mode which is fundamentally different to those of the perfluoroalkanes (e.g., through the N atom lone pair).

Despite the presence of these two features, a spin-forbidden reaction does occur on the nanosecond timescale, as expected. In this case, $^3CpMn(CO)_2$ decays to form a species which exhibits two ν(CO) bands at 1965 and 1899 cm^{-1}. Following this reaction, the intensity of the ν(CO) bands of this new species is observed to be much larger than that of the unidentified intermediate above, suggesting that formation of this new product dominates in this case. The two ν(CO) bands at 1965 and 1899 cm^{-1} are assigned to $^1CpMn(CO)_2(N(C_2F_5)_3)$. The spin-forbidden reaction itself occurs with a lifetime of τ = 36 ($\pm$4) ns, *ca.* 2x slower than observed in PFMCH, suggesting that PFTEA may be more inert than even the perfluoroalkane. TRIR kinetic traces for this process are given in Figure 2.35. $^1CpMn(CO)_2(N(C_2F_5)_3)$ exhibits no evidence of decay to form the dimer on a nanosecond timescale.

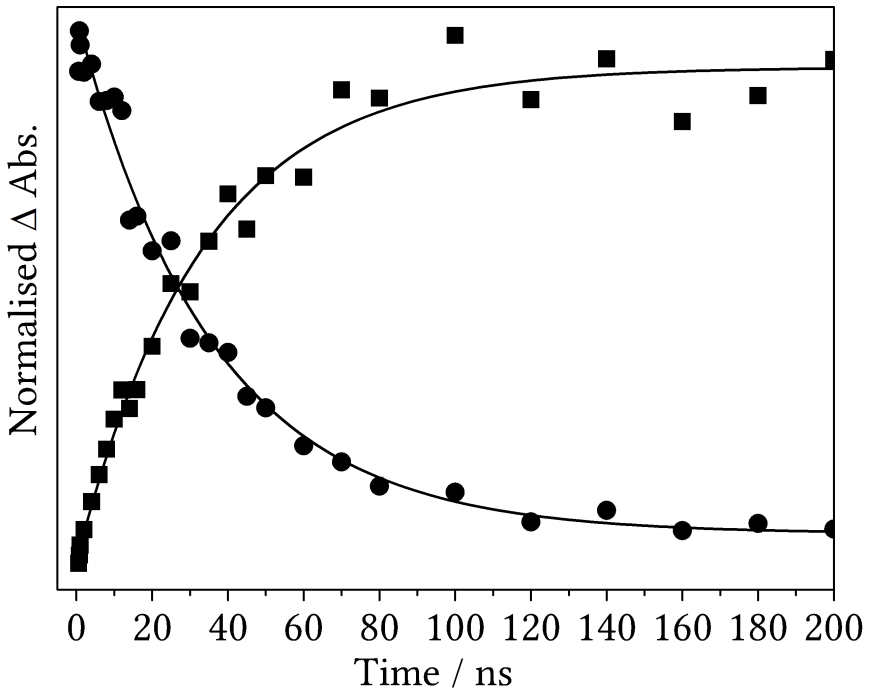


FIGURE 2.35: Nanosecond kinetic traces from $TR^{M}PS$ difference spectra recorded following 266 nm irradiation of $CpMn(CO)_3$ in PFTEA solution, under Ar atmosphere, showing matching rates for the decay of $^{3}CpMn(CO)_2$ at 2006 cm^{-1} (circles) and formation of $^{1}CpMn(CO)_2(N(C_2F_5)_3)$ at 1899 cm^{-1} (squares). Solid lines are mono-exponential fits.

As above for the perfluorinated alkane PFH, solutions of $CpMn(CO)_3$ in PFTEA were doped with *n*-heptane and Xe in order to determine if this solvent will allow coordination of these weakly binding ligands at room temperature. *n*-heptane was added to a solution of $CpMn(CO)_3$ in PFTEA doped with *n*-heptane (0.5 M), as above. This solution was photolysed at 266 nm, and a series of $TR^{M}PS$ difference spectra were recorded. On a picosecond timescale following photolysis, the ν(CO) bands of the parent $CpMn(CO)_3$ were bleached and two new bands at 2005 and 1855 cm^{-1} were observed, indicating fast formation of $^{3}CpMn(CO)_2$ as expected from experiments in pure PFTEA. After 100 ps, the two additional ν(CO) bands at 1973 and 1904 cm^{-1} observed previously were also present. As seen previously, these bands were stable on a

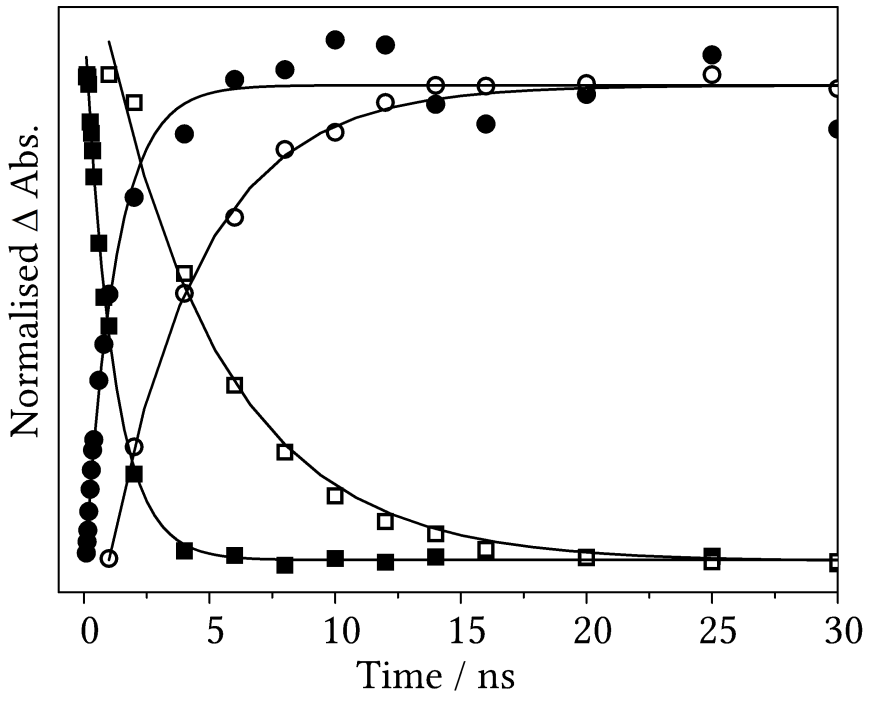


FIGURE 2.36: Kinetic traces from TR^MPS spectra recorded following 266 nm irradiation of $CpMn(CO)_3$ in PFTEA doped with *n*-heptane (0.5 M) under 1.5 bar Ar showing matching rates for the decay of $^3CpMn(CO)_2$ at 2006 cm^{-1} (closed squares) and formation of $^1CpMn(CO)_2(C_7H_{16})$ at 1897 cm^{-1} (closed circles). Nanosecond kinetic traces from TR^MPS spectra recorded following 266 nm irradiation of $CpMn(CO)_3$ in Xe saturated PFTEA solution, under 1.5 bar Xe. Matching rates for the decay of $^3CpMn(CO)_2$ at 2006 cm^{-1} (open squares) and formation of $^1CpMn(CO)_2Xe$ at 1898 cm^{-1} (open circles) can be seen. Solid lines are mono-exponential fits. Note, the first time delay reported for photolysis in the presence of Xe is 1 ns.

nanosecond timescale and did not increase in intensity concurrently with the decay of $^3CpMn(CO)_2$. As expected, the ν(CO) bands of $^3CpMn(CO)_2$ were observed to decay, giving way to two new ν(CO) bands at 1963 and 1897 cm^{-1}. This process occurred at a faster rate than that observed in pure PFTEA ($\tau = 1.0$ (± 0.1) ns), matching the lifetime for the analogous process observed in PFTEA doped with *n*-heptane (0.5 M). The product of the spin-forbidden reaction in this case is assigned as $^1CpMn(CO)_2(C_7H_{16})$, which is stable on a nanosecond timescale.

Following this, a solution of $CpMn(CO)_3$ in PFTEA was prepared under a Xe

atmosphere and held under 1.5 bar pressure of Xe during recording of a series of TR^MPS difference spectra. On a picosecond timescale after 266 nm photolysis, the two ν(CO) bands of the 16-electron triplet $^3CpMn(CO)_2$ were observed as above, as were the two ν(CO) bands at 1973 and 1904 cm^{-1}. $^3CpMn(CO)_2$ was observed to decay to form a species with ν(CO) bands at 1965 and 1898 cm^{-1}. The rate of this process was observed to match that of the analogous reaction in Xe-doped PFH, as well as Xe-doped PFMCH (τ = 4.1 ($\pm$0.4) ns). TRIR kinetic traces for *n*-heptane and Xe-doped solutions of $CpMn(CO)_3$ in PFTEA are shown in Figure 2.36, and observed rate constants for all processes observed following photolysis of $CpMn(CO)_3$ in pure and doped PFTEA solution are given in Table 2.20. The product in this case was assigned as $^1CpMn(CO)_2Xe$, which was observed to be stable on a nanosecond timescale.

TABLE 2.20: Observed rate constants for the processes observed following 266 nm photolysis of $CpMn(CO)_3$ in PFTEA solution under Ar, PFTEA doped with *n*-heptane under Ar and PFTEA solution under 1.5 bar Xe, all experiments recorded at 298 K.

ν(CO) (cm^{-1})	**Assignment**	**k_{obs} (s^{-1})**
2006	$^3CpMn(CO)_2$	2.8 ($\pm$0.3) x 10^7
1855	$^3CpMn(CO)_2$	2.6 ($\pm$0.4) x 10^7
1965	$^1CpMn(CO)_2(N(C_2F_5)_3)$	2.7 ($\pm$0.3) x 10^7
1899	$^1CpMn(CO)_2(N(C_2F_5)_3)$	2.8 ($\pm$0.2) x 10^7
2005	$^3CpMn(CO)_2$	1.0 ($\pm$0.1) x 10^9
1855	$^3CpMn(CO)_2$	1.1 ($\pm$0.2) x 10^9
1963	$^1CpMn(CO)_2(C_7H_{16})$	9.1 ($\pm$1.0) x 10^8
1897	$^1CpMn(CO)_2(C_7H_{16})$	1.0 ($\pm$0.1) x 10^9
2006	$^3CpMn(CO)_2$	2.5 ($\pm$0.3) x 10^8
1855	$^3CpMn(CO)_2$	2.4 ($\pm$0.4) x 10^8
1965	$^1CpMn(CO)_2Xe$	2.5 ($\pm$0.2) x 10^8
1898	$^1CpMn(CO)_2Xe$	2.4 ($\pm$0.3) x 10^8

Both PFH and PFTEA have been shown to be useful non-coordinating solvents

for the characterisation of organometallic alkane and noble gas complexes at room temperature. This is especially surprising in the case of the perfluorinated amine PFTEA, which appears to exhibit high inertness despite the expected presence of a lone pair on the central N atom. Many of the small transition metal complexes of interest in these studies are more soluble in PFTEA than in PFH, or indeed even PFMCH. This increased ability to solvate molecules may lead PFTEA to be a very useful solvent in future spectroscopic studies.

2.2.6.5 TRIR Spectroscopy of (MeCp)Mn(CO)$_3$ in Perfluoro(methylcyclohexane)

Following experiments on the photochemistry of CpMn(CO)$_3$ in a variety of perfluorinated solvents, as presented above, this study was expanded to include other organometallic complexes which have been reported to form a long-lived coordinatively unsaturated intermediate upon photolysis. The first of such species to be studied was a widely available Cp-substituted derivative of CpMn(CO)$_3$, (MeCp)Mn(CO)$_3$ (MeCp = methylcyclopentadienyl). The chemistry of these Cp-substituted derivatives is known to be similar to that of CpMn(CO)$_3$, however the increased electron density on the Cp ring may lead to different kinetic behaviour in weakly binding solvents due to the change in electron density at the central Mn atom.

In order to examine the interactions of this Cp-substituted derivative with PFMCH, it was first photolysed at 266 nm in PFMCH solution under an Ar atmosphere. A series of TR^{M}PS difference spectra recorded following photolysis are presented in Figure 2.37. Within 1 ps of photolysis, the two ν(CO) bands of the parent (MeCp)Mn(CO)$_3$

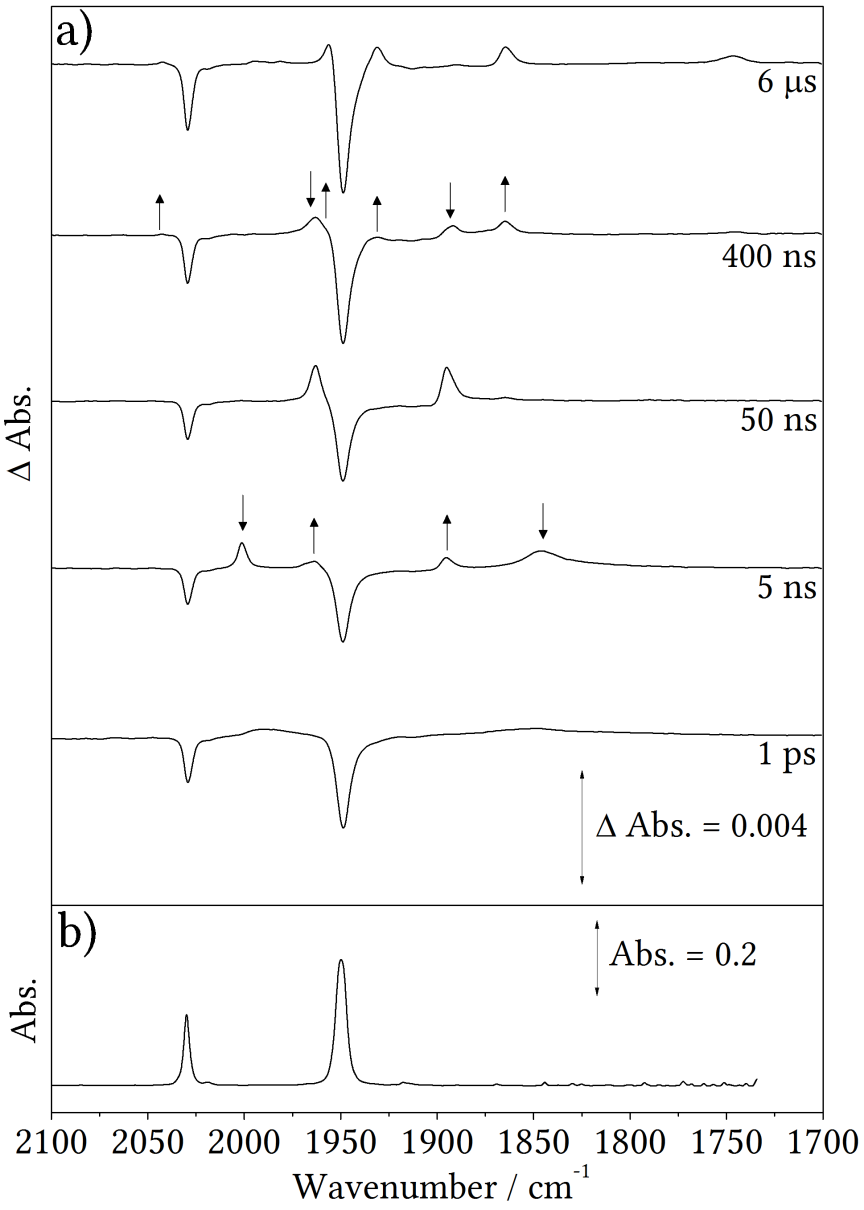


FIGURE 2.37: a) Selected picosecond, nanosecond and microsecond TR^{M}PS difference spectra recorded at a series of time delays following 266 nm photolysis of a solution of (MeCp)Mn(CO)$_3$ in PFMCH. Formation and decay of ^{3}(MeCp)Mn(CO)$_2$, subsequent formation and decay of ^{1}(MeCp)Mn(CO)$_2$(C_7F_{14}), and finally formation of (MeCp)$_2$Mn$_2$(CO)$_5$ can be observed. b) FTIR spectrum of same solution.

complex (2030 and 1950 cm^{-1}) were depleted and two new broad features were observed. These new features were seen to sharpen and blue-shift indicating vibrational cooling over the first 30 ps of the experiment. This rate of vibrational cooling of the initial

intermediate is as expected from photolysis of $CpMn(CO)_3$ in PFMCH, described earlier in this Chapter. Following this vibrational cooling process, these features yield two ν(CO) bands at 2002 and 1846 cm^{-1}, exhibiting the characteristically large $\Delta\nu$ of the coordinatively unsaturated 16-electron complex $^3(MeCp)Mn(CO)_2$.[53] These two ν(CO) bands are therefore assigned to this complex. The TR^MPS difference spectrum recorded 5 ns after photolysis shows the two ν(CO) bands of $^3(MeCp)Mn(CO)_2$, as well as two new ν(CO) bands at 1962 and 1895 cm^{-1}. These two bands continue to grow as those of $^3(MeCp)Mn(CO)_2$ decay, indicating formation of a Mn-solvent complex directly from $^3(MeCp)Mn(CO)_2$, as observed previously in this Chapter for both $Fe(CO)_5$ and $CpMn(CO)_3$. These two new bands are therefore assigned to $^1(MeCp)Mn(CO)_2(C_7F_{14})$. The rate of the reaction of $^3(MeCp)Mn(CO)_2$ with the PFMCH solvent in this case (lifetime τ = 18 ($\pm$2) ns) is within error of that observed for the reaction of the unsubstituted $^3CpMn(CO)_2$ with PFMCH. This indicates that although there is a small change in electron density on the metal centre upon moving from $CpMn(CO)_3$ to $(MeCp)Mn(CO)_3$, as indicated by the decreased ν(CO) band frequencies observed for $(MeCp)Mn(CO)_3$, $^3(MeCp)Mn(CO)_2$ and $^1(MeCp)Mn(CO)_2(C_7F_{14})$ compared to their Cp-unsubstituted equivalents, this change in electron density does not affect the rate of the spin-forbidden reaction.

Examination of spectra recorded at later time delays, however, does reveal a difference between the photochemistry of $CpMn(CO)_3$ and $(MeCp)Mn(CO)_3$ following photolysis in PFMCH solvent. The difference spectrum recorded 50 ns following photolysis shows a new small feature at 1865 cm^{-1}, which continues to grow concurrently with the decay of the two ν(CO) bands of $^1(MeCp)Mn(CO)_2(C_7F_{14})$. The growth of

TABLE 2.21: ν(CO) absorption band frequencies of (MeCp)Mn(CO)$_3$ and intermediates produced following photolysis of (MeCp)Mn(CO)$_3$ in pure PFMCH, as well as PFMCH doped with 1.5 bar Xe, 1.5 bar methane and 1.5 bar ethane.

Compound	**Dopant**	**ν(CO) (cm^{-1})**
(MeCp)Mn(CO)$_3$		2030, 1950
	Xe	2030, 1950
	CH_4	2030, 1950
	C_2H_6	2030, 1950
^{3}(MeCp)Mn(CO)$_2$		2002, 1846
	Xe	2002, 1846
	CH_4	2002, 1846
	C_2H_6	2002, 1846
^{1}(MeCp)Mn(CO)$_2$X		1962, 1895
	Xe	1960, 1893
	CH_4	1961, 1892
	C_2H_6	1959 , 1892
(MeCp)$_2$Mn$_2$(CO)$_5$		2046, 1956, 1930, 1865, 1746

this new ν(CO) band is accompanied by the growth of an additional small feature at 2046 cm^{-1}, and features at 1956, 1930 and 1746 cm^{-1}. A summary of all ν(CO) band positions for (MeCp)Mn(CO)$_3$ and any intermediates or photoproducts observed during these experiments is present in Table 2.21.

Earlier in this Chapter, formation of $Cp_2Mn_2(CO)_5$ was considered as a possible decay pathway for the singlet solvent complex formed following photolysis of CpMn(CO)$_3$ in perfluorohexane. In that case, there was insufficient evidence to conclusively assign this photoproduct. In this study however, it appears that the final photoproduct is a dimeric species. Several of the ν(CO) bands observed in this study (1956, 1930 and 1746 cm^{-1}) show agreement those observed by Creaven *et al.* in *n*-heptane solution (1955, 1934 and 1740 cm^{-1}).[162] Of particular note is the presence of the bridging ν(CO) band at 1746 cm^{-1}. In addition to this agreement with previous work, the two bleached ν(CO) parent bands of (MeCp)Mn(CO)$_3$ were seen undergo further

bleaching on the same timescale as formation of the final photoproduct. This additional bleaching of the parent ν(CO) bands suggests further depletion of the parent complex, indicative of a possible reaction between (MeCp)Mn(CO)$_3$ and ^{1}(MeCp)Mn(CO)$_2$(C_7F_{14}) to form the dinuclear complex (MeCp)$_2$Mn$_2$(CO)$_5$. The final photoproduct in this study is therefore assigned as (MeCp)$_2$Mn$_2$(CO)$_5$. In contrast to the experiments presented above for CpMn(CO)$_3$ in PFMCH, in which the solvent complex was shown to be stable on the nanosecond and early microsecond timescales, ^{1}(MeCp)Mn(CO)$_2$(C_7F_{14}) decays to form (MeCp)$_2$Mn$_2$(CO)$_5$ on the nanosecond timescale. It is unlikely that this increased propensity to formation of the dimeric complex comes as a result of the increased amount of electron density donated to the metal centre by the methylcyclopentadienyl ring, compared to the unsubstituted cyclopentadienyl ring. In addition, due to the small change in electron density donated from the ring, confirmed by the small *ca.* 2-5 cm^{-1} change in ν(CO) band frequencies between CpMn(CO)$_3$ and (MeCp)Mn(CO)$_3$, any other effects caused by this change in electron density would also be expected to be subtle. Previously, sterics have been shown to be an important factor in formation of such dimeric complexes.[163] It is probable in this case that other factors (e.g., solution concentration) are affecting the formation of this dimeric species.

Following photolysis of a solution of (MeCp)Mn(CO)$_3$ in pure PFMCH solution, a series of experiments were performed to examine the effect of gaseous dopants on the photochemistry of (MeCp)Mn(CO)$_3$ in perfluorinated solvents. In this case, the gaseous dopants of interest were the noble gas Xe, and the alkanes methane and ethane. Samples solutions were prepared under an atmosphere of the dopant gas of interest as above, and held under 1.5 bar for the duration of the experiment.

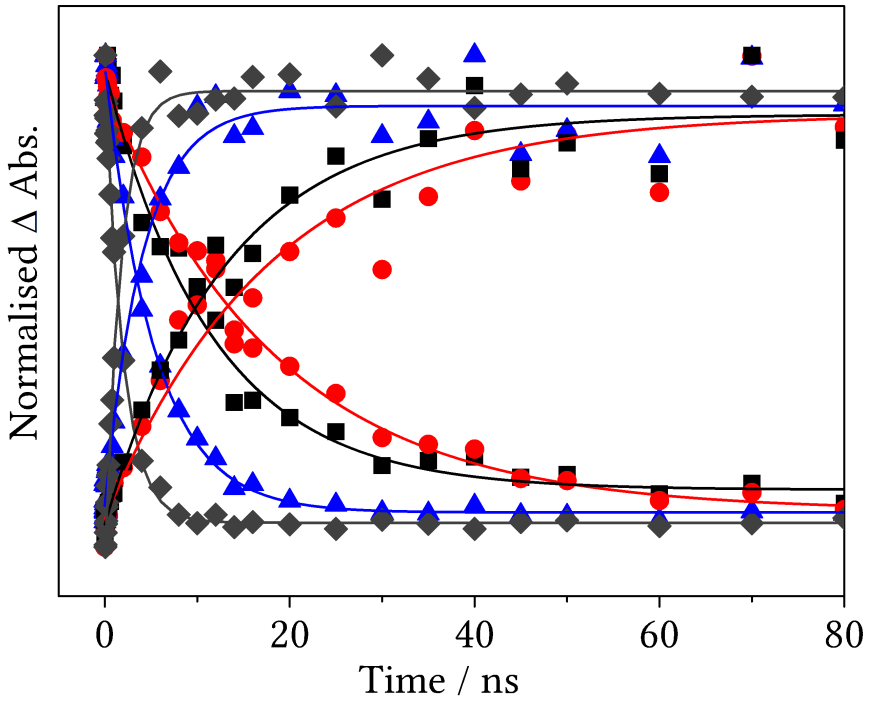


FIGURE 2.38: Kinetic traces from TR^{M}PS spectra recorded following 266 nm irradiation of $(MeCp)Mn(CO)_3$ in a series of PFMCH solutions. Matching rates for the decay of $^{3}(MeCp)Mn(CO)_2$ and formation of $^{1}(MeCp)Mn(CO)_2X$ are shown, where X = PFMCH (red circles), Xe (blue triangles), CH_4 (black squares) and C_2H_6 (grey diamonds). Solid lines are mono-exponential fits.

In all three cases photolysis was followed immediately by depletion of the two parent ν(CO) bands, and formation of two broad features. These features sharpened and blue-shifted over the first 30 ps of the experiment to yield two ν(CO) bands at 2002 and 1846 cm^{-1}, consistent with those observed in the pure solvent. These bands were observed to decay concurrently with formation of two new bands, corresponding to the dopant complex $^{1}(MeCp)Mn(CO)_2X$. The rate of this spin-forbidden reaction was observed to be different for each dopant, and was shown to be faster than that observed in pure PFMCH in every case. Kinetic traces from TR^{M}PS difference spectra are given in Figure 2.38, while lifetime values for the reaction of $^{3}CpMn(CO)_2$ with solvent or dopant in pure and doped PFMCH solutions are given in Table 2.22.

TABLE 2.22: Lifetimes (in ns) for the spin-forbidden reaction of ^{3}(MeCp)Mn(CO)$_2$ to form ^{1}(MeCp)Mn(CO)$_2$X (X = solvent or dopant) following photolysis of (MeCp)Mn(CO)$_3$ in a series of PFMCH/dopant systems (all data recorded at 298 K). Values for corresponding reactions following photolysis of CpMn(CO)$_3$ in various PFMCH/dopant solutions are included for comparison

Complex	**Dopant**	**Lifetime τ (ns)**
CpMn(CO)$_3$		18 (±2)
	Xe	4.5 (±0.5)
	CH_4	13 (±2)
	C_2H_6	2 (±0.2)
(MeCp)Mn(CO)$_3$		18 (±2)
	Xe	3.9 (±0.4)
	CH_4	19 (±4)*
	C_2H_6	1.9 (±0.2)

Both Xe and ethane undergo a reaction with the unsaturated 16-electron complex ^{3}(MeCp)Mn(CO)$_2$ at a rate many times faster than that of the pure PFMCH solvent. Both of these lifetime values are consistent with those observed for formation of the equivalent complexes following photolysis of CpMn(CO)$_3$, suggesting that the addition of a methyl substituent to the Cp ring has little, if any, effect on the spin-forbidden reaction. These matching lifetime values are also consistent with the agreement between lifetimes observed for formation of ^{1}CpMn(CO)$_2$X in pure PFMCH solvent for CpMn(CO)$_3$ and (MeCp)Mn(CO)$_3$. These observations suggest the formation of ^{1}(MeCp)Mn(CO)$_2$Xe and ^{1}(MeCp)Mn(CO)$_2$(C_2H_6) in solution following photolysis of (MeCp)Mn(CO)$_3$.

Results presented earlier in this Chapter recorded following photolysis of CpMn(CO)$_3$ in PFMCH doped with CH_4, showed no conclusive evidence for formation of ^{1}CpMn(CO)$_2$(CH_4) in room temperature solution. The rate of the spin-forbidden reaction in that case was found to be within error of that for the PFMCH solvent alone, suggesting either a very similar rate of reaction for these two ligands, or the absence of any formation of ^{1}CpMn(CO)$_2$(CH_4). In this case however, the lifetime for this

process (τ = 13 ($\pm$2) ns) is faster than that observed in the pure solvent. The product of the spin-forbidden reaction is tentatively assigned as ^{1}(MeCp)Mn(CO)$_2$(CH$_4$), due to the difference in observed reaction rate between pure PFMCH solution, and CH$_4$ doped PFMCH solution, as well as the difference in ν(CO) band positions of the ^{1}(MeCp)Mn(CO)$_2$X complexes formed in these cases, as shown in Figure 2.39. A summary of the observed rate constants for the spin-forbidden reaction of ^{3}(MeCp)Mn(CO)$_2$ to form ^{1}(MeCp)Mn(CO)$_2$X (X = solvent or dopant) is given in Table 2.23.

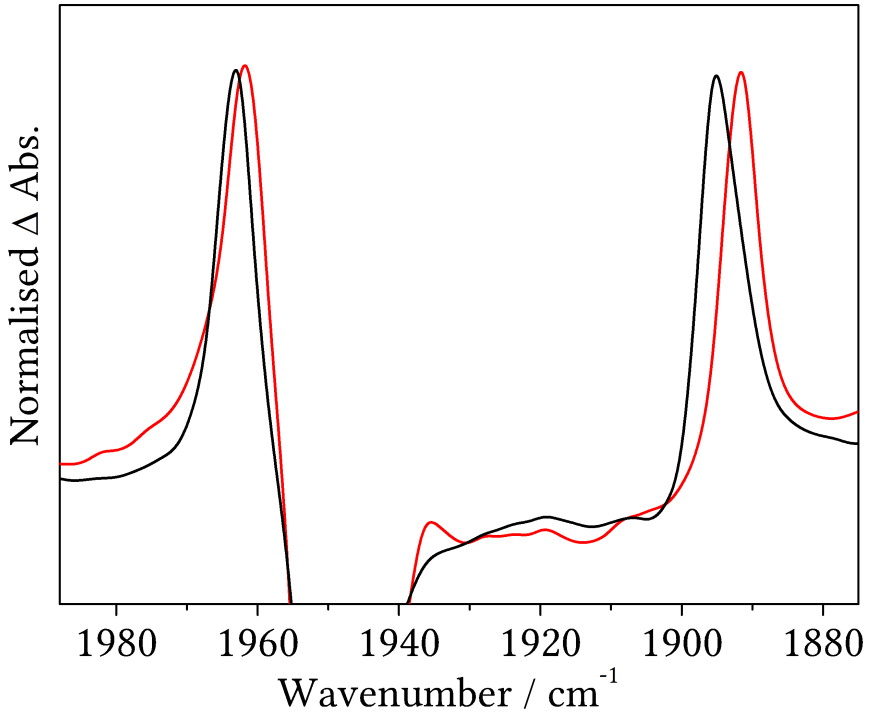


FIGURE 2.39: Expanded TR^{M}PS spectrum recorded 30 ns following photolysis of (MeCp)Mn(CO)$_3$ in PFMCH showing ν(CO) bands of ^{1}(MeCp)Mn(CO)$_2$(C$_7$F$_{14}$) (black), and 30 ns following photolysis of (MeCp)Mn(CO)$_3$ in PFMCH doped with 1.5 bar CH$_4$ (red), showing ν(CO) bands of ^{1}(MeCp)Mn(CO)$_2$(CH$_4$).

The overall trend for reaction rate to form ^{1}(MeCp)Mn(CO)$_2$X in the series of doped solutions studied above is as follows, from fastest to slowest: C$_2$H$_6$ > Xe > CH$_4$ > PFMCH. These observations are largely consistent with the observed trend

TABLE 2.23: Observed rate constants for the spin-forbidden reaction following 266 nm photolysis of $(MeCp)Mn(CO)_3$ in a series of PFMCH solutions at 298 K.

ν(CO) (cm^{-1})	Assignment	k_{obs} (s^{-1})
2002	$^3(MeCp)Mn(CO)_2$	5.6 (±0.5) x 10^7
1846	$^3(MeCp)Mn(CO)_2$	5.8 (±0.4) x 10^7
1962	$^1(MeCp)Mn(CO)_2(C_7F_{14})$	5.5 (±0.3) x 10^7
1895	$^1(MeCp)Mn(CO)_2(C_7F_{14})$	5.6 (±0.3) x 10^7
2002	$^3(MeCp)Mn(CO)_2$	2.5 (±0.3) x 10^8
1846	$^3(MeCp)Mn(CO)_2$	2.3 (±0.3) x 10^8
1960	$^1(MeCp)Mn(CO)_2Xe$	2.4 (±0.4) x 10^8
1893	$^1(MeCp)Mn(CO)_2Xe$	2.6 (±0.4) x 10^8
2002	$^3(MeCp)Mn(CO)_2$	7.7 (±1) x 10^7
1846	$^3(MeCp)Mn(CO)_2$	7.3 (±0.8) x 10^7
1962	$^1(MeCp)Mn(CO)_2(CH_4)$	7.5 (±0.7) x 10^7
1894	$^1(MeCp)Mn(CO)_2(CH_4)$	7.1 (±1) x 10^7
2002	$^3(MeCp)Mn(CO)_2$	5.1 (±0.4) x 10^8
1846	$^3(MeCp)Mn(CO)_2$	5.2 (±0.3) x 10^8
1959	$^1(MeCp)Mn(CO)_2(C_2H_6)$	5.2 (±0.3) x 10^8
1893	$^1(MeCp)Mn(CO)_2(C_2H_6)$	5.4 (±0.4) x 10^8

reported for the rate of the recombination reaction of $^1CpMn(CO)_2X$ with CO in a series of pure liquid and supercritical alkanes and noble gases.[34] This trend also closely follows observations reported above for $CpMn(CO)_3$. It is evident from these studies that the addition of a methyl substituent onto the Cp ring has little to no effect on the spin-forbidden reaction of $^3(MeCp)Mn(CO)_2$ with PFMCH, or indeed gaseous dopants, when compared with $CpMn(CO)_3$.

2.2.7 Discussion of the Reaction Mechanism Following Photolysis of $CpMn(CO)_3$

It is clear from the results presented in this Chapter that the intermediates and photoproducts formed following photolysis of $CpMn(CO)_3$ and $(MeCp)Mn(CO)_3$ are dependent on the nature of the solvent, as well as any dopants present in the solution. Following 266 nm photolysis, a 16-electron coordinatively unsaturated species of the form $^3CpMn(CO)_2$ is formed. This species appears to be a primary photoproduct, appearing in a vibrationally hot state immediately following photolysis. As stated above, this is the expected route for formation of this triplet species when utilising short-duration laser pulses.[150–152,186,187] When photolysis is performed with a low intensity light source in steady-state, the primary photoproduct is $^1CpMn(CO)_2$.[53] Some evidence for formation of $^1CpMn(CO)_2$ has been observed during the studies presented in this Chapter following photolysis of $CpMn(CO)_3$ in the perfluorinated amine PFTEA. In this case, $^1CpMn(CO)_2$ was formed as a minor primary photoproduct, which decayed on the nanosecond timescale either to further form the major primary photoproduct $^3CpMn(CO)_2$, or the dicarbonyl solvent complex $^1CpMn(CO)_2(N(C_2F_5)_3)$.

Following formation of $^3CpMn(CO)_2$ within 1 ps of irradiation, the triplet species undergoes a spin-forbidden reaction to form $^1CpMn(CO)_2X$ (X = solvent or dopant). This reaction occurs on a picosecond or nanosecond timescale, with the rate seemingly dependent on the solvent or dopant with which $^3CpMn(CO)_2$ is reacting. While the rate of reaction and the ν(CO) band positions of $^1CpMn(CO)_2X$ appear to be dependent on the nature of X, the ν(CO) absorption frequencies of $^3CpMn(CO)_2$ do not. This

suggests that any interaction of $^3CpMn(CO)_2$ with the solvent or dopant prior to spin-state change is very weak.

In order to examine the nature of interaction between $^3CpMn(CO)_2$ and the ligands it subsequently undergoes spin-forbidden reaction with, theoretical calculations were carried out by Dr. Zhen Liu and Prof. Jeremy Harvey at KU Leuven. Preliminary results are presented below. Firstly, relative energies (including zero-point energy) were calculated for the triplet and singlet states of a series of $^3CpMn(CO)_2$ and $^1CpMn(CO)_2X$ systems, and the minimum energy crossing point (MECP) for spin-crossover between the two states. The MECP is defined at the lowest energy point at which the potential energy surfaces of the triplet and singlet species cross. The energies were calculated by DFT, using a dispersion correctly modified form of B3LYP. Preliminary calculations showed the possibility of two distinct triplet states, differing in terms of orbital occupation and geometry, specifically the OC-M-CO bond angles, with the complex exhibiting the largest bond angles predicted to be the most stable. Table 2.24 shows the results of these calculations for a number of solvent and dopant systems.

TABLE 2.24: Calculated relative energies for $^3CpMn(CO)_2$ and $^1CpMn(CO)_2X$ for a series of ligands (X = None, Xe, CO_2, ethane, *n*-heptane, PFMCH). Energies were calculated by DFT using dispersion corrected B3LYP**-D3BJ. Energies are presented in kcal/mol.

X =	**None**	**Xe**	**CO_2**	**Ethane**	**Heptane**	**PFMCH**
$^3CpMn(CO)_2$	0.0	0.0	0.0	0.0	0.0	0.0
$^1CpMn(CO)_2X$	2.9	-4.6	-6.2	-9.3	-6.9	-2.2
MECP	3.8	4.2	2.6	1.6	0.8	4.1

Table 2.24 shows the results of these calculations for a number of solvent and dopant systems. In the absence of a ligand, it can be seen that the triplet state is the ground state, while in the presence of a ligand, the singlet state is the ground state in

all cases. The MECP is highest for reactions with Xe and PFMCH, and smallest for reaction with heptane, in agreement with experimentally measured reaction rates for spin-forbidden reaction reported previously in this Chapter. A correlation is also noted between the calculated energy of the singlet state and the experimentally determined reaction rate for this series of ligands, with $^{1}CpMn(CO)_2(C_7F_{14})$ lying highest in energy, and the alkane complexes $^{1}CpMn(CO)_2(C_2H_6)$ and $^{1}CpMn(CO)_2(C_7H_{16})$ lying lowest in energy. It should be noted that for PFMCH and heptane, there is a large amount of conformational complexity for both singlet and triplet adducts. Although all best efforts have been made to find the lowest energy state of each of these species, it is conceivable that this complexity will have an effect on calculated energies, as well as calculated reaction rates.

Spin-forbidden rate constants for the series of ligand and dopant systems were also calculated in a similar fashion to those reported previously.[125] Rate constants for passage through the MECP from triplet to singlet for each of the ligands were calculated, and are presented in Table 2.25 along with experimentally determined observed rate constants.

While the calculated absolute values for the rate constants of these spin-forbidden reactions do not appear to match particularly well with experimentally obtained values, it is still interesting to note the general trend in rate. The reaction with PFMCH is calculated to be the slowest, in agreement with experimental results presented earlier in this Chapter, while the reaction with heptane is calculated to be the fastest. One possible reason for the poor match may lie in the structure of the triplet species used in these calculations. Interestingly, the lowest energy configuration for the triplet state was

TABLE 2.25: Calculated rate constants for the spin-crossover reaction of $^3CpMn(CO)_2$ to form $^1CpMn(CO)_2X$ for a series of ligands (X = None, Xe, CO_2, ethane, heptane, PFMCH). Experimentally measured observed rate constants for the same process are also given for comparison. All values in s^{-1}. *The rate constant for the reaction of ethane with $^3CpMn(CO)_2$ is subject to a discrepancy caused by sensitivity to the procedure for moderation of vibrational frequencies, however this value has been included for consistency.

Ligand	**Calculated**	**Experimental**
None	3.6×10^9	
Xe	1.1×10^9	2.5×10^8
CO_2	4.9×10^{10}	2×10^8
Ethane	4.6×10^7*	5×10^8
Heptane	2.3×10^{11}	9.0×10^9
PFMCH	1.8×10^9	6×10^7

obtained when the metal complex of interest is weakly solvated by the ligand of interest. In most cases however, this interaction is very weak and an equilibrium between the free and solvated forms of the triplet species would be expected in solution. Calculated structures for all species are shown in Figure 2.40. This opens up the possibility of of competing reaction pathways to form the singlet species. Further studies will be undertaken to determine the effect of these competing pathways.

The possibility of a triplet species that interacts weakly with the solvent or dopant of interest before undergoing a spin-state change presents an interesting contrast to kinetic studies reported previously.[83,125,139,219] In these studies, the potential energy surface of the unsaturated triplet species was assumed to remain unchanged by the addition of a ligand, with the MECP for the reaction being controlled by any changes in the potential energy surface of the bound singlet species, caused by interaction with the ligand. In the case of a bound triplet state however, the ligand may exert influence on the potential energy surfaces of both triplet and singlet species. This mechanism of influence is in stark contract to the one presented by Besora *et al.*,[125] in which

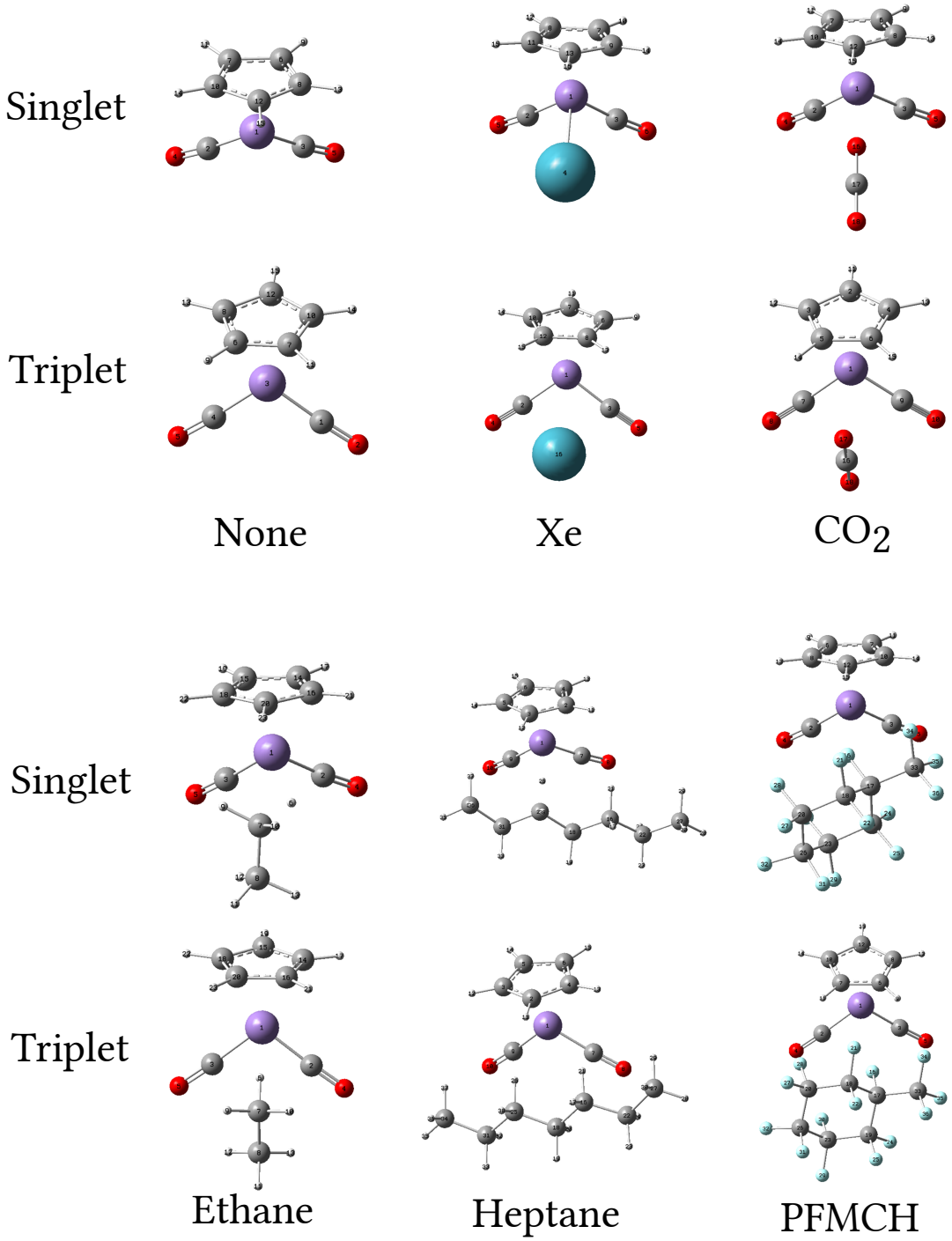
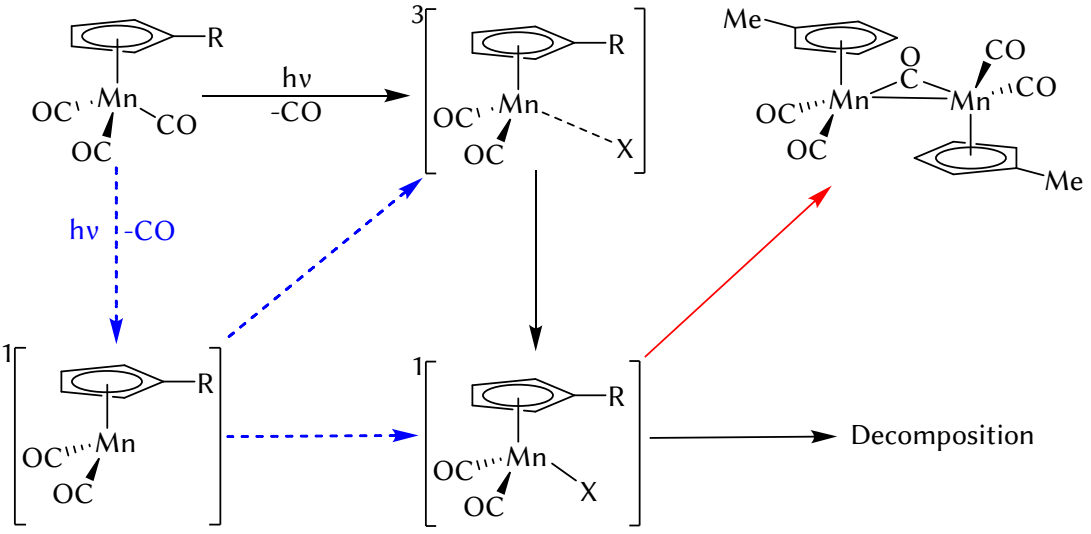


FIGURE 2.40: Calculated lowest energy geometries for $^3CpMn(CO)_2$ and $^1CpMn(CO)_2X$ intermediates formed following photolysis of $CpMn(CO)_3$ in a series of solutions, where X = None, Xe, CO_2, ethane, heptane and PFMCH.

a 'naked' $^{3}Fe(CO)_4$ undergoes a single-body spin-crossover to form $^{1}Fe(CO)_4$, which either reverts to the triplet, or is trapped by the ligand and undergoes a barrierless process to form $^{1}Fe(CO)_4X$. Through combination of experimental and theoretical results, a reaction mechanism for photolysis of $CpMn(CO)_3$ can be proposed, shown in Scheme 2.6.



SCHEME 2.6: Proposed reaction mechanism following photolysis of $CpMn(CO)_3$ or $(MeCp)Mn(CO)_3$ in a series of alkane and perfluorinated alkane or amine solvent systems, including various doped and mixed solvent systems. (R = H, Me. X = *n*-heptane, *c*-pentane, PFMCH, PFH, PFTEA, Xe, CO_2, ethane. Blue dashed arrows represent minor pathways only observed for $CpMn(CO)_3$ in PFTEA. Red arrows represent pathways only observed for $(MeCp)Mn(CO)_3$. Products of the final decomposition step have not been identified.

2.2.8 TR^{M}PS of $CpCo(CO)_2$ and $CpV(CO)_4$ in Perfluoroalkanes

Following examination of the photochemistry of iron and manganese containing complexes in various alkane and perfluorinated solvents, these studies were expanded to include two other organometallic species which have been shown to form

metastable 16-electron triplet species upon UV photolysis, namely $CpCo(CO)_2$[142,220] and $CpV(CO)_4$.[54,147,193]

The first of these species to be examined was $CpCo(CO)_2$. A solution of $CpCo(CO)_2$ in PFMCH was prepared under an argon atmosphere and irradiated with 266 nm light, as above. Following irradiation, a series of TR^MPS difference spectra were recorded across the ps, ns and μs timescales, which are presented in Figure 2.41.

Within the first time delay following photolysis, the two ν(CO) bands of the parent $CpCo(CO)_2$ (2038 and 1978 cm^{-1}) have bleached and a new broad feature can be seen, lying across the lower energy of the two parent bands. These new features undergoes vibrational cooling over the first 30 ps of the experiment to yield a single ν(CO) band at 2001 cm^{-1}. This species is stable on the picosecond timescale, but on the nanoseond timescale begins to decay. Concurrent with this observed decay is the growth of two new ν(CO) bands, one in the terminal carbonyl region at 1971 cm^{-1}, and one in the bridging carbonyl region at 1825 cm^{-1}. The growth of these bands is accompanied by further consumption of the parent, indicating a reaction between an intermediate and the parent complex to form this new bridged dimeric product. The lifetime of this process was recorded as τ = 50 ($\pm$7) ns. This new bridged species is stable into the microsecond timescale. Rate constants for all observed processes are given in Table 2.27

It is clear from the presence of the bridging carbonyl band that the final product of this process is dimeric in nature, similar to the $(MeCp)_2Mn_2(CO)_5$ product observed earlier in this Chapter. However, unlike previous experiments involved photolysis

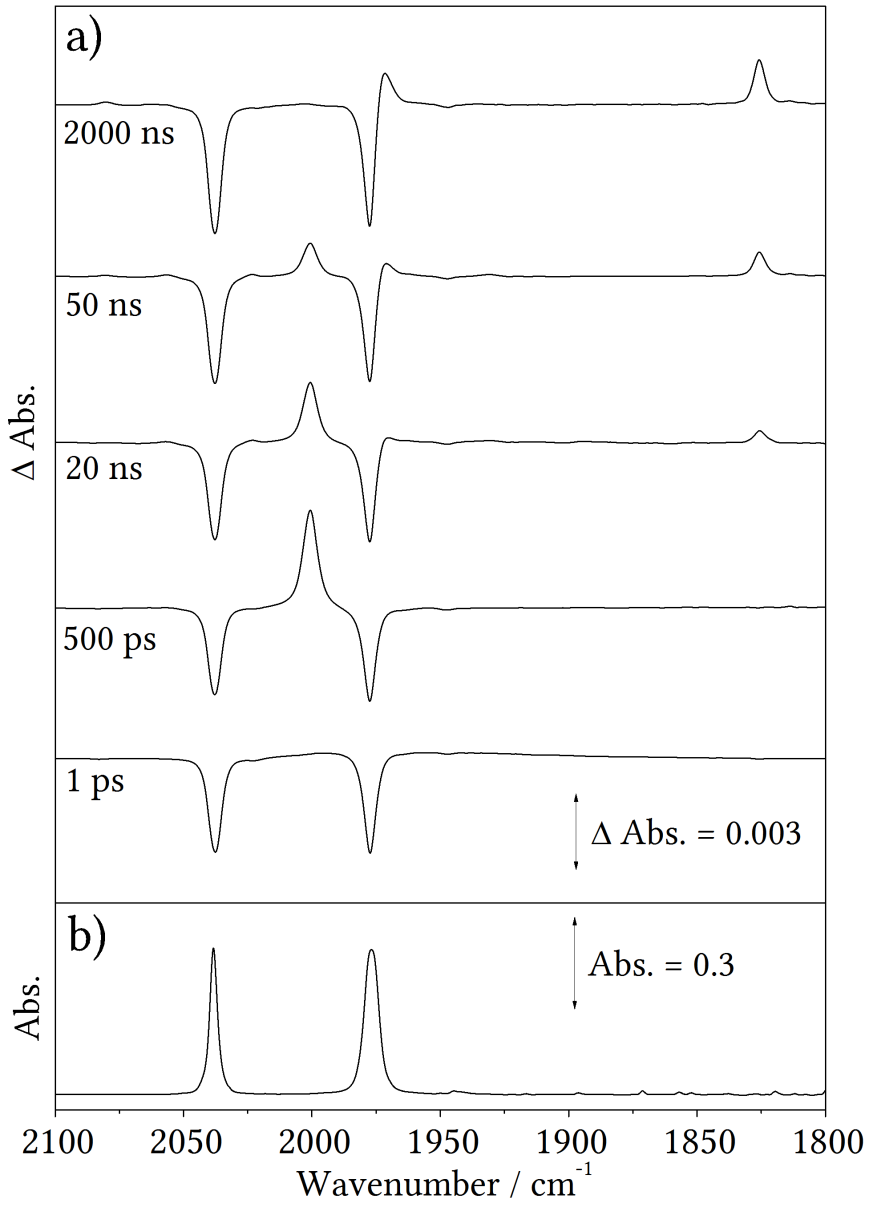


FIGURE 2.41: a) Selected picosecond, nanosecond and microsecond $TR^{M}PS$ difference spectra recorded at a series of time delays following 266 nm photolysis of a solution of $CpCo(CO)_2$ in PFMCH under Ar. Formation and decay of $^3CpCo(CO)$ and subsequent formation $Cp_2Co_2(CO)_3$ can be seen. Spectra recorded at 298 K. b) FTIR spectrum of same solution.

of $CpMn(CO)_3$ and $(MeCp)Mn(CO)_3$, $CpCo(CO)_2$ appears to form only a single intermediate following UV photolysis. This result is in agreement with the studies reported by Bengali *et al.*, in which $CpCo(CO)_2$ was photolysed in liquid noble gas

TABLE 2.26: ν(CO) absorption band frequencies of $CpCo(CO)_2$ and intermediates and photoproducts formed following photolysis of $CpCo(CO)_2$ and in pure liquid solvents.

Compound	Solvent	ν(CO) (cm^{-1})	Reference
$CpCo(CO)_2$	PFMCH	2038, 1978	This work
	PFH	2039, 1980	This work
	*liq*Kr	2037, 1977	142
	*liq*Xe	2031, 1971	142
	Cyclohexane	2030, 1969	191
$^3CpCo(CO)$	PFMCH	2001	This work
	PFH	2002	This work
	*liq*Kr	1999	142
	*liq*Xe	1993	142
	Cyclohexane	1990	191
$Cp_2Co_2(CO)_3$	PFMCH	1971, 1825	This work
	PFH	1973, 1826	This work
	*liq*Kr	1972, 1823	142
	*liq*Xe	1969, 1819	142
	Cyclohexane	1965, 1812	191
$Cp_2Co_2(CO)_2$	*liq*Xe	1805	142

solvents.[142] The authors reported initial formation of a single ν(CO) band at 1999 cm^{-1} or 1993 cm^{-1} in *liq*Kr and *liq*Xe, respectively, which they go on to assign to a coordinatively unsaturated 16-electron species $^3CpCo(CO)$. This fragment is assigned as a triplet with reference to previously published computational studies.[221–223] This unsaturated species then went on to decay, yielding three new ν(CO) bands, one in the terminal carbonyl region, and two in the bridging carbonyl region of the spectrum. Bands at 1969 cm^{-1} and 1819 cm^{-1} were assigned to the tricarbonyl dimer species $Cp_2Co_2(CO)_3$, in agreement with our results. The second bridging carbonyl band was assigned to a second dimer species, $Cp_2Co_2(CO)_2$, which was not observed during our experiments. ν(CO) band positions for all cobalt carbonyl species observed in these studies are summarised in Table 2.26. No evidence of coordination of the noble gas solvent was reported, and indeed the agreement of our results seems to suggest

a lack of coordination of PFMCH in this case. The results presented herein are also in agreement with those of Wasserman *et al.*, who noted no evidence of coordination of cyclohexane to the unsaturated ^{3}CpCo(CO) fragment, despite known interactions observed in comparable metal carbonyl fragments e.g., $^3Fe(CO)_4$ and $^3CpMn(CO)_2$.[191]

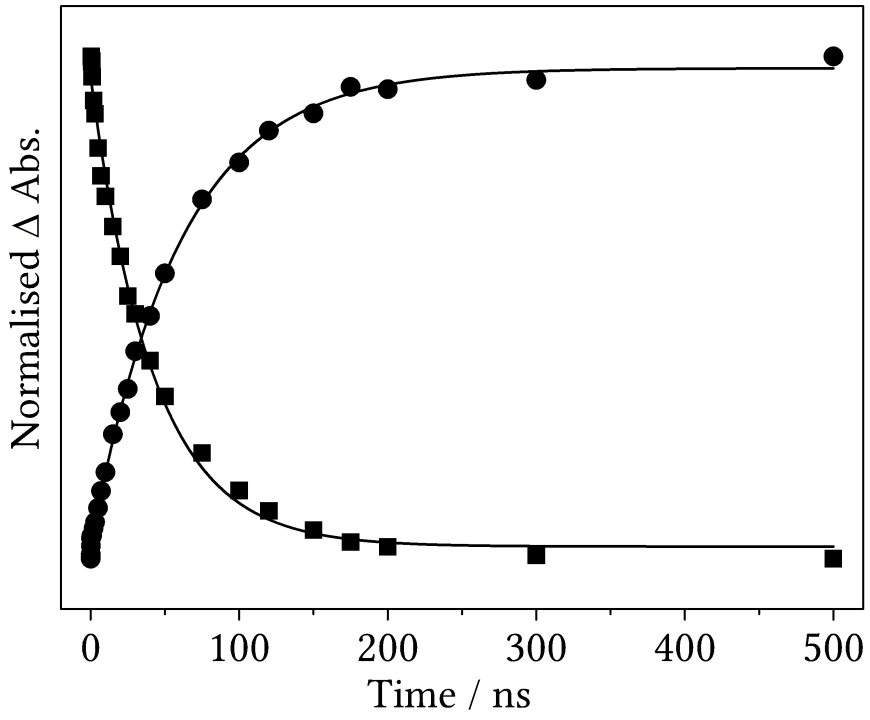


FIGURE 2.42: Kinetic traces from TR^{M}PS spectra recorded following 266 nm irradiation of $CpCo(CO)_2$ in PFMCH under Ar. Matching rates for the decay of ^{3}CpCo(CO) (squares) and formation of $Cp_2Co_2(CO)_3$ (circles) are shown. Solid lines are mono-exponential fits.

From these previous results, it might be expected that addition of Xe or liquid alkane to a solution of $CpCo(CO)_2$ in PFMCH would have little or no effect on the rate of reaction of $CpCo(CO)_2$ with ^{3}CpCo(CO) to form the dimer $Cp_2Co_2(CO)_3$, and this is indeed the case. Upon addition of Xe or *n*-heptane to the solution, neither the ν(CO) band positions of the photoproducts, nor the rate of formation of $Cp_2Co_2(CO)_3$ changes in a significant way. TR^{M}PS kinetic traces for the decay of ^{3}CpCo(CO) and

formation of $Cp_2Co_2(CO)_3$ are shown in Figure 2.42. Upon changing the solvent from PFMCH to PFH, the rate of reaction to form $Cp_2Co_2(CO)_3$ is still unchanged, while the positions of all ν(CO) parent bands show a small change of 1-2 cm^{-1}, indicative only of a change in the solvent environment. Somewhat expectedly, addition of Xe or *n*-heptane to a solution of $CpCo(CO)_2$ in PFH also yields no significant kinetic changes.

Compared to $CpMn(CO)_3$ and $Fe(CO)_5$, the photochemistry of $CpCo(CO)_2$ is unusual, and it appears to represent an exception regarding the coordination of solvents to its triplet intermediate. Previous experiments in THF and alcohol solvents have shown strong interactions between the solvent and the cobalt carbonyl fragment in both the triplet and singlet states.[145] Similar results were also observed in alkyne and alkene solutions.[146] DFT calculations have shown that the triplet state of $^3CpCo(CO)$ is favoured over the singlet by 13-26 kcal/mol, compared to 0-9 kcal/mol for $^3Fe(CO)_4$.[144] This result may go some way to explaining the exceptional photochemistry of $CpCo(CO)_2$.

As mentioned above, $CpV(CO)_4$ has also been previously reported to form a 16-electron unsaturated complex upon UV photolysis. In order to examine the effect of perfluoroalkane solvents on the formation and subsequent decay of this intermediate, TR^MPS spectra were recorded following 266 nm photolysis of $CpV(CO)_4$ in PFMCH and PFH solutions. A series of difference spectra recorded following photolysis of $CpV(CO)_4$ in PFMCH is shown in Figure 2.43.

The TR^MPS difference spectrum recorded 1 ps after photolysis clearly shows bleaching of the two parent ν(CO) bands at 2034 and 1942 cm^{-1}, and formation of a broad feature between the two parent bleaches. This feature sharpens and blue-shifts

TABLE 2.27: Observed rate constants for the spin-forbidden reaction observed following 266 nm photolysis of $CpCo(CO)_2$ and $CpV(CO)_4$ in a series of perfluoroalkane solutions at 298 K.

ν(CO) (cm^{-1})	Assignment	k_{obs} (s^{-1})
2001	$^3CpCo(CO)$	2.2 (±0.3) x 10^7
1971	$Cp_2Co_2(CO)_3$	1.9 (±0.2) x 10^7
1825	$Cp_2Co_2(CO)_3$	2.0 (±0.2) x 10^7
2024	$^3CpV(CO)_3$	3.1 (±0.3) x 10^6
1974	$^1CpV(CO)_3(C_7F_{14})$	3.3 (±0.6) x 10^6
1878	$^1CpV(CO)_3(C_7F_{14})$	3.0 (±0.2) x 10^6
2022	$^3CpV(CO)_3$	1.4 (±0.1) x 10^6
1975	$^1CpV(CO)_3(C_6F_{14})$	1.4 (±0.2) x 10^6
1879	$^1CpV(CO)_3(C_6F_{14})$	1.3 (±0.1) x 10^6
2022	$^3CpV(CO)_3$	1.7 (±0.1) x 10^6
1974	$^1CpV(CO)_3Xe$	1.8 (±0.2) x 10^6
1879	$^1CpV(CO)_3Xe$	1.7 (±0.1) x 10^6
2022	$^3CpV(CO)_3$	2.6 (±0.2) x 10^6
1974	$^1CpV(CO)_3(C_7H_{16})$	2.8 (±0.3) x 10^6
1878	$^1CpV(CO)_3(C_7H_{16})$	2.7 (±0.2) x 10^6

over *ca.* 40 ps consistent with vibrational cooling, to yield a single ν(CO) band at 2024 cm^{-1}. This species decays on a nanosecond timescale, giving way to two ν(CO) bands at 1974 and 1878 cm^{-1}. A further feature is observed at 1923 cm^{-1}, however the intensity of this feature is not consistent over time. The origin of this feature is unknown, and it will remain unassigned.

These results show some agreement with those of Snee *et al.*, who examined the photolysis of $CpV(CO)_4$ in *n*-heptane and triethylsilane solutions.[147] In *n*-heptane, the authors note initial formation of a single feature at 2020 cm^{-1}, assigned to an

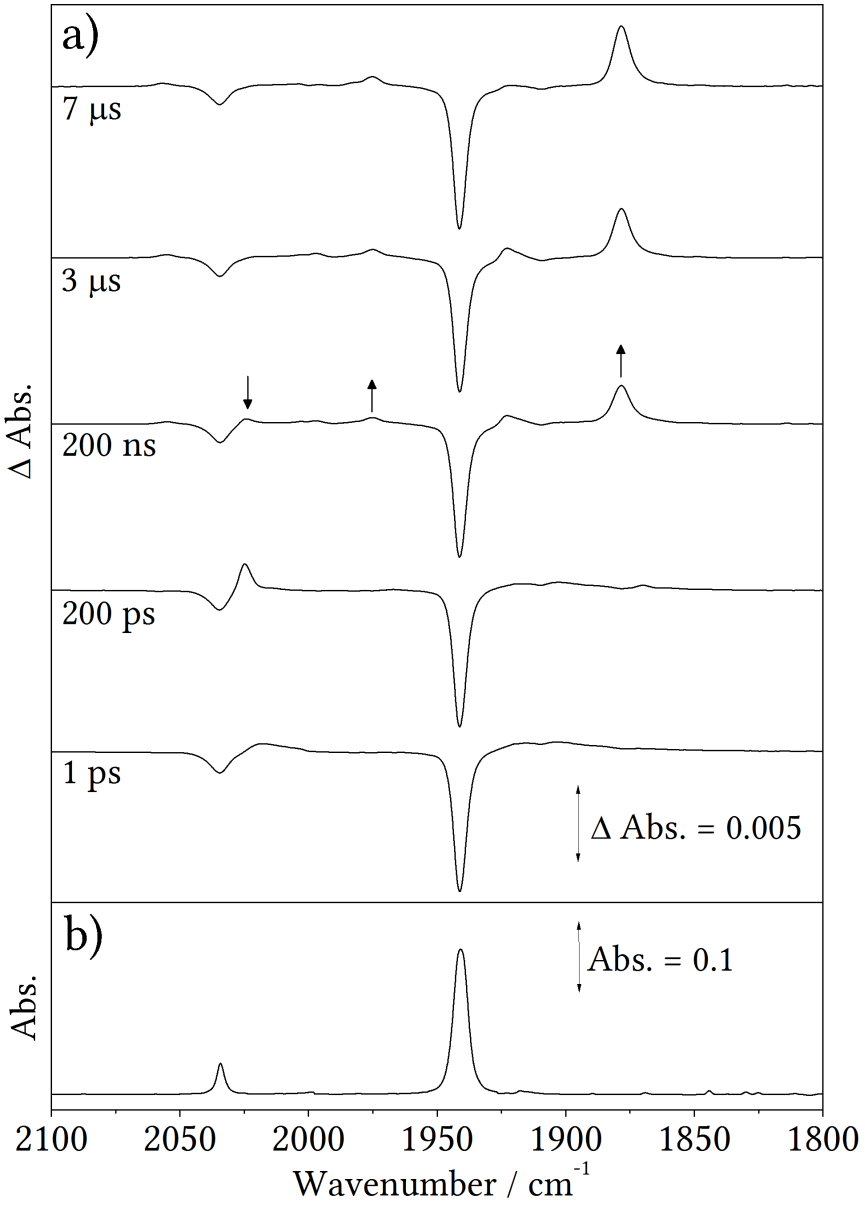


FIGURE 2.43: a) Selected picosecond, nanosecond and microsecond TR^{M}PS difference spectra recorded at a series of time delays following 266 nm photolysis of a solution of $CpV(CO)_4$ in PFMCH. Formation and decay of $^3CpV(CO)_3$ and concurrent formation of $^1CpV(CO)_3(C_7F_{14})$ can be observed. b) FTIR spectrum of same solution.

unsaturated intermediate $^3CpV(CO)_3$. This species was observed to decay, yielding a new species with ν(CO) bands at 1895 and 1990 cm^{-1}, assigned as the solvent complex $^1CpV(CO)_3(C_7H_{16})$. The band observed at 2020 cm^{-1} is consistent with our results, which show a band at 2024 cm^{-1}. This band is therefore assigned as the same unsaturated

intermediate observed by Snee *et al.*, $^{3}CpV(CO)_3$, in both *n*-heptane and triethylsilane solutions. The ν(CO) bands of the second species observed during our experiments show some agreement with those observed by Snee *et al.*, as well as other previously published room temperature[149,224] and matrix isolation studies of $CpV(CO)_4$.[54,148] As well as room temperature IR studies of $CpTa(CO)_4$ and $CpNb(CO)_4$, and $Cp^*V(CO)_4$.[224] The ν(CO) band positions for all assigned species are summarised in Table 2.28.

TABLE 2.28: ν(CO) absorption band frequencies of $CpV(CO)_4$ and intermediates and photoproducts formed following photolysis of $CpV(CO)_4$ in pure PFMCH and PFH solution, as well as Xe and *n*-heptane doped solutions of PFMCH and PFH. Literature values recorded in *n*-heptane and triethylsilane are also included, despite parent ν(CO) band positions not being fully reported.

Compound	**Solvent/ Matrix**	**Dopant**	**ν(CO) (cm^{-1})**	**Reference**
$CpV(CO)_4$	PFMCH		2034, 1942	This work
	PFH		2035, 1942	This work
		Xe	2035, 1942	This work
		n-heptane	2035, 1942	This work
	n-heptane		2030	147
	triethylsilane		1931	147
$^{3}CpV(CO)_3$	PFMCH		2024	This work
	PFH		2022	This work
		Xe	2022	This work
		n-heptane	2022	This work
	n-heptane		2020	147
	triethylsilane		2020	147
$^{1}CpV(CO)_3X$	PFMCH		1974, 1878	This work
	PFH		1975, 1879	This work
		Xe	1974, 1879	This work
		n-heptane	1974, 1978	This work
	n-heptane		1990, 1895	147
	n-heptane		1895	224
	CH_4 matrix		1954, 1887, 1859, 1856	54
	Ar matrix		1964, 1902, 1867	224
	triethylsilane		1973, 1876	147

While it may be expected that our results in PFMCH (1974 and 1978 cm^{-1}) would match more closely with those reported by Snee and co-workers in *n*-heptane solvent

(1990 and 1895 cm^{-1}), the ν(CO) band positions of this second species are more akin to those observed in triethylsilane solution (1973 and 1876 cm^{-1}). This is somewhat unexpected considering earlier results in this Chapter. This decrease in ν(CO) frequency upon moving from *n*-heptane to PFMCH suggests an increased donation of electron density from the solvent ligand to the metal centre, however the binding mode of the PFMCH solvent to the metal is still unknown, and other factors e.g., sterics may affect the interaction between solvent molecule and metal centre. ν(CO) bands observed at 1974 and 1878 cm^{-1} are tentatively assigned to the solvent complex $^1CpV(CO)_3(C_7F_{14})$.

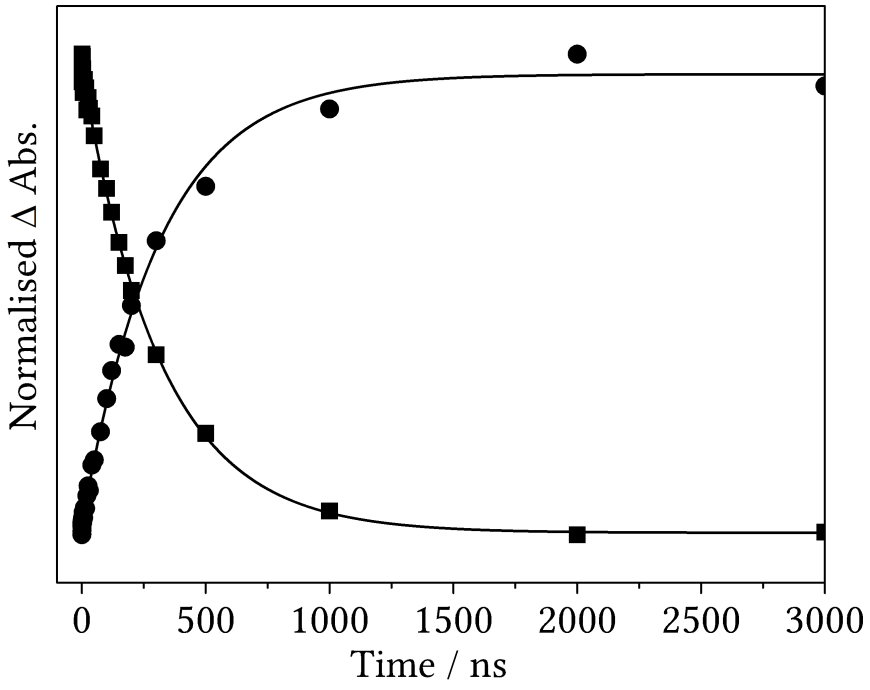


FIGURE 2.44: Kinetic traces from TR^MPS spectra recorded following 266 nm irradiation of $CpV(CO)_4$ in PFMCH solution. Matching rates for the decay of $^3CpV(CO)_3$ (circles) and formation of $^1CpV(CO)_3(C_7F_{14})$ (squares) are shown. Solid lines are mono-exponential fits.

Despite the assumed increased donation of electron density upon moving from *n*-heptane to PFMCH, reaction of $^3CpV(CO)_3$ with PFMCH to form $^1CpV(CO)_3(C_7F_{14})$ is remarkably slow (lifetime τ = 320 ($\pm$30) ns) compared to previous results. TR^MPS

kinetic traces for this process are shown in Figure 2.44, and observed rate constants for all processes observed following photolysis of $CpV(CO)_4$ are given in Table 2.27. Snee *et al.* reported a lifetime for growth of $^1CpV(CO)_3(C_7H_{16})$ as 39 ps, while decay of $^3CpV(CO)_3$ was not complete. Results reported in triethylsilane showed complete decay of the 16-electron intermediate, with a lifetime of 360 ps. It has been shown previously in this Chapter that PFMCH can increase the lifetime of unsaturated intermediates beyond that observed in alkanes and even some liquid or supercritical noble gases, however the difference in this case is remarkably large, 4 orders of magnitude slower than in *n*-heptane. Following this result, the experiment was repeated with the addition of Xe and *n*-heptane dopants, however no change in either the rate of reaction or the ν(CO) band positions of $^3CpV(CO)_3$ or $^1CpV(CO)_3X$ could be observed, indicating formation of the same photoproduct in all cases.

This result is somewhat surprising, however corresponding experiments performed in PFH solvent, both pure and doped with Xe or *n*-heptane (0.5 M) show very different behaviour. In pure PFH solution, the lifetime for the spin-forbidden reaction of $^3CpV(CO)_3$ with the solvent to form PFH is observed to be slower than in PFMCH (τ = 700 ($\pm$50) ns), while addition of Xe and *n*-heptane to this solution does yield a change in lifetime for this process, indicating formation of a new species, namely $^1CpV(CO)_3Xe$ and $^1CpV(CO)_3(C_7H_{16})$ respectively. The trend in rates of these reactions is as expected, with PFH yielding the slowest rate of reaction, while Xe is faster (τ = 580 ($\pm$30) ns), and *n*-heptane is faster still (τ = 380 ($\pm$30) ns). TR^MPS kinetic traces for these processes are shown in Figure 2.45, while a comparison of lifetime values with those in the literature is given in Table 2.29.

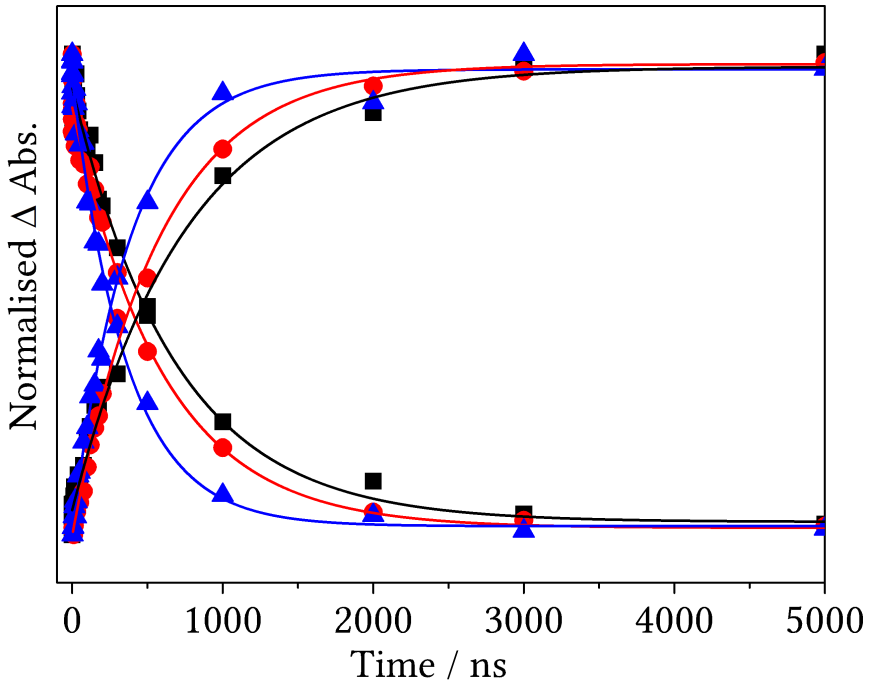


FIGURE 2.45: Kinetic traces from TR^{M}PS spectra recorded following 266 nm irradiation of $CpV(CO)_4$ in PFH solution (black squares), as well as Xe doped (red circles) and *n*-heptane doped (blue triangles) PFH solutions. Matching rates for the decay of $^3CpV(CO)_3$ and formation of $^1CpV(CO)_3(C_6F_{14})$ are shown. Solid lines are mono-exponential fits.

TABLE 2.29: Lifetimes (in ns) for the spin-forbidden reaction of $^3CpV(CO)_3$ to form $^1CpV(CO)_3X$ (X = solvent or dopant) following photolysis of $CpV(CO)_4$ in a series of PFMCH/dopant and PFH/dopant systems (all data recorded at 298 K). Literature data for the same process in *n*-heptane and triethylsilane are given for comparison.

Solvent	**Dopant**	**Lifetime τ (ns)**	**Reference**
PFMCH		320 (±30)	This work
PFH		700 (±50)	This work
	Xe	580 (±30)	This work
	n-heptane	380 (±20)	This work
n-heptane		0.039 (±0.003)	147
Triethylsilane		0.36 (±0.01)	147

All three of these processes show a slower rate of reaction that that observed in PFMCH, indicating that PFMCH may be binding to the metal more strongly than expected in this case. While this is somewhat in agreement with the observation that ν(CO) band positions of $^1CpV(CO)_3(C_7F_{14})$ lie lower in energy than those of

$^1CpV(CO)_3(C_7H_{16})$ reported by Snee and co-workers,[147] it should be noted that the ν(CO) bands of $^1CpV(CO)_3(C_6F_{14})$ lie within *ca.* 2 cm^{-1} of those of the PFMCH adduct. It is also interesting to note that although a faster rate of reaction is observed upon addition of *n*-heptane to a solution of $CpV(CO)_4$ in PFH, the ν(CO) band positions for the product of spin-crossover do not match those reported previously for $^1CpV(CO)_3(C_7H_{16})$, and are in fact very close to those reported for the PFMCH and PFH solvent adducts above. The reason for this discrepancy is currently unknown, though theoretical studies are under way. Through these studies we hope to determine the cause of the exceptionally long lifetime of $^3CpV(CO)_3$ in PFMCH and PFH solutions, and determine the source of the aforementioned disparity between our results and those previously published.

2.3 Conclusions

In this Chapter, the photochemistry of a series of model transition metal carbonyl complexes has been examined using time-resolved infrared spectroscopic techniques, as well as *ab initio* calculations.

The photochemistry of $Fe(CO)_5$ was examined in the perfluorinated alkane solvent perfluoro(methylcyclohexane). Upon photolysis, formation of both $^3Fe(CO)_3$ and $^3Fe(CO)_4$ was observed, and possible reasoning behind the observed ratio of the ν(CO) bands of these complexes was discussed. $^3Fe(CO)_4$ was observed to undergo a spin-forbidden reaction, most likely with the solvent to form $^1Fe(CO)_4X$, at a rate much slower than reported in the literature for weakly coordinating solvents e.g., alkanes.

This rate is even observed to be slower than previous experiments performed using the noble gas Xe as a solvent, and represents the slowest rate observed for this spin-forbidden process in conventional solution at room temperature. It is proposed that this slow rate is due to a weak interaction between the perfluorinated solvent and the metal. A mechanism for this process, including final formation of the dimer $Fe_2(CO)_8$ is proposed.

Photolysis of $CpMn(CO)_3$ was also carried out in a series of solvents, including alkanes, perfluoro(methylcyclohexane), perfluoro(hexane) and perfluoro(triethylamine). In agreement with results observed for $Fe(CO)_5$, the perfluorinated solvents greatly extended the lifetime of a coordinatively unsaturated intermediate $^3CpMn(CO)_2$. DFT calculations, carried out by Dr. Magnus Hanson-Heine were used to assign the structure and spin-state of this intermediate. It was determined that this molecule is indeed an unsaturated 16-electron triplet, and that it exists in a pyramidal structure in its ground state. Addition of various weakly binding dopants to solutions of $CpMn(CO)_3$ in PFMCH, including the liquid alkane cyclopentane, and gaseous species C_2H_6, Xe and CO_2 was shown to cause a change in the rate of the spin-forbidden reaction to form $^1CpMn(CO)_2X$ (X = dopant). This change in rate was also accompanied by small changes in the ν(CO) band positions of the bound species, indicating binding of different ligands in each case. These results represent the first instance of binding of many of these ligands to $CpMn(CO)_2$ in liquid solution at room temperature, and demonstrates the utility of weakly coordinating solvents for generation of noble gas and alkane complexes. Somewhat surprisingly, the perfluorinated amine perfluoro(triethylamine) was found to react with $^3CpMn(CO)_2$ even more slowly than PFMCH, and some

evidence for formation of the unsaturated singlet species $^{1}CpMn(CO)_2$ was observed in this solvent. Photolysis of $(MeCp)Mn(CO)_3$ in PFMCH doped with methane showed evidence for formation of a methane complex in room temperature solution, whereas results observed for $CpMn(CO)_3$ were inconclusive. Further preliminary DFT studies by Prof. Jeremy Harvey and Dr. Zhen Liu showed some agreement with experimental data, and suggested a weak interaction between the triplet species and the solvent in each case. The possibility that interaction with the solvent or dopant affects not only the potential energy surface of the singlet species, but also the 'unsaturated' triplet species is considered, along with the subsequent effect on the minimum energy crossing point between the two.

Finally, the photochemistry of $CpCo(CO)_2$ and $CpV(CO)_4$ were examined in perfluorinated alkane solvents. $CpCo(CO)_2$ was found not to coordinate to PFMCH, or to any of the added weak ligand dopants, and simply formed the dimeric species $Cp_2Co_2(CO)_3$ through a reaction between the initial photoproduct $^{3}CpCo(CO)$ and the parent $CpCo(CO)_2$. Upon photolysis in PFMCH, $CpV(CO)_4$ was found to form a coordinatively unsatured 16-electron species, which undergoes reaction with what is presumed to be the solvent. Addition of alkane and noble gas dopants to this solution did not change the rate of this spin-forbidden process. Photolysis in PFH solutions with alkanes and noble gas dopants showed a change in rate similar to that observed previously for $CpMn(CO)_3$. The timescale of this spin-forbidden reaction and the $\nu(CO)$ band positions of the resulting species were found not to match with those previously published. The reason for the discrepancy is still unknown, however it is hoped that further DFT calculations will allow us to determine the reason for this change.

Chapter 3

Further Time-Resolved Studies of Alkane and Noble Gas Complexes in Room Temperature Perfluoroalkane Solutions

3.1 Introduction

Organometallic noble gas and alkane complexes have garnered much interest over the past few decades. In particular, organometallic alkane complexes have attracted great interest due to their identification as intermediates in transition metal mediated C-H

activation processes.[37,41,56,225–235] Chemistry of this nature is particularly appealing due to the possibility of converting methane or methanol, through the activation of strong C-H bonds, to useful sources of energy and chemical feedstocks.[236]

Organometallic noble gas complexes, while less desirable in the study of catalytic processes, possess their own varied and interesting chemistry. Of the six noble gases, only krypton, xenon and radon have been shown to form isolable compounds with other atoms, usually the highly electronegative oxygen or fluorine.[237,238]

Observation of a series of organometallic alkane and noble gas complexes was described 40 years ago by Perutz and Turner.[80] In that study, $M(CO)_6$ (M= Cr, Mo, W) were photolysed in a series of cryogenic matrices, including frozen alkanes, tetrafluoromethane, neon and xenon. Evidence for coordination of the matrix material to the metal centre came in form of a shift in the λ_{max} following photolysis. While this case is often cited as the first observation of an organometallic noble gas complex, an earlier study of photolysis of $Cr(CO)_6$ in an Ar matrix showed the possibility of coordination of Ar to the Cr metal centre.[239] However, the potential importance of this interaction was not discussed until several years later.

Early work on the chemistry of the organometallic noble gas and alkane complexes was intrinsically tied together through the use of matrix isolation, flash photolysis and UV/visible and IR absorption techniques. Later studies of these interesting classes of organometallic complexes required very different tools and conditions. Further introduction to organometallic noble gas and alkane complexes will be given separately, below.

3.1.1 Organometallic Alkane Complexes

In order to fully understand the desirable C-H activation chemistry of the organometallic alkane complexes, an understanding of their structure, formation and reactivity is vital. The aim of much of the work described in this introduction section was to generate and characterise an organometallic alkane complex which is stable in solution at room temperature.

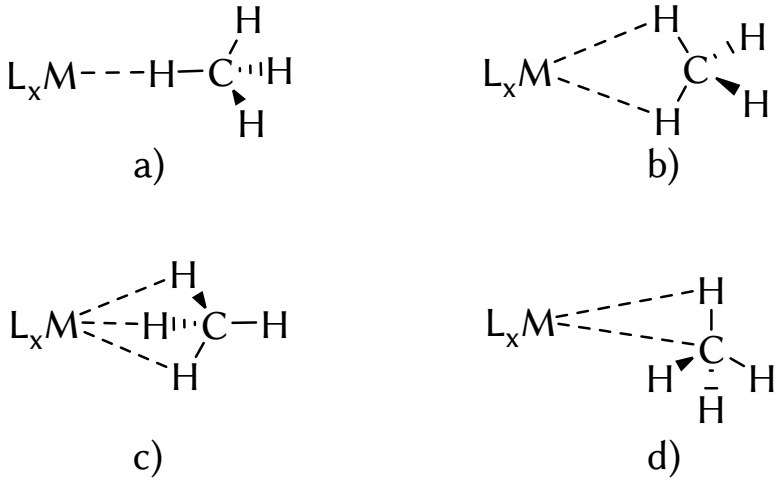


FIGURE 3.1: The various ways in which an alkane (CH_4 in this example) may bond to a metal centre. a) η^1-H mode, b) η^2-H,H mode, c) η^3-H,H,H mode d) η^2-C,H mode. Adapted from ref 240.

Organometallic alkane complexes are generally very short-lived at room temperature, due to the HOMO and LUMO orbitals of the C-H σ-bond being poorly suited to accept or donate electron density from or to the metal centre.[240] The first observation of an organometallic alkane complex in the solution phase was reported following photolysis of $Cr(CO)_6$ in room temperature cyclohexane solution.[81] These studies confirmed that the cyclohexane solvent coordinated to the metal centre within 50 ns of photolysis, and suggested that $Cr(CO)_5$ is significantly stabilised in solution

by interaction with the cyclohexane solvent. However during these studies it was found that the alkane complex formed was particularly sensitive to impurities in the solution. Upon photolysis of $Cr(CO)_6$ in the perfluorinated alkane perfluoro(methylcyclohexane), the generated $Cr(CO)_5$ fragment was found to be shorter-lived, indicating the pefluoroalkane exhibits a weaker interaction with the metal centre compared to cyclohexane, or possible no coordinative interaction at all.[78,79] Further studies of the formation of $Cr(CO)_5$(cyclohexane) in solution showed that solvation of the unsaturated $Cr(CO)_5$ by cyclohexane actually occurs within 1 ps of photolysis.[19]

The first IR spectrum of an organometallic alkane complex in room temperature solution was reported by Grevels.[241] During this study, the authors photolysed $Cr(CO)_6$ in cyclohexane, in the presence of a series of other solvents, known to form strong coordination complexes with Cr, including acetone, benzene, methanol and water, as shown in Figure 3.2. A shift in the position of the ν(CO) bands corresponding to the complex $Cr(CO)_5X$ (X = cyclohexane, acetone, benzene, methanol, water) was observed upon addition of the corresponding solvent, suggesting formation of a different complex in each case. IR spectroscopy was shown to be a powerful tool for the study of organometallic alkane complexes, particularly those which include carbonyl ligands, due to the sensitivity of the ν(CO) band frequencies to changes in coordination number, geometry and electron density at the metal centre.

Additional studies of alkane complexes of the form $M(CO)_5$(alkane) (M = Cr, Mo, W) have examined the strength of the M-alkane bond interaction. Initial studies of utilised transient absorption spectroscopy of the photolysis of $W(CO)_6$ in methylcyclohexane. During this study, the rate of the reaction between the alkane complex

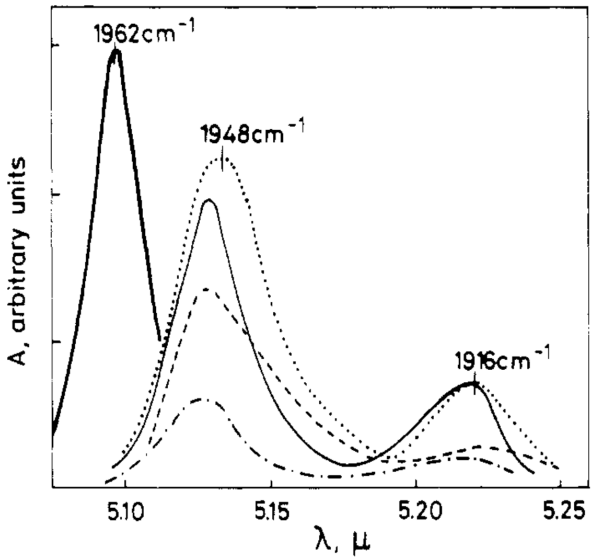


FIGURE 3.2: IR spectra recorded following photolysis of $Cr(CO)_6$ in CO-saturated cyclohexane doped with other solvents. Showing $Cr(CO)_5$(cyclohexane) (bold line), $Cr(CO)_5$(acetone) (narrow line), $Cr(CO)_5$(benzene) (dashed line), $Cr(CO)_5$(methanol) (dotted line) and $Cr(CO)_5$(X) (unassigned, dot-dashed line). Reproduced from ref 241.

$W(CO)_5$(methylcyclohexane) with added pyridine has examined, and W-alkane bond energy estimated to be 16 kJ/mol.[242] Further experiments have utilised TRIR to examine the reactions of $M(CO)_5$(alkane) with a variety of competing ligands,[243–245] while photoacoustic calorimetry (PAC) has been used to determine the binding energy of a series of Cr- and Mo- alkane complexes.[178,246,247] Systematic studies of the reactivity of a series of organometallic alkane complexes have shown that their reactivity decreases across and down groups V, VI and VII.[185,206,224] In these studies, TRIR spectroscopy has been used to examine the formation and reactivity of a series of organometallic alkane complexes of the form Cp'$M(CO)_2$(alkane), (Cp' = η^5-C_5R_5, R = H, CH_3, C_2H_5) following photolysis of the parent Cp'$M(CO)_3$ in an alkane solvent at room temperature. The reactivity of the alkane complex formed in these cases is measured through examination of the second-order rate constant k_2 for the reaction of the alkane

complex with a competing ligand (e.g., CO). Through these studies, the reactivity of Cp'Mn(CO)$_2$(heptane) (Cp' = η^5-C$_5$R$_5$, R = H, CH$_3$, C$_2$H$_5$) has been shown to vary according to the substituent on the Cp ring, however it was found that the steric bulk of the incoming ligand has the greatest effect on the stability of the alkane complex, indicating that sterics rather than electronics controls this process.[163,207] Such studies have led to the identification of CpRe(CO)$_2$(heptane) an organometallic alkane complex which has been shown to have a lifetime > 20 ms at room temperature in the absence of CO.[174] This Re-alkane complex has been shown to 50,000 times less reactive than the analogous vanadium complex CpV(CO)$_3$(heptane).[224]

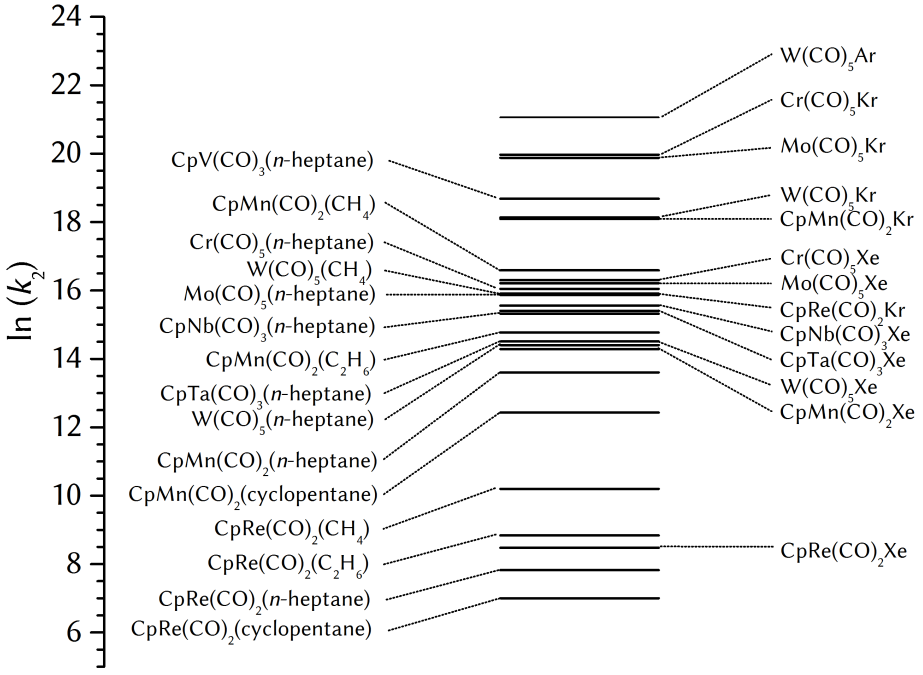


FIGURE 3.3: Plot of natural log of the rate constant (lnk_2 for the reaction of a series of organometallic noble gas and alkane complexes with CO to reform their respective parent species. Figure adapted from ref 34, original plot kindly provided by Dr. James Calladine.

The high relative stabilities of the Re-alkane complexes have led to their subsequent characterisation by NMR spectroscopy. CpRe(CO)$_2$(cyclopentane) was probed by Ball

et al. at low temperature (180 K), and was found to persist for several hours following initial formation.[40] A study of the related complex $CpRe(CO)_2(PF_3)$ showed that this compound not only formed the σ-alkane complex as expected, there was also evidence of formation of the C-H activated alkyl hydride species, in contrast to previous studies of $CpRe(CO)_3$.[41] A TRIR study comparing the stabilities of $CpRe(CO)_2$(heptane) and $CpRe(CO)_2$(cyclopentane) found that the cyclopentane complex was almost twice as stable as the heptane complex.[48] The binding modes of a series of alkane solvents have been investigated at room temperature. Photolysis of $CpRe(CO)_3$ in cyclopentane and cyclohexane results in binding of the alkane *via* the η^2-C,H mode, with a rapid equilibrium between the two H atoms of the CH_2 moiety. Experiments in the linear alkanes have shown that although all C-H bonds are capable of binding to the metal centre, the preferred mode of coordination is through the secondary C-H bonds.[44] NMR studies in cyclohexane have shown a slight preference towards binding of the axial C-H to the metal.[248] A recent theoretical and experimental study undertaken within our group examined the effect of increasing alkane chain-length on the rate of C-H activation mediated by $Cp'Rh(CO)_2$ (Cp' = η^5-C_5H_5 or η^5-C_5Me_5).[235] It was found that a large increase in the lifetime of activation was observed upon moving from cyclohexane to cycloheptane and cyclooctane. Theoretical studies confirmed that migration of the Rh fragment along the different C-H units of the ring does have an effect on the rate of the activation process. The lifetime of organometallic alkane complexes has been found to be highly dependent on the nature of the alkane ligand itself. Cyclic alkanes have been found to form more stable complexes than their linear counterparts,[48,206,207,249] while the shorter chain linear alkanes show weaker binding to the metal centre than their longer chain analogues, with CH_4 showing the lowest binding

energy.[249,250] Despite this, a TRIR study of the reactivity of alkane complexes of the form (benzene)$Cr(CO)_2$(alkane) with CO was found to increase as the chain length of the alkane solvent was increased. It was determined that this effect was due to entropic factors caused by the increasing chain length, rather than a change in the activation enthalpy.[207] NMR studies such as those described above have subsequently been expanded and various other organometallic alkane complexes have been characterised in this way. Ball *et al.* have reported NMR studies of Re-cycloheptane and Re-cyclooctane complexes, facilitated by the use of lower melting point alkanes as solvents, to overcome the high melting point of the larger cycloalkanes.[251,252] Brookhart and Goldberg have reported the formation of a rhodium-methane complex, formed through protonation of a Rh^I-CH_3 resulting in the formation of $[Rh(PONOP)(CH_4)][BAr^F{}_4]$ (PONOP = 2,6-bis(di-tert-butyl-phosphinito)pyridine, $BAr^F{}_4 = B[3,5\text{-}(CF_3)_2C_6H_3]^-_4$).[253] Despite the reduced stability compared to their Re analogues,[185] Mn-alkane complexes (alkane = *n*-propane, *n*-butane, neopentane, cyclopentane) have also been observed by NMR,[46,47] as have W-alkane complexes (alkane = cyclopentane, *n*-pentane, isobutane, neohexane and cycloheptane[45] and even methane and ethane complexes of rhodium.[253,254]

In comparison to the relative wealth of NMR spectroscopic studies described above, few x-ray crystallographic studies of transition metal alkane complexes have been reported, with only two examples currently reported. The first of these examples is the Fe^{II}-porphyin *n*-heptane complex $[Fe(DAP)(C_7H_{16})]$ (DAP = double A-frame porphyrin).[255] The reported interaction between the metal and alkane in this iron species is ambiguous, with both the iron atom and heptane molecule exhibiting significant disorder. The reported Fe-C distances (2.52 and 2.83 Å) are, however within

those expected for agostic interactions from calculated C-H-M angles.[256] Additional evidence for coordination comes from slight displacement of the Fe atom out of the porphyrin plane, as expected for some 5-coordinate iron species, in agreement with calculated geometries for this complex. The second, and more compelling example of an x-ray structure was reported by Weller *et al.*[257] The rhodium-norbornane complex $[Rh(P^iBu_2(CH_2)P^iBu_2)(C_7H_{12})][BAr^F{}_4]$ was generated in the solid state by hydrogenation of a Rh-diene complex precursor. In addition to crystallographic characterisation of this species, Weller *et al.* utilised solid-state NMR spectroscopy to provide additional characterisation of the interaction between metal and alkane, ultimately assigning it as an η^2-C,H interaction.

Nitrogen donor ligands have also found an important role in the formation and stabilisation of organometallic alkane complexes in recent times, expanding upon previous work on Cp-ligated Re-alkane complexes. $TpRe(CO)_2$(cyclopentane) (Tp = hydrotris(pyrazol-1-yl)borate) was found to have a shorter lifetime than its Cp analogue.[232] Later, Ball *et al.* characterised the first oxygen-supported Re-alkane complex, $KpRe(CO)_2$(alkane) (Kp = cyclopentadienyltris(diethylphosphito)cobaltate), (alkane = cyclopentane, cyclohexane or *n*-pentane).[258]

Organometallic complexes of the shortest chain alkanes methane and ethane have been found to be the least stable to reaction with CO. Theoretical and experimental studies have determined a link between the strength of the C-H bond of an alkane, and the subsequent strength of the M-CH_3 bond following metal-mediated C-H activation.[259–262] Methane and ethane possess particularly strong C-H bonds, and the Rh-CH_3 bond formed following C-H activation of CH_4 has been shown to be very

strong.[252,260] Theoretical studies have shown that the M-CH_4 bond has a particularly low binding energy.[263] This, along with the low barrier to C-H activation, makes the study of short-chain alkane complexes more difficult, as they are predicted to be very short-lived at room temperature. Previously, organometallic complexes of methane have been characterised using low temperature matrix isolation,[19,80,95,239,264,265] and in the gas phase.[266] More recently, organometallic methane complexes have been characterised spectroscopically in room temperature solution. The first such observation characterised formation of $^1Fe(CO)_4(CH_4)$ following photolysis of $Fe(CO)_5$ in *sc*CH_4. Following formation of the 16-electron unsaturated triplet species $^3Fe(CO)_4$, the methane complex was observed to form on the nanosecond timescale.[103] Further studies observed formation of $W(CO)_5(CH_4)$ following photolysis of $W(CO)_6$ in *sc*CH_4 at room temperature. The resulting methane complex was found to be very short lived and much more reactive than its longer-chain alkane analogues.[37,198] Theoretical studies have examined the coordination and subsequent activation of methane at transition metal centres.[232,263,267–269] A theoretical and experimental study undertaken by Cowan *et al.* examined the photolysis of $CpRe(CO)_3$ and $Cp^*Re(CO)_3$ in *sc*CH_4 and *liq*C_2H_6, as shown in Figure 3.4.[37,198] It was demonstrated that the initial methane or ethane complex formed within a few nanoseconds of photolysis. The methane and ethane sigma complexes are then found to enter an equilibrium with the resulting C-H activation product, the alkyl hydride of the form Cp'$Re(CO)_2$(R)H. The ratio of alkane:alkyl hydride complex was found to depend on both the nature of the organometallic fragment (i.e., the electron density donated by the Cp ring), as well as the alkane itself, with $Cp^*Re(CO)_2(CH_4)$ exhibiting the largest amount of activated product, and $CpRe(CO)_2(C_2H_6)$ the smallest.

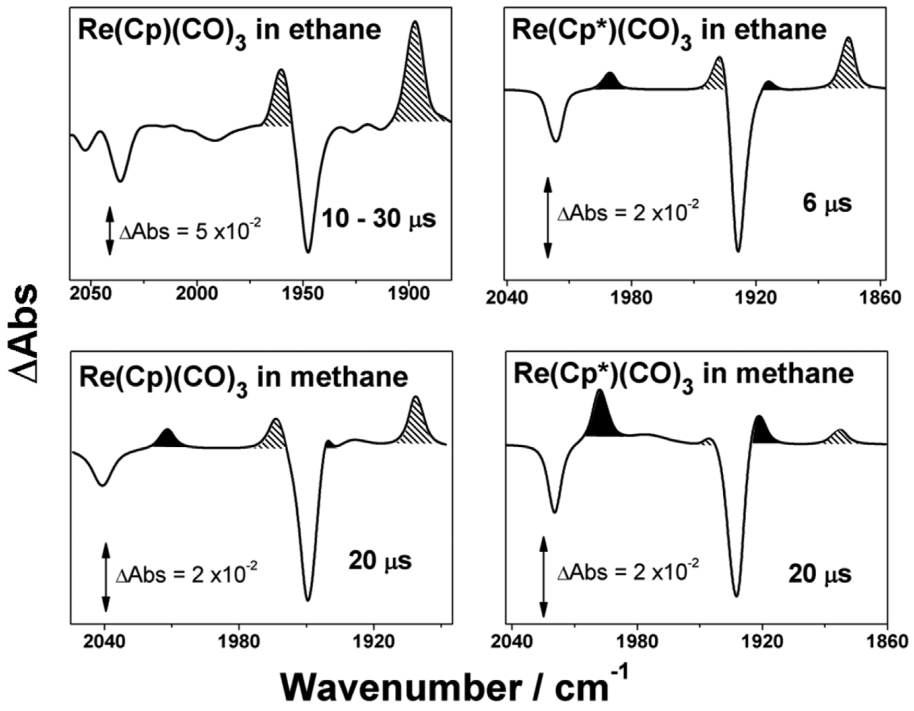


FIGURE 3.4: TRIR difference spectra obtained following photolysis of $CpRe(CO)_3$ and $Cp^*Re(CO)_3$ in *sc*CH_4 or *liq*C_2H_6 at room temperature. Striped bands indicate the dicarbonyl solvent complex, solid filled bands indicate the C-H activated oxidative addition products. Figure adapted from ref 37.

3.1.2 Organometallic Noble Gas Complexes Complexes

The chemistry of the noble gases is comparatively limited. As stated above, only Kr, Xe and Rn have been shown to form stable compounds with other atoms.[237] The lack of reactivity of the other noble gases can be attributed to the decreasing energy required to promote the atom to a state with an unpaired electron, as well as reduced ionisation energy, upon moving down the group.

In theory, radon should be the most reactive of the noble gases, however its longest lived isotope (^{222}Rn) is highly radioactive, with a half-life of only 3.8 days. This makes the chemistry of radon difficult to study. However, several compounds of radon

have been reported, including RnF_2 and RnO_3.[237]

The stable compounds of xenon and krypton have been more widely studied. Krypton has been shown to form KrF_2, as well as many different species containing the krypton fluoride cation $[KrF]^+$. The chemistry of Xe is comparatively rich. Bartlett was the first to observe a stable noble gas complex in 1962, the orange/yellow solid $Xe^+[PtF_6]^-$. Since then, various different complexes of Xe with fluorine and oxygen have been synthesised, with Xe oxidation states ranging from +2 to +8, and coordination numbers and geometries ranging from simple linear XeF_2 to the trigonal bipyramidal XeO_3F_2 and the octahedron XeF_6.[184] More recently, there has been considerable interest in the use of the noble gas fluorides as ligands for the formation of coordination complexes and adducts.[270–273] All of the compounds discussed above involve a bond between a noble gas and a main group element, usually fluorine or oxygen. However, there should be no reason why a noble gas atom cannot act as a ligand, and bond coordinatively to a metal centre. Noble gas atoms do, after all have "at least one pair of electrons that can donate", thus filling the definition of a 'ligand' put forth by Cotton and Wilkinson.[237] Observation of these elusive and short-lived species has remained largely spectroscopic in nature, with only a single x-ray crystal structure of a metal-noble gas complex reported to date, that of $[AuXe_4](Sb_2F_{11})_2$.[274,275] However, with continued improvement in detector rise-time and gating technology in various fields such as time-resolved crystallography, additional crystallographic determination of the existence of such a species may only be a matter of time. The nature of the transition metal-noble gas bond has been successfully modelled using DFT methods, and has been shown to be highly dependent on orbital interactions between the noble gas and

carbonyl ligands.[276] Various methods have been utilised in the formation of these highly reactive short-lived species. These methods hinge on the absence of competing ligands in the reaction medium, and therefore usually utilise the noble gas itself as the solvent or matrix. All of these methods involve initial UV photolysis of the parent complex to remove a ligand, usually CO (though H^- has also been used),[277] creating an unsaturated organometallic fragment with which the noble gas atom can react.

Following initial matrix isolation experiments by Perutz and Turner described above,[80] a wealth of spectroscopic observations of various organometallic noble gas complexes have been reported. Poliakoff *et al.* also used matrix isolation to characterise $Fe(CO)_4Xe$ following photolysis of a $Fe(CO)_5$ in a Xe matrix.[95] EPR spectroscopy has also been utilised to characterise noble gas complexes. The isoelectronic 17-electron species $[KrFe(CO)_5]^+$ and $KrMn(CO)_5$ were detected following γ-radiolysis in krypton matrices.[278] More recent examples of noble gas complexes formed using matrix isolation techniques include: $Ru(CO)_2(PMe_3)_2X$ (X = Ar, Xe),[277] (dmpe)$Ru(CO)_2X$ (X = Ar, Xe; dmpe = $Me_2PCH_2CH_2PMe_2$),[279] and (dfepe)$Cr(CO)_3X$ (X = Ar, Xe; dfepe = $(C_2F_5)PCH_2CH_2P(C_2F_5)_2$).[280] Matrix isolation has proven to be an incredibly useful technique for the characterisation of such complexes, however a need to understand the subsequent reactivity and stability of such complexes has prompted a move towards gas and solution phase studies, utilising both liquid and supercritical noble gas solvents.

The first solution phase observation of an organometallic noble gas complex was reported by Simpson and co-workers.[281] Following photolysis of $Cr(CO)_6$ in *liq*Xe, as well as *liq*Kr doped with 5 % Xe at approx. 180 K. The characteristic ν(CO) bands of $Cr(CO)_5Xe$ were observed in both solvent systems, and the complex was found to be

remarkably long-lived ($t_{1/2}$ = 2 s). Further studies utilised 5d metals to produce more stable organometallic Xe complexes. An extensive rapid-scan IR study of the formation of $M(CO)_5X$ (M = Cr, W; X = Kr, Xe) was undertaken by Weiller.[49] It was found that the krypton complexes of both Cr and W have lifetimes *ca.* 0.1 s at 150 K in *liq*Kr solvent, while photolysis of $W(CO)_6$ in *liq*Xe was shown to produce $W(CO)_5Xe$, with a lifetime of approx. 1.5 minutes at *ca.* 170 K. During this study, the rate of reaction of the noble gas complex $W(CO)_5Xe$ with CO to regenerate the parent $W(CO)_6$ was measured as a function of temperature (173-198 K). Application of the steady-state approximation to this reaction predicted a linear dependence of the rate constant, k_{obs}, on the concentration of CO in the solution. From the resulting Arrhenius plot, an estimate of the bond dissociation energy of W-Xe was reported as *ca.* 35 kJ/mol, much lower than the W-heptane bond dissociation enthalpy (65 kJ/mol).[282]

In addition to the study of group 6 metal-noble gas complexes, Bergman *et al.* have reported the formation of $Cp^*Rh(CO)X$ (X = Xe and Kr), following photolysis of $Cp^*Rh(CO)_2$ in *liq*Kr or *liq*Xe in the presence of alkanes; cyclohexane[142,284] and neopentane.[226] It was observed that the Kr complex decayed much more quickly than the Xe complex, indicating a stronger M-Xe bond. Additional studies attempted to measure the Rh-Xe bond energy of $Cp^*Rh(CO)Xe$ in *liq*Xe solution with TRIR spectroscopy.[285] The reaction of this species with CO as found to be very fast, and using the same method as the previous study above, also by Weiller *et al.*, the Rh-Xe bond enthalpy was calculated as *ca.* 12 kJ/mol, weaker than the W-Xe bond energy.

Studies of $CpRe(CO)_3$ and its derivatives have been particularly interesting. Initial photolysis studies of $CpRe(CO)_3$ in *liq*Xe showed the Re-Xe complex $CpRe(CO)_2Xe$

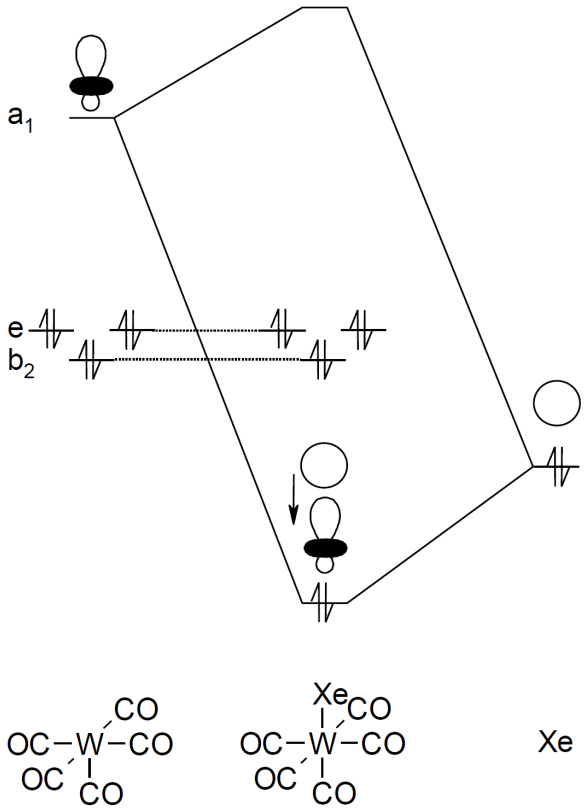


FIGURE 3.5: Proposed orbital interactions for the coordination of Xe to coordinatively unsatured $W(CO)_5$. Electron flow from Xe to W is indicated by an arrow. Figure adapted from ref[283].

to be much longer lived than $W(CO)_5Xe$, with a lifetime of 3.5 minutes at *ca.* 170 K,[48] compared to 1.5 minutes for $W(CO)_5Xe$. This observation, along with the previously reported NMR spectrum of the closely related $CpRe(CO)_2$(alkane),[40] led to the first attempted NMR characterisation of an organometallic noble gas complex. Due to the poor solubility of $CpRe(CO)_3$ in *liq*Xe, $CpRe(CO)_2(PF_3)$ and (^{i}PrCp)$Re(CO)_2(PF_3)$ were chosen as the materials of study for this NMR investigation. The addition of NMR active ^{19}F and ^{31}P nuclei to the molecules also increased the breadth of NMR techniques with which the resulting Xe complex could be detected.[42] FTIR studies showed that upon photolysis, two different Re-Xe photoproducts were produced, the monocarbonyl

Cp'Re(CO)(PF_3)Xe, and the dicarbonyl Cp'Re$(CO)_2$Xe, with the monocarbonyl being the longest lived.

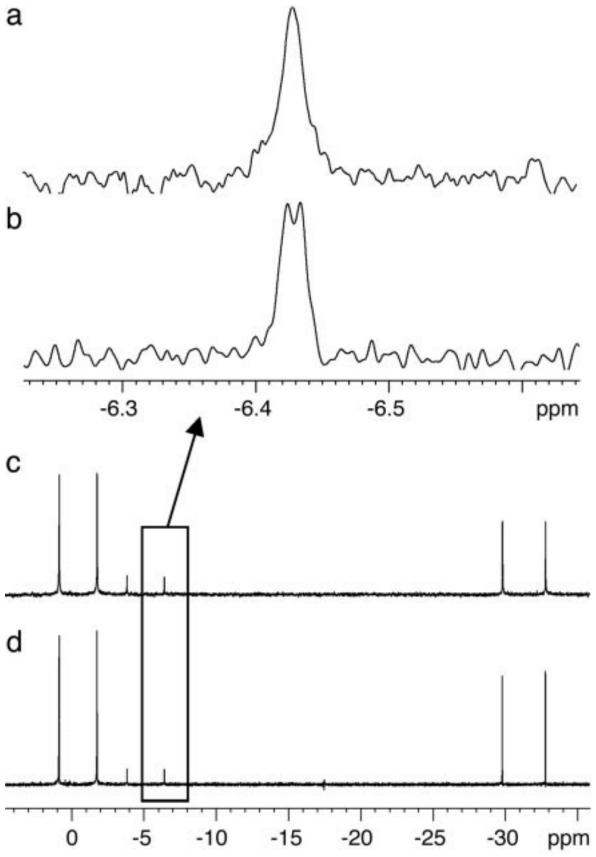


FIGURE 3.6: ^{19}F spectra of (^{i}PrCp)Re$(CO)_2(PF_3)$ recorded during prolonged photolysis in *liq*Xe at 163 K. a) is an expansion of c) which shows the spectrum recorded in unlabelled Xe. b) is an expansion of d) which shows the spectrum recorded in ^{129}Xe. A small splitting due to $^3J_{XeF}$ coupling can be seen. Figure reproduced from ref 42.

NMR studies following photolysis of these complexes in *liq*Xe at *ca.* 160 K showed the first NMR spectroscopic evidence for formation of a transition metal-noble gas bond. 2D NMR experiments showed coupling constants of $^3J_{XeF} = 5$ Hz and $^2J_{XeP} = 42$ Hz, indicating that Xe may be acting as a ligand, and the interaction between the metal and noble gas atom is not simply a weak solvation interaction. This study contains the only published observation of an organometallic Xe complex by NMR to date.

In recent years, as attention has turned towards formation of noble gas complexes which are stable at room temperature, supercritical fluids have been heavily exploited. Supercritical fluids allow the reactivity and stability of organometallic noble gas complexes to be examined at room temperature, with the added advantage that they exhibit a high capacity for dissolving CO gas. The first observation of one of these complexes in room temperature solution was reported by Sun and co-workers.[286] TRIR spectroscopy was used to characterise $W(CO)_5Ar$ and $M(CO)_5X$ (M = Cr, Mo, W; X = Kr, Xe) at room temperature in supercritical Ar, Kr or Xe. Temperature dependence studies of the rate of reaction of $W(CO)_5Xe$ were reported, along with a calculated bond enthalpy for W-Xe of *ca.* 34 kJ/mol in agreement with work previously published by Weiller[49] and Wells.[148] Studies in *sc*Kr showed a small shift in the ν(CO) bands of $W(CO)_5X$ to higher wavenumber, indicating weaker coordination to the metal centre in the case of Kr compared to Xe. This observation was also echoed by the comparative decay lifetimes of Xe and Kr complexes, with the Kr complexes reported to be much shorter lived. Experiments utilising *sc*Kr solvent doped with 7 % Xe showed that the ν(CO) band positions of $W(CO)_5Xe$ are consistent in both *sc*Xe and *sc*Kr. Similar experiments in *sc*Ar doped with Kr also confirmed the coordination of Kr to the metal centre. Further studies of Cr and Mo hexacarbonyl species showed weaker coordination of the Cr and Mo metals to Kr and Xe compared to W. Subsequently, these methods have been used to characterise a wide variety of organometallic noble gas complexes, including $CpM(CO)_3Xe$ (M = V, Nb, Ta),[287] Cp'$Mn(CO)_2X$ (Cp' = η^5-C_5H_5, η^5-C_5Me_5, η^5-C_5Et_5; X = Kr, Xe),[183] CpRh(CO)X (X = Kr, Xe),[288] and η^n-Tp^*Rh(CO)Xe (n = 2, 3).[289]

3.1.3 Aims

Expanding on the work presented in the previous Chapter, the aim of the work presented within this Chapter was to examined the photochemistry of a series of model transition metal carbonyl complexes in perfluorinated solutions at room temperature and near-ambient pressure.

By utilising the weakly coordinating nature of the perfluoroalkane solvent, we hoped to be able to observe organometallic Xe, methane and ethane complexes for a variety of transition metals. Many of these target complexes have been characterised previously in supercritical fluid solutions or cryogenic matrices, however we aimed to characterise these complexes using milder conditions; room temperature and near-ambient pressures.

By examining the rate of formation and subsequent decay of these complexes, an organometallic complex, solvent and dopant system which would be suitable for future study by either XAFS or NMR spectroscopy could potentially be found.

3.2 Results and Discussion

In the preceding Chapter, it was shown that photolysis of a solution of $CpMn(CO)_3$ in perfluorinated alkane or amine solvent, in the presence of an alkane or noble gas dopant, can result in the formation of an organometallic noble gas or alkane complex following a spin-forbidden reaction of an unsaturated 16-electron triplet intermediate. In previous studies, various other transition metals have been shown to form long-lived organometallic alkane and noble gas complexes at room temperature in noble gas or

alkane solutions,[34] including 2nd and 3rd row transition metals (Re and Rh), and the Group VI metals Cr, Mo and W. In these cases however, no spin-forbidden reaction has been previously reported, therefore the changing rate of this process can not be used as evidence for the formation of a new species. Previous time-resolved studies have utilised supercritical or liquid xenon, krypton, alkanes as solvent to form these weakly-bound complexes, many of which require harsh conditions of pressure or temperature. In this Chapter, the photochemistry of a series of transition metal compounds which do not exhibit spin-forbidden chemistry is reported. The photochemistry of these complexes was examined in room temperature perfluoroalkane solution, at ambient or near-ambient (1.5 bar) pressures.

3.2.1 TRIR Studies of $CpRe(CO)_3$ in Perfluoroalkane Solvents

The photochemistry or $CpRe(CO)_3$ in the presence of alkanes and noble gases is well reported, and previous studies have shown the formation of remarkably stable alkane and noble gas complexes.[34] In order to attempt to characterise noble gas and alkane complexes of rhenium in perfluorinated solvents, the photochemistry of $CpRe(CO)_3$ in PFMCH was examined.

A solution of $CpRe(CO)_3$ in PFMCH under an Ar atmosphere was photolysed at 266 nm, and a series of TRIR difference spectra were recorded across the picosecond, nanosecond and microsecond timescales. A selection of these difference spectra can be seen in Figure 3.7. The difference spectrum recorded immediately following photolysis shows two negative features at 2037 and 1948 cm^{-1}, which persist throughout the experiment. These features correspond to a bleaching of the parent $CpRe(CO)_3$. Also

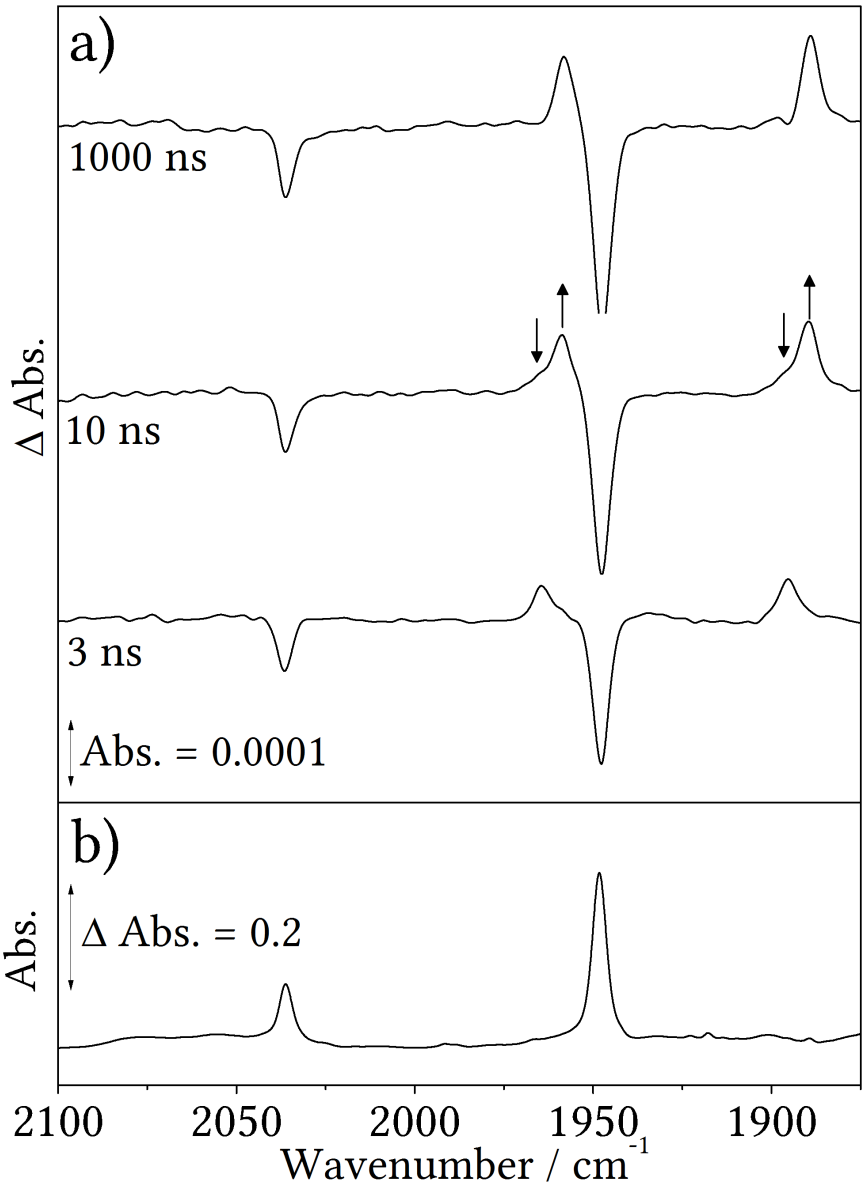


FIGURE 3.7: a) Selected nanosecond TRIR difference spectra recorded at a series of time delays following 266 nm photolysis of a solution of $CpRe(CO)_3$ in PFMCH. The interchange between two dicarbonyl species on the fast nanosecond timescale can be seen clearly. b) FTIR spectrum of the same solution.

present in the spectra on the fast picosecond timescale are large, broad features which decay over the first 100 ps of the experiment concurrent with partial reformation of the parent bleaches. Various previous studies have shown that vibrationally excited electronic ground states of organometallic carbonyl complexes can be formed following

photolysis, and decay on the picosecond timescale.[150,290] The broad features observed during this study are therefore assigned to as vibrationally hot $CpRe(CO)_3$. Following this process, two positive ν(CO) bands are observed, at 1964 and 1895 cm^{-1}. These ν(CO) bands appear stable on the picosecond timescale, and the spectrum recorded 1 ns following photolysis shows only the presence of these two positive features. The number and position of these ν(CO) features are consistent with formation of a dicarbonyl complex of the form $CpRe(CO)_2X$, by comparison with previous photolysis studies.[37,42,48,183,198,216]

In most previous cases, this initially formed transient remains stable into the microsecond timescale, and is assigned as the product of a reaction with the solvent, $CpRe(CO)_2$(Sol). However, in this case the difference spectrum recorded 10 ns following photolysis shows that the two initial ν(CO) bands have decayed, and two new ν(CO) features which appear at slightly lower frequency (1958 and 1889 cm^{-1}) have formed. The difference in ν(CO) frequency between the two bands of the 2nd transient species is similar to those of the 1st transient species, indicating formation of two distinct dicarbonyl species following photolysis of $CpRe(CO)_3$. The lower frequency of the ν(CO) bands of the 2nd transient compared to the 1st, suggests an increased amount of electron density present on the metal.

The rate of decay of the 1st transient species matches the rate of growth of the 2nd, as shown in Figure 3.8, indicating direct formation of the 2nd dicarbonyl species from the 1st. The lifetime of this process was measured as $\tau = 3.5$ (± 0.5) ns. Difference spectra recorded on the microsecond timescale following photolysis show only the two ν(CO) bands of the 2nd dicarbonyl species. These features do not decay fully on the

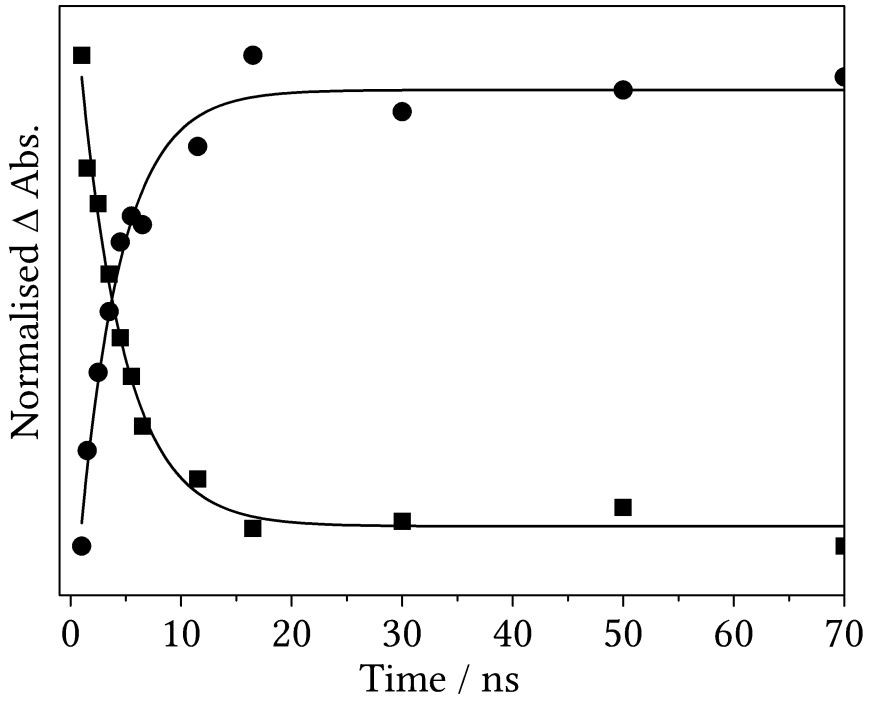


FIGURE 3.8: Normalised, single-point kinetic traces from TRIR spectra recorded following photolysis of $CpRe(CO)_3$ in PFMCH under Ar, showing matching rates for the decay of the 1st transient (1895 cm^{-1}, squares) and growth of the 2nd transient (1889 cm^{-1}, circles) on a nanosecond timescale. Solid black lines represent mono-exponential fits.

timescale of the experiment (70 μs), losing only 20 % of their maximum intensity over this time. No recovery of the ν(CO) bands of the parent complex is observed on this timescale.

Attempting to assign these two dicarbonyl species presents several different possibilities. Direct formation of the 2nd transient from the 1st, as well as the lower frequency of the ν(CO) bands of the 2nd transient suggests the 2nd transient is the product of the reaction of the 1st with a solvent, parent complex or other ligand. The sample solution in this case contains only $CpRe(CO)_3$, the PFMCH solvent, and dissolved Ar gas. While a reaction of a dicarbonyl species of the form $CpRe(CO)_2X$ has been reported to undergo reaction with the parent $CpRe(CO)_3$ to form $Cp_2Re_2(CO)_5$

in the absence of CO,[174] ν(CO) band positions for the dimeric species do not match those observed for the 2nd transient in this case, and no increased bleaching of the parent ν(CO) bands is observed during the experiment.[167] Due to these observations, formation of a dimeric species can be ruled out.

A further possibility involves a reaction of either a solvent complex or coordinatively unsaturated dicarbonyl species with Ar to form $CpRe(CO)_2Ar$, which has previously been tentatively assigned following photolysis of $CpRe(CO)_3$ in *sc*Ar.[216] However, this species was found to be short lived in the presence of CO, and it is likely due to the long-lived nature of the 2nd transient that this Ar complex is not formed during these studies. The ν(CO) bands of $CpRe(CO)_2Ar$ were also found to appear to higher energy than those of the 2nd transient, when compared with their respective parent ν(CO) frequencies, indicating a weaker mode of binding than observed in this case. While $CpRe(CO)_2Ar$ may appear to be a candidate for assignment of the 1st transient which exhibits higher energy ν(CO) bands, the low concentration of Ar in the solution compared to the solvent makes formation of this species on a fast picosecond timescale unlikely.

A further possibility is that the 1st transient complex represents a coordinatively unsaturated complex, which undergoes a reaction with the solvent to form $CpRe(CO)_2(C_7F_{14})$. This situation is similar to that observed for $CpMn(CO)_3$ in the previous Chapter as well as previously published work.[53,118,150] As stated above, no unsaturated triplet intermediate has ever been observed following photolysis of $CpRe(CO)_3$, however singlet unsaturated $CpRe(CO)_2$ has been previously reported in Nujol at 77 K.[167] The authors reported ν(CO) band positions for $CpRe(CO)_2$ of

1947 and 1879 cm^{-1}, with parent $CpRe(CO)_3$ ν(CO) bands at 2029 and 1934 cm^{-1}. Comparison with the ν(CO) bands of the 1st observed dicarbonyl transient in this experiment (1964 and 1895 cm^{-1}, parent bands 2037 and 1948 cm^{-1}) with those of $CpRe(CO)_2$ in Nujol at 77 K shows some agreement between for the difference between the lower energy parent ν(CO) band and lower energy transient ν(CO) band ($\Delta\nu$ = 55 and 53 cm^{-1} for Nujol and PFMCH, respectively), while a comparison of the higher energy bands is less convincing ($\Delta\nu$ = 82 and 73 cm^{-1} for Nujol and PFMCH, respectively). Coordinatively unsaturated complexes have also been previously assigned following photolysis of $M(CO)_6$ (M = Cr, Mo, W) in PFMCH, suggesting that the non-coordinating nature of the solvent may allow for detection of such species.[78,79]

An interchange of this nature has been previously observed following photolysis of $CpRe(CO)_3$ in *sc*Kr doped with Xe.[216] The author reported initial formation of a Kr solvent complex, which underwent reaction with Xe to form the more stable $CpRe(CO)_2Xe$. This change in the nature of the dicarbonyl complex was observed as a shift to lower wavenumber on the nanosecond timescale upon reaction with Xe. This result was reported in contrast to previous studies of photolysis of $W(CO)_6$ in *sc*Kr doped with Xe, in which preferential coordination of $W(CO)_5$ by Xe was observed less than 50 ns following photolysis.[286] In both of these cases, the interchange between the two observed dicarbonyl species was observed on the long nanosecond timescale (50-1000 ns) if it was observed at all. The 2nd dicarbonyl transient observed during this study was seen to form on a fast nanosecond timescale (<10 ns). It is therefore possible that further dicarbonyl species were present at earlier times in the previously published studies discussed above, however they were not observed.

A final possibility for the assignment of the 1st observed transient is fast formation of a short-lived, weak binding mode of the PFMCH solvent, which undergoes isomerisation to a more stable binding mode, or reaction with a trace impurity, resulting in formation of the 2nd more stable transient species. An isomerisation mechanism would likely be highly dependent on the structure of the solvent molecule. PFMCH possesses multiple binding sites which are chemically different, including a CF_3 moiety, attached to a CF centre, which is bound to a series of CF_2 groups which make up the cyclohexyl ring. In order to test this hypothesis, it would be necessary to repeat the above experiment in a perfluorinated solvent which possesses only one type of C-F environment with which the Re metal centre can interact, e.g., non-branched cyclic perfluoroalkanes, to determine if this interchange between two different dicarbonyl species is still present. Unfortunately, the low availability of unbranched cyclic perfluoroalkanes (e.g., perfluoro(cyclohexane)) prohibits such studies, and the synthesis of perfluorinated alkanes on a scale necessary for their use as a solvent is far beyond the scope of this work. The possibility of the presence of a small amount of perfluoroalkene impurity was also considered as a potential cause of the observed interchange. The presence of C=C double bonds in solution would likely cause formation of a more strongly bound coordination complex than a perfluoroalkane complex. In order to determine if this was the case, a small amount of perfluoro(hexene) was doped into a solution of $CpRe(CO)_3$ in PFMCH. TRIR spectra recorded on the nanosecond timescale following 266 nm photolysis of $CpRe(CO)_3$ in PFMCH doped with perfluoro(hexene) (0.5 M) is shown in Figure 3.9. Photolysis resulted in initial bleaching of the two parent ν(CO) bands of $CpRe(CO)_3$ and formation of two new ν(CO) features at (1964 and 1895 cm^{-1}) within 1 ns, in agreement with experiments in neat PFMCH. Decay of these two

features is concurrent with formation of two new ν(CO) features at which have not been previously observed at 1990 and 2052 cm^{-1}. These features are assigned to the perfluoro(hexene) complex $CpRe(CO)_2(C_6F_{10})$. The ν(CO) bands of this species do not match those of either of the dicarbonyl transient observed in neat PFMCH, indicating that perfluoroalkene impurities are unlikely to play a role in the photochemistry of metal carbonyls in PFMCH.

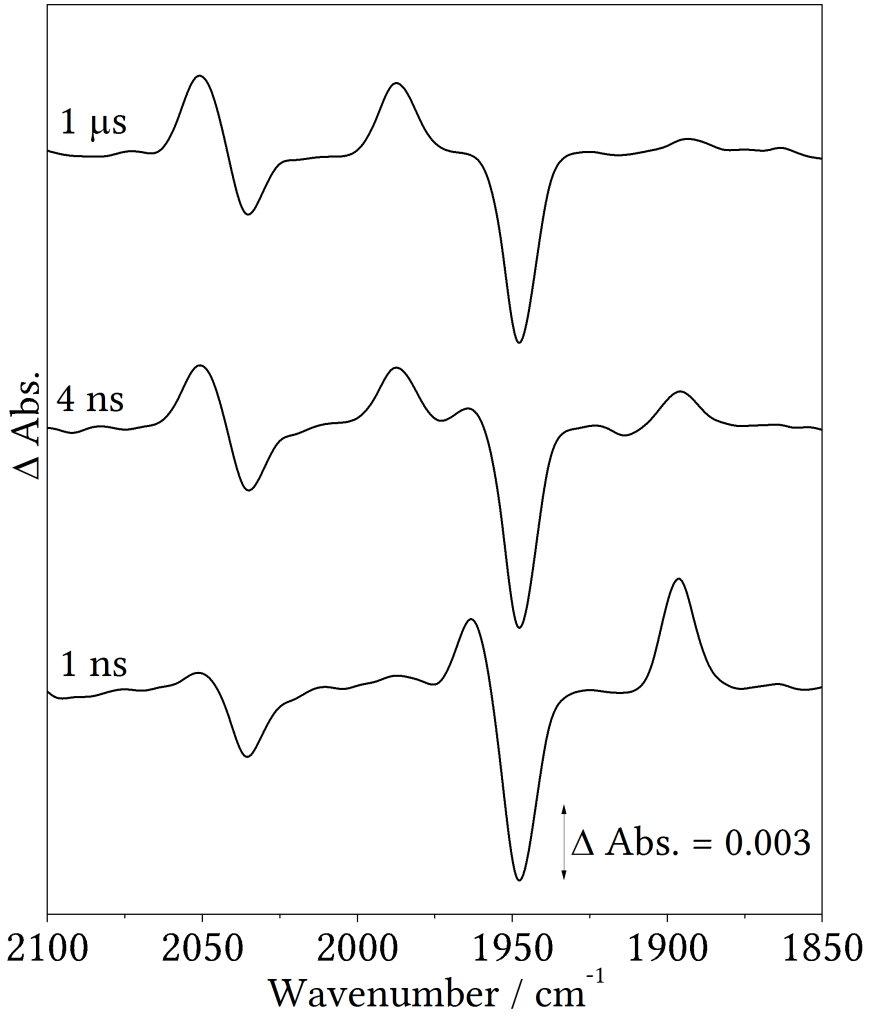


FIGURE 3.9: Selected nanosecond TRIR difference spectra recorded at a series of time delays following 266 nm photolysis of a solution of $CpRe(CO)_3$ in PFMCH doped with perfluoro(hexene) (0.5 M), showing initial formation of a dicarbonyl transient, followed by growth of the perfluoro(hexene) complex $CpRe(CO)_2(C_6F_{10})$.

In addition to experiments involving photolysis of $CpRe(CO)_3$ in PFMCH, photolysis of a solution of $CpRe(CO)_3$ in perfluoro(hexanes) was also undertaken. Following photolysis, the parent ν(CO) bands (2038 and 1950 cm^{-1}) were bleached, resulting in formation of two ν(CO) bands corresponding to a carbonyl loss species (1965 and 1896 cm^{-1}). These features are stable on the picosecond timescale, however on the nanosecond timescale they decay to form two new ν(CO) features (1960 and 1890 cm^{-1}) to lower energy compared to the initial transient species, also consistent with a dicarbonyl species. The rate of decay of the 1st transient was found to match the rate of growth of the 2nd (lifetime $\tau = 10$ ($\pm$1) ns). This interchange between the two dicarbonyl species is consistent with that observed in PFMCH, however the rate of this interchange is slower.

It is clear from this study that the rate of formation of the 2nd dicarbonyl species in this case is dependent on the nature of the solvent. While this interchange behaviour is not altered on changing the solvent from PFMCH to PFH, this does not rule out the possibility of different binding modes of the solvent causing the formation of two different dicarbonyl species, as PFH also possesses two different C-F environments with which the metal centre can interact. Alternatively, the solvent may undergo a change between an η^1-F interaction with the metal, and an η^2-C,F interaction. This interchange behaviour was not observed in the previous Chapter following photolysis of $CpMn(CO)_3$ in perfluorinated solvents. This could be due to the shorter lived species not being observed due to the presence of a long-lived coordinatively unsaturated triplet intermediate. It is possible that the interchange between the triplet and singlet states is slower than the decay of the shorter lived dicarbonyl transient initially observed

following photolysis of $CpRe(CO)_3$.

3.2.2 TRIR Studies of $CpRe(CO)_3$ in Perfluoroalkane Solvents with Noble Gas and Liquid Alkane Dopants

Following studies in pure PFMCH solvent, solutions of $CpRe(CO)_3$ in PFMCH were doped with cyclopentane and Xe, in order to attempt to characterise any resulting organometallic noble gas and alkane complexes. These two dopant systems were chosen due to high stability reported for xenon and cyclopentane complexes of $CpRe(CO)_2$.[34]

The TRIR difference spectrum recorded 1 ps following 266 nm photolysis of a solution of $CpRe(CO)_3$ in PFMCH doped with cyclopentane (0.5 M) resulted in bleaching of the two parent ν(CO) bands at 2037 and 1948 cm^{-1}, accompanied by broad, vibrationally excited features. Two distinct ν(CO) bands are also present at 1952 and 1887 cm^{-1}. These bands are consistent with a dicarbonyl complex of the form $CpRe(CO)_2X$. These features were observed to be stable on the nanosecond timescale, and the TRIR difference spectrum recorded 1 ns following photolysis shows only the ν(CO) bands of this species, shown in Figure 3.10. The ν(CO) bands of the single photoproduced species observed during this experiment lie closer to those of the 2nd, more stable dicarbonyl observed following photolysis in PFMCH than to the 1st, less stable dicarbonyl. It is possible that the 1st dicarbonyl species is present on the fast picosecond timescale, however its presence may be obscured by the broad vibrationally excited ground state features present at early time. This new species was observed to

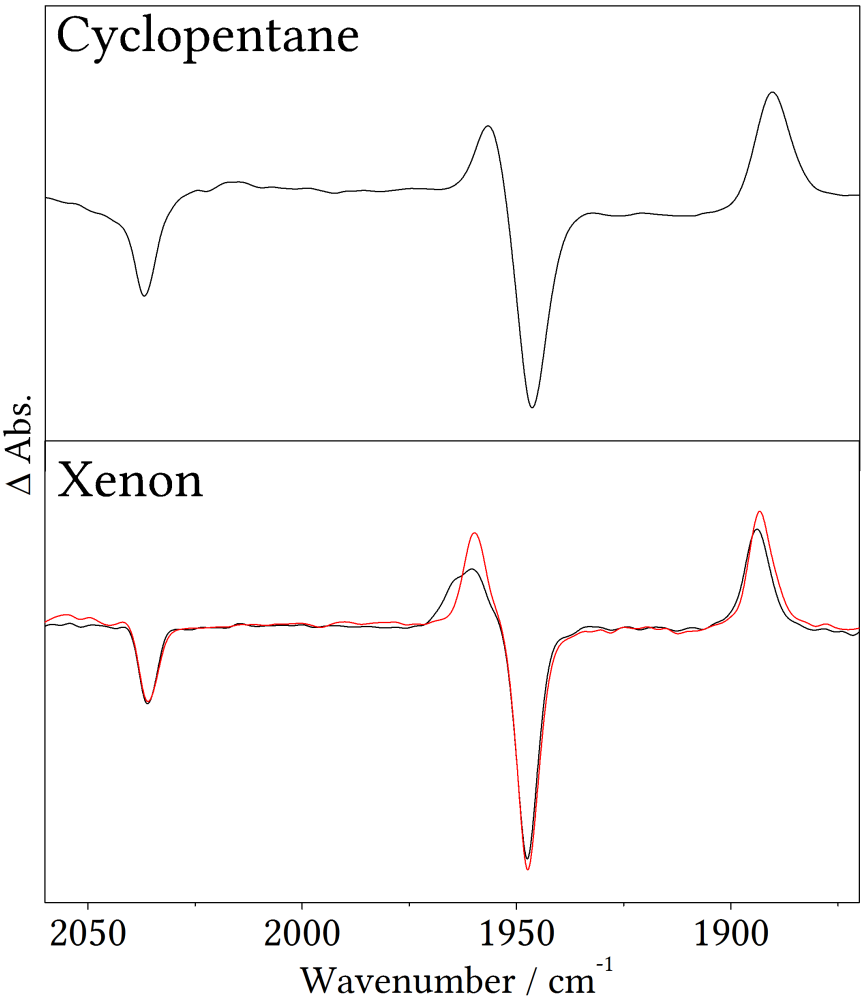


FIGURE 3.10: TRIR difference spectra recorded 1 ns following photolysis of a solution of $CpRe(CO)_3$ in PFMCH doped with cyclopentane (0.5 M) (top, black), 1 ns following photolysis of $CpRe(CO)_3$ in PFMCH under 1.5 bar Xe (bottom, black), and 50 ns following photolysis of $CpRe(CO)_3$ in PFMCH under 1.5 bar Xe (bottom, red).

decay only slightly over the course of the experiment, losing *ca.* 5 % of its maximum intensity after 70 μs.

Photolysis of a solution of $CpRe(CO)_3$ in PFMCH under Xe (1.5 bar) resulted in initial bleaching of the two parent ν(CO) absorption bands (2037 and 1948 cm) along with formation of vibrationally hot features. These new features cool over the first 100 ps of the experiment to yield two ν(CO) bands at 1964 and 1895 cm^{-1}. In

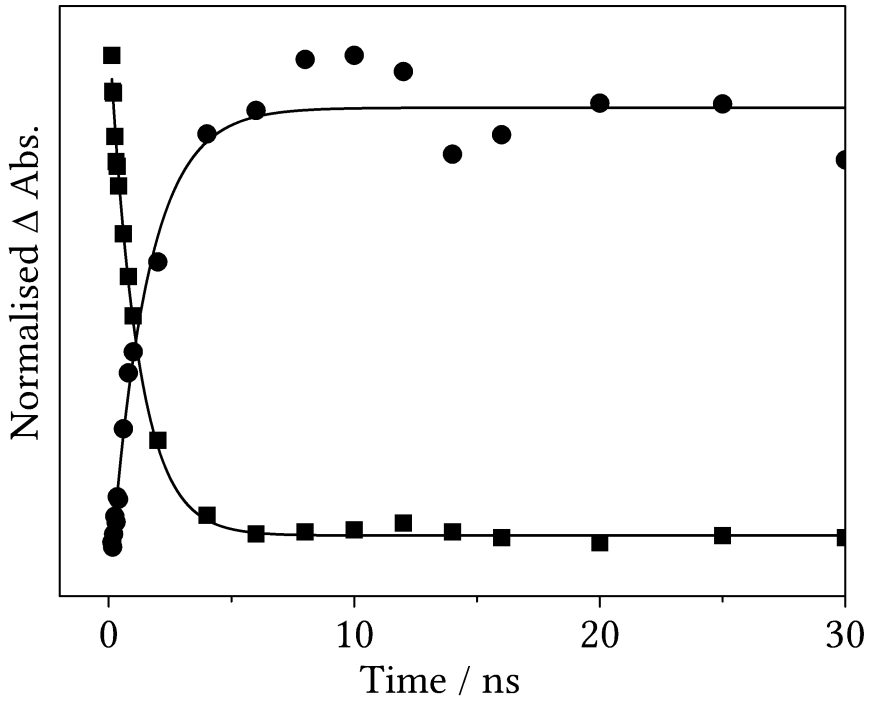


FIGURE 3.11: Kinetics traces from TRIR spectra recorded following photolysis of a solution of $CpRe(CO)_3$ in PFMCH under 1.5 bar Xe, showing decay of the 1st dicarbonyl transient (squares) and growth of the 2nd dicarbonyl species (circles). Solid lines show mono-exponential fits.

this case, this initial dicarbonyl transient species begins to decay on the picosecond timescale, giving way to a second dicarbonyl species with ν(CO) bands at 1959 and 1893 cm^{-1}. The TRIR difference spectrum recorded 1 ns following photolysis exhibits some evidence of the first dicarbonyl transient, as a small shoulder on the higher energy transient band of the final dicarbonyl species, as shown in Figure 3.10. The rate of growth of the 2nd dicarbonyl and the rate of decay of the 1st were found to match, as shown in Figure 3.11, indicative of direct formation of the second species from the first. This observation is consistent with spectra recorded in pure PFMCH (τ = 3.5 ($\pm$0.5) ns), however in the case of the Xe doped solution, the rate of interchange between the two transient species is faster (τ = 1.2 ($\pm$0.2) ns). This second transient was observed to be stable on the nanosecond and early microsecond timescales, losing *ca.* 18 % of

its maximum intensity over the course of the 70 μs experiment. Addition of Xe to a solution of $CpRe(CO)_3$ in perfluoro(hexanes) also gave similar results. In this case, the formation of the 2nd dicarbonyl species from the 1st occurred at a similar rate to that observed in Xe doped PFMCH (τ = 1.3 ($\pm$0.2) ns). A summary of the lifetimes for this process is given in Table 3.1, and associated rate constants are summarised in Table 3.3 The fact that this rate remains the same upon changing the solvent suggests that in doped solutions, the solvent itself plays little or no role in this process.

TABLE 3.1: Lifetimes (in ns) for the interchange between the 1st and 2nd $CpRe(CO)_2X$ transients formed following photolysis of $CpRe(CO)_3$, $Cp^*Re(CO)_3$ and $CpRe(CO)_2(N_2)$ in a series of pure and Xe doped PFMCH and PFH solutions at 298 K.

Compound	**Solvent**	**Dopant**	**Lifetime τ (ns)**
$CpRe(CO)_3$	PFMCH		3.5 ($\pm$0.5)
		Xe	1.2 ($\pm$0.2)
	PFH		10 ($\pm$1.0)
		Xe	1.3 ($\pm$0.2)
$Cp^*Re(CO)_3$	PFMCH		3.3 ($\pm$0.4)
		Xe	1.1 ($\pm$0.2)
$CpRe(CO)_2(N_2)$	PFMCH		3.7 ($\pm$0.4)
		Xe	1.3 ($\pm$0.2)

Figure 3.12 shows a comparison of the TRIR difference spectra recorded 5 μs following photolysis of $CpRe(CO)_3$ in PFMCH, Xe doped PFMCH and *c*-pentane doped PFMCH. In the case of the solution containing cyclopentane only a single photoproduct is observed, the ν(CO) bands of which appear to lower energy than those observed during the other two experiments. By comparison with previous studies, this species is assigned as the cyclopentane complex $CpRe(CO)_2(C_5H_{10})$.[48] Addition of Xenon to the solution also results in a change of ν(CO) frequency of the 2nd dicarbonyl complex

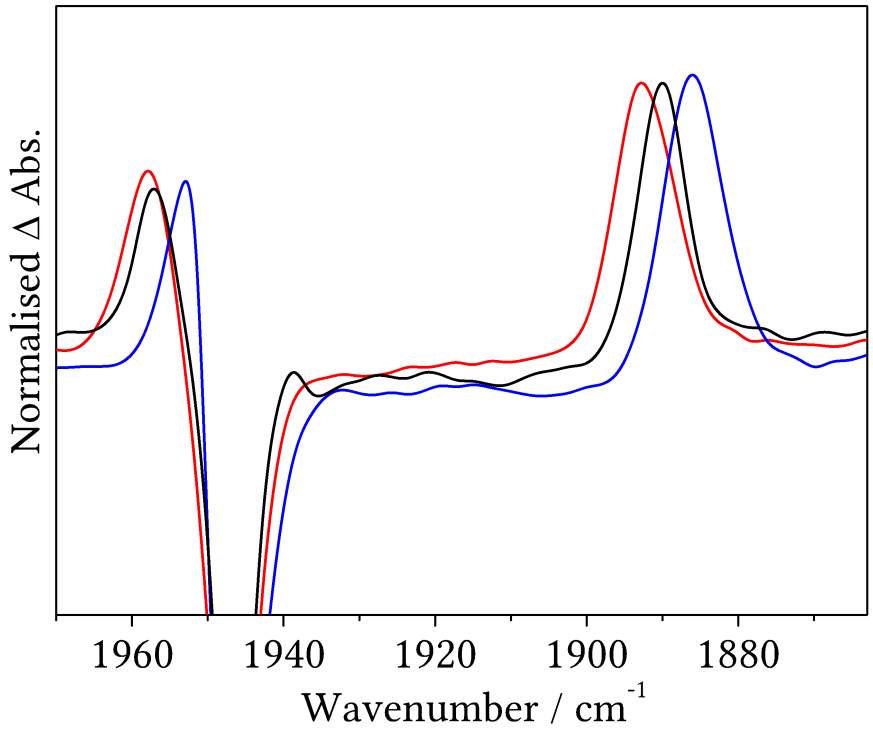


FIGURE 3.12: TRIR difference spectra recorded 5 μs following photolysis of a solution of $CpRe(CO)_3$ in PFMCH (black), $CpRe(CO)_3$ in PFMCH doped with *c*-pentane (blue) and $CpRe(CO)_3$ in PFMCH under 1.5 bar Xe (red). The effect of addition of alkane and noble gas dopants on the ν(CO) band positions of the second dicarbonyl transient species can be seen clearly.

compared to experiments in pure PFMCH, while those of the 1st dicarbonyl complex remain the same. The rate of interchange between these two species is also faster upon addition of Xe when compared to pure PFMCH, indicating formation of a different species. From this, as well as previously reported studies,[48,174,183] the 2nd dicarbonyl species observed following photolysis of $CpRe(CO)_3$ in PFMCH under Xe (1.5 bar) is assigned as the Xe complex $CpRe(CO)_2Xe$. Due to its comparable stability and similar ν(CO) band positions to both $CpRe(CO)_2(C_5H_{10})$ and $CpRe(CO)_2Xe$, it is likely that the 2nd dicarbonyl transient produced following photolysis of $CpRe(CO)_3$ in pure PFMCH is $CpRe(CO)_2(C_7F_{14})$.

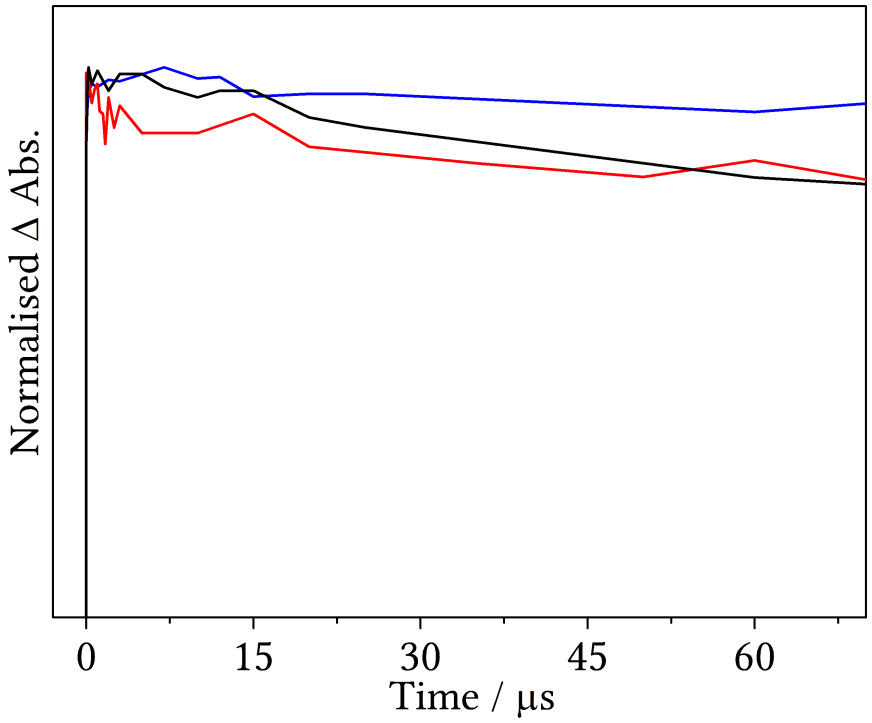


FIGURE 3.13: Kinetics traces from TRIR spectra recorded following photolysis of a solution of $CpRe(CO)_3$ in PFMCH (black), $CpRe(CO)_3$ in PFMCH doped with *c*-pentane (0.5 M) (blue) and $CpRe(CO)_3$ in PFMCH under 1.5 bar Xe (red). The decay of the final dicarbonyl species in each case is shown.

Examination of the decay of the final dicarbonyl photoproduct in each case reveals the remarkable stability of all three complexes, shown in Figure 3.13. As expected, the decay of $CpRe(CO)_2(C_5H_{10})$ appears to be the slowest, as expected due to the high stability of this complex reported previously.[34] Photoproducts formed following photolysis of in pure PFMCH and PFMCH doped with Xe show similar stability on the microsecond timescale, however both are less stable than $CpRe(CO)_2(C_5H_{10})$. From the studies presented above, it is clear that the formation, stability and ν(CO) band positions of the 2nd dicarbonyl species produced following photolysis of $CpRe(CO)_3$ in PFMCH are dependent on the nature of the solvent or dopant, while the ν(CO) frequencies of the 1st dicarbonyl transient species appears to be independent of it. This

observations somewhat reflects the spin-crossover system observed for $CpMn(CO)_3$ in the previous chapter, in which a coordinatively unsaturated or weakly coordinated intermediate undergoes a reaction with the solvent or dopant to produce a more stable dicarbonyl species. In the case of $CpMn(CO)_3$ however, there was considerable precedent for the assignment of the triplet dicarbonyl intermediate, while in the case of $CpRe(CO)_3$, this study represents the first observation of such an intermediate by time-resolved spectroscopy. It seems likely considering the results presented above that this species is either the coordinatively unsaturated species $CpRe(CO)_2$, or a more weakly coordinated form of $CpRe(CO)_2(C_7F_{14})$.

3.2.3 TRIR Studies of $CpRe(CO)_3$ Derivatives in Perfluoroalkane Solvents

Following TRIR studies of $CpRe(CO)_3$ in PFMCH and PFH, studies of the Cp-substituted derivative $Cp^*Re(CO)_3$ (Cp^* = pentamethylcyclopentadienyl) were also undertaken, to examine any difference in photochemistry due to the addition of 5 electron donating substituents onto the Cp ring.

Figure 3.14 shows TRIR difference spectra recorded following 266 nm photolysis of $Cp^*Re(CO)_3$ in PFMCH under Ar, as well as in PFMCH under Xe. Immediately following photolysis, the parent ν(CO) bands of $Cp^*Re(CO)_3$ (2018 and 1928 cm^{-1}) were bleached, and new broad features were observed over the first 100 ps of the experiment, consistent with vibrationally excited ground state features observed above. The spectra also showed two distinct ν(CO) bands at 1941 and 1871 cm^{-1}, consistent with formation

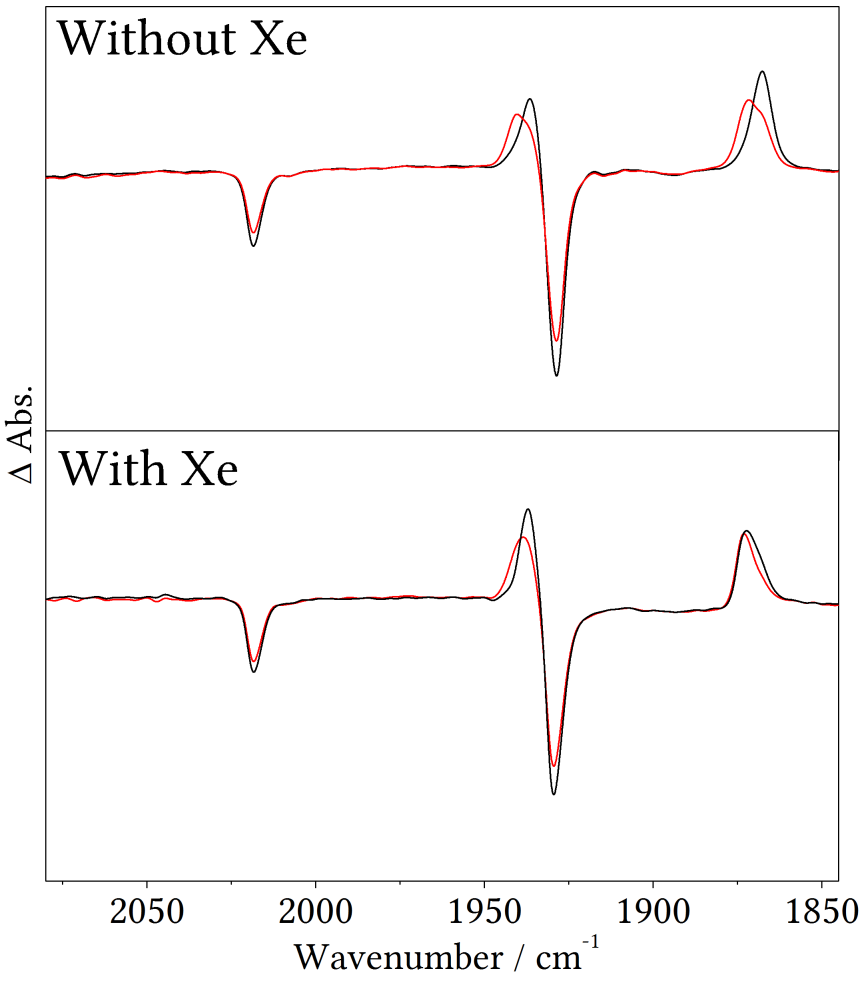


FIGURE 3.14: TRIR difference spectra recorded 1 ns (red) and 100 ns (black) following 266 nm photolysis of a solution of $Cp^*Re(CO)_3$ in PFMCH under 1.5 bar Ar (top) and a solution of $Cp^*Re(CO)_3$ in PFMCH under 1.5 bar Xe (bottom). The difference in behaviour of the first dicarbonyl transient, and the difference in ν(CO) frequency of the second dicarbonyl transient can be seen.

of the 1st dicarbonyl transient observed for $CpRe(CO)_3$ experiments above. ν(CO) band positions of this 1st transient species were consistent for both photolysis in pure PFMCH and Xe doped PFMCH, suggesting formation of the same initial transient species. In both cases, this dicarbonyl species was observed to decay to yield a 2nd more stable species, with ν(CO) bands at 1936 and 1867 cm^{-1}, and 1937 and 1870 cm^{-1} for pure PFMCH and Xe doped PFMCH, respectively. The difference spectra recorded

100 ns following photolysis show only the presence of the 2nd dicarbonyl transient in each case.

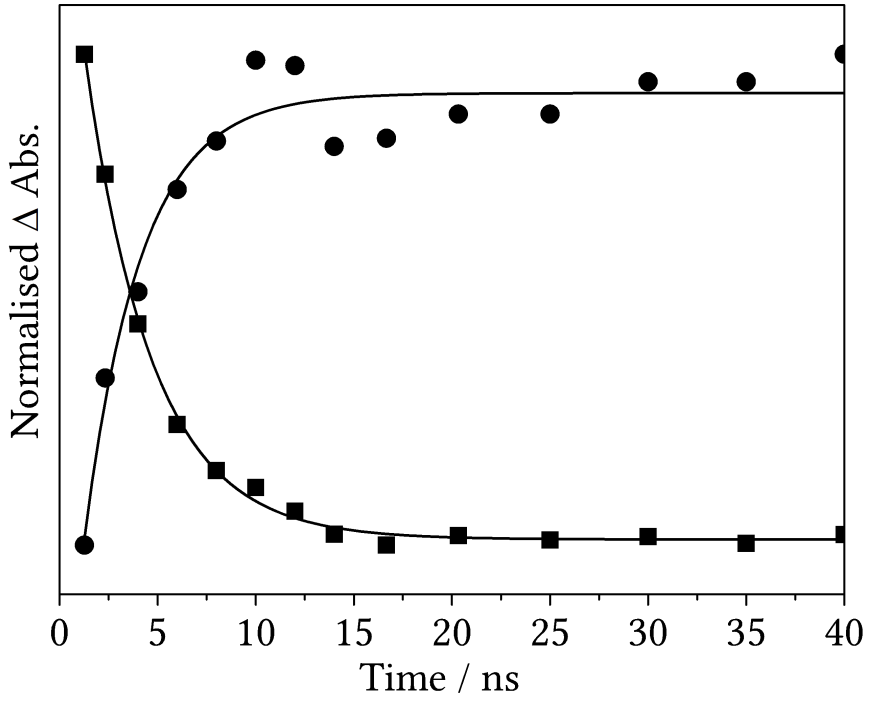


FIGURE 3.15: Normalised, single-point kinetic traces from TRIR difference spectra recorded following photolysis of $Cp^*Re(CO)_3$ in PFMCH under Ar, showing matching rates for the decay of the first dicarbonyl species (1941 cm^{-1}, squares) and growth of the second transient (1936 cm^{-1}, circles) on a nanosecond timescale. Solid black lines represent mono-exponential fits.

As above, this difference in ν(CO) frequencies of the 2nd dicarbonyl transient species suggests formation of a different species upon addition of Xe to a solution of $Cp^*Re(CO)_3$ in PFMCH. Further evidence is observed in the rate of the interchange between these two species. In pure PFMCH solution, this process is observed to be slower (lifetime τ = 3.3 ($\pm$0.4) ns, Figure 3.15), than the same process observed in Xe doped PFMCH (lifetime τ = 1.1 ($\pm$0.2) ns, Figure 3.16). It should be noted that these values are within error of those reported for analogous processes following photolysis of

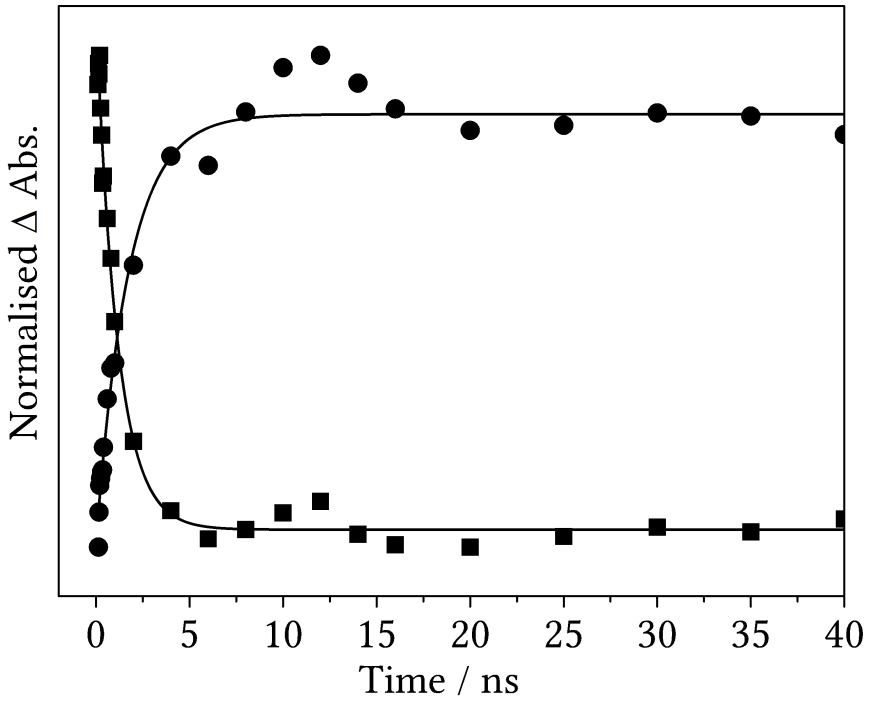


FIGURE 3.16: Normalised, single-point kinetic traces from TRIR difference spectra recorded following photolysis of $Cp^*Re(CO)_3$ in PFMCH under Xe 1.5, showing matching rates for the decay of the first dicarbonyl species (1941 cm^{-1}, squares) and growth of the second transient (1937 cm^{-1}, circles) on a nanosecond timescale. Solid black lines represent mono-exponential fits.

$CpRe(CO)_3$ in PFMCH, indicating that the addition of methyl substituents onto the Cp ring has little or no effect on the formation of this 2nd dicarbonyl species. Consistent with observations reported for $CpRe(CO)_3$ above, the 2nd dicarbonyl species does not decay fully on the timescale of this experiment (70 μs), with both species losing only *ca.* 20 % of their maximum intensity. By comparison with results for $CpRe(CO)_3$ presented above, as well as the difference in their rates of formation and ν(CO) band positions, the 2nd dicarbonyl species formed during these experiments are assigned as $Cp^*Re(CO)_2(C_7F_{14})$ and $Cp^*Re(CO)_2Xe$, for pure PFMCH and Xe doped PFMCH, respectively.

The photochemistry of an additional $CpRe(CO)_3$ derivative, $CpRe(CO)_2(N_2)$,

was also examined during these studies. This species is known to undergo facile loss of N_2 following photolysis at 355 nm.[43,291] It was hoped that this species would exhibit the same photochemistry in the presence of Xe in PFMCH solution as $CpRe(CO)_3$, but at a longer photolysis wavelength. Initiating this chemistry with 355 nm rather than 266 nm irradiation would allow access to a broader range of cell window materials for use in future TR-XAFS experiments. 355 nm photolysis of $CpRe(CO)_2(N_2)$ in PFMCH resulted in bleaching of the parent ν(CO) and ν(NN) bands, and formation of the same 1st dicarbonyl species observed previously following photolysis of $CpRe(CO)_3$, which subsequently decayed to form $CpRe(CO)_2(C_7F_{14})$ at a rate consistent with results presented above. Addition of Xe to this solution resulted in formation of $CpRe(CO)_2Xe$, as expected.

TABLE 3.2: ν(CO) absorption band frequencies of $CpRe(CO)_3$, $Cp^*Re(CO)_3$ and intermediates and photoproducts formed following photolysis of $CpRe(CO)_3$ and $Cp^*Re(CO)_3$ in a series of pure and doped PFMCH and PFH solutions. Experiments performed in solution phase at 298 K unless otherwise stated.

Compound	Solvent/Matrix	Dopant	ν(CO) (cm^{-1})	Reference/Notes
$CpRe(CO)_3$	PFMCH		2037, 1948	This work
		c-pentane	2037, 1948	This work
		Xe	2037, 1948	This work
	PFH		2038, 1950	This work
		Xe	2038, 1950	This work
	Nujol		2029, 1934	167, 77 K
	*sc*Ar		2040, 1954	216
	*sc*Xe		2035, 1946	216
	n-heptane		2031, 1940	216
1st transient	PFMCH		1964, 1895	This work
		Xe	1964, 1895	This work
	PFH		1965, 1896	This work
		Xe	1965, 1896	This work
$CpRe(CO)_2X$	PFMCH		1958, 1889	This work
		c-pentane	1952, 1887	This work
		Xe	1959, 1893	This work
	PFH		1960, 1890	This work
		Xe	1961, 1983	This work
	Nujol		1957, 1879	167, 77 K
	*sc*Ar		1970, 1907	216
	*sc*Xe		1957, 1894	216
	n-heptane		1954, 1890	216
$Cp^*Re(CO)_3$	PFMCH		2018, 1928	This work
		Xe	2018, 1928	This work
1st transient	PFMCH		1941, 1871	This work
		Xe	1941, 1871	This work
$Cp^*Re(CO)_2X$	PFMCH		1936, 1867	This work
		Xe	1937, 1870	This work
$CpRe(CO)_2(N_2)$	PFMCH		1981, 1927	This work
		Xe	1981, 1927	This work
1st transient	PFMCH		1964, 1895	This work
		Xe	1964, 1895	This work
$CpRe(CO)_2X$	PFMCH		1958, 1889	This work
		Xe	1959, 1893	This work

TABLE 3.3: Observed rate constants (k_{obs}) for the reaction of the initial dicarbonyl transient with solvent or dopant to form $CpRe(CO)_2X$ or $Cp^*Re(CO)_2X$ following 266 ns photolysis of $CpRe(CO)_3$ in pure and Xe doped PFMCH and PFH solutions, and $Cp^*Re(CO)_3$ and $CpRe(CO)_2(N_2)$ in pure and Xe doped PFMCH solutions. All data recorded at 298 K.

Compound	**Solvent**	**ν(CO) (cm^{-1})**	**Assignment**	**k_{obs} (s^{-1})**
$CpRe(CO)_3$	PFMCH	1964	1st transient	2.8 (±0.2) x 10^8
		1895	1st transient	2.6 (±0.5) x 10^8
		1958	$CpRe(CO)_2(C_7F_{14})$	2.5 (±0.3) x 10^8
		1889	$CpRe(CO)_2(C_7F_{14})$	3.0 (±0.6) x 10^8
		1964	1st transient	8.4 (±1) x 10^8
		1895	1st transient	9.0 (±1.4) x 10^8
		1959	$CpRe(CO)_2Xe$	8.6 (±0.9) x 10^8
		1893	$CpRe(CO)_2Xe$	8.3 (±1.5) x 10^8
	PFH	1965	1st transient	1.1 (±0.1) x 10^8
		1896	1st transient	1.2 (±0.2) x 10^8
		1960	$CpRe(CO)_2(C_6F_{14})$	1.0 (±0.1) x 10^8
		1890	$CpRe(CO)_2(C_6F_{14})$	9.1 (±1.5) x 10^7
		1965	1st transient	7.8 (±1.2) x 10^8
		1896	1st transient	8.3 (±1.6) x 10^8
		1961	$CpRe(CO)_2Xe$	8.3 (±1.2) x 10^8
		1893	$CpRe(CO)_2Xe$	9.0 (±1.5) x 10^8
$Cp^*Re(CO)_3$	PFMCH	1941	1st transient	3.0 (±0.2) x 10^8
		1871	1st transient	2.7 (±0.4) x 10^8
		1936	$CpRe(CO)_2(C_7F_{14})$	3.0 (±0.3) x 10^8
		1867	$CpRe(CO)_2(C_7F_{14})$	2.9 (±0.4) x 10^8
		1941	1st transient	9.1 (±1.2) x 10^8
		1871	1st transient	1.0 (±0.2) x 10^9
		1937	$CpRe(CO)_2Xe$	9.4 (±1.0) x 10^8
		1870	$CpRe(CO)_2Xe$	1.1 (±0.3) x 10^9
$CpRe(CO)_2(N_2)$	PFMCH	1964	1st transient	2.7 (±0.3) x 10^8
		1895	1st transient	2.5 (±0.3) x 10^8
		1958	$CpRe(CO)_2(C_7F_{14})$	2.6 (±0.4) x 10^8
		1889	$CpRe(CO)_2(C_7F_{14})$	2.6 (±0.5) x 10^8
		1964	1st transient	7.8 (±0.6) x 10^8
		1895	1st transient	8.3 (±1.3) x 10^8
		1959	$CpRe(CO)_2Xe$	7.9 (±1.0) x 10^8
		1893	$CpRe(CO)_2Xe$	8.6 (±1.5) x 10^8

3.2.4 DFT Studies of Transient Species Produced Following Photolysis of $CpRe(CO)_3$

In order to aid our spectral assignment of the transient species produced following photolysis of $CpRe(CO)_3$ in perfluorinated solvents, DFT calculations of the vibrational frequencies of a series of potential structures were undertaken. DFT has proven to be an extremely useful tool for the study of organometallic alkane and noble gas complexes in recent years.[53,125,232,267,292] All of the calculations reported below were carried out using the Gaussian 03 software package, and Gaussview graphical user interface.[293,294]

In order to reduce computational cost, relativistic effective core potentials (RECPs) were used for Re and Xe atoms. RECPs are known to reproduce experimental trends well at lower computational cost than comparable calculations performed using all-electron basis sets. Previous work within the group has utilised the B3LYP hybrid functional along with the LANL2DZ RECP basis set for heavier atoms and the 6-311G** basis set for all other atoms to calculate the vibrational frequencies of similar species, with some success at modest computational cost.[41] These parameters have therefore been selected for use herein, and will be denoted as B3LYP/LANL2DZ/6-311G**.

The calculated vibrational frequencies of a series of structures of the form $CpRe(CO)_2X$ (X = None, CO, Ar, Xe, C_2F_6, cyclopentane and PFMCH) are given in Table 3.4, along with experimentally obtained values in PFMCH, some of which are tentatively assigned. The reported calculations returned no negative frequencies, indicating that structures had reached the minimum on the potential energy surface. The calculations systematically overestimate the ν(CO) frequencies of all of the studied

TABLE 3.4: Experimental and theoretical ν(CO) absorption band frequencies of $CpRe(CO)_3$and intermediates and photoproducts formed following photolysis of $CpRe(CO)_3$. DFT calculations were carried out on energy minimised structures in the gas phase at 298 K, using the B3LYP/LANL2DZ/6-311G** method described above. Experimental ν(CO) band positions were obtained following photolysis in pure PFMCH solution, cyclopentane doped PFMCH solution, or PFMCH solution in the presence of 1.5 bar Ar or Xe, all at 298 K.

	ν(CO) (cm^{-1})	
Compound	**Calculated**	**Experimental**
$\mathbf{CpRe(CO)_3}$	2111, 2035	2037, 1948
$\mathbf{CpRe(CO)_2}$	2049, 1998	1964, 1895
$\mathbf{CpRe(CO)_2Ar}$	2046, 1994	
$\mathbf{CpRe(CO)_2Xe}$	2045, 1993	1959, 1893
$\mathbf{CpRe(CO)_2(C_5H_{10})}$	2038, 1988	1952, 1887
$\mathbf{CpRe(CO)_2(C_2F_6)}$	2044, 1991	
$\mathbf{CpRe(CO)_2(C_7F_{14})}$ **($\mathbf{CF_3}$-bound)**	2044, 1991	1958, 1889
$\mathbf{CpRe(CO)_2(C_7F_{14})}$ **($\mathbf{CF_2}$-bound)**	2045, 1992	

complexes. However, despite this difference interesting trends can be observed in the calculated frequencies.

The calculated frequencies were shown to reproduce the trend in ν(CO) band positions of the final photoproduct observed following photolysis of $CpRe(CO)_3$ in pure PFMCH, and Xe and cyclopentane doped PFMCH. The ν(CO) band positions increase in the order $CpRe(CO)_2(C_5H_{10}) < CpRe(CO)_2(C_7F_{14}) < CpRe(CO)_2Xe$, matching the trend observed in experimental studies, and indicating that our assignment of these three species is likely correct.

Calculation of the ν(CO) band positions of $CpRe(CO)_2$ resulted in ν(CO) frequencies which were approximately 5-7 cm^{-1} higher in energy than those of the PFMCH solvent complex $CpRe(CO)_2(C_7F_{14})$. This difference in ν(CO) frequency matches the difference between the observed bands of the PFMCH complex and the first dicarbonyl transient observed in all experiments, giving a further indication that the first dicarbonyl

transient observed following photolysis is the coordinatively unsaturated $CpRe(CO)_2$. Calculations of the ν(CO) frequencies of the argon complex $CpRe(CO)_2Ar$ show did not show such a large difference in ν(CO) frequency when compared to the PFMCH complex, presumably due to a weak but favourable interaction with the Ar atom. Again, it is concluded that the presence of this species in solution is unlikely.

In order to determine whether the two distinct dicarbonyl species observed following photolysis represent different binding modes of the PFMCH solvent, two different structures of the PFMCH complex were considered. In the first structure the metal interacts with one of the CF_2 units in the perfluoro(cyclohexyl) ring, and another in which the metal interacts with the CF_3 moiety. The difference between the ν(CO) bands of these two species was found to be slight (1-2 cm^{-1}). This is in contrast to experimental studies, which showed a difference in ν(CO) band position between the two dicarbonyl species of 5-7 cm^{-1}. Binding enthalpies were calculated by subtracting the minimised energies of the individual components of the solvated species ($CpRe(CO)_2$ and PFMCH) from that of the PFMCH complex $CpRe(CO)_2(C_7F_{14})$. The binding energy of the CF_3-bound species was found to be larger than that of the CF_2-bound structure (28 and 25 kJ/mol, respectively). It is therefore possible that the PFMCH complex observed experimentally is the CF_3-bound structure, and the CF_2-bound structure is not observed.

In order to aid future computational studies of such species, the structure $CpRe(CO)_2(C_2F_6)$ was also calculated, to determine if this species represents a reasonable computational model of $CpRe(CO)_2(C_7F_{14})$, with fewer atoms and therefore lower computational cost. The calculated ν(CO) frequencies of this species were found

to match well with those of the CF_3-bound PFMCH complex, and was found to have a similar binding enthalpy (27 kJ/mol), indicating that this may indeed by a useful computational model for future calculations at higher levels of theory. In all of these cases, the perfluoroalkane was found to bind to the metal centre through a lone pair located on an F atom. Attempts to calculate structures involving an η^2 interaction between the C-F bond and the metal, as observed for alkanes, resulted in either rearrangement to the F-bound geometry, or breaking of the C-F bond and the return of negative frequencies, indicating that the complex is not at an energy minimum. Despite this, an isomerisation mechanism still represents a possible explanation for the presence of two different dicarbonyl species following photolysis. The errors present in such calculations mean that these results cannot be taken as definitive.

3.2.5 TRIR Studies of C-H Activation at Re in Perfluoro(methylcyclohexane)

An array of different organometallic methane and ethane complexes have been previously examined by matrix isolation,[80,95,265] time-resolved techniques,[37,103,198,249,250] as well as computational studies.[220,232,263,268,269] Of particular interest are the methane and ethane complexes produced following photolysis of $CpRe(CO)_3$ and $Cp^*Re(CO)_3$, due to the observed ability of the Re centre to activate the C-H bonds of methane and ethane following formation of the initial alkane σ-complex.[37,198] Previous room temperature TRIR studies of the formation of methane and ethane complexes of Re have been undertaken using *sc*CH_4 or *liq*C_2H_6 as a solvent. The use of these alkanes as a solvent

requires high pressure conditions (>100 bar), which is not only energy intensive, but requires the use of specially designed high-pressure spectroscopic cells.[202]

3.2.5.1 Characterisation of $CpRe(CO)_2$(alkane) (Alkane = Methane, Ethane) in Room Temperature Perfluoroalkane Solution

In the following studies, characterisation of methane and ethane complexes of Re in room temperature perfluoroalkane solution, at near-ambient (1.5 bar) pressure, using a conventional TRIR transmission flow cell was attempted.

Figure 3.17 shows a series of selected TRIR difference spectra, recorded following 266 nm photolysis of $CpRe(CO)_3$ in PFMCH under 1.5 bar CH_4. Within 1 ps of photolysis, the two parent ν(CO) bands of $CpRe(CO)_3$ (2036 and 1948 cm^{-1}) are bleached and new broad features were observed. Over the first 100 ps of the experiment, these new features are observed to sharpen and blue-shift, yielding two distinct ν(CO) bands at 1964 and 1895 cm^{-1}. These bands match those observed previously for the 1st dicarbonyl transient species formed following photolysis of $CpRe(CO)_3$ in pure PFMCH. These two ν(CO) bands are observed to partially decay on the early nanosecond timescale, along with the formation of four new ν(CO) bands at 2010, 1960, 1937 and 1893 cm^{-1}. This is in stark contrast to previous studies, in which the two ν(CO) bands of the 1st transient species were found to decay completely resulting in formation of a further dicarbonyl solvent or dopant complex of the form $CpRe(CO)_2X$, with only two ν(CO) bands.

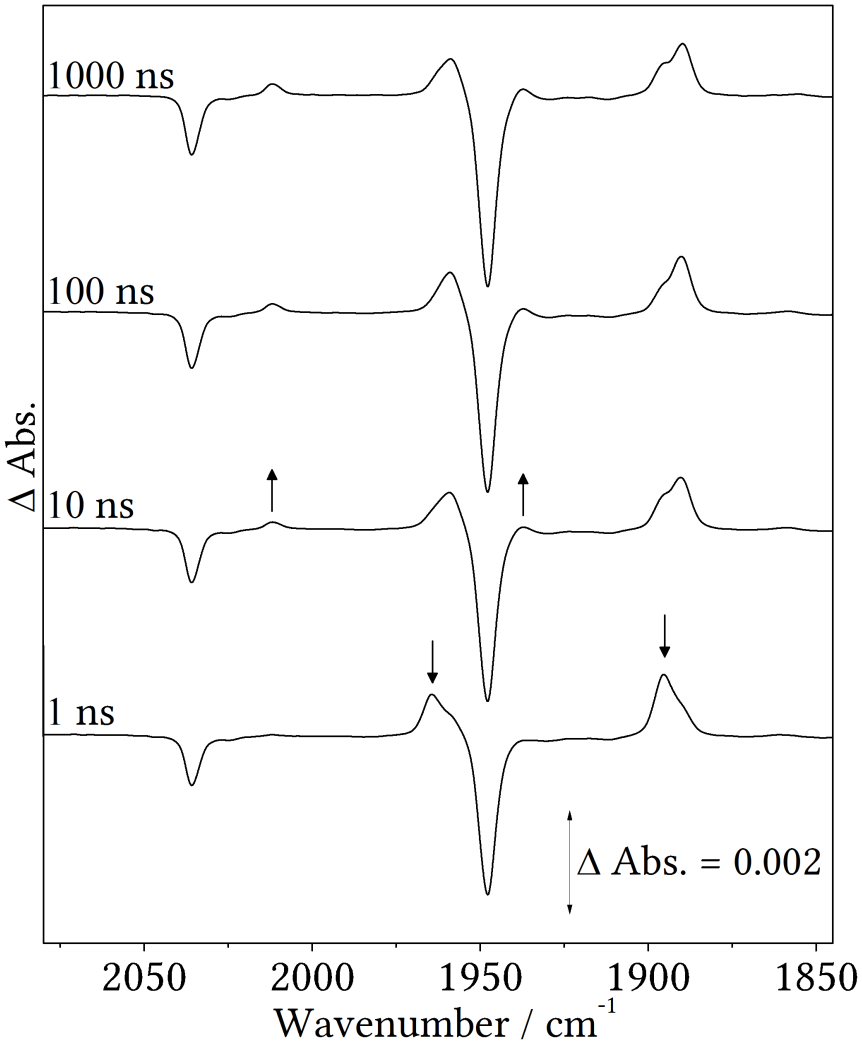


FIGURE 3.17: Selected nanosecond TRIR difference spectra recorded at a series of time delays following 266 nm photolysis of a solution of $CpRe(CO)_3$ in PFMCH under 1.5 bar CH_4. Initial formation of two dicarbonyl species, followed by subsequent C-H activation can be seen.

In this case, it appears that there is more than one species produced following the decay of the 1st dicarbonyl transient. The ν(CO) band positions of these species so not match those reported previously for a dimeric species.[167,174] Two of the ν(CO) bands (1960 and 1893 cm^{-1}) closely match those assigned previously to both $CpRe(CO)_2(C_7F_{14})$ and $CpRe(CO)_2Xe$, suggesting coordination of a weak-binding ligand to the metal centre, possibly methane or the PFMCH solvent. Previous studies have reported the ν(CO)

bands of $CpRe(CO)_2(CH_4)$ in $scCH_4$ as 1963 and 1902 cm^{-1},[198] in agreement with previous matrix isolation, TRIR and NMR studies.[40,48] These values appear at higher energy than those observed in this case, however this shift down in frequency may be partially accounted for by the change in solvent from $scCH_4$ to PFMCH, which also causes the parent ν(CO) bands of $CpRe(CO)_3$ to shift down in energy by 3-5 cm^{-1}.

The two additional ν(CO) bands observed at 2010 and 1937 cm^{-1}, are shifted to higher energy compared to the expected position of $CpRe(CO)_2(CH_4)$ or related dicarbonyl complexes. This shift is consistent with oxidation of the metal centre from Re^{I} to Re^{III}, due to oxidative addition of an alkane. This process has not been observed during photolysis studies of $CpMn(CO)_3$ in perfluorinated solvent presented in the previous Chapter, or in the above studies of $CpRe(CO)_3$ in PFMCH. Activation of C-H bonds by a Re metal centre has been observed previously.[37,234] and ν(CO) bands positions of the activated species $CpRe(CO)_2(CH_3)H$ have been reported as 2012 and 1942 cm^{-1}, which closely match those observed in this case. The two ν(CO) bands observed at 2010 and 1937 cm^{-1} are therefore assigned to the C-H activated alkyl hydride complex $CpRe(CO)_2(CH_3)H$. Previous DFT studies have reported that $CpRe(CO)_2(CH_4)$ and $CpRe(CO)_2(CH_3)H$ lie very close in energy, with a low activation barrier between the two species (approx. 28 kJ/mol).[232]

Figure 3.18 shows kinetic traces from TRIR showing the decay of the 1st transient species (lifetime τ = 2.4 ($\pm$0.2) ns) and growth of bands tentatively assigned to $CpRe(CO)_2(CH_4)$ (τ = 2.9 ($\pm$0.2) ns) and $CpRe(CO)_2(CH_3)H$ (τ = 3.8 ($\pm$0.3) ns). It should be initially noted that decay of the 1st transient species in this case is faster than that observed previously for pure PFMCH solvent (τ = 3.5 ($\pm$0.5) ns), but slower

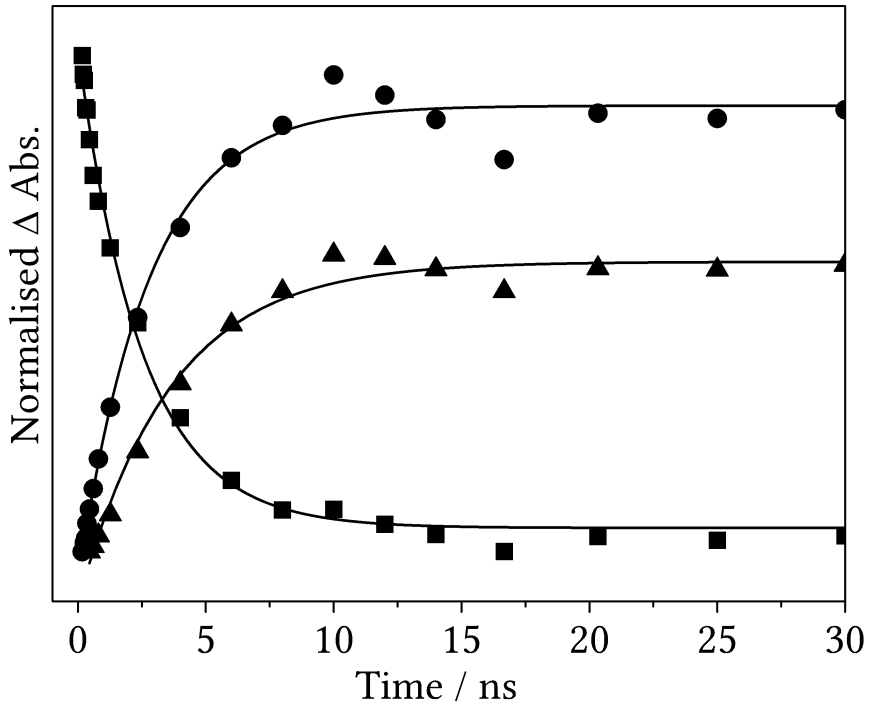


FIGURE 3.18: Normalised single-point kinetic traces from TRIR difference spectra recorded following 266 nm photolysis of $CpRe(CO)_3$ in PFMCH under CH_4 (1.5 bar), showing decay of the 1st dicarbonyl transient species (squares), formation of $CpRe(CO)_2(CH_4)$ (circles) and formation of $CpRe(CO)_2(CH_3)H$ (triangles). Solid lines are mono-exponential fits.

than that observed for PFMCH doped with 1.5 bar Xe (τ = 1.2 ($\pm$0.2) ns). Growth of the transient species assigned as $CpRe(CO)_2(CH_4)$ appears slightly slower than the decay of the 1st transient. Formation of $CpRe(CO)_2(CH_3)H$ was observed to be slower than both of these processes.

It would be expected that $CpRe(CO)_2(CH_3)H$ would form directly from the alkane complex, $CpRe(CO)_2(CH_4)$. Indeed this has previously been directly observed by TRIR following photolysis of $Cp^*Re(CO)_3$ in *sc*CH_4 along with subsequent establishment of an equilibrium between $Cp^*Re(CO)_2(CH_4)$ and $Cp^*Re(CO)_2(CH_3)H$.[37] The unequivocal observation of a C-H activated species, $CpRe(CO)_2(CH_3)H$, would indeed suggest the presence of $CpRe(CO)_2(CH_4)$ in solution. While the 1st observed dicarbonyl transient

species may decay on the same timescale as the formation of $CpRe(CO)_2(CH_3)H$, the rates of decay and formation of these species, respectively do not match, making it unlikely that the activated species forms directly from this 1st transient. Harris *et al.* have previously described the ability of 16-electron unsaturated triplet species (e.g., $^3CpMn(CO)_2$ and $^3CpCo(CO)$) to directly activate the Si-H bond of a silane, without a Si-H-bound σ-complex intermediate being observed spectroscopically.[144,147,150] However, the authors also reported that second and third row transition metals do not exhibit this phenomenon due to the lack of a long-lived triplet intermediate.[56,190] The small difference between the rate of decay of the 1st transient and rate of growth of the 2nd observed above raises the possibility of contribution from another process, possibly formation of a low concentration of $CpRe(CO)_2(CH_3)H$, contributing to the growth of this second transient, tentatively assigned to $CpRe(CO)_2(CH_4)$. However, a contribution of this type would be expected to cause the growth of this species to deviate from simple behaviour. Additionally, the incomplete decay of the 1st transient raises the possibility of an equilibrium between the 1st transient and $CpRe(CO)_2(CH_4)$.

In addition to photolysis of $CpRe(CO)_3$ in PFMCH under a CH_4 atmosphere, this study was expanded to examine photolysis of $CpRe(CO)_3$ in PFMCH under C_2H_6. Immediately upon photolysis, the parent ν(CO) bands (2037 and 1948 cm^{-1}) were observed to bleach. The TRIR difference spectra recorded on the picosecond timescale show the presence of two ν(CO) bands at 1965 and 1895 cm^{-1}, similar to those observed previously for the 1st dicarbonyl transient formed following photolysis of $CpRe(CO)_3$ in PFMCH under a CH_4 atmosphere. However, in this case, this species decays fully on a fast nanosecond timescale, along with the formation of four new ν(CO) features at 2009,

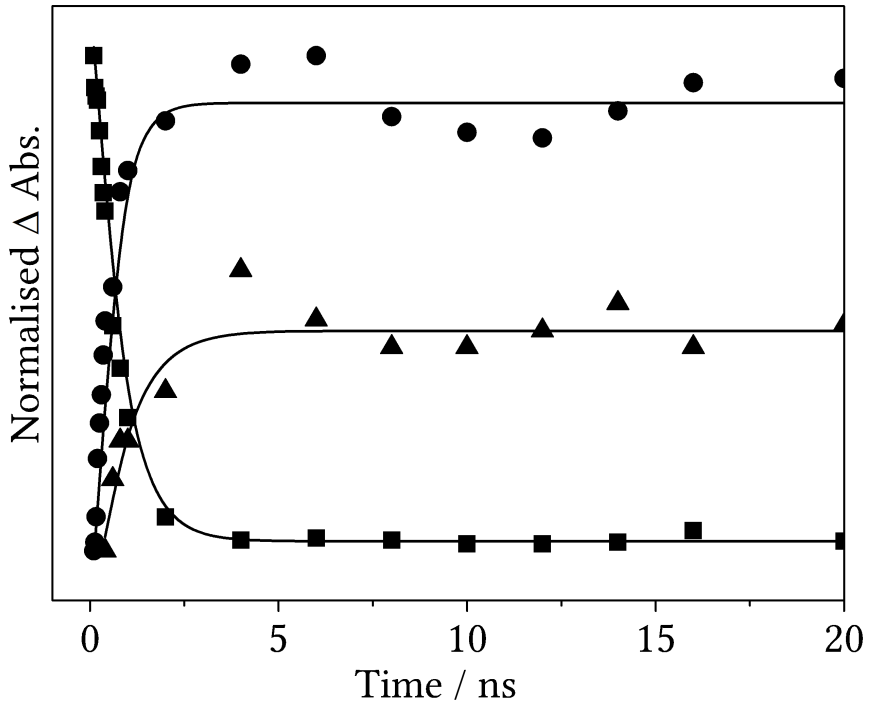


FIGURE 3.19: Single-point kinetic traces from TRIR difference spectra recorded following 266 nm photolysis of $CpRe(CO)_3$ in PFMCH under C_2H_6 (1.5 bar), showing decay of the 1st dicarbonyl transient species (squares), formation of $CpRe(CO)_2(C_2H_6)$ (circles) and formation of $CpRe(CO)_2(C_2H_5)H$ (triangles). Solid lines are mono-exponential fits.

1960, 1936 and 1893 cm^{-1}. The two ν(CO) bands at 2009 and 1936 cm^{-1} are consistent with formation of a small amount of the C-H activated species $CpRe(CO)_2(C_2H_5)H$. The other two ν(CO) features observed on this timescale are shifted to lower energy compared to the ν(CO) bands of the 1st transient, suggesting addition of electron density to the metal centre through coordination of a weak ligand. This species is tentatively assigned as $CpRe(CO)_2(C_2H_6)$.

Figure 3.19 shows TRIR kinetic traces for the decay of the 1st dicarbonyl transient (lifetime τ = 0.5 ($\pm$0.1) ns) and the formation of $CpRe(CO)_2(C_2H_6)$ (τ = 0.6 ($\pm$0.1) ns) and $CpRe(CO)_2(C_2H_5)H$ (τ = 1.1 ($\pm$0.2) ns). The rate of decay of the 1st transient species and the rate of growth of $CpRe(CO)_2(C_2H_6)$ were observed to

match, indicating direct formation of the latter from the former. The growth of the C-H activated species $CpRe(CO)_2(C_2H_5)H$ is slower than both of these rates. In contrast to studies under a CH_4 atmosphere, the 1st dicarbonyl transient was shown to decay completely, eliminating the possibility of an equilibrium between this transient and $CpRe(CO)_2(C_2H_6)$. In this case it seems likely that $CpRe(CO)_2(C_2H_5)H$ is forming directly from $CpRe(CO)_2(C_2H_6)$, and not from the 1st transient. The faster rate of formation of $CpRe(CO)_2(C_2H_6)$ compared to its CH_4 analogue, as well as the complete decay of the 1st transient are consistent with previous observations of the increased stability of $CpRe(CO)_2(C_2H_6)$ compared to $CpRe(CO)_2(CH_4)$.[198]

3.2.5.2 Characterisation of $Cp^*Re(CO)_2$(alkane) (Alkane = Methane, Ethane) in Room Temperature Perfluoroalkane Solution

The C-H activation chemistry observed in the above experiments following photolysis of $CpRe(CO)_3$ in PFMCH under CH_4 or C_2H_6 was further investigated by repeating these experiments with $Cp^*Re(CO)_3$, in order to examine the effect of the increased electron density on the metal centre afforded by the addition of electron donating methyl substituents onto the Cp ring.

TABLE 3.5: Observed rate constants (k_{obs}) for the C-H activation of CH_4 and C_2H_6 by $CpRe(CO)_3$ and $Cp^*Re(CO)_3$, in PFMCH solvent. All data recorded at 298 K.

ν(CO) (cm^{-1})	Assignment	k_{obs} (s^{-1})
2010	$CpRe(CO)_2(CH_3)H$	2.6 (±0.2) x 10^8
1937	$CpRe(CO)_2(CH_3)H$	2.7 (±0.3) x 10^8
2009	$CpRe(CO)_2(C_2H_5)H$	8.6 (±0.7) x 10^8
1936	$CpRe(CO)_2(C_2H_5)H$	9.1 (±1.0) x 10^8
1995	$Cp^*Re(CO)_2(CH_3)H$	2.7 (±0.4) x 10^8
1919	$Cp^*Re(CO)_2(CH_3)H$	2.8 (±0.5) x 10^8
1993	$Cp^*Re(CO)_2(C_2H_5)H$	7.1 (±1.4) x 10^8
1917	$Cp^*Re(CO)_2(C_2H_5)H$	7.5 (±1.5) x 10^8

TRIR spectra recorded following 266 nm photolysis of $Cp^*Re(CO)_3$ in PFMCH under CH_4 (1.5 bar) showed very similar results to those observed for $CpRe(CO)_3$. Photolysis resulted in immediate bleaching of the two ν(CO) parent bands of $Cp^*Re(CO)_3$ (2018 and 1928 cm^{-1}) and formation of two initial ν(CO) bands (1941 and 1870 cm^{-1}) consistent with the unassigned dicarbonyl transient species observed above. As above, these ν(CO) features decay partially, giving way to four new ν(CO) features at 1995, 1936, 1919 and 1870 cm^{-1}. The two ν(CO) bands at 1995 and 1919 cm^{-1} are consistent with a C-H activated species, as observed above, and are therefore assigned as $Cp^*Re(CO)_2(CH_3)H$. The two additional ν(CO) bands are consistent with a dicarbonyl species, similarly to those tentatively assigned to $CpRe(CO)_2(CH_4)$ and $CpRe(CO)_2(C_2H_6)$ above. These ν(CO) features are assigned as $Cp^*Re(CO)_2(CH_4)$. As above, the rate of decay of the 1st dicarbonyl (τ = 2.6 (±0.3) ns) and the rate of growth of $Cp^*Re(CO)_2(CH_4)$ (τ = 3.0 (±0.8) ns) are similar, while the rate of growth of $Cp^*Re(CO)_2(CH_3)H$ (τ = 3.7 (±0.5) ns) is slower. It would once again be expected that direct formation of $Cp^*Re(CO)_2(CH_3)H$ from $Cp^*Re(CO)_2(CH_4)$ would introduce some deviation from simple behaviour into the growth of $Cp^*Re(CO)_2(CH_4)$. The large

(<25 %) error reported for the lifetime of this growth process may be due to such a contribution, however the processes occurring here have very similar rates, making determination of kinetic behaviour difficult.

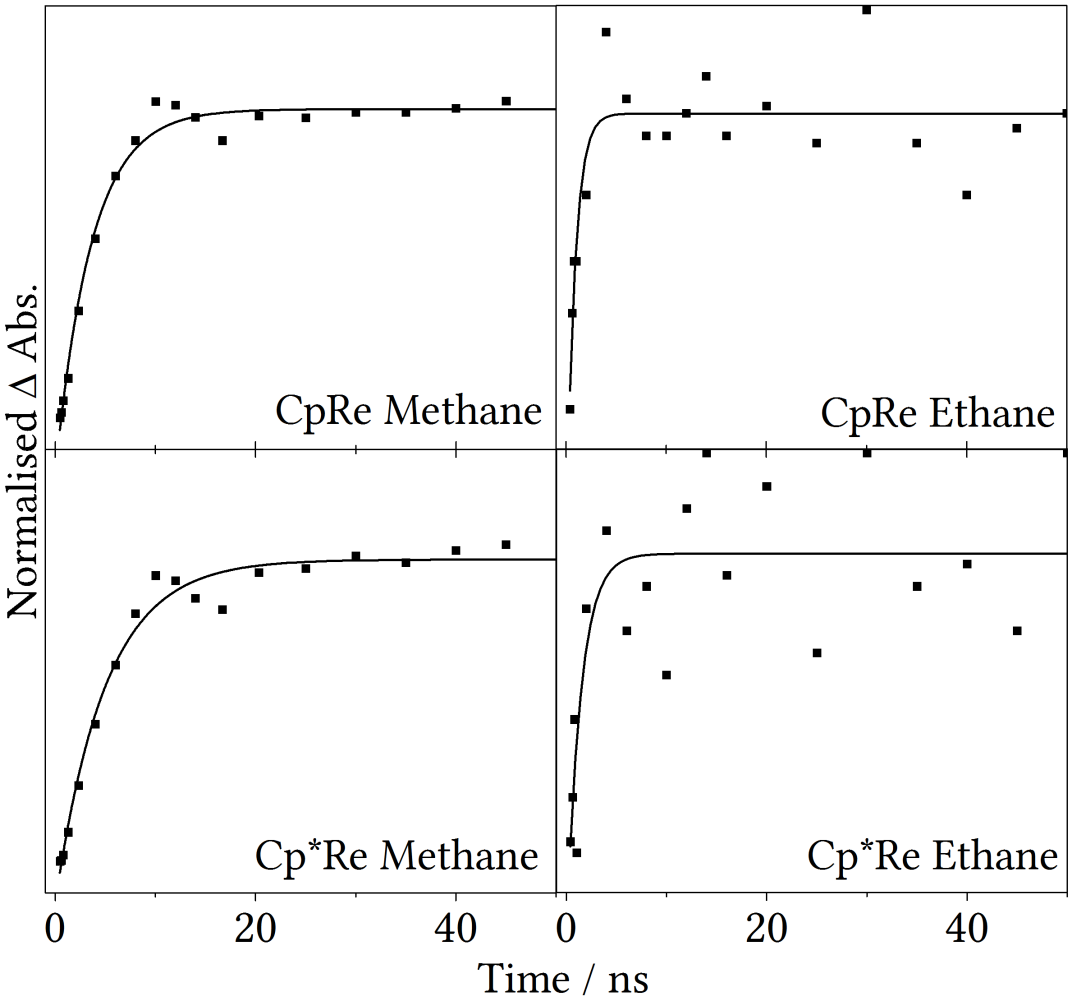


FIGURE 3.20: Single-point kinetic traces from TRIR difference spectra showing C-H activation following photolysis of a solution of $CpRe(CO)_3$ in PFMCH under 1.5 bar CH_4 (top left), under 1.5 bar C_2H_6 (top right), $Cp^*Re(CO)_3$ in PFMCH under 1.5 bar CH_4 (bottom left) and under 1.5 bar C_2H_6 (bottom right). Solid lines are mono-exponential fits.

Photolysis of $Cp^*Re(CO)_3$ in PFMCH under C_2H_6 (1.5 bar) resulted in the bleaching of the parent ν(CO) bands (2018 and 1928 cm^{-1}) and initial formation of two ν(CO) bands consistent with the unassigned transient observed above (1941 and 1871

cm^{-1}). This species was shown to decay fully on a fast nanosecond timescale, resulting in four new ν(CO) bands. The rate of formation of $Cp^*Re(CO)_2(C_2H_5)H$ (τ = 1.4 ($\pm$0.6) ns) was observed to form faster than $Cp^*Re(CO)_2(CH_3)H$, as expected. Two of these new ν(CO) bands (1937 and 1870 cm^{-1}) are assigned to the dicarbonyl ethane complex $Cp^*Re(CO)_2(C_2H_6)$, while the final two (1993 and 1917 cm^{-1}) are assigned as the C-H activation product $Cp^*Re(CO)_2(C_2H_5)H$. Figure 3.20 shows a comparison of the rate of C-H activation for the systems examined in this study.

Figure 3.21 shows a comparison of TRIR difference spectra recorded 100 ns following 266 nm photolysis of $CpRe(CO)_3$ and $Cp^*Re(CO)_3$ in PFMCH under CH_4 or C_2H_6 atmospheres. A comparison of the ratio of the intensity of the ν(CO) bands of the σ-alkane complex to those of the C-H activated alkyl hydride (alkane:alkyl hydride) shows that the increased amount of electron density on the metal in the case of $Cp^*Re(CO)_3$ results in a greater amount of the C-H activated alkyl hydride forming following photolysis. Previous studies have reported that the strength of the C-H bond in the alkane is correlated with the strength of the resulting metal-carbon bond.[260–262] In this case, the nature of the alkane also affects the amount of the C-H activated alkyl hydride produced, with methane resulting in more C-H activation than ethane. The ratio of alkane:alkyl hydride formed was observed to vary in the order: $CpRe(CO)_3$ with ethane > $Cp^*Re(CO)_3$ with ethane > $CpRe(CO)_3$ with methane > $Cp^*Re(CO)_3$ with methane. This result is in agreement with previously published studies.[198]

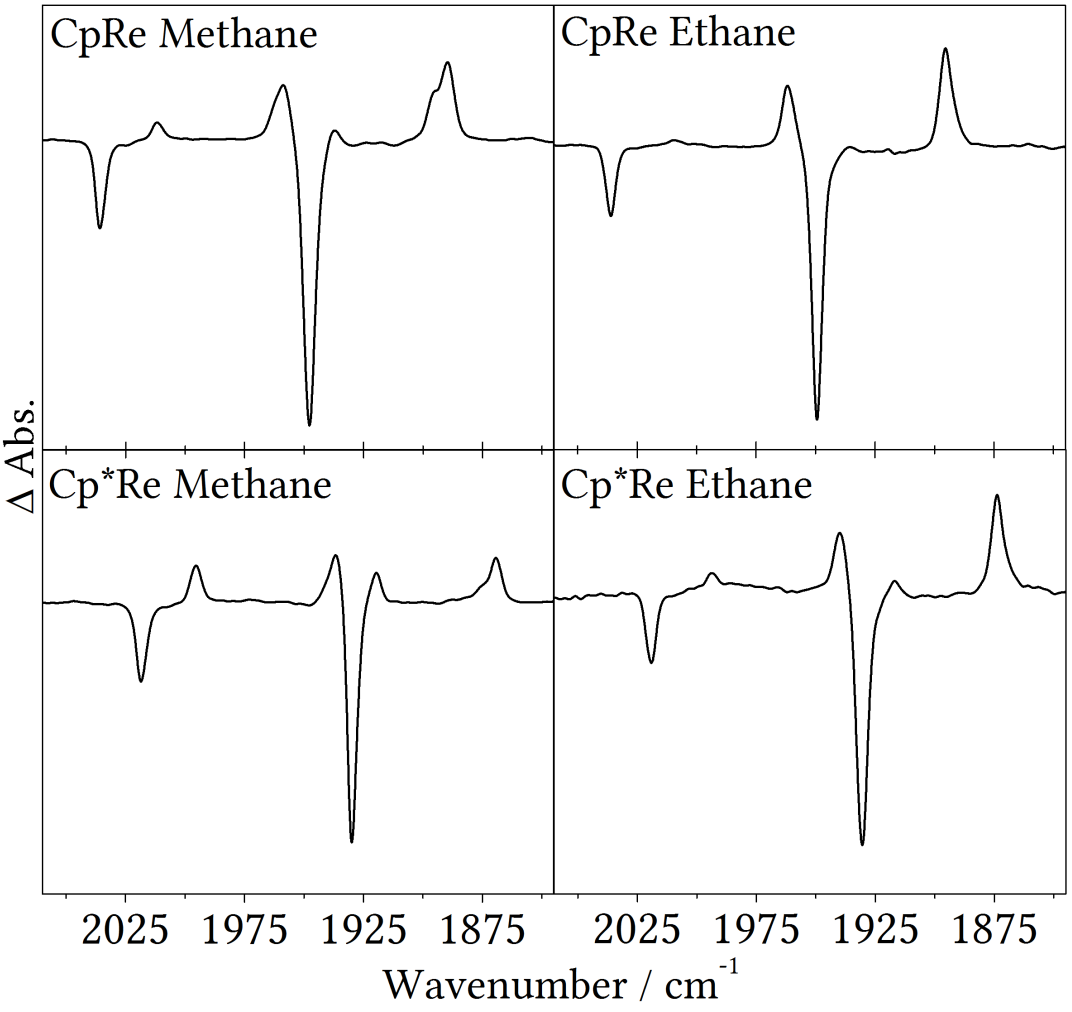


FIGURE 3.21: Nanosecond TRIR difference spectra recorded 100 ns following 266 nm photolysis of a solution of $CpRe(CO)_3$ in PFMCH under 1.5 bar CH_4 (top left), under 1.5 bar C_2H_6 (top right), $Cp^*Re(CO)_3$ in PFMCH under 1.5 bar CH_4 (bottom left) and under 1.5 bar C_2H_6 (bottom right). ν(CO) bands of the C-H activated species can be seen in all cases.

3.2.6 TRIR Studies of $CpRh(CO)_2$ in Perfluoroalkane Solvents

Noble gas and alkane complexes formed following photolysis of $CpRe(CO)_3$ have been shown to be remarkably stable,[37,40–42,48,174,183] noble gas complexes of rhodium are also well reported,[56,226,285,288,289,295] and have also shown high stability to reaction with CO in some cases, albeit less than analogous Re complexes.

TABLE 3.6: ν(CO) absorption band frequencies of $CpRe(CO)_3$, $Cp^*Re(CO)_3$ and intermediates and photoproducts formed following photolysis of $CpRe(CO)_3$ and $Cp^*Re(CO)_3$ in a series of pure PFMCH and PFMCH doped with 1.5 bar CH_4 or C_2H_6. Experiments performed in solution phase at 298 K unless otherwise stated.

Compound	**Solvent/Matrix**	**Dopant**	**ν(CO) (cm^{-1})**	**Reference/Notes**
$CpRe(CO)_3$	PFMCH		2037, 1948	This work
		CH_4	2036, 1948	This work
		C_2H_6	2037, 1948	This work
	*sc*Ar	CH_4	2040, 1950	198
1st transient	PFMCH		1964, 1895	This work
		CH_4	1964, 1895	This work
		C_2H_6	1965, 1895	This work
$CpRe(CO)_2X$	PFMCH		1958, 1899	This work
		CH_4	1960, 1893	This work
		C_2H_6	1960, 1893	This work
	*sc*Ar	CH_4	1966, 1905	198
$CpRe(CO)_2(R)H$	PFMCH	CH_4	2010, 1937	This work
		C_2H_6	2009, 1936	This work
	*sc*Ar	CH_4	2018, 1943	198
$Cp^*Re(CO)_3$	PFMCH		2018, 1928	This work
		CH_4	2018, 1928	This work
		C_2H_6	2018, 1928	This work
	scCH_4		2020, 1933	198
1st transient	PFMCH		1941, 1871	This work
		CH_4	1941, 1871	This work
		C_2H_6	1941, 1871	This work
$Cp^*Re(CO)_2X$	PFMCH		1936, 1867	This work
		CH_4	1936, 1870	This work
		C_2H_6	1937, 1870	This work
	scCH_4		1943, 1883	198
$Cp^*Re(CO)_2(R)H$	PFMCH	CH_4	1995, 1919	This work
		C_2H_6	1993, 1917	This work
	scCH_4		1998, 1923	198

In continuation of the work presented above, studies on the photochemistry of $CpRh(CO)_2$ were undertaken in perfluoroalkane solutions, and subsequently in Xe-doped perfluoroalkane solutions in an attempt to characterise CpRh(CO)Xe in room temperature solution at near-ambient pressure. $CpRh(CO)_2$ is a liquid at room temperature, and exhibited relatively high miscibility with both PFMCH and PFH.

TABLE 3.7: Lifetimes (in ns) for the growth of C-H activated alkyl hydride species formed following photolysis of $CpRe(CO)_3$ and $Cp^*Re(CO)_3$ under CH_4 or C_2H_6.

Compound	**Lifetime τ (ns)**
$\mathbf{CpRe(CO)_2(CH_3)H}$	3.8 (±0.3)
$\mathbf{CpRe(CO)_2(C_2H_5)H}$	1.1 (±0.2)
$\mathbf{Cp^*Re(CO)_2(CH_3)H}$	3.7 (±0.5)
$\mathbf{Cp^*Re(CO)_2(C_2H_5)H}$	1.4 (±0.6)

The ability to attain higher concentrations of this material in perfluorinated solvents when compared to $CpRe(CO)_3$ could make the solution phase chemistry presented in this Thesis more versatile, and assist us in achieving our ultimate goal of characterising an organometallic noble gas complex with TR-XAFS.

$CpRh(CO)_2$ was photolysed at 266 nm in PFMCH solution under Ar. Figure 3.22 shows a selection of TRIR difference spectra recorded at various time delays following photolysis. TRIR spectra recorded on the picosecond timescale showed that photolysis resulted in immediate bleaching of the two ν(CO) parent bands of $CpRh(CO)_2$ (2054, 1990 cm^{-1}) and formation of three broad features (2048, 2028 and 1978 cm^{-1}) which decay over the first 200 ps of the experiment along with concurrent reformation of the parent complex. These broad features likely represent a transient excited state, much like the one observed previously following photolysis of $CpRe(CO)_3$.[150,290] Following the decay of this excited state species, a single ν(CO) transient band remained at 1968 cm^{-1}, the spectrum recorded 1 ns following photolysis shows only this ν(CO) feature. By comparison to previously published photolysis studies, this ν(CO) band is assigned as a monocarbonyl species of the form CpRh(CO)X.[235,288,295] This species is assigned as the PFMCH solvent complex $CpRh(CO)(C_7F_{14})$.

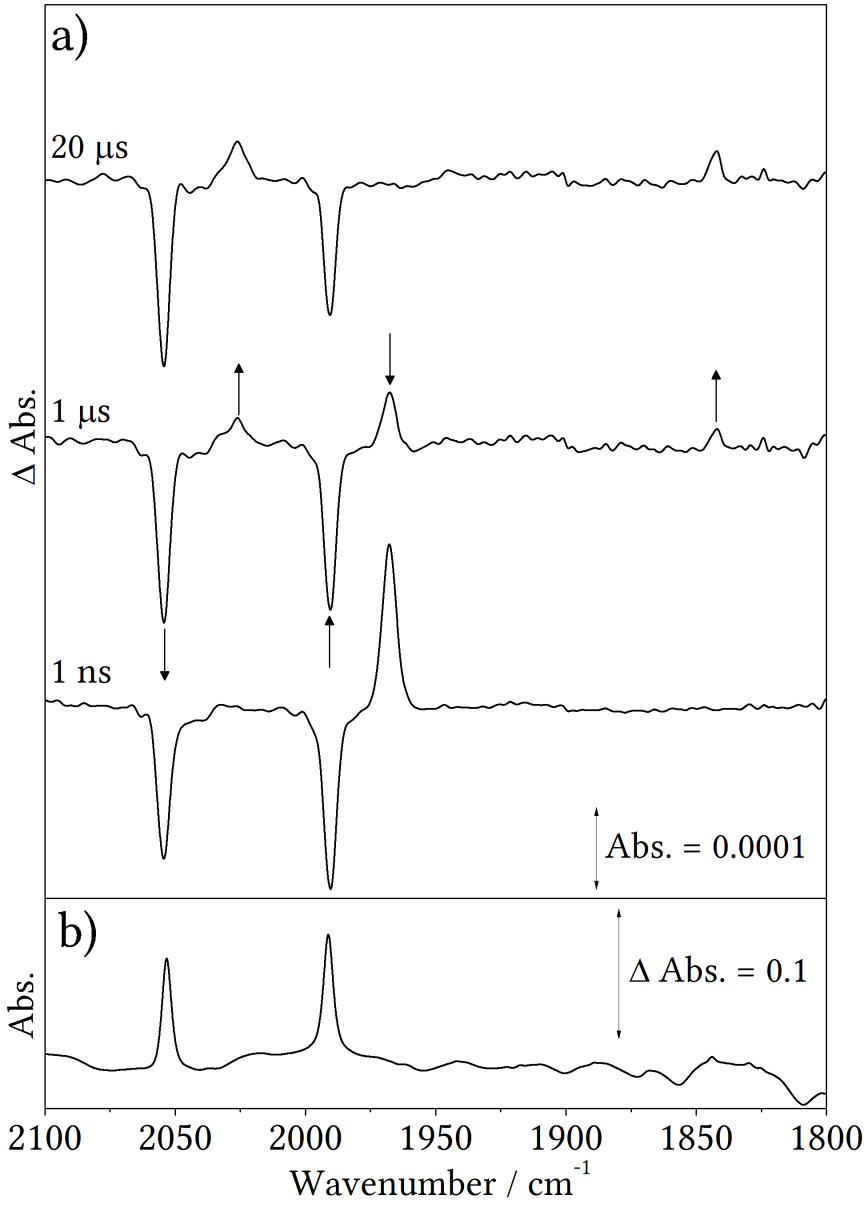


FIGURE 3.22: a) Selected nanosecond TRIR difference spectra recorded at a series of time delays following 266 nm photolysis of a solution of $CpRh(CO)_2$ in PFMCH under Ar (1.5 bar). The decay of a monocarbonyl species, as well as growth of a dimer and oxidative addition product can be seen b) FTIR spectrum of the same solution.

Decay of the monocarbonyl solvent complex was observed to occur on a microsecond timescale, and was accompanied by the formation of two new positive ν(CO) features, as well as increased bleaching of the higher energy parent band, and apparent recovery of the other parent ν(CO) band. One of the these new positive ν(CO) features

(1841 cm^{-1}) appears at very low energy in the bridging carbonyl region of the spectrum. The appearance of this band could suggest formation of a dinuclear species, and indeed a dinuclear species has been observed previously following photolysis of $CpRh(CO)_2$ in alkane solvent.[56] The authors observed ν(CO) bands at 1837 and 1984 cm^{-1} in cyclohexane solution, assigned to the dimer *trans*-$Cp_2Rh_2(CO)_3$. The low energy bridging band observed in our study closely matches the band at 1837 cm^{-1} reported by Belt *et al.*, and it is likely that the higher energy band expected for this dimer (1984 cm^{-1}) appears at slightly higher energy in PFMCH. An increase of 4-6 cm^{-1} compared to the higher energy band reported by Belt and co-workers, consistent with the shift observed in the bridging band upon changing from cyclohexane to PFMCH solution, would place the higher energy dimer band at approximately the same frequency as the lower energy parent band (1990 cm^{-1}). This is consistent with the apparent decrease of this parent bleach on the same timescale as growth of the dimer band at 1841 cm^{-1}. The two competing processes occurring at *ca.* 1990 cm^{-1} make the kinetics difficult to deconvolute. However, the apparent increased bleaching of the higher energy parent band is also consistent with formation of *trans*-$Cp_2Rh_2(CO)_3$, through a reaction of CpRh(CO)X with parent $CpRh(CO)_2$. The lifetime of this increased bleaching (τ = 550 ($\pm$80) ns) is consistent with the growth of the bridging carbonyl band at 1841 cm^{-1} (τ = 600 ($\pm$60) ns).

The final ν(CO) feature observed following the decay of the monocarbonyl comes at 2026 cm^{-1}. The appearance of this band at higher wavenumber compared to the monocarbonyl complex is suggestive of a decrease in electron density at the Rh centre. Such a shift has been observed previously following photolysis of $CpRh(CO)_2$ in alkane

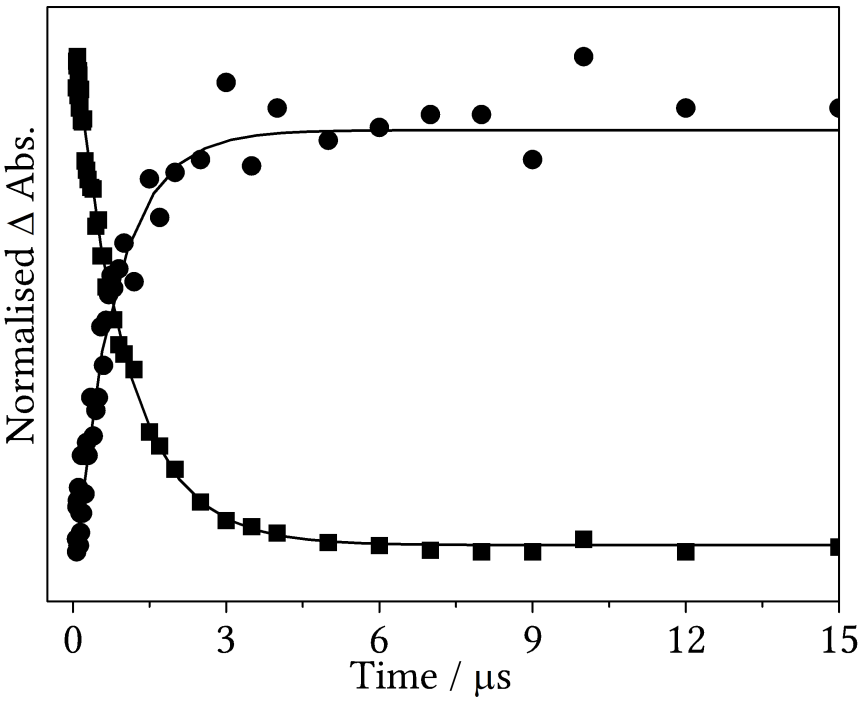


FIGURE 3.23: Single-point kinetic traces from TRIR difference spectra recorded following 266 nm photolysis of $CpRh(CO)_2$ in PFMCH under Ar (1.5 bar), showing decay of the monocarbonyl transient species $CpRh(CO)(C_7F_{14})$ (squares), and formation of the major decay product tentatively assigned as $CpRh(CO)(C_7F_{13})F$ (circles). Solid lines are mono-exponential fits.

solutions, and have been assigned as C-H activation of the alkane through oxidative addition to the rhodium metal.[233,235] Figure 3.23 shows kinetic traces from this TRIR study. The lifetime values for the decay of the monocarbonyl species and growth of this new ν(CO) band are observed to be within error of each other (τ = 960 ($\pm$50) and 850 ($\pm$80) ns, respectively), with both being slower than the observed rate for formation of the dimer species.

The presence of a small amount of alkane impurity was considered as a possible source for this apparent oxidative activation product. Any alkane would likely be in very low concentration, and the lack of any change in the ν(CO) band position of the monocarbonyl complex assigned to $CpRh(CO)(C_7F_{14})$, even on the picosecond

timescale, suggests that only a single monocarbonyl complex is present following photolysis in PFMCH. The rate of formation of this oxidative addition product is also much slower than would be expected for C-H activation of a linear[233] or cyclic alkane[235] by $CpRh(CO)_2$, which has been reported to occur between 10-100 ns.

An additional possibility for the assignment of the ν(CO) band at 2026 cm^{-1} is a C-F activation product. C-F activation would result in the same oxidation state change as C-H activation, leading to a ν(CO) band which would appear at lower wavenumber compared to the monocarbonyl product. C-F activation by $CpRh(CO)_2$ derivatives has been observed previously. Photolysis of $Cp^*Rh(\eta^2\text{-}C_2H_4)(PMe_3)$ in perfluorobenzene resulted in the formation of $Cp^*Rh(F)(C_6F_5)(PMe_3)$.[296] While a matrix isolation study reported formation of $CpRh(F)(C_6F_5)(PMe_3)$ in small quantities following photolysis of $CpRh(\eta^2\text{-}C_2H_4)(PMe_3)$.[297] A recent study has even suggested that in some cases, C-F activation may occur alongside C-H activation in cases where both bonds are present.[298] No observations of C-F activation of a perfluoroalkane by $CpRh(CO)_2$ have been reported however, and therefore no comparisons of the kinetics of this activation can be drawn. The ν(CO) band at 2026 cm^{-1} will be very tentatively assigned to a C-F activation product $CpRh(CO)(C_7F_{13})F$, however additional studies will be required to confirm this assignment, as the presence of a small amount of impurity which contains C-H bonds is still a possibility.

Following the study reported above in pure PFMCH, the experiment was repeated under 1.5 bar of Xe to examine any differences caused by addition of the noble gas. Figure 3.24 shows a series of TRIR spectra recorded following photolysis of this solution. Immediately following photolysis, the two parent ν(CO) bands (2054 and 1990 cm^{-1})

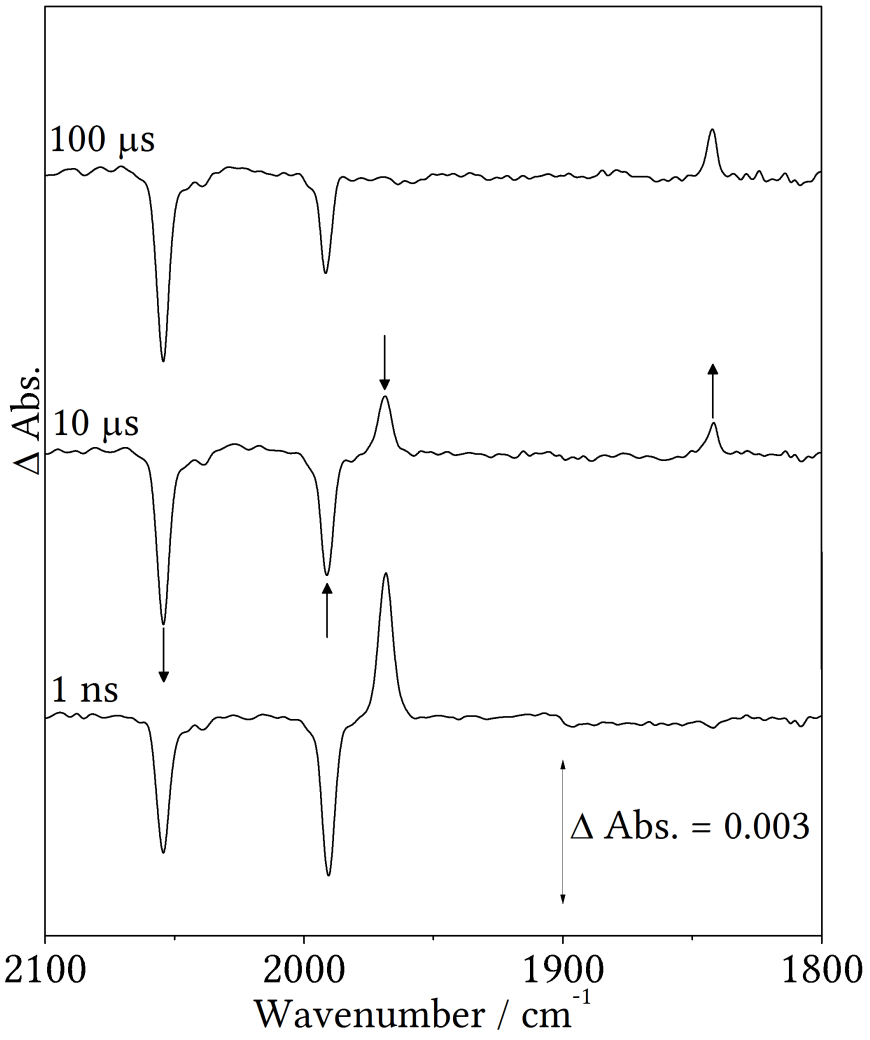


FIGURE 3.24: Selected nanosecond TRIR difference spectra recorded at a series of time delays following 266 nm photolysis of a solution of $CpRh(CO)_2$ in PFMCH under Xe (1.5 bar), showing decay of the monocarbonyl species and formation of a dimeric species as the major photoproduct.

are bleached. Similarly to the above case, the spectrum recorded 1 ns following photolysis shows only a single ν(CO) band, consistent with a monocarbonyl of the form CpRh(CO)X. In this case, the ν(CO) band of this monocarbonyl (1970 cm^{-1}) appears at slightly higher energy than the one observed above, assigned to the solvent complex (1968 cm^{-1}). This small shift in band position is indicative of a change in electron density present on the metal centre, and is consistent with the small positive

shift in ν(CO) frequency observed upon addition of Xe to a solution of $CpRe(CO)_3$ in PFMCH, reported earlier in this Chapter.

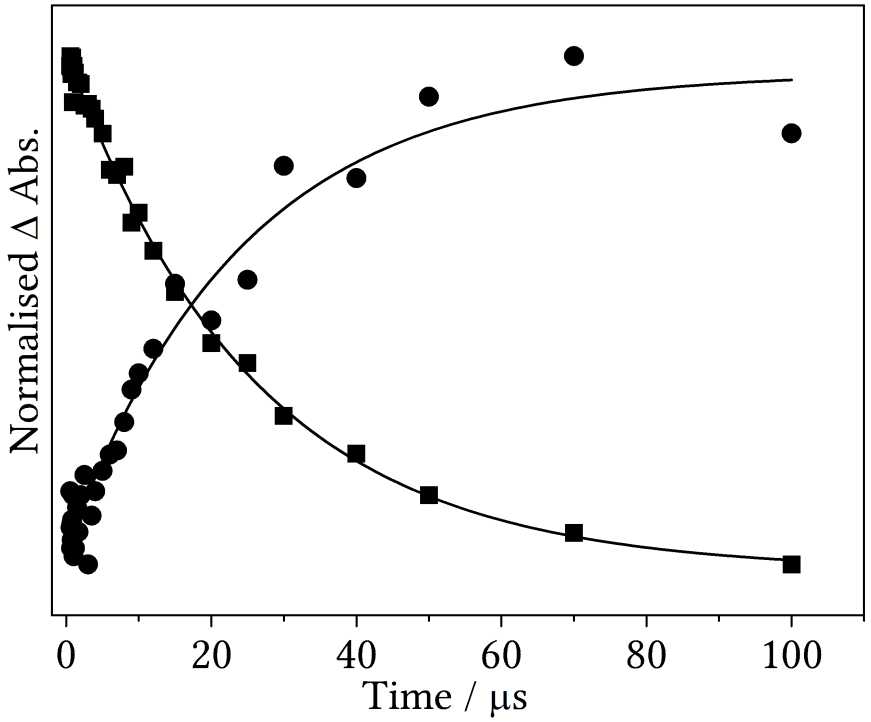


FIGURE 3.25: Single-point kinetic traces from TRIR difference spectra recorded following 266 nm photolysis of $CpRh(CO)_2$ in PFMCH under Xe (1.5 bar), showing decay of the monocarbonyl transient species CpRh(CO)Xe (squares), and formation of the major decay product assigned as $Cp_2Rh_2(CO)_3$ (circles). Solid lines are mono-exponential fits.

This monocarbonyl species is observed to decay, resulting in formation of a single positive ν(CO) band at 1841 cm^{-1}. This band is consistent with the dinuclear species assigned above, $Cp_2Rh_2(CO)_3$. The growth of this ν(CO) band is concurrent with increased bleaching of the higher energy parent band and decreased bleaching of the lower energy parent band. This observation is once again consistent with formation of the dimeric species assigned above. The higher energy ν(CO) band observed in the previous experiment, very tentatively assigned to the C-F activation product is not observed following addition of Xe to the solution. The rate of decay of the monocarbonyl species

in this case (τ = 24.0 ($\pm$3) μs) matches the rate of growth of the bridging carbonyl band of the dimeric species $Cp_2Rh_2(CO)_3$(τ = 25.5 ($\pm$2) μs), as shown in the TRIR kinetics traces presented in Figure 3.25. The increase in lifetime of the monocarbonyl complex, the slight shift in its ν(CO) band position following addition of Xe to the solution suggests preferential formation of an Xe complex. The monocarbonyl species in this case is therefore assigned as CpRh(CO)Xe. This observation of preferential binding of Xe in solution also bolsters the previous assignment of CpRh(CO)(C_7F_{14}) following photolysis in pure PFMCH, as any alkane complex formed due to impurities in the solution would be expected to form preferentially over the Xe complex.

TABLE 3.8: Observed rate constants (k_{obs}) for processes observed following photolysis of $CpRh(CO)_2$ in PFMCH and PFH solutions. All data recorded at 298 K.

Solvent	**ν(CO) (cm^{-1})**	**Assignment**	**k_{obs} (s^{-1})**
C_7F_{14} (PFMCH)	1968	CpRh(CO)(C_7F_{14})	1.0 ($\pm$0.1) x 10^6
	2026	CpRh(CO)(C_7F_{13})F	1.1 ($\pm$0.1) x 10^6
	1970	CpRh(CO)Xe	4.1 ($\pm$0.3) x 10^4
	1841	$Cp_2Rh_2(CO)_3$	3.9 ($\pm$0.3) x 10^4
C_6F_{14} (PFH)	1970	CpRh(CO)(C_6F_{14})	7.6 ($\pm$1.0) x 10^6
	2030	CpRh(CO)(C_6F_{13})F	8.3 ($\pm$1.0) x 10^6
	1971	CpRh(CO)Xe	3.6 ($\pm$0.5) x 10^4
	1842	$Cp_2Rh_2(CO)_3$	3.7 ($\pm$0.5) x 10^4

The above experiments were subsequently repeated in PFH solution. As above, formation of a single monocarbonyl species was initially observed, following by formation of $Cp_2Rh_2(CO)_3$, as well as the oxidative addition product CpRh(CO)(C_6F_{13})F. Addition of Xe to the solution resulted in formation of only the dimeric species following decay of the monocarbonyl, with no observation of any activated species. In the case of photolysis in pure PFH, the oxidative addition product is observed to form much faster than in PFMCH (τ = 120 ($\pm$20) ns), suggesting formation of a different activated

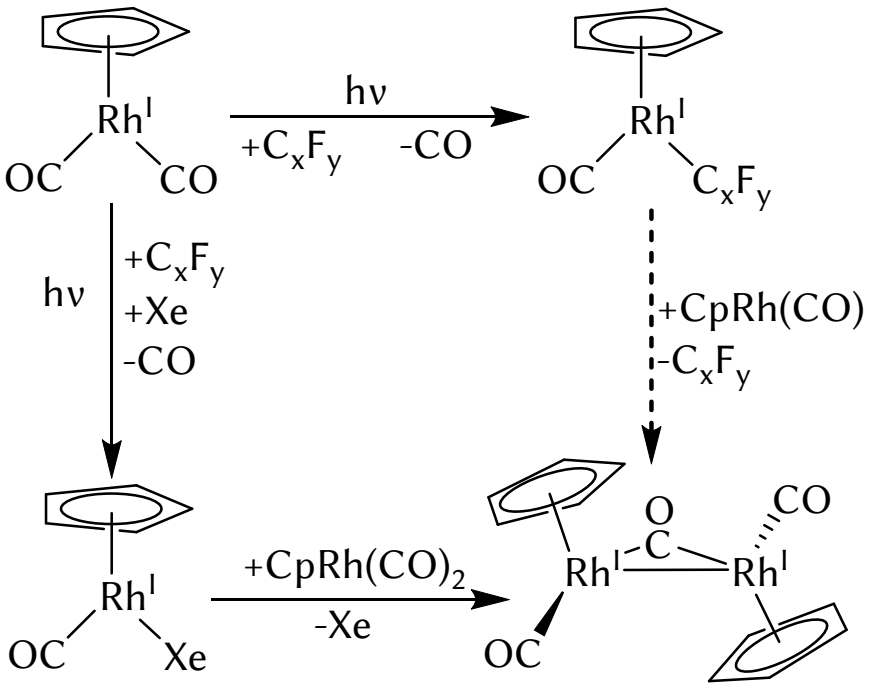
TABLE 3.9: ν(CO) absorption band frequencies of $CpRh(CO)_2$, and intermediates and photoproducts formed following photolysis in a series of pure and Xe doped PFMCH and PFH solutions. Literature values recorded in *sc*Xe, *sc*Kr and cyclohexane are given for comparison. Experiments performed in solution phase at 298 K.

Compound	Solvent/Matrix	Dopant	ν(CO) (cm^{-1})	Reference
$CpRh(CO)_2$	PFMCH		2054, 1990	This work
		Xe	2054, 1990	This work
	PFH		2055, 1992	This work
		Xe	2055, 1992	This work
	*sc*Xe		2051, 1988	288
	*sc*Kr		2056, 1994	288
CpRh(CO)X	PFMCH		1968	This work
		Xe	1970	This work
	PFH		1970	This work
		Xe	1971	This work
	*sc*Xe		1967	288
	*sc*Kr		1975	288
$Cp_2Rh_2(CO)_3$	PFMCH		1990, 1841	This work
		Xe	1990, 1841	This work
	PFH		1992, 1842	This work
		Xe	1992, 1842	This work
	Cyclohexane		1837, 1984	56
$CpRh(CO)(R^F)F$	PFMCH		2026	This work
	PFH		2030	This work

species. Following addition of Xe to the solution, the decay of the monocarbonyl (τ = 28 ($\pm$4) μs) and growth of the dimer species (τ = 27 ($\pm$3) μs) are observed to occur on the same timescale as the previous experiment in PFMCH, suggesting formation of the same species in both cases. A summary of all ν(CO) band positions of $CpRh(CO)_2$ and intermediates produced following photolysis is given in Table 3.9. A proposed reaction mechanism, as discussed throughout this section, is presented in Scheme 3.1

The above experiments were also attempted for the Cp-substituted derivative of $CpRh(CO)_2$, $Cp^*Rh(CO)_2$. However, this compound was found to be insufficiently soluble in perfluoroalkanes solvent to yield spectra with an acceptable signal-to-noise

ratio.



SCHEME 3.1: Proposed reaction mechanism following 266 nm photolysis of $CpRh(CO)_2$ in PFMCH and PFH, with and without Xe dopant. Dashed lines show minor pathways.

3.2.7 Spectroscopic Studies of $M(CO)_6$ (M = Cr, Mo, W) in Perfluoroalkane Solvents

The first photolysis studies resulting in the formation of an organometallic noble gas or alkane complex involved irradiation of matrix isolated group-6 metal carbonyl species.[80,239] The first identification of an organometallic alkane complex in solution was also reported following photolysis of $Cr(CO)_6$ in cyclohexane solution,[81] and subsequent work used perfluoroalkanes as a solvent, characterising an interaction between the metal centre and the perfluoroalkane which was weaker than that observed in alkane solution.[78,79] The group-6 metal hexacarbonyls are still used today as a model

photochemical system, and have recently been used to examine the effectiveness of a new time-resolved technique which is utilised within this Thesis, TR^{M}PS.[39] It is for these reasons that the study presented within this Chapter was expanded to incorporate photolysis of $M(CO)_6$ (M = Cr, Mo, W) in perfluoroalkane solutions.

Figure 3.26 shows a series of TRIR difference spectra recorded following photolysis of $W(CO)_6$ in PFMCH solution under Ar (1.5 bar). Within 1 ps of photolysis, the parent ν(CO) band of $W(CO)_6$ (1989 cm^{-1}) was observed to bleach, and new broad ν(CO) features were observed. These features were seen to sharpen and blue-shift, yielding two new ν(CO) bands after *ca.* 100 ps (1966 and 1930 cm^{-1}). These bands are consistent with loss of a carbonyl ligand following photolysis to form a pentacarbonyl complex of the form $W(CO)_5X$.[49] This species is not stable, however, and gives way to a further two ν(CO) bands (1961 and 1935 cm^{-1}) which are slightly shifted compared to the initial transient. The number of ν(CO) bands and their band positions are also consistent with formation of a pentacarbonyl complex of the form $W(CO)_5X$. The rate of decay of the initial pentacarbonyl species (τ = 6.4 ($\pm$0.4) ns) and the rate of growth of the second (τ = 6.2 ($\pm$0.5) ns) were observed to be within error, indicating direct formation of one species from the other.

This second pentacarbonyl species was observed to decay on the microsecond timescale, leading to formation of a further complex with ν(CO) bands at 1977, 1940 and 1918 cm^{-1}. This complex is stable on the timescale of this experiment (70 μs). This species has been observed previously on the microsecond timescale following photolysis of $W(CO)_6$ in *n*-heptane solution, and assigned to the water complex $W(CO)_5(H_2O)$, due

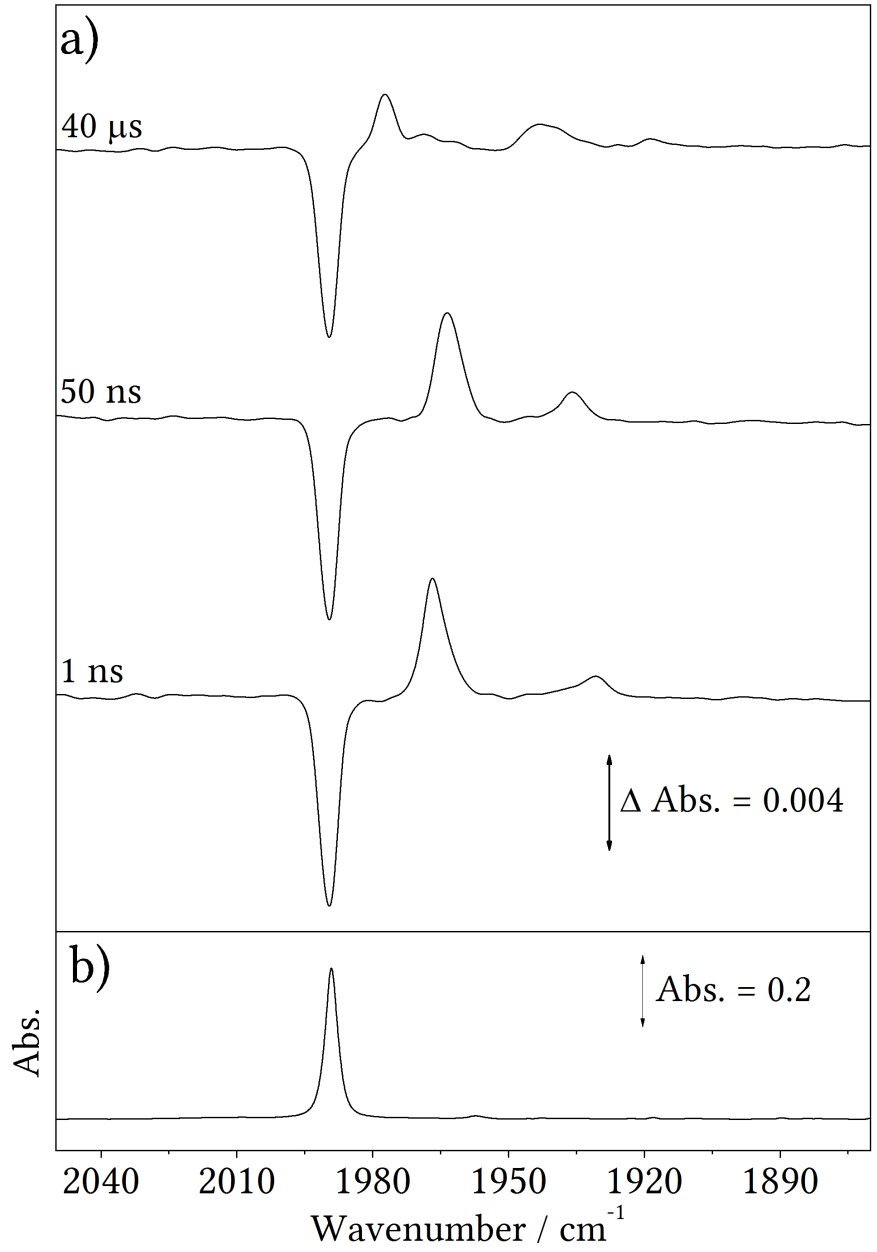


FIGURE 3.26: Selected nanosecond TRIR difference spectra recorded at a series of time delays following 266 nm photolysis of a solution of $W(CO)_6$ in PFMCH under Ar (1.5 bar), bleaching of the parent ν(CO) band and subsequent formation and decay of two different pentacarbonyl transients can be seen.

to reaction between the transient alkane complex and a small amount of water impurity in the solution.[39,241] Despite taking every precaution to avoid contamination with water in this case, it appears that the final photoproduct formed following photolysis

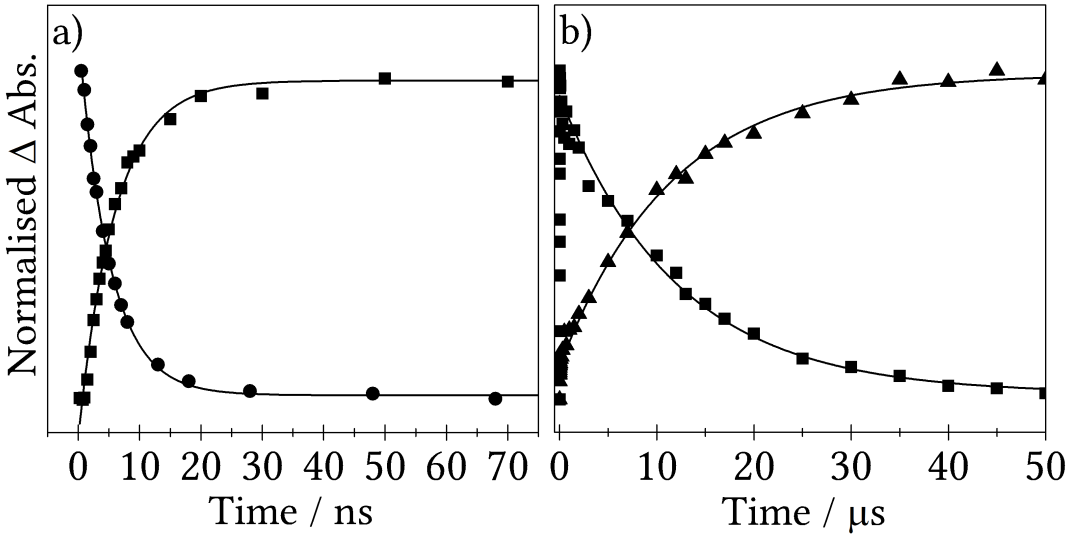


FIGURE 3.27: Kinetic traces from TRIR difference spectra recorded following photolysis of $W(CO)_6$ in PFMCH under Ar (1.5 bar) showing a) decay of the first pentacarbonyl transient (circles) and growth of the second (squares) and b) subsequent decay of the second pentacarbonyl species (squares), and finally formation of the water complex $W(CO)_5(H_2O)$ (triangles). Solid lines show mono-exponential fits.

of $W(CO)_6$ in PFMCH was the water complex $W(CO)_5(H_2O)$, and the ν(CO) bands at 1977, 1940 and 1918 cm^{-1} are assigned to this species.

The rate of growth of the water complex (τ = 11.5 ($\pm$1) μs) and the rate of decay of the second pentacarbonyl transient species (τ = 12.0 ($\pm$1) μs) were observed to match, indicating direct formation of the former from the latter, and the reaction path following photolysis is A $\longrightarrow$ B $\longrightarrow$ C in nature. Kinetic traces from TRIR difference spectra showing these processes are shown in Figure 3.27.

The spectra presented above in Figure 3.26 are representative of those obtained following photolysis of $Mo(CO)_6$ and $Cr(CO)_6$, with only slight differences in the ν(CO) band positions of each of the photoproduced species. The ν(CO) band positions of all observed species are summarised in Table 3.11. In all cases, initial formation of a pentacarbonyl transient is observed which decays to form a second, which in turn decays

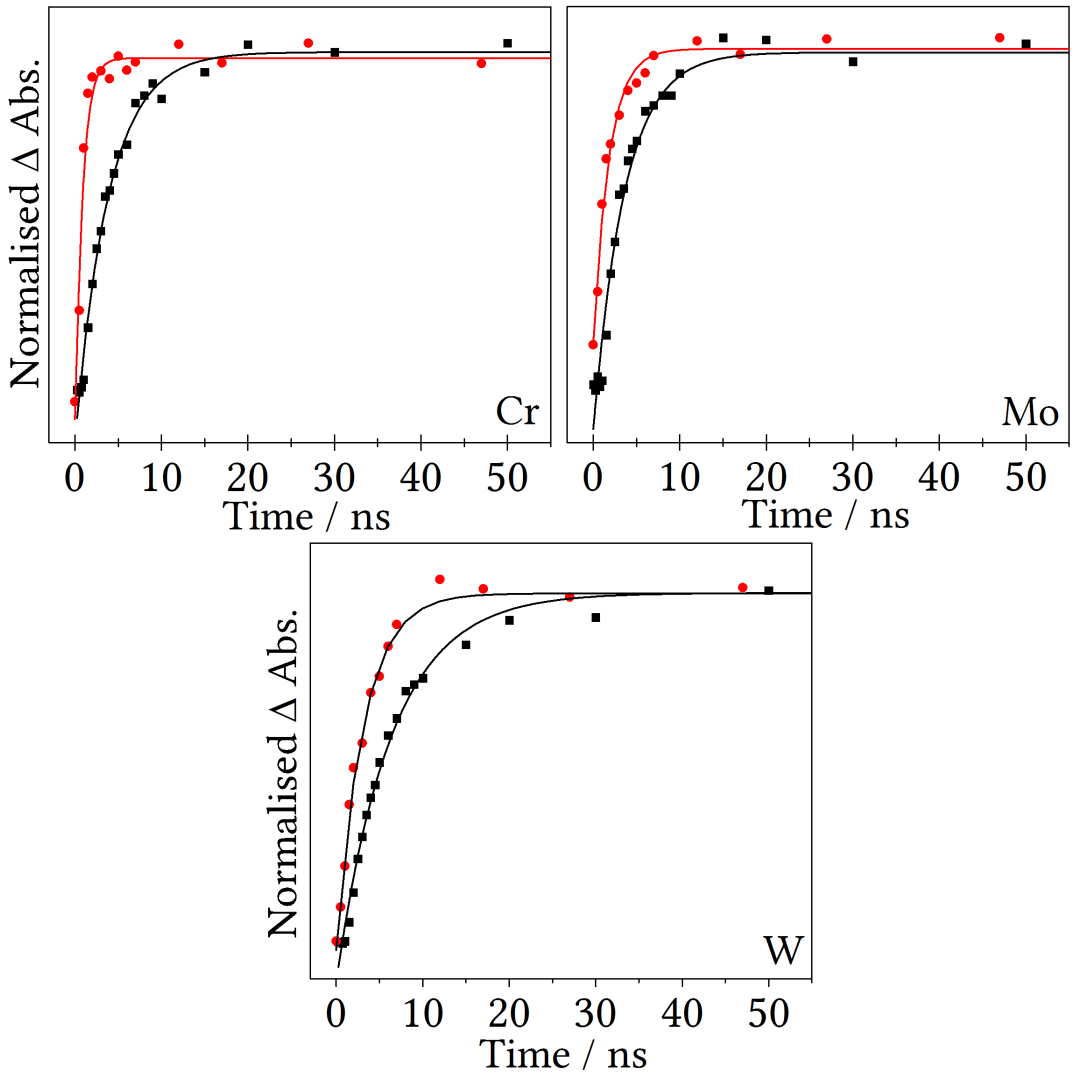


FIGURE 3.28: Kinetic traces from TRIR difference spectra recorded following photolysis of a series of solutions of $M(CO)_6$ (M = Cr (top left), Mo (top right), W (bottom)) in PFMCH under Ar (1.5 bar) or Xe (1.5 bar), showing growth of bands assigned as $M(CO)_5(C_7F_{14})$ (black squares), and $M(CO)_5Xe$ in each case. Solid lines show mono-exponential fits.

to form the water complex, in the same A $\longrightarrow$ B $\longrightarrow$ C mechanism observed above. The main observed difference between the three metals is the rates at which these reactions occur. The rate of formation of both the second pentacarbonyl transient and the water complex is found to increase in the series W < Mo < Cr. This observation is consistent with the relative stabilities of alkane and noble gas complexes of these three

metals to reaction with CO, with W forming the most stable complexes and Cr the lease stable.[34]

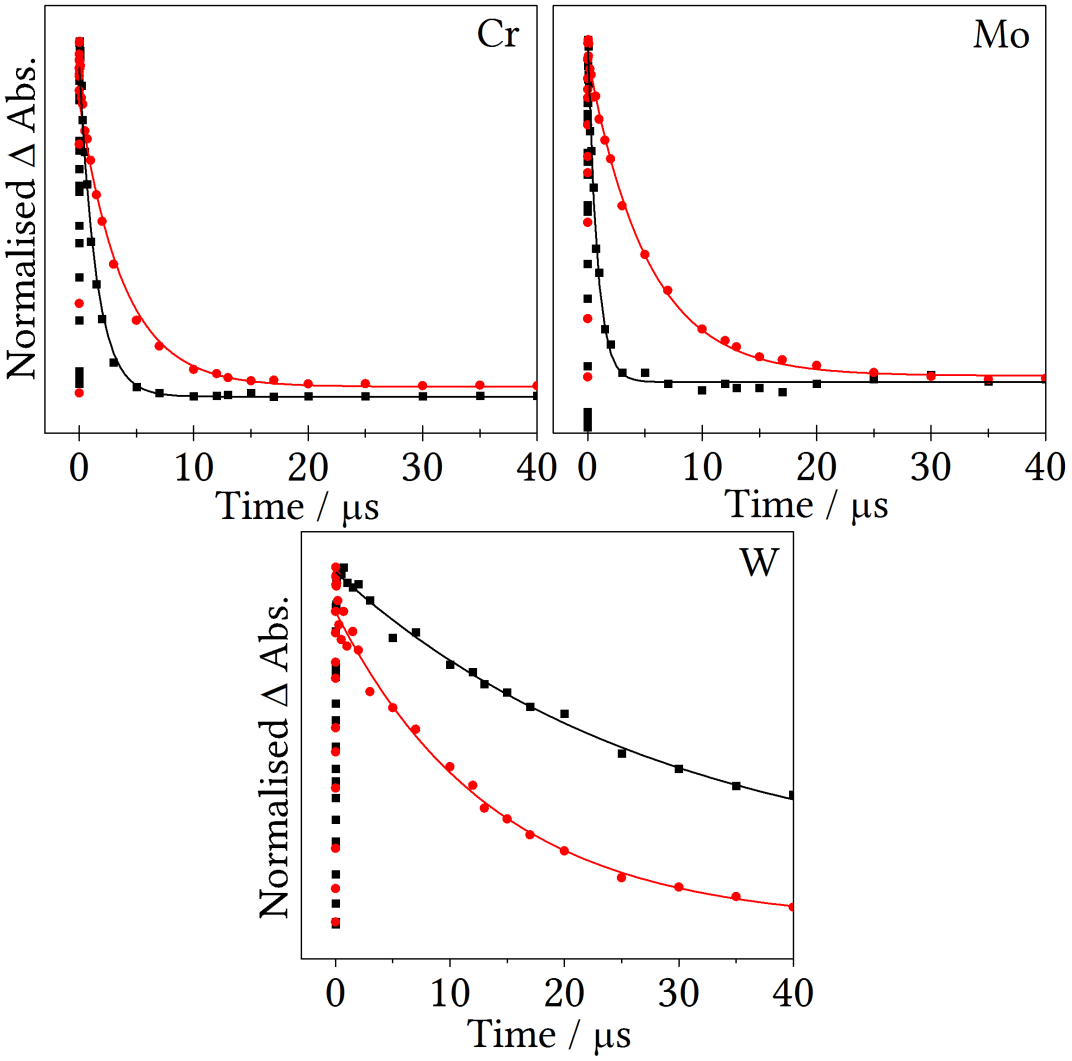


FIGURE 3.29: Kinetic traces from TRIR difference spectra recorded following photolysis of a series of solutions of $M(CO)_6$ (M = Cr (top left), Mo (top right), W (bottom)) in PFMCH under Ar (1.5 bar) or Xe (1.5 bar), showing decay of bands assigned as $M(CO)_5(C_7F_{14})$ (black squares), and $M(CO)_5Xe$ in each case. Solid lines show mono-exponential fits.

Experiments were repeated following the addition of Xe (1.5 bar) to each solution. 266 nm photolysis of the resulting solutions resulted in initial formation of the same pentacarbonyl transient species as in pure PFMCH, which decayed to form a second

pentacarbonyl transient, as above. However, upon addition of Xe the ν(CO) band positions of the second pentacarbonyl species were observed to be different to those seen in pure PFMCH. The observed shift to higher energy indicates a differing amount of electron density on the metal centre. While the same A $\longrightarrow$ B $\longrightarrow$ C reaction mechanism is observed in each case following the addition of Xe, with all experiments resulting in the ultimate formation of the water complex, the rates of each step in the reaction are altered upon addition of Xe. The rate of formation of the second pentacarbonyl transient from the first is increased upon addition of Xe (Figure 3.28), while the rate of decay of this second transient to form the water complex is slowed (Figure 3.29), indicating increased stability of the second transient. The increased rate of formation, slowed rate of decay and change in ν(CO) frequency of the second pentacarbonyl species indicate that the structure of this species was altered upon addition of Xe, and possibly indicated formation of an Xe complex in solution in each case.

TABLE 3.10: Observed rate constants (k_{obs}) for growth and decay processes of solvent or Xe complexes observed following photolysis of $M(CO)_6$ (M = Cr, Mo, W) in PFMCH and PFH solutions. All data recorded at 298 K.

			k_{obs} (s^{-1})	
Solvent	**ν(CO) (cm^{-1})**	**Assignment**	**Growth**	**Decay**
C_7F_{14} (PFMCH)	1962	$Cr(CO)_5(C_7F_{14})$	2.6 ($\pm$0.2) x 10^8	6.7 ($\pm$0.6) x 10^5
	1966	$Cr(CO)_5Xe$	1.3 ($\pm$0.1) x 10^9	2.7 ($\pm$0.2) x 10^5
	1971	$Mo(CO)_5(C_7F_{14})$	2.9 ($\pm$0.2) x 10^8	9.1 ($\pm$0.8) x 10^5
	1973	$Mo(CO)_5Xe$	5.6 ($\pm$0.5) x 10^8	2.0 ($\pm$0.2) x 10^5
	1961	$W(CO)_5(C_7F_{14})$	1.6 ($\pm$0.1) x 10^8	8.3 ($\pm$1.0) x 10^4
	1963	$W(CO)_5Xe$	3.3 ($\pm$0.2) x 10^8	3.3 ($\pm$0.3) x 10^4
C_6F_{14} (PFH)	1964	$Cr(CO)_5(C_6F_{14})$	3.0 ($\pm$0.3) x 10^8	3.3 ($\pm$0.4) x 10^6
	1968	$Cr(CO)_5Xe$	1.5 ($\pm$0.1) x 10^9	2.5 ($\pm$0.4) x 10^5

While assignment of the final photoproduct as the water complex in each case

may be straightforward by examining previously published work, assignment of the two pentacarbonyl species observed prior to formation of this final product is less trivial. The appearance of two different transients which interchange on a nanosecond timescale is similar to the regime observed previously following photolysis of $CpRe(CO)_3$ in PFMCH. Similarly, the rate of this interchange is altered by the addition of Xe, and is no longer seen upon addition of a small amount of cyclopentane to the solution. Addition of cyclopentane to a solution of $W(CO)_6$ in PFMCH in this case was also observed to result in the formation of a single transient species with ν(CO) bands at 1959 and 1934 cm^{-1} (parent: 1989 cm^{-1}), which was stable on the timescale of the experiment, similar to those previously reported following photolysis of $W(CO)_6$ in liquid Kr in the presence of cyclohexane (1959 and 1935 cm^{-1}, parent: 1988 cm^{-1}).[49] The ν(CO) bands of the second transient species observed following photolysis of $W(CO)_6$ in PFMCH under Xe (1963 and 1937 cm^{-1}) also closely match those reported by Weiller following photolysis of $W(CO)_6$ in *sc*Kr doped with Xe (1963 and 1936 cm^{-1}), which is assigned as the Xe complex $W(CO)_5Xe$. As observed following photolysis of $CpRe(CO)_3$ in PFMCH and PFH, the ν(CO) band positions of the second, more stable transient species are more akin to those of the cyclopentane complex, as well as the previously reported cyclohexane complex, indicating coordination of a weak ligand to the metal centre. It seems likely therefore due to its ν(CO) band positions and its changing rate of growth and decay upon addition of Xe, that the second pentacarbonyl transient in this case is the solvent complex $M(CO)_5(C_7F_{14})$ following photolysis in pure solvent, or the Xe complex $M(CO)_5Xe$ upon addition of Xe to the solution.

As in the case of $CpRe(CO)_3$, there are several candidates for assignment of

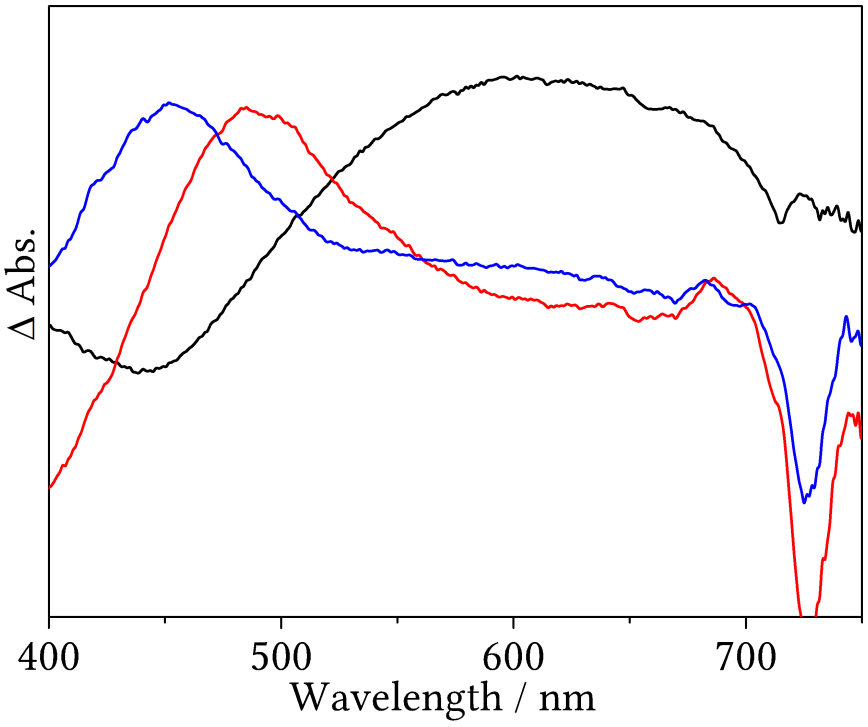


FIGURE 3.30: Selected nanosecond TA difference spectra recorded 1 ns (black), 200 ns (red) and 20,000 ns (blue) following 266 nm photolysis of a solution of $Cr(CO)_6$ in PFMCH under Ar (1.5 bar), formation of three different transient absorption bands can be seen over time.

the initial carbonyl loss product. The most likely candidates are a coordinatively unsaturated species of the form $M(CO)_5$, or a weak complex with the PFMCH solvent. A short lived, and possibly coordinatively unsaturated species of this type has been observed previously by Kelly *et al.* following photolysis of $M(CO)_6$ in perfluoro(methylcyclohexane), by transient absorption (TA) UV/visible spectroscopy.[78,79] In addition to the TRIR experiments presented above, TA spectra were also recorded following photolysis of $M(CO)_6$ in PFMCH solution. Figure 3.30 shows TA difference spectra on the nanosecond timescale recorded following 266 nm photolysis of $Cr(CO)_6$ in PFMCH under Ar. The spectrum recorded 1 ns following photolysis showed a single broad absorption band with λ_{max} *ca.* 610 nm. This band was observed to decay on the fast

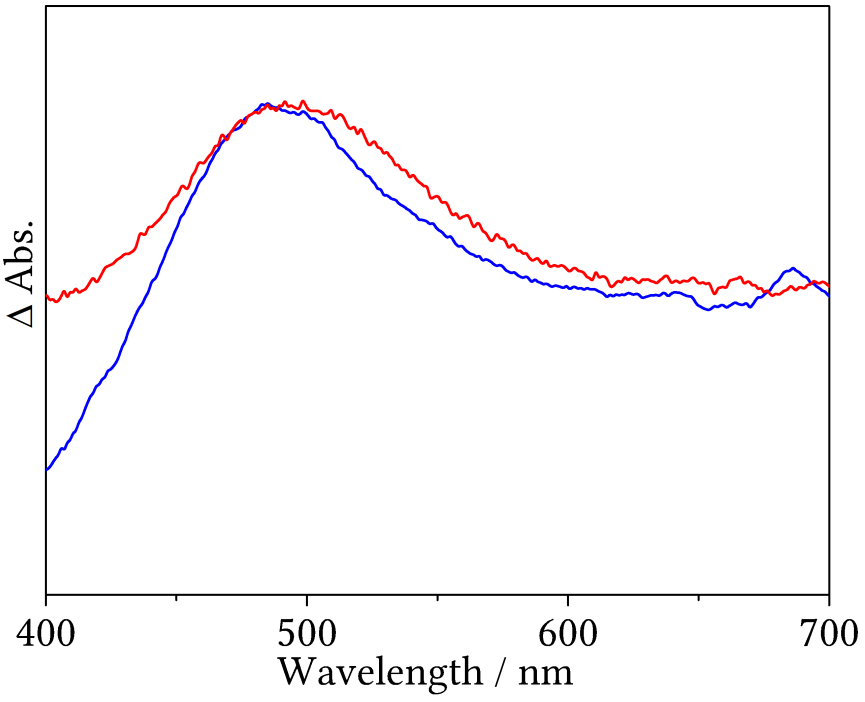


FIGURE 3.31: Nanosecond TA difference spectra recorded 200 ns following 266 nm photolysis of a solution of $Cr(CO)_6$ in PFMCH under Ar (1.5 bar) (blue) and $Cr(CO)_6$ in PFMCH under Xe (1.5 bar) (red).

nanosecond timescale, consistent with TRIR studies, to yield a further absorption band with λ_{max} *ca.* 490 nm. It is clear that this absorption band at *ca.* 610 nm represents the first pentacarbonyl transient observed during our TRIR experiments. These results show good agreement with the work of Kelly *et al.*, who report an initial transient following photolysis of $Cr(CO)_6$ with a λ_{max} *ca.* 620 nm. Studies of $Mo(CO)_6$ and $W(CO)_6$ are also in agreement with previous work, exhibiting initial absorption bands at λ_{max} *ca.* 470 nm and 475 nm respectively (Kelly *et al.*: 460 and 475 nm). Kelly and co-workers assigned this band as coordinatively unsaturated $M(CO)_5$ following photolysis in PFMCH. Photolysis in cyclohexane was shown to yield a single product, which was assigned as the cyclohexane complex $M(CO)_5(C_6H_{12})$. In all cases, decay of this initial absorption band was accompanied by growth of a further absorption

at higher energy. Matrix isolation studies by Perutz and Turner have indicated that a shift to higher energy may indicate stronger coordination of a ligand to the metal centre.[80] Photolysis of $Cr(CO)_6$ in a Ne matrix resulting in a λ_{max} at 624 nm, while repeating the experiment in a CH_4 matrix increased the energy of λ_{max} to 489 nm. This previous observation is somewhat in agreement with our TA and TRIR observations, with both techniques presenting evidence for binding of a weak ligand (PFMCH or Xe) following initial formation of a coordinatively unsaturated species. Based on the assignment by Kelly and co-workers, the initially formed pentacarbonyl species formed following photolysis of $M(CO)_6$ (M = Cr, Mo, W) is tentatively assigned as $M(CO)_5$. A comparison of the difference spectrum recorded 200 ns following photolysis of solutions of $Cr(CO)_6$ in PFMCH under Ar or Xe, shows a small change in the λ_{max} of the second transient species, shown in Figure 3.31. In neat PFMCH, λ_{max} = 490 nm, and this species is assigned as the solvent complex $Cr(CO)_5(C_7F_{14})$, while upon addition of Xe λ_{max} = 500 nm, suggesting a small change in the binding interaction between metal and ligand upon addition of Xe, possibly indicating formation of $Cr(CO)_5Xe$.

TABLE 3.11: ν(CO) absorption band frequencies and λ_{max} of $M(CO)_6$ (M = Cr, Mo, W) and intermediates and photoproducts formed following photolysis in a series of pure and Xe doped PFMCH and PFH solutions. Experiments performed in solution phase at 298 K unless otherwise stated.

Compound	**Solvent**	**Dopant**	**ν(CO) (cm^{-1})**	**λ_{max} (nm)**	**Reference/ Notes**
$Cr(CO)_6$	PFMCH		1993		This work
		Xe	1993		This work
	PFH		1995		This work
		Xe	1995		This work
$Cr(CO)_5$	PFMCH		1967, 1936	610	This work
		Xe	1967, 1936		This work
	PFH		1968, 1938		This work
		Xe	1968, 1937		This work
$Cr(CO)_5X$	PFMCH		1962, 1937	490	This work
		Xe	1966, 1939	500	This work
	PFH		1964, 1939		This work
		Xe	1968, 1940		This work
	*liq*Xe		1960, 1934		49, 140 K
	*liq*Kr	C_6H_{12}	1961, 1939		49, 140 K
$Cr(CO)_5(H_2O)$	PFMCH		1980, 1969, 1950(br), 1917	451	This work
		Xe	1980, 1969, 1950(br), 1917		This work
	PFH		1983, 1970, 1950(br), 1920		This work
		Xe	1983, 1970, 1950(br), 1920		This work
$Mo(CO)_6$	PFMCH		1995		This work
		Xe	1995		This work
$Mo(CO)_5$	PFMCH		1975, 1930	470	This work
		Xe	1975, 1931		This work
$Mo(CO)_5X$	PFMCH		1971, 1935	435	This work
		Xe	1973, 1937		This work
$Mo(CO)_5(H_2O)$	PFMCH		1983, 1967, 1950(br), 1917	403	This work
		Xe	1983, 1967, 1950(br), 1918		This work
$W(CO)_6$	PFMCH		1989		This work
		Xe	1989		This work
$W(CO)_5$	PFMCH		1966, 1930	475	This work
		Xe	1966, 1930		This work
$W(CO)_5X$	PFMCH		1961, 1935	420	This work
		Xe	1963, 1937		This work
		C_5H_{10}	1959, 1934		This work
	*liq*Kr	Xe	1963, 1936		49, 183 K
		C_6H_{12}	1959, 1935		49, 180 K
$W(CO)_5(H_2O)$	PFMCH		1977, 1940(br), 1918		This work
		Xe	1977, 1940(br), 1918		This work

3.2.8 DFT Studies of Transient Species Produced Following Photolysis of $M(CO)_6$ (M = Cr, Mo, W)

In addition to the DFT study of the transients produced following photolysis of $CpRe(CO)_3$ reported above, calculations were also carried out to aid assignment of the ν(CO) band of species produced following photolysis of $M(CO)_6$ (M = Cr, Mo, W). As above, all calculations were carried out using Gaussian 03 and the Gaussview interface.[293,294] The B3LYP functional was used, along with the LANL2DZ RECP basis set for W and Xe atoms, and the 6-311G** basis set for all other atoms.

TABLE 3.12: Experimental and theoretical ν(CO) absorption band frequencies of $M(CO)_6$ and intermediates and photoproducts formed following photolysis of $M(CO)_6$ (M = Cr, Mo, W). DFT calculations were carried out on energy minimised structures in the gas phase at 298 K, using the B3LYP/LANL2DZ/6-311G** method described above. Experimental ν(CO) band positions were obtained following photolysis in pure PFMCH solution, or in the presence of 1.5 bar Ar or Xe at 298 K.

	ν(CO) (cm^{-1})	
Compound	**Calculated**	**Experimental**
$\mathbf{Cr(CO)_6}$	2083	1993
$\mathbf{Cr(CO)_5}$	2066, 2047	1967, 1936
$\mathbf{Cr(CO)_5Xe}$	2062, 2045	1966, 1939
$\mathbf{Cr(CO)_5(C_2F_6)}$	2060, 2043	
$\mathbf{Cr(CO)_5(C_7F_{14})}$ **($\mathbf{CF_3}$-bound)**	2060, 2043	1962, 1937
$\mathbf{Cr(CO)_5(C_7F_{14})}$ **($\mathbf{CF_2}$-bound)**	2061, 2043	
$\mathbf{Mo(CO)_6}$	2081	1995
$\mathbf{Mo(CO)_5}$	2067, 2037	1975, 1930
$\mathbf{Mo(CO)_5Xe}$	2063, 2038	1973, 1937
$\mathbf{Mo(CO)_5(C_2F_6)}$	2062, 2037	
$\mathbf{W(CO)_6}$	2076	1989
$\mathbf{W(CO)_5}$	2059, 2033	1966, 1930
$\mathbf{W(CO)_5Xe}$	2054, 2035	1961, 1935
$\mathbf{W(CO)_5(C_2F_6)}$	2044, 1991	

Calculated vibrational frequencies for a series of possible transient species produced following photolysis of $M(CO)_6$ (M = Cr, Mo, W) are given in Table 3.12.

Calculations returned no imaginary frequencies, indicating that the structures had reached a minimum on the potential energy surface. As with the calculations for various rhenium complexes reported previously in this Chapter the calculations systematically overestimate the ν(CO) frequencies of all species studied, however interesting trends still emerge upon comparison of the calculated frequencies.

An interesting trend which arose from experimental studies was the difference in $\Delta\nu$ between the two ν(CO) bands of the initially formed dicarbonyl species, tentatively assigned as $M(CO)_5$ ($\Delta\nu$ = 31, 45 and 36 cm^{-1} for M = Cr, Mo and W respectively) compared with those of the other assigned pentacarbonyl species, assigned as $M(CO)_5X$, where X is the solvent or dopant of interest ($\Delta\nu$ = 26, 36 and 26 cm^{-1} for M = Cr, Mo and W respectively). The calculated vibrational frequencies were observed to reproduce this trend, with the coordinatively unsaturated $M(CO)_5$ exhibiting a larger $\Delta\nu$ than any of the coordinatively saturated structures studies, which all exhibited very similar $\Delta\nu$ values. In all cases, the calculated highest energy ν(CO) absorption band of species of the form $M(CO)_5X$ and $M(CO)_5$ were observed to exhibit a general shift down in wavenumber compared to the ν(CO) band of the parent $M(CO)_6$. The trend observed in the magnitude of this shift is in agreement with that observed in experimental studies, following the order $M(CO)_5(C_7F_{14}) > M(CO)_5Xe > M(CO)_5$. This observation is further indication that that initially formed transient species may be the coordinatively unsaturated species $M(CO)_5$, which undergoes a reaction with the solvent or dopant on a nanosecond timescale to form $M(CO)_5X$, though the calculations presented herein are far from conclusive.

Similar to calculations reported previously in this Chapter, two different structures

of $Cr(CO)_5(C_7F_{14})$ were calculated, one in which the metal is bound to a CF_2 moiety, and one in which the metal is bound to the CF_3 unit. Calculations showed only a small difference between the ν(CO) bands of the two structures, while a comparison of the binding enthalpies of the two structures showed, as above, that the CF_3-bound structure (37 kJ/mol) is likely to be favoured over the CF_2-bound (35 kJ/mol). As above for complexes of Re, all interactions between metal and perfluoroalkane were found to occur through the lone pair of an F atom, and not through the C-F bond, as would be expected for the C-H bond of alkanes. Attempts to calculate species bound in an η^2 fashion through the C-F were not successful, leading to either a change in geometry or the return of imaginary frequencies, indicating that the structure was not at a minimum on the potential energy surface. Isomerisation between different binding modes of the solvent still represents a possible explanation for the presence of two distinct pentacarbonyl species in solution, and the true binding mode of the perfluoroalkane solvent is still unknown. C_2F_6 was once again found to be a reasonable computational model for the CF_3-bound PFMCH complex $Cr(CO)_5(C_7F_{14})$, producing calculated ν(CO) frequencies in good agreement with those of $Cr(CO)_5(C_7F_{14})$. In order to reduce computational cost, C_2F_6 was used as a computational model for calculations of the ν(CO) band positions of $Mo(CO)_5(C_7F_{14})$ and $W(CO)_5(C_7F_{14})$. In these studies, the C_2F_6 complex was found to satisfactorily reproduce experimental trends in ν(CO) band positions and $\Delta\nu$, indicating that this model may be useful for future calculations of transition metal perfluoroalkane complexes.

3.3 Conclusions

In this Chapter, the photochemistry of a series of model transition metal complexes has been examined using various time-resolved spectroscopic techniques in the perfluorinated solution phase. It has been demonstrated that addition of various dopants, including noble gases and gaseous alkanes, alters the photochemistry of such complexes in the perfluorous phase, indicating formation of a series of weakly-bound organometallic noble gas and alkane complexes in room temperature solution.

The photochemistry of $CpRe(CO)_3$ and its derivatives, $Cp^*Re(CO)_3$ and $CpRe(CO)_2(N_2)$, has been examined using TRIR spectroscopy following photolysis in perfluoroalkane solvents. Upon photolysis, these compounds were observed to undergo carbonyl loss, resulting in formation of a dicarbonyl species, likely to be either the coordinatively unsaturated species $CpRe(CO)_2$, or a weakly-bound solvent complex. This dicarbonyl species was found to be unstable, decaying to yield a second dicarbonyl species of the form $CpRe(CO)_2X$ on the fast nanosecond timescale. Kinetic studies showed that this second dicarbonyl species is formed directly from the first. The ν(CO) bands of the second dicarbonyl species were observed to be shifted to lower energy compared to the first, indicating an increase of electron density on the Re metal centre. The direct formation of the second dicarbonyl from the first, and the shift in ν(CO) band positions suggested direct reaction of the first dicarbonyl transient with the solvent or dopant to form a more strongly bound species. In all cases, the second dicarbonyl species was found not to decay on the timescale of the experiment. Addition of cyclopentane to a solution of $CpRe(CO)_3$ in PFMCH resulting in the formation of only a single dicarbonyl intermediate, while addition of Xe (1.5 bar) to the solution

was found to increase the rate of formation of the second dicarbonyl transient, as well as subtly altering its ν(CO) band frequencies. This change is suggestive of formation of an organometallic Xe complex in room temperature solution. DFT calculations were undertaken, and were found to reproduce trends in experimental ν(CO) band positions well, offering further indication that the initially formed dicarbonyl may indeed be the coordinatively unsaturated $CpRe(CO)_2$. Photolysis studies of $CpRe(CO)_3$ and $Cp^*Re(CO)_3$ were conducted using 266 nm irradiation, while studies of $CpRe(CO)_2(N_2)$ were conducted using 355 nm excitation. Results obtained following 355 nm photolysis of $CpRe(CO)_2(N_2)$ in PFMCH were comparable to those obtained following photolysis of $CpRe(CO)_3$ at 266 nm, and suggest that careful choice of the leaving ligand may allow this interesting chemistry to be accessed at various photolysis wavelengths.

Doping of methane or ethane into solutions of $CpRe(CO)_3$ and $Cp^*Re(CO)_3$ in PFMCH resulted in initial formation of the same dicarbonyl species as seen in pure PFMCH, following by formation of a σ-alkane complex which went on to undergo oxidative addition to the metal centre to form an alkyl hydride complex of the form $CpRe(CO)_2(R)H$. The observation of oxidative addition unequivocally proves binding of methane and ethane to the metal centre in room temperature perfluoroalkane solution. The ratio of alkane:alkyl hydride formed was observed to vary in the order: $CpRe(CO)_3$ with ethane > $Cp^*Re(CO)_3$ with ethane > $CpRe(CO)_3$ with methane > $Cp^*Re(CO)_3$ with methane. This result is in agreement with previously published studies.[37]

The above study was expanded to examine the photochemistry of $CpRh(CO)_2$ in PFMCH and PFH, with and without the presence of Xe in solution, using TRIR spectroscopy. Photolysis at 266 nm in the pure solvent resulted in initial formation

of a monocarbonyl species assigned as $CpRh(CO)(C_7F_{14})$. Decay of this species is accompanied by formation of a small amount of the dimeric species $Cp_2Rh_2(CO)_3$, confirmed by further consumption of the parent complex. The major product of the decay of the monocarbonyl solvent complex is a species with a single ν(CO) band shifted to higher energy compared to the monocarbonyl. This band is very tentatively assigned as an oxidative addition product, $CpRh(CO)(R^F)F$. Addition of Xe to the solution resulted in formation of a monocarbonyl complex with ν(CO) bands at slightly higher energy than those assigned to $CpRh(CO)(C_7F_{14})$. No evidence of the tentatively assigned C-F activated species was observed, instead the dimeric species was observed to be the only product. A reaction mechanism was proposed, including different reaction pathways with and without Xe. The monocarbonyl species formed following addition of Xe to the solution was assigned as CpRh(CO)Xe.

The photochemistry of $M(CO)_6$ (M = Cr, Mo, W) was also examined by TRIR spectroscopy in PFMCH. Following photolysis as 266 nm in all case, a single pentacarbonyl product of the form $M(CO)_5$ was observed to form. Similarly to the above case of $CpRe(CO)_3$, this initial carbonyl loss product was found to be unstable, decaying on the fast nanosecond timescale, at a rate matching the formation of a second, more stable pentacarbonyl species. This second product was also found to be unstable, decaying on the microsecond timescale to form a complex with a trace water impurity. Addition of cyclopentane to a solution of $W(CO)_6$ in PFMCH resulted in the formation of only a single pentacarbonyl species. Addition of Xe to each of the solutions resulted in formation of the same initial pentacarbonyl transient, however the rate of decay of this species and formation of the second pentacarbonyl transient were found to increase.

The rate of decay of the second pentacarbonyl transient was also observed to slow upon addition of Xe. Due to the increased rate of formation, decreased rate of decay and change in ν(CO) band positions upon addition of Xe, the second pentacarbonyl species formed following photolysis was assigned as the Xe complex $M(CO)_5Xe$. In addition to TRIR studies, TA spectroscopic study of $M(CO)_6$ in PFMCH was also undertaken. Three different transient absorption bands were observed in each case, in agreement with TRIR results. The first of these absorption bands, corresponding to the initially formed pentacarbonyl species, was found to match absorption bands reported previously in PFMCH solution, assigned as the coordinatively unsaturated species $M(CO)_5$. DFT calculations were again utilised to aid in the assignment of ν(CO) bands, and were shown to produce experimental trends well, further indicating initial formation of $M(CO)_5$ following photolysis. The initially formed pentacarbonyl transient formed following photolysis of $M(CO)_6$ in PFMCH was therefore assigned as $M(CO)_5$.

In the previous Chapter, perfluorinated solvents were shown to be able to extend the lifetime of highly reactive, coordinatively unsaturated 16-electron triplet species compared to liquid alkane solvents, and even some noble gases. In this Chapter, perfluorinated solvents have further shown their potential as solvent systems for formation of weakly-bound organometallic complexes in room temperature solution. Formation of such complexes in solution requires a solvent which will bind to the metal even less strongly than the weak ligand of interest, be it a gaseous alkane or noble gas. Perfluorinated solvents appear to form very weak complexes with organometallic species, evidenced by the changing chemistry, changing kinetics and changing ν(CO) band

positions of transient species upon addition of alkane or noble gas dopants to sample solutions. When coupled with pump-probe spectroscopic techniques incorporating fast detection, perfluorinated solvents may allow the detection of such species by a variety of techniques, potentially including TR-XAFS and pump-probe NMR spectroscopy.

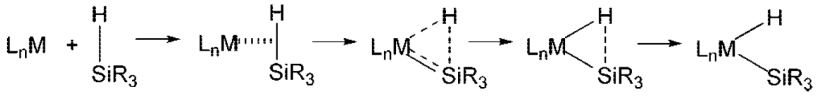
Chapter 4

Time-Resolved Spectroscopic Studies of Organometallic Triethylsilane Complexes

4.1 Introduction

The chemistry of σ-complexes formed through η^2 interaction between a transition metal and an X-H bond (X = H, C, Si etc.) has been a source of much interest throughout the past few decades.[299] Much of this interest centres around their identification as intermediates in the activation of such X-H bonds.[227,236,300–302] The interaction between a hydrosilane and a transition metal can range from a weak σ-interaction, to formation two full formal bonds, one between the metal and the hydrogen, and the other between

the metal and the silicon atom. This oxidative addition process results in a change in both the oxidation state and coordination number at the metal centre.[303]



SCHEME 4.1: Steps in the activation of a hydrosilane Si-H bond by a transition metal centre. Reproduced from ref 300.

Scheme 4.1 shows the various stages of Si-H activation by a metal centre. The nature of the η^2 σ-interaction of the Si-H bond with the metal centre has been investigated in great detail previously,[301,304–308] and has been described as a nonclassical 3-centre/2-electron bond, arising from interaction between the Si-H σ-bonding orbital and an empty metal *d*-orbital. Silane σ-complexes were first identified in 1969,[309] and are often studied as a model for similar complexes, e.g., C-H σ-complexes.[40] In comparison with similar σ-complex systems (e.g., H-H and C-H), the increased basicity of the Si-H bond makes the unit a superior electron donor, creating a strong interaction between σ-bond and metal centre. Additionally, interactions between the Si-H bond and other ligands attached to the metal centre have also been observed.[304,305,310] The σ*-antibonding orbital of the Si-H bond is a better π-acceptor than the comparable C-H and H-H antibonding orbitals, leading to increased back-bonding from the metal centre, and ultimately more facile oxidative addition of the Si-H to the metal.

The coordinatively unsaturated 16-electron transition metal species required is usually generated through loss of a carbonyl or phosphine ligand, by photochemical or thermal means. Structural investigations of silane σ-bonded complexes have mostly utilised x-ray diffraction, with a small number of studies using other techniques such as

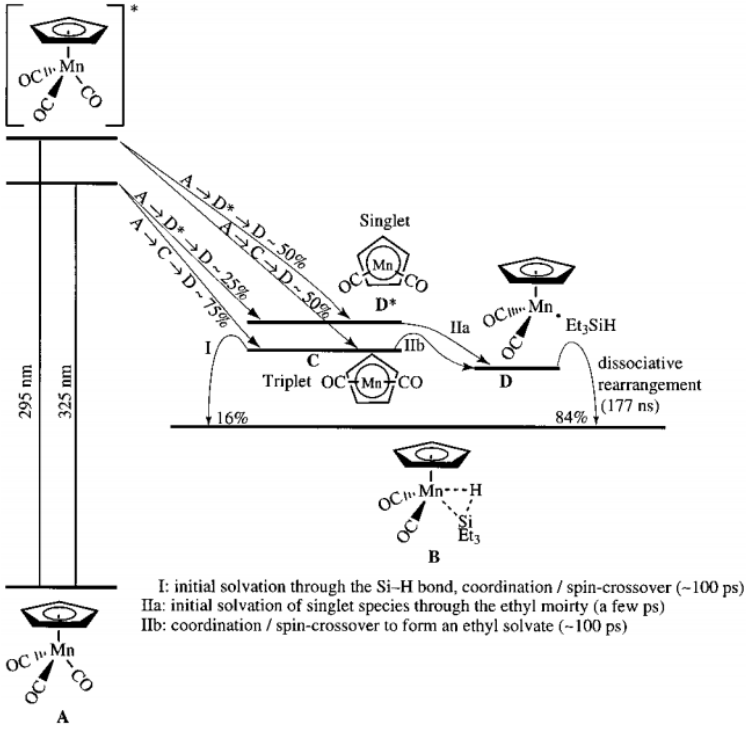
neutron diffraction[308,311,312] and NMR spectroscopy.[312,313] Vibrational spectroscopic techniques have also been widely utilised in the study of such σ-complexes, as well as any subsequent activation chemistry. These techniques are well suited to the study of Si-H interactions with transition metal carbonyl complexes due to the high sensitivity of the ν(CO) absorbance frequency to the electron density at the metal centre. The remainder of this Introduction will focus on infrared spectroscopic investigations of transition metal hydrosilane interactions.

4.1.1 IR Spectroscopy of Transition Metal Hydrosilane Complexes

While the use of metal carbonyl species as precursors for silane activation may not be as extensive as that of their phosphine analogues, there is still a wealth of evidence for the use of IR spectroscopic techniques to characterise both Si-H σ-complexes and Si-H activated species. Much of the work presented herein was undertaken by the Harris group, who have amply demonstrated the power of TRIR spectroscopy for characterisation of such species.

Harris and co-workers used TRIR spectroscopy to examine the photochemistry of $CpMn(CO)_3$ following photolysis in triethylsilane solution, providing the first reported study of silicon-hydrogen bond activation using ultrafast infrared spectroscopy.[150,186] Initially, two transient species were reported, which were assigned to the silane σ-complex $CpMn(CO)_2(EtSiHEt_2)$, and the unsaturated 16-electron intermediate $CpMn(CO)_2$. A single confirmed ν(CO) band of this intermediate was observed in this case, while the other, lower energy band observed previously by Zheng *et al.*[152] lay outside of the spectroscopic window of the instrument. Later studies attempted to give further insight

into the mechanism of Si-H bond activation at manganese carbonyl centres using a combination of TRIR spectroscopic studies and density functional theory calculations.



SCHEME 4.2: Proposed reaction mechanism following UV irradiation of $CpMn(CO)_3$ in triethylsilane solution. Proposed structures (C and D*) for the triplet and singlet 16-electron species $^3CpMn(CO)_2$ and $^1CpMn(CO)_2$ are also shown. Reproduced from ref 150.

Based on the findings of this study, a reaction mechanism was proposed, shown in Scheme 4.2. Initial formation of the Si-H 'activated' species was proposed to occur directly through the triplet unsaturated intermediate $^3CpMn(CO)_2$, while further activation was shown to occur through formation of the σ-complex $CpMn(CO)_2(EtSiHEt_2)$ from a singlet unsaturated intermediate, which was not observed spectroscopically. In this case, the 'activated' species did not show conclusive evidence for breaking of the Si-H bond. While the shift in the ν(CO) bands to higher energy were shown to be consistent with a reduction in electron density at the Mn centre, the length of the Si-H

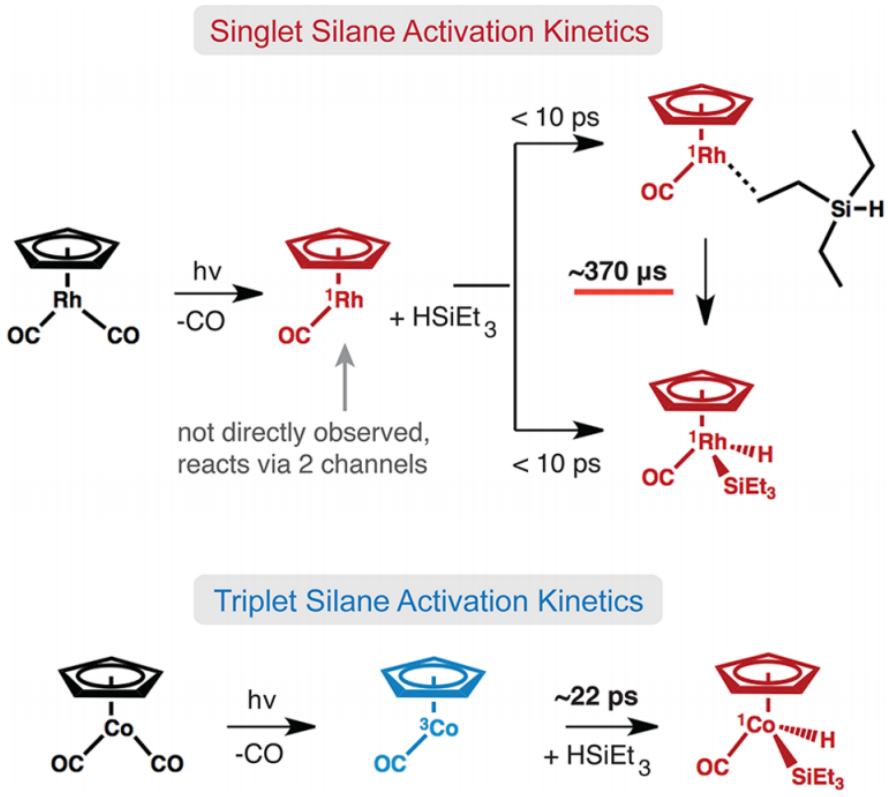
bond is such that activation was not confirmed, in agreement with the work of Schubert *et al.*[311] This species was designated as an η^2 Si-H σ-complex, $CpMn(CO)_2(\eta^2\text{-H-SiEt}_3)$, which exhibits significant $CpMn(CO)_2H(SiEt_3)$ character, designated as the 'partially activated' $CpMn(CO)_2(H\text{---}SiEt_3)$ for the remainder of this Chapter. The ratio of the triplet and singlet complexes initially formed was found to be dependent on the excitation wavelength selected, with the longer wavelength (325 nm) resulting in increased formation of the triplet $^3CpMn(CO)_2$. Spin-forbidden reaction of the triplet to form the solvated singlet state in this case was found to occur on the picosecond timescale (*ca.* 100 ps) in triethylsilane solution. Photolysis of $CpRe(CO)_3$ in triethylsilane resulted in only the formation of a singlet species, which was preferentially solvated by the ethyl moiety of the silane molecule to give $CpRe(CO)_2(EtSiHEt_2)$, which was identified spectroscopically. This ethyl-bound species was then shown to undergo a rearrangement-activation reaction to form the Si-H activated species $CpRe(CO)_2(SiEt_3)H$ on the fast microsecond timescale. The interaction between the Si-H bond and the metal centre in the final photoproduct (the Si-H 'activated' species) was assigned as a nonclassical interaction for $CpMn(CO)_2(H\text{---}SiEt_3)$, while its Re analogue exhibited full oxidative addition. This difference was assigned due to a shorter Si-H bond lengths in reported *ab initio* calculations for the Mn species.

The solution phase photochemistry of $CpV(CO)_4$ in the presence of $HSiEt_3$, $HSiEtCl_2$ or $HSiCl_3$ was studied at low and room temperatures by George *et al.* using TRIR spectroscopy.[224] Photolysis in the presence of $HSiEtCl_2$ or $HSiCl_3$ resulted is observation of ν(CO) bands which were shifted to higher wavenumber than those of the parent $CpV(CO)_4$, indicating oxidation at the metal centre. In the presence of $HSiEt_3$,

however, photolysis resulted in formation of a species with ν(CO) which appear to lower energy compared to those of $CpV(CO)_4$. This species was assigned as the η^2 Si-H complex $CpV(CO)_3(HSiEt_3)$. The authors conclude that oxidative addition is arrested in the case of $HSiEt_3$. A later study by Snee *et al.* also examined the photochemistry of $CpV(CO)_4$ in triethylsilane using TRIR spectroscopy.[147] The reaction of $CpV(CO)_4$ and $HSiEt_3$ was found to be similar to that described above with $CpMn(CO)_3$. Initial formation of an unsaturated 16-electron complex $^3CpV(CO)_3$ was observed, followed by coordination of the silane solvent through a concerted spin-crossover/solvation mechanism, forming the ethyl-bound silane complex $CpV(CO)_3(EtSiHEt_2)$. An additional product was observed to form on the picosecond timescale, with ν(CO) bands at lower energy compared to the parent complex, in agreement with results reported by George *et al.*,[224] described above. With reference to photolysis of $CpMn(CO)_3$ in $HSiEt_3$,[150,186] this species is assigned as a η^2 Si-H σ-complex, $CpV(CO)_3(\eta^2$-H-$SiEt_3)$, which exhibits some $CpV(CO)_3H(SiEt_3)$ character. As above for $CpMn(CO)_3$, *ab initio* calculations suggested an elongated Si-H bond when compared with free silane, however this bond length was not consistent with full oxidative activation at the V centre.

Harris and co-workers have also investigated the photochemistry of $Fe(CO)_5$ in triethylsilane.[118] The 16-electron coordinatively unsaturated species $^3Fe(CO)_4$ was observed in triethylsilane as the first photoproduct, however it was found to be unstable on the picosecond timescale, decaying completely to form the silyl activated complex $^1Fe(CO)_4H(SiEt_3)$ within 1.2 ns.

Lomont, Nguyen and Harris highlighted the ability of 16-electron triplet species to directly or partially activate Si-H bonds in their recent review.[190] The authors draw



SCHEME 4.3: Silane activation by singlet and triplet photoproducts following photolysis of $CpRh(CO)_2$ and $CpCo(CO)_2$ in $HSiEt_3$. Reproduced from ref 190.

an interesting comparison between the cases of $CpRh(CO)_2$ and $CpCo(CO)_2$, shown in Scheme 4.3 In the case of $CpRh(CO)_2$, photolysis in $HSiEt_3$ results in formation of a singlet coordinatively unsaturated species, which is not observed spectroscopically, which goes on to react with the solvent *via* two different pathways within 10 ps of photolysis. Direct activation of the Si-H activated species is observed, along with formation of the ethyl-bound σ-complex. Subsequently, this σ-complex then undergoes slow activation on the microsecond timescale.[56] In contrast, $CpCo(CO)_2$ shows fast Si-H activation on the picosecond timescale, directly from the 16-electron intermediate $^3CpCo(CO)$, which is observed spectroscopically.[144]

While all of the studies reported above involve formation of an Si-H activated or

partially activated species, with either a nonclassical interaction or formal oxidative addition to the metal centre, this scenario is not universal among the transition metal complexes. A 2000 study by Harris and co-workers, reported photolysis of $M(CO)_6$ (M = Cr, Mo, W) in triethylsilane and triisopropylsilane.[314] Following photolysis and subsequent carbonyl loss, the unsaturated species $M(CO)_5$ was observed to be rapidly solvated through the ethyl-moiety of the silane to form a σ-complex. This species is not stable however, giving way to the Si-H bound σ-complex on the picosecond to nanosecond timescale. A dissociative rearrangement mechanism is proposed, with the silane solvent dissociating from the metal centre, before re-coordinating in a different orientation to allow bonding through the Si-H moiety.

4.1.2 Aims

The initial aim of the work presented in this Chapter was to study silane coordination and activation using time-resolved XAFS spectroscopy. Initially, TR^MPS spectroscopy was used to examine the photochemistry of a series of model transition metal complexes in $HSiEt_3$. The transition metal complexes selected for study herein have previously shown strong evidence for formation of transition metal noble gas and alkane complexes in room temperature perfluoroalkane solution (Chapters 2 and 3 of this Thesis).

By replicating the solution concentration, solvent conditions and photoexcitation wavelength that will be utilised in future TR-XAFS experiments, hydrosilane photochemistry was used as a model system to test the methodology for formation of transition metal noble gas and alkane complexes described in previous Chapters. Hydrosilane chemistry, particularly Si-H bond activation offers an interesting test case

for TR-XAFS due to the change in oxidation state which occurs at the metal centre. Changes in oxidation state are known to result in changes in the near-edge and edge regions of the XAFS spectrum, while the change from coordination of a CO ligand to coordination through an Si-H bond should also result in changes to the EXAFS region of the spectrum, potentially allowing structural identification of a silane σ-complex, and observation of activation kinetics.

4.2 Results and Discussion

As stated above, the photochemistry of transition metal carbonyl species in neat triethylsilane solvent has been studied in great detail previously by the Harris group, and much of the TRIR work presented in this Chapter will begin by repeating the work of Harris and co-workers. Repeating the work of Harris and co-workers has allowed us to examine known chemistry under conditions which may be conducive to future TR-XAFS studies. Despite the wealth of previously published work, there is still much to examine in this field, and the advent of techniques such as TR^{M}PS allow for kinetics observations to be made across the picosecond, nanosecond and microsecond timescale in a single experiment. The work presented in this Chapter represents a major step towards our ultimate aim of characterising organometallic noble gas and alkane complexes in room temperature solution using TR-XAFS.

4.2.1 TR^{M}PS Studies of $CpMn(CO)_3$ in Neat Triethylsilane

The photolysis of $CpMn(CO)_3$ in neat triethylsilane has been previously studied in detail by Harris and co-workers, utilising 295 and 325 nm photolysis.[150,186,187] All studies presented within this Chapter are undertaken using 266 nm photolysis, which is selected due to its wide availability.

Figure 4.1 shows a series of TR^{M}PS difference spectra recorded following 266 nm photolysis of $CpMn(CO)_3$ in pure $HSiEt_3$ under an Ar atmosphere at 298 K. Immediately following photolysis the two parent ν(CO) bands of $CpMn(CO)_3$ (2027 and 1945 cm^{-1}) were observed to bleach, along with formation of four vibrationally hot ν(CO) features. These features were observed to narrow and blue-shift over the first 30 ps following photolysis, to yield four distinct ν(CO) bands, the lowest energy of which appears very broad (2001, 1959, 1892 and 1840 cm^{-1}). Yang *et al.* assign two initially formed ν(CO) bands following photolysis of $CpMn(CO)_3$ in $HSiEt_3$ as the triplet unsaturated dicarbonyl $^3CpMn(CO)_2$. However, the ν(CO) bands of the species assigned by Yang (*ca.* 2000 and 1883 cm^{-1}) do not match those observed here. Recent matrix isolations studies have indicated that the ν(CO) band reported at *ca.* 1883 cm^{-1} by Yang *et al.* may not be due to the triplet species $^3CpMn(CO)_2$,[53] and that a further ν(CO) at lower energy is expected, which was not observed by Yang due to experimental constraints on the spectroscopic window. The observation of two ν(CO) bands at 2001 and 1840 cm^{-1}, assigned to $^3CpMn(CO)_2$, is in agreement with previous matrix isolation studies, as well as work presented in Chapter 1 of this Thesis.

In addition to the presence of $^3CpMn(CO)_2$, the TR^{M}PS difference spectra

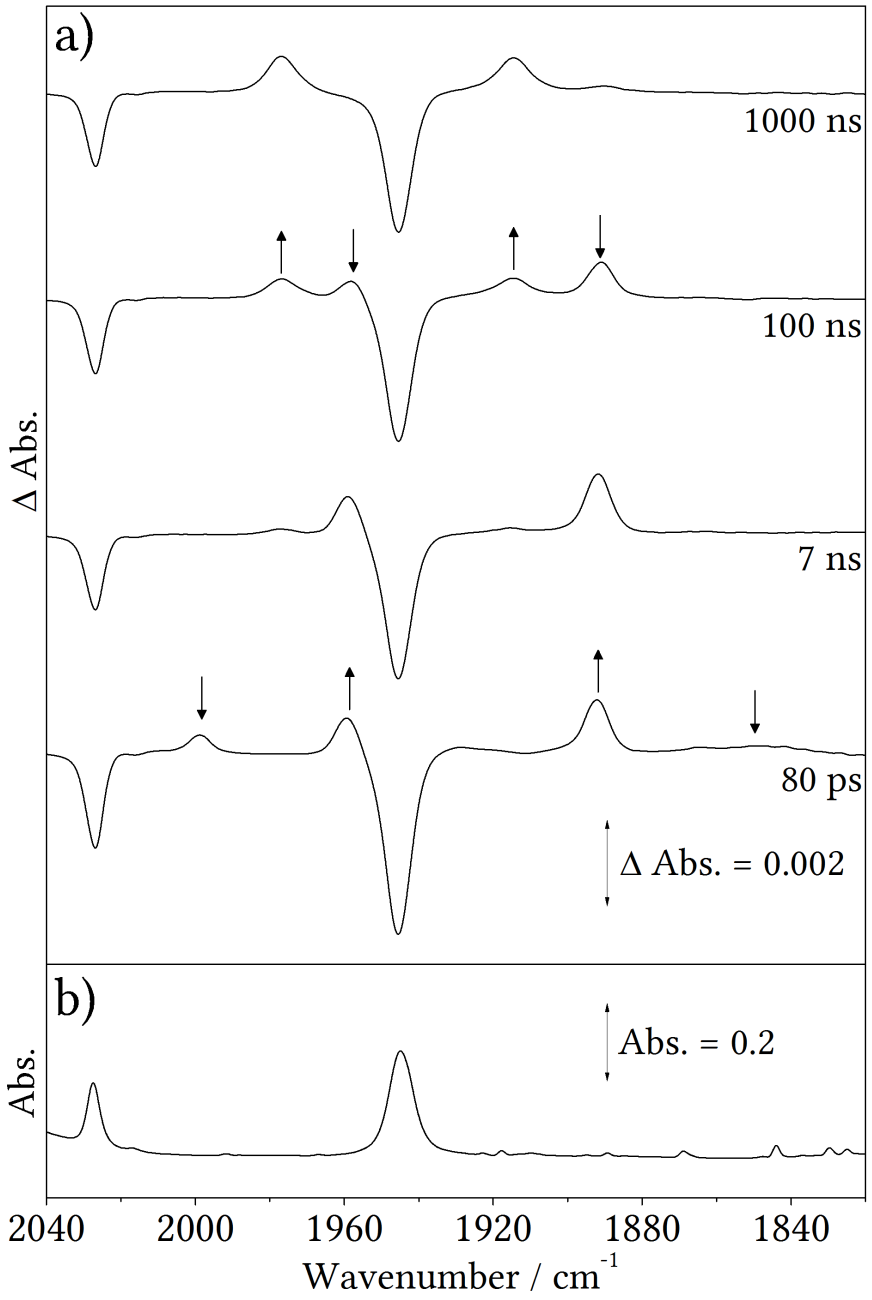


FIGURE 4.1: Selected ps and ns $TR^{M}PS$ difference spectra recorded at a series of time delays following 266 nm photolysis of a solution of $CpMn(CO)_3$ in $HSiEt_3$ under an Ar atmosphere. Initial formation of $^3CpMn(CO)_2$, followed by direct partial Si-H activation from $^3CpMn(CO)_2$ to form $CpMn(CO)_2(H\text{--}SiEt_3)$, and indirect partial Si-H activation through formation of the silane σ-complex $CpMn(CO)_2(HSiEt_3)$ can be seen.

recorded on the picosecond timescale following photolysis shows two ν(CO) bands at 1959 and 1892 cm^{-1}. These two bands correspond to formation of a solvated singlet complex of the form $^{1}CpMn(CO)_2X$, in agreement with previous studies.[53,150,173,186,187] The ν(CO) band positions of this species agree with those reported by Yang *et al.*, who assign this species as a triethylsilane σ-complex, bound through an ethyl moiety $CpMn(CO)_2(EtSiHEt_2)$.[150,186,187]

Two additional ν(CO) bands are observed in the spectra recorded 7, 100 and 1000 ns following photolysis. These ν(CO) bands (1977 and 1914 cm^{-1}) appear at higher energy relative to those of the silane σ-complex, suggestive of a decrease in electron density present on the metal centre. Two similar ν(CO) bands (1979 and *ca.* 1915 cm^{-1}) were assigned by Yang *et al.* as the Si-H partial activation product $CpMn(CO)_2(H\text{---}SiEt_3)$.

Examination of the growth and decay of the three species involved in this reaction reveals two different pathways for formation of the final partially activated species $CpMn(CO)_2(H\text{---}SiEt_3)$. Figure 4.2 shows kinetic traces from $TR^{M}PS$ difference spectra recorded on the picosecond timescale following 266 nm photolysis of $CpMn(CO)_3$ in $HSiEt_3$. The decay of the triplet dicarbonyl species $^{3}CpMn(CO)_2$ (τ = 100 ($\pm$10) ps) is accompanied by the growth of both $CpMn(CO)_2(EtSiHEt_2)$ (τ = 85 ($\pm$10) ps) and the initial growth of the partially Si-H activated product $CpMn(CO)_2(H\text{---}SiEt_3)$ (τ = 90 ($\pm$15) ps). The good agreement between the experimental lifetimes of these three processes is indicative of direct formation of both the silane solvent complex and the Si-H partially activated species from the unsaturated 16-electron triplet species. These

results show good agreement with Yang *et al.*, who also observed a correlation between the decay of $^{3}CpMn(CO)_2$ and the growth of the partially activated species.

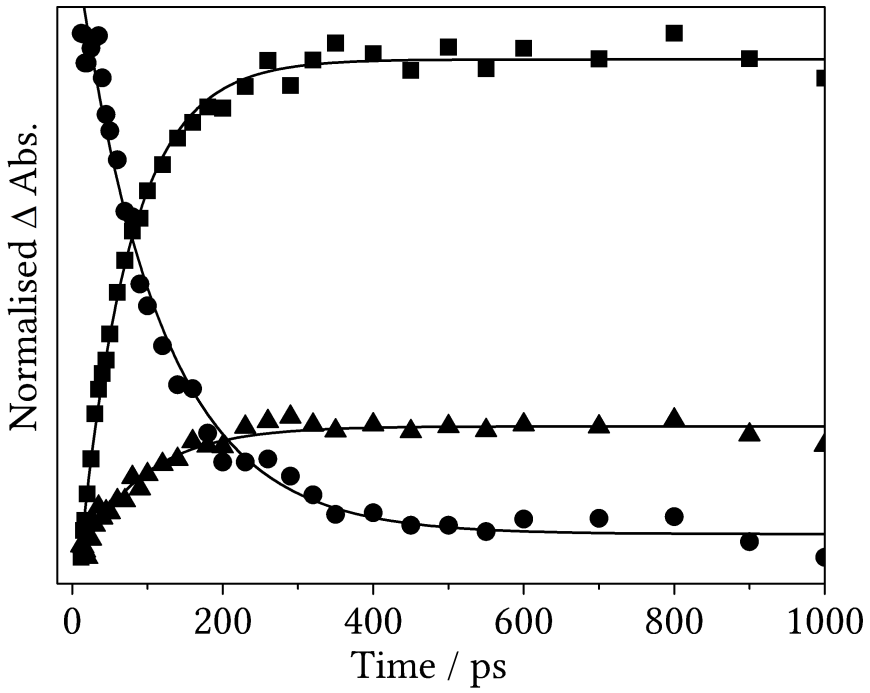


FIGURE 4.2: Single-point kinetic traces from TR^{M}PS difference spectra recorded on the picosecond timescale following 266 nm photolysis of $CpMn(CO)_3$ in $HSiEt_3$ under Ar, showing decay of $^{3}CpMn(CO)_2$ (2001 cm^{-1}, circles), formation of $CpMn(CO)_2(EtSiHEt_2)$ (1959 cm^{-1}, squares) and initial direct formation of $CpMn(CO)_2(H{-}SiEt_3)$ (1977 cm^{-1}, triangles). Solid lines are mono-exponential fits.

Examination of the nanosecond kinetics from TR^{M}PS difference spectra shows the second pathway through which $CpMn(CO)_2(H{-}SiEt_3)$ is formed. Figure 4.3 shows kinetic traces from difference spectra recorded on the nanosecond timescale, showing the decay of the silane solvent complex (τ = 155 ($\pm$15) ns) and further formation of $CpMn(CO)_2(H{-}SiEt_3)$ (τ = 145 ($\pm$10) ns). The matching rates of formation and decay of these two species is indicative of direct formation of $CpMn(CO)_2(H{-}SiEt_3)$ from the ethyl-bound silane σ-complex. Again, this observation is in agreement with the work of Yang *et al.*, who proposed a reaction mechanism based on their photolysis studies,

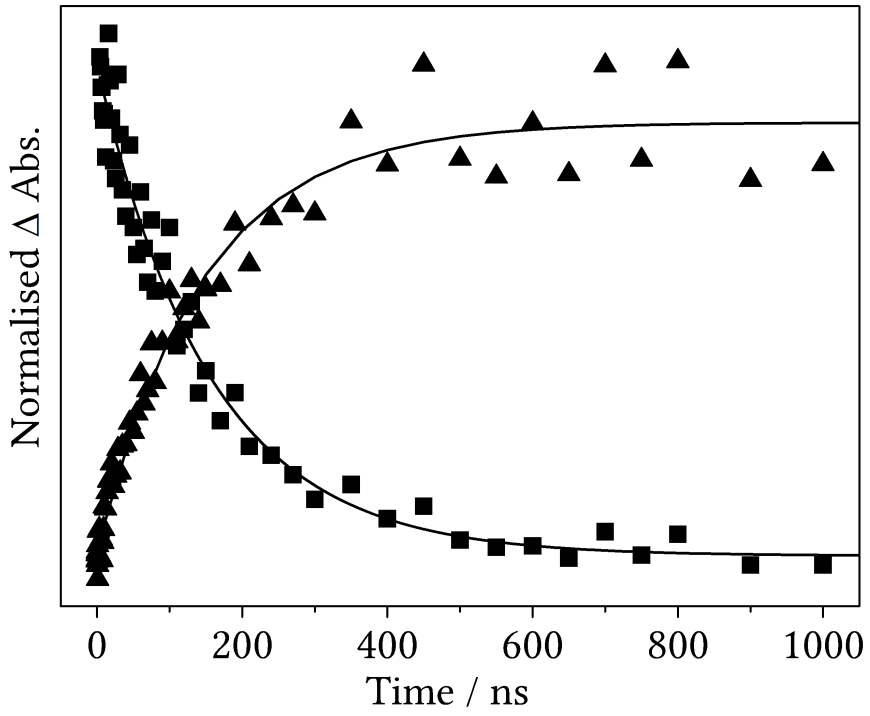


FIGURE 4.3: Single-point kinetic traces from $TR^{M}PS$ difference spectra recorded on the nanosecond timescale following 266 nm photolysis of $CpMn(CO)_3$ in $HSiEt_3$ under Ar, showing decay of $CpMn(CO)_2(EtSiHEt_2)$ (1959 cm^{-1}, squares) and further formation of $CpMn(CO)_2(H{-}SiEt_3)$ (1977 cm^{-1}, triangles), which is the final photoproduct. Solid lines are mono-exponential fits.

shown in Scheme 4.2.[150] The ratio of the two initially formed species, $^3CpMn(CO)_2$ and $CpMn(CO)_2(EtSiHEt_2)$ was observed to be *ca.* 1:1 (assuming the same extinction coefficient), in agreement with observations following short-wavelength photolysis experiments by Yang *et al.*, while the ratio of $CpMn(CO)_2(H{-}SiEt_3)$ formed directly from the triplet to $CpMn(CO)_2(H{-}SiEt_3)$ formed through the singlet solvent complex is *ca.* 4:1, again in good agreement with previously published work.

Changing the excitation wavelength from 295 to 266 nm appears to results in very little change in the observed chemistry following photolysis. 295 nm resides in a well between two electronic absorption bands of $CpMn(CO)_3$, leading Yang *et al.* to conclude that two different reaction mechanisms can be accessed dependent upon the

excitation wavelength selected. 266 nm resides on the shoulder of the higher energy of these two absorption bands. Excitation at 266 nm should therefore, according to the reported hypothesis, result in increased initial formation the solvated singlet compared to the unsaturated triplet species. No significant different in the triplet:singlet ratio is observed following 266 nm photolysis in this study, compared to previous studies using longer excitation wavelengths. However, the observed ratio of these two species is difficult to determine accurately at shorter excitation wavelengths due to increased formation of vibrationally hot species on the fast picosecond timescale.

TABLE 4.1: ν(CO) absorption band frequencies of $CpMn(CO)_3$, $CpRe(CO)_3$, $Cp^*Re(CO)_3$, intermediates and photoproducts formed following photolysis in pure triethylsilane. All experiments performed in solution phase at 298 K.

Compound	**ν(CO) (cm^{-1})**	**Reference**
$\mathbf{CpMn(CO)_3}$	2027, 1945	This work
	2029, 1946	150
$\mathbf{^3CpMn(CO)_2}$	2001, 1840	This work
	2000, 1883	150
$\mathbf{CpMn(CO)_2(EtSiHEt_2)}$	1959, 1892	This work
	1960, 1892	150
$\mathbf{CpMn(CO)_2(H{-}SiEt_3)}$	1977, 1914	This work
	1979, 1915	150
$\mathbf{CpRe(CO)_3}$	2029, 1939	This work
	2030, 1939	150
$\mathbf{CpRe(CO)_2(EtSiHEt_2)}$	1949, 1885	This work
	1948, 1887	150
$\mathbf{CpRe(CO)_2(SiEt_3)H}$	1989, 1918	This work
	1990, 1918	150
$\mathbf{Cp^*Re(CO)_3}$	2009, 1945	This work
$\mathbf{Cp^*Re(CO)_2(EtSiHEt_2)}$	1925, 1863	This work
$\mathbf{Cp^*Re(CO)_2(SiEt_3)H}$	1966, 1897	This work

TABLE 4.2: Observed rate constants (k_{obs}) for growth and decay processes of triplet intermediates, solvent complexes and Si-H activation or partial activation products observed following photolysis of $CpMn(CO)_3$, $CpRe(CO)_3$ and $Cp^*Re(CO)_3$ in pure $HSiEt_3$. All data recorded at 298 K. a = Formation from a triplet intermediate. b = Formation from a silane complex intermediate.

	k_{obs} (s^{-1})		
Compound	**Growth[a]**	**Growth[b]**	**Decay**
^{3}**CpMn(CO)$_2$**			1.0 (±0.1) x 10^{10}
CpMn(CO)$_2$(EtSiHEt$_2$)	1.2 (±0.1) x 10^{10}		6.5 (±0.6) x 10^6
CpMn(CO)$_2$(H···SiEt$_3$)	1.1 (±0.1) x 10^{10}	6.9 (±0.5) x 10^6	
CpRe(CO)$_2$(EtSiHEt$_2$)			1.3 (±0.1) x 10^5
CpRe(CO)$_2$(SiEt$_3$)H		1.4 (±0.1) x 10^5	
Cp*Re(CO)$_2$(EtSiHEt$_2$)			4.2 (±0.3) x 10^5
Cp*Re(CO)$_2$(SiEt$_3$)H		4.2 (±0.3) x 10^5	

4.2.2 TR^{M}PS Studies of CpRe(CO)$_3$ and Cp*Re(CO)$_3$ in Neat Triethylsilane

Further to the studies presented above, TR^{M}PS difference spectra were also recorded following photolysis of $CpRe(CO)_3$ in neat $HSiEt_3$. As above, this experiment has been previously reported by the Harris group,[150,187] however once again these experiments were performed using 295 nm as a photolysis wavelength to induce carbonyl loss. In this study, 266 nm irradiation was utilised.

Figure 4.4 shows a series of selected TR^{M}PS difference spectra recorded following 266 nm photolysis of $CpRe(CO)_3$ in $HSiEt_3$. Following photolysis, the two parent ν(CO) absorptions (2029 and 1939 cm^{-1}) bands were observed to bleach within 1 ps, followed by formation of three broad ν(CO) features which have been previously assigned as absorption due to the vibrationally excited electronic ground state of the parent $CpRe(CO)_3$ observed in Chapter 3 of this Thesis, as well as in previously published

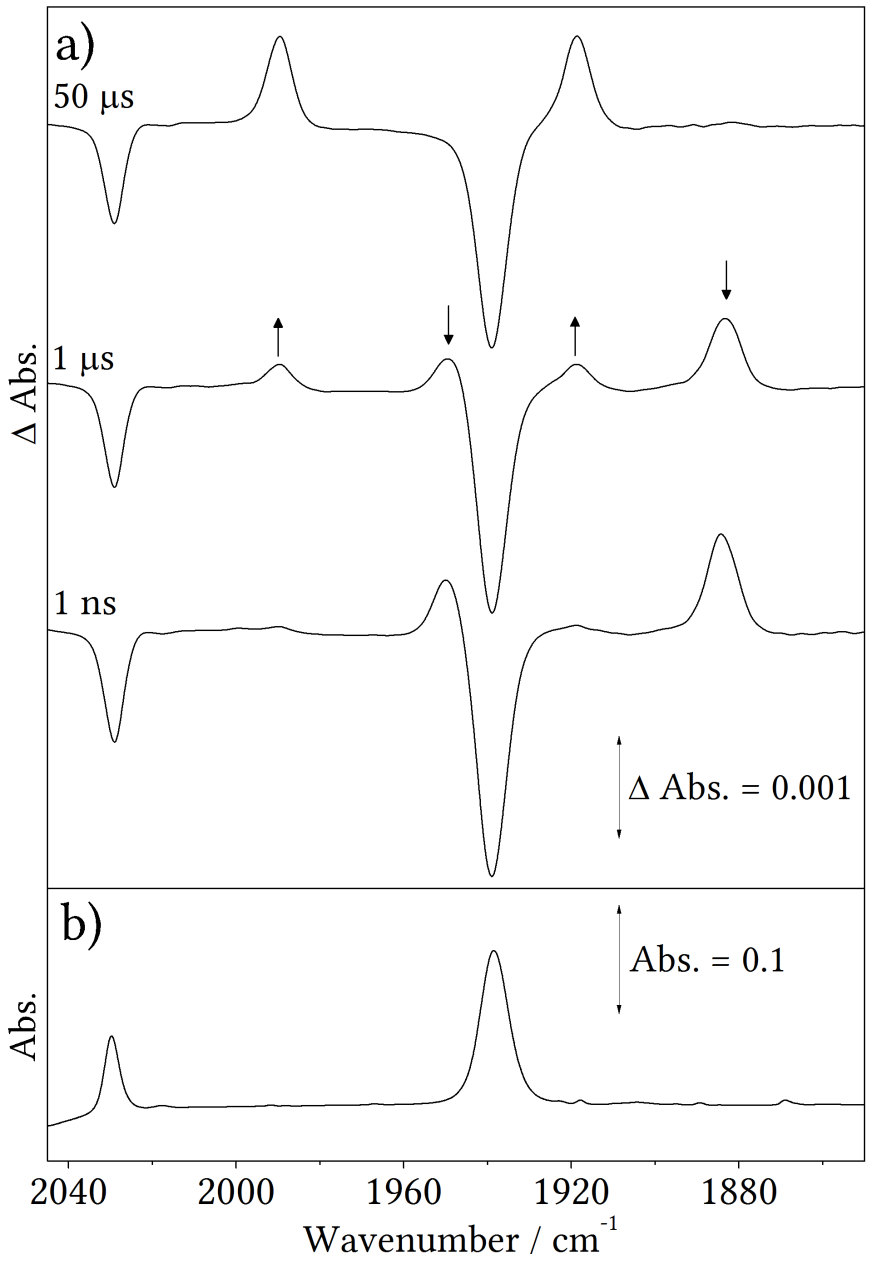


FIGURE 4.4: Selected ns TR^{M}PS difference spectra recorded at a series of time delays following 266 nm photolysis of a solution of $CpRe(CO)_3$ in $HSiEt_3$ under an Ar atmosphere. Initial formation of $CpRe(CO)_2(EtSiHEt_2)$, followed by direct Si-H activation to form $CpRe(CO)_2(SiEt_3)H$ can be seen.

work.[150,290] Following decay of this vibrationally excited state on the picosecond timescale, four new ν(CO) bands were observed at 1989, 1949, 1918 and 1885 cm^{-1}. Two of these ν(CO) bands (1949 and 1885 cm^{-1}) are consistent with formation of

a dicarbonyl intermediate of the form $CpRe(CO)_2X$, assigned by Yang *et al.* as the ethyl-bound silane σ-complex $CpRe(CO)_2(EtSiHEt_2)$. The two remaining ν(CO) bands observed at 1989 and 1918 $cm^{-1}$are shifted to higher wavenumber compared to those of the silane σ-complex, indicative of an Si-H activation product. These two ν(CO) bands are therefore assigned to $CpRe(CO)_2(SiEt_3)H$, in accordance with previous studies.[150,187] Appearance of a small amount of the Si-H activation product on the picosecond timescale is indicative of fast formation small concentration of the Si-H bound σ-complex $CpRe(CO)_2(H{-}SiEt_3)$, which then undergoes fast activation.

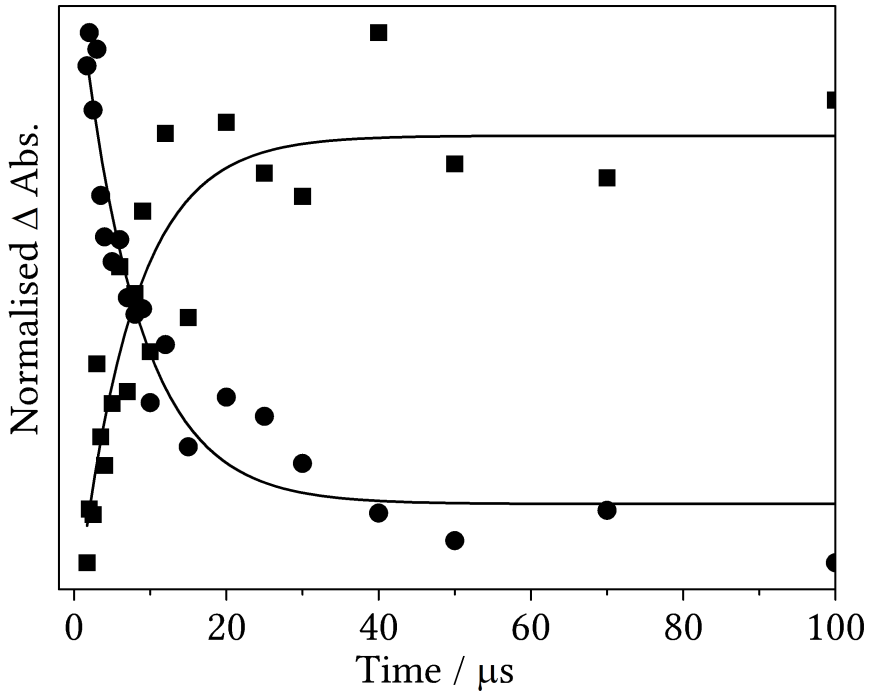


FIGURE 4.5: Single-point kinetic traces from TR^MPS difference spectra recorded on the nanosecond timescale following 266 nm photolysis of $CpRe(CO)_3$ in $HSiEt_3$ under Ar, showing decay of $CpRe(CO)_2(EtSiHEt_2)$ (1949 cm^{-1}, circles) and formation of $CpRe(CO)_2(SiEt_3)H$ (1989 cm^{-1}, squares). Solid lines are mono-exponential fits.

The two ν(CO) bands corresponding to the $CpRe(CO)_2(EtSiHEt_2)$ were observed to decay on the same timescale as additional formation of $CpRe(CO)_2(SiEt_3)H$. Kinetic

traces from TR^{M}PS difference spectra showing this process are shown in Figure 4.5. The rates of decay of $CpRe(CO)_2(EtSiHEt_2)$ (τ = 7.6 ($\pm$0.8) μs) and growth of $CpRe(CO)_2(SiEt_3)H$ (τ = 7.3 ($\pm$1.2) μs) were observed to match, indicating direct Si-H activation from the ethyl-bound complex via the same rearrangement-activation mechanism observed for $CpMn(CO)_3$. This observation is in agreement with previously reported photolysis experiments.[150]

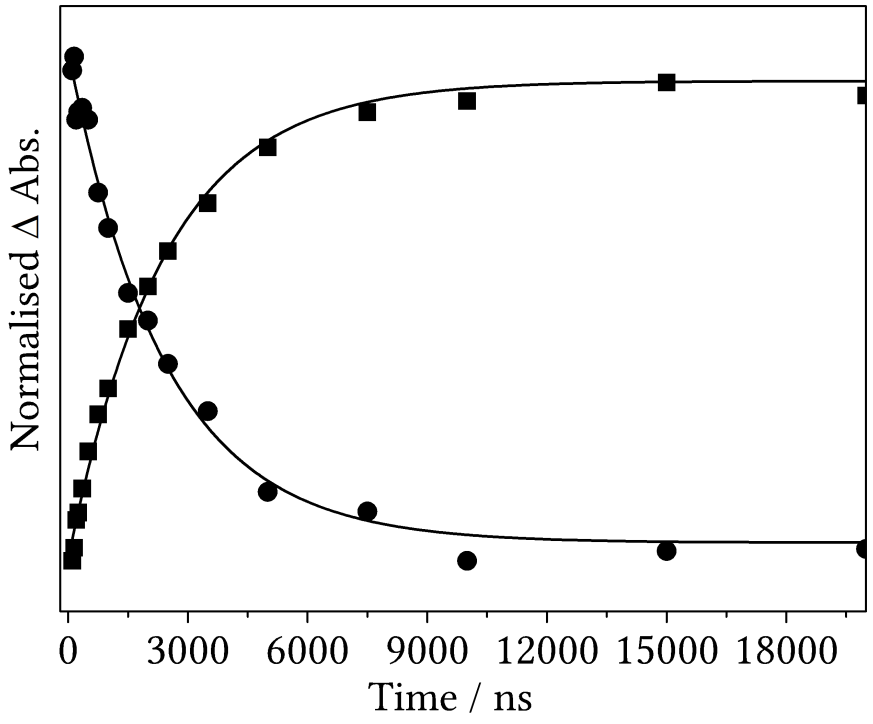


FIGURE 4.6: Single-point kinetic traces from TR^{M}PS difference spectra recorded on the nanosecond and microsecond timescale following 266 nm photolysis of $Cp^*Re(CO)_3$ in $HSiEt_3$ under Ar, showing decay of $Cp^*Re(CO)_2(EtSiHEt_2)$ (1925 cm^{-1}, circles) and formation of $Cp^*Re(CO)_2(SiEt_3)H$ (1966 cm^{-1}, squares). Solid lines are mono-exponential fits.

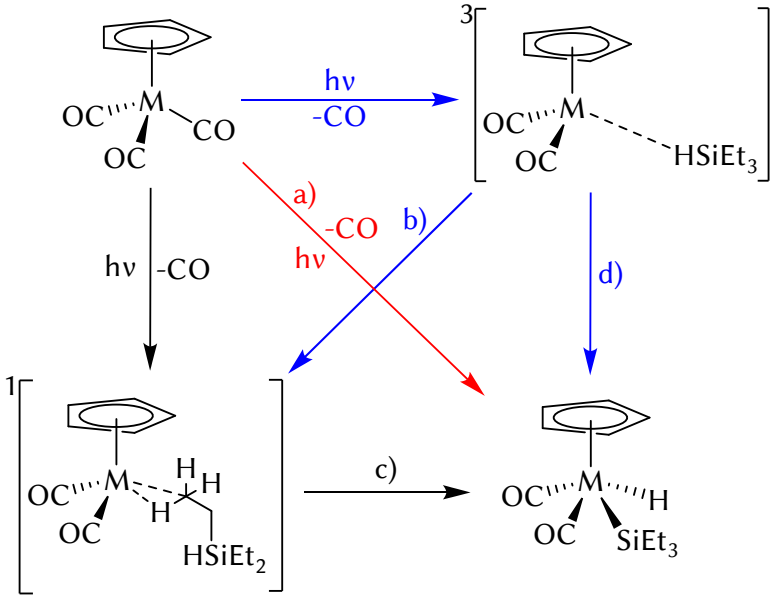
The photochemistry of $Cp^*Re(CO)_3$ in $HSiEt_3$ following 266 nm irradiation was also examined as part of this study. As above for $CpRe(CO)_3$, photolysis resulted in bleaching of the parent ν(CO) bands (2009 and 1945 cm^{-1}) and formation of vibrationally hot ground state ν(CO) bands, which decay on the picosecond timescale to yield

four ν(CO) bands assigned to $Cp^*Re(CO)_2(EtSiHEt_2)$ (1925 and 1863 cm^{-1}) and $CpRe(CO)_2(SiEt_3)H$ (1966 and 1897 cm^{-1}). Decay of the silane σ-complex (τ = 2.4 ($\pm$0.2) μs) is accompanied by growth of the Si-H activation product (τ = 2.4 ($\pm$0.3) μs), as observed above. Kinetic traces from TR^MPS spectra showing this process are shown in Figure 4.6. The rate of this process is observed to be faster than for the unsubstituted $CpRe(CO)_3$. It is possible that this increased rate of activation is a result of the increased electron density on the metal centre due to the addition of electron donating methyl groups to the Cp-ring.

The reaction mechanism observed following photolysis of $CpRe(CO)_3$ and $Cp^*Re(CO)_3$ is less complex that that observed for $CpMn(CO)_3$ due to the absence of formation of a 16-electron intermediate. However, there are still two possible routes to the final photoproduct, the Si-H activated species. Scheme 4.4 shows the observed reaction mechanism following 266 nm photolysis of $CpMn(CO)_3$, $CpRe(CO)_3$ and $Cp^*Re(CO)_3$, in agreement with the work of Harris and co-workers.[150,187]

4.2.3 TR^MPS Studies of $CpMn(CO)_3$ and $CpRe(CO)_3$ in Triethylsilane-Doped Perfluoro(methylcyclohexane)

Any future TR-XAFS studies on the room temperature formation of organometallic noble gas, methane or ethane complexes will necessitate the use or perfluorinated solvents, in order to ensure formation of the desired coordination complex, in accordance with the methodology outlined in Chapters 2 and 3 of this Thesis. In this Thesis, as well as in previously reported studies,[77–79] perfluoro(methylcyclohexane) (PFMCH)



SCHEME 4.4: Reaction mechanism observed following 266 nm photolysis of $CpMn(CO)_3$, $CpRe(CO)_3$ and $Cp^*Re(CO)_3$. Reaction pathways concerning only by $CpMn(CO)_3$ are shown in blue, while reaction pathways concerning only $CpRe(CO)_3$ and $Cp^*Re(CO)_3$ are shown in red. a) Direct formation of Si-H activated or partially activated species through Si-H bound σ-complex. b) Spin-crossover to form ethyl-bound σ-complex. c) Rearrangement-activation of the ethyl-bound σ-complex. d) Direct Si-H activation from the triplet species. The structure of the final activated or partially activated species is shown with a formally broken Si-H bond for simplicity.

has been shown to be an incredibly useful solvent environment for the formation of weakly coordinated organometallic complexes. It is to this end that the photolysis of $CpMn(CO)_3$ and $CpRe(CO)_3$ will be reexamined in PFMCH doped with triethylsilane, to determine if the activation chemistry described above is still accessible.

Figure 4.7 shows a series of TR^{M}PS difference spectra recorded on the nanosecond timescale following 266 nm photolysis of $CpMn(CO)_3$ in PFMCH doped with 0.5 M $HSiEt_3$ under an Ar atmosphere. Immediately following photolysis, the two parent bands of $CpMn(CO)_3$ (2033 and 1953 cm^{-1}) were observed to bleach. Following vibrational cooling processes on the picosecond timescale, four new ν(CO) bands were observed to form within 1 ns following photolysis at 2007, 1966, 1897 and 1849 cm^{-1}. Two

of these bands (2007 and 1847 cm^{-1}) are assigned to the 16-electron triplet species $^3CpMn(CO)_2$, in accordance with previous work reported in this Chapter, as well as Chapter 2 of this Thesis and previously published studies.[53] The other two ν(CO) bands (1966 and 1897 cm^{-1}) are indicative of formation of a singlet dicarbonyl solvent complex of the form $^1CpMn(CO)_2X$. The spectrum recorded 8 ns following photolysis shows two additional ν(CO) bands at 1985 and 1919 cm^{-1}, appearing to lower energy compared to the ν(CO) bands of the singlet dicarbonyl species, indicating formation of an Si-H partial activation product. These ν(CO) bands are therefore assigned as the silyl hydride $CpMn(CO)_2(H\text{---}SiEt_3)$.

Similarly to studies presented above in neat triethylsilane, $CpMn(CO)_2(H\text{---}SiEt_3)$ appears to form through two different pathways. The decay of the 16-electron triplet species $^3CpMn(CO)_2$ (τ = 4.3 ($\pm$0.2) ns) is accompanied by both initial growth of the partially activated species (τ = 4.7 ($\pm$0.5) ns), as well as growth of the singlet dicarbonyl complex (τ = 4.2 ($\pm$0.4) ns). The growth of this dicarbonyl species from the unsaturated species is observed to be faster than the growth of $^1CpMn(CO)_2(C_7F_{14})$ from $^3CpMn(CO)_2$ as observed in Chapter 2 of this Thesis (τ = 18 ($\pm$2) ns). This dicarbonyl species is therefore assigned as the ethyl-bound silane σ-complex $CpMn(CO)_2(EtSiHEt_2)$. The growth of this silane complex is slower than that observed in pure $HSiEt_3$, however this can be attributed to the decreased concentration of $HSiEt_3$ in this solvent system.

Figure 4.8 shows kinetic traces from TR^MPS spectra recorded following 266 nm photolysis. In addition to initial formation of the partially Si-H activated species

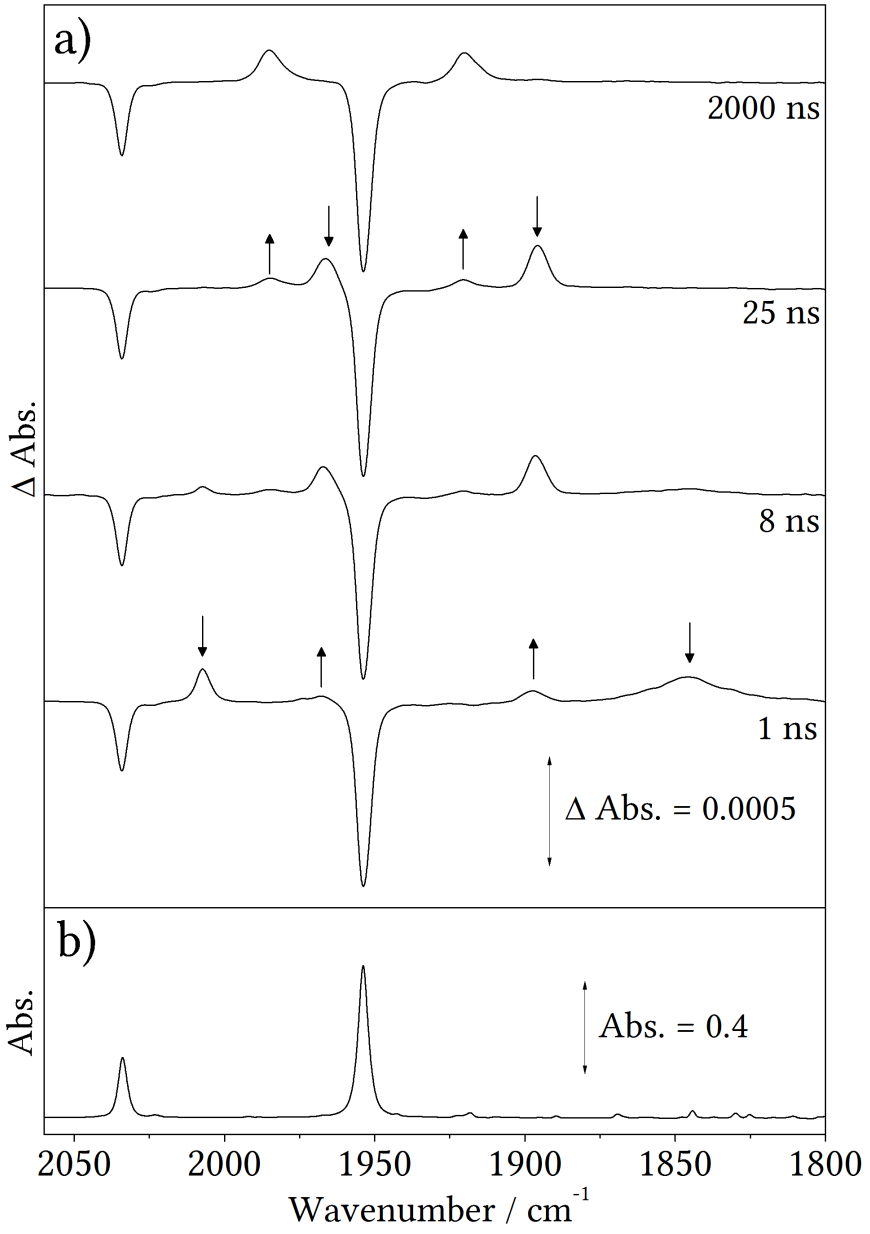


FIGURE 4.7: Selected ns TR^{M}PS difference spectra recorded at a series of time delays following 266 nm photolysis of a solution of $CpMn(CO)_3$ PFMCH with 0.5 M $HSiEt_3$ under an Ar atmosphere. Decay of $^3CpMn(CO)_2$, accompanied by direct Si-H activation to form $CpMn(CO)_2(H{-}SiEt_3)$ and formation of $CpMn(CO)_2(EtSiHEt_2)$, followed by additional formation of $CpMn(CO)_2(H{-}SiEt_3)$ can be seen.

from $^3CpMn(CO)_2$, further formation is observed on the nanosecond timescale through decay of $CpMn(CO)_2(EtSiHEt_2)$. The rate of decay of $CpMn(CO)_2(EtSiHEt_2)$ (τ = 135 ($\pm$15) ns) and further growth of $CpMn(CO)_2(H{-}SiEt_3)$ (τ = 155 ($\pm$20) ns) were

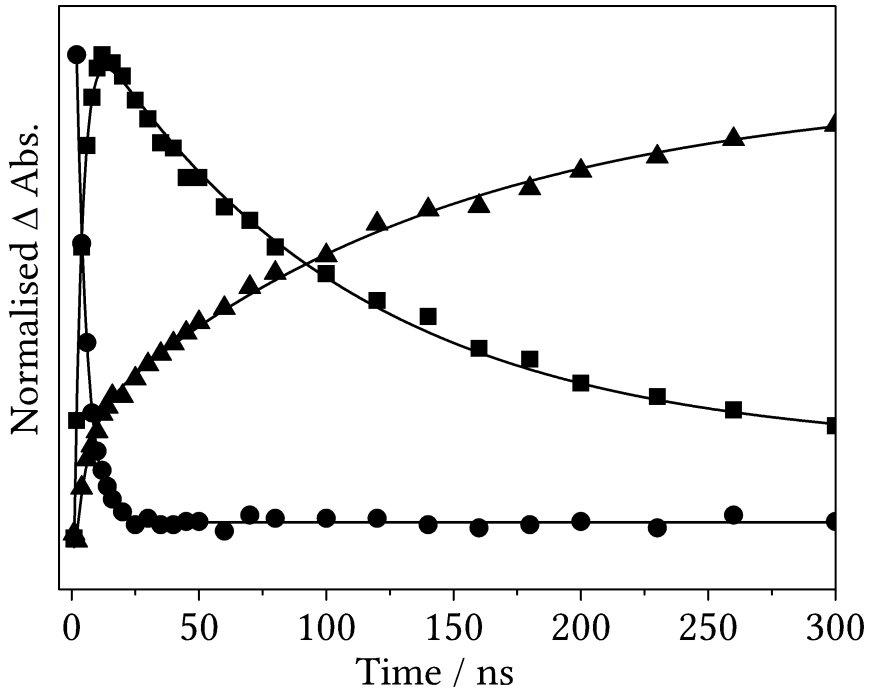


FIGURE 4.8: Single-point kinetic traces from $TR^{M}PS$ difference spectra recorded on the nanosecond timescale following 266 nm photolysis of $CpMn(CO)_3$ in $HSiEt_3$ doped PFMCH under Ar, showing decay of $^3CpMn(CO)_2$ (circles), formation and subsequent decay of $CpMn(CO)_2(EtSiHEt_2)$ (squares) and formation of $CpMn(CO)_2(H\text{---}SiEt_3)$ (triangles). Solid lines are mono-exponential or bi-exponential fits.

observed to be within error of each other, and are also in agreement with lifetime values reported above in pure $HSiEt_3$ as well as previously published values.[150,187] From this study it can be concluded that Mn-mediated silane activation chemistry is still accessible upon doping of $HSiEt_3$ into PFMCH.

TABLE 4.3: Observed rate constants (k_{obs}) for growth and decay processes of triplet intermediates, solvent complexes and Si-H activation or partial activation products observed following photolysis of $CpMn(CO)_3$, $CpRe(CO)_3$ in PFMCH doped with $HSiEt_3$ (0.5 M) under Ar. All data recorded at 298 K.

	k_{obs} (s^{-1})	
Compound	**Growth**	**Decay**
^{3}**CpMn(CO)$_2$**		2.3 (±0.1) x 10^8
CpMn(CO)$_2$(EtSiHEt$_2$)	2.4 (±0.2) x 10^8	7.3 (±0.7) x 10^6
CpMn(CO)$_2$(H···SiEt$_3$)	2.1 (±0.2) x 10^8	
	6.5 (±0.7) x 10^6	
CpRe(CO)$_2$(EtSiHEt$_2$)		9.9 (±1.0) x 10^5
		6.7 (±0.6) x 10^4
CpRe(CO)$_2$(SiEt$_3$)H	9.6 (±1.0) x 10^5	
	7.4 (±0.6) x 10^4	

In neat $HSiEt_3$, the photochemistry of $CpRe(CO)_3$ was found to be relatively uncomplicated when compared to $CpMn(CO)_3$, due to lack of a coordinatively unsaturated intermediate. Upon photolysis of $CpRe(CO)_3$ in PFMCH doped with 0.5 M $HSiEt_3$, however, this chemistry becomes more complex. Figure 4.9 shows a series of TR^{M}PS difference spectra recorded on the nanosecond timescale following 266 nm photolysis of $CpRe(CO)_3$ in $HSiEt_3$ doped PFMCH. Immediately following photolysis, the two parent ν(CO) bands of $CpRe(CO)_3$ are bleached (2037 and 1948 cm^{-1}).

The spectrum recorded 1 ns following photolysis shows several ν(CO) features. A broad ν(CO) feature is observed at 1964 cm^{-1}, along with additional features at lower wavenumber (1895 and 1889 cm^{-1}). Over the first few nanosecond following photolysis, the higher energy broad feature is observed to blue-shift and sharpen, while the small feature at 1889 cm^{-1}decays completely, concurrently with additional formation of the ν(CO) band at 1895 cm^{-1}. This scenario is reminiscent of the interchange between two different dicarbonyl transients of the form $CpRe(CO)_2X$ observed in neat

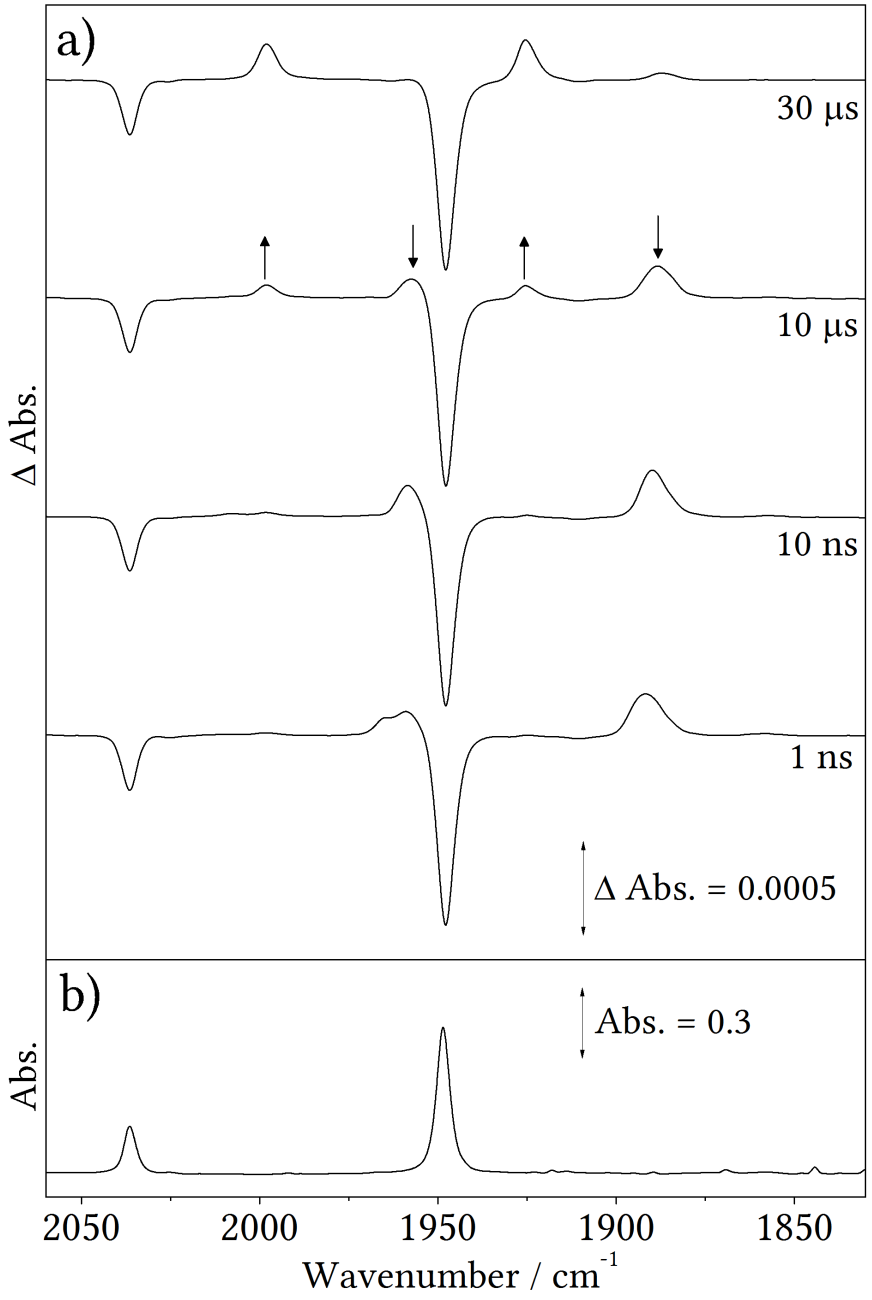


FIGURE 4.9: Selected ns TR^{M}PS difference spectra recorded at a series of time delays following 266 nm photolysis of a solution of $CpRe(CO)_3$ in PFMCH doped with $HSiEt_3$ (0.5 M) under an Ar atmosphere. Decay of $CpRe(CO)_2X$, accompanied by Si-H activation to form $CpRe(CO)_2(SiEt_3)H$ can be seen.

perfluoroalkane solvents, reported in Chapter 3 of this Thesis. In those studies, the initial dicarbonyl intermediate was tentatively assigned as the singlet unsaturated

intermediate $CpRe(CO)_2$ by examination of both experimental and calculated ν(CO) band frequencies. It is concluded that the dicarbonyl intermediate initially observed in this case is likely to be the same as that observed in neat PFMCH, reported in Chapter 3.

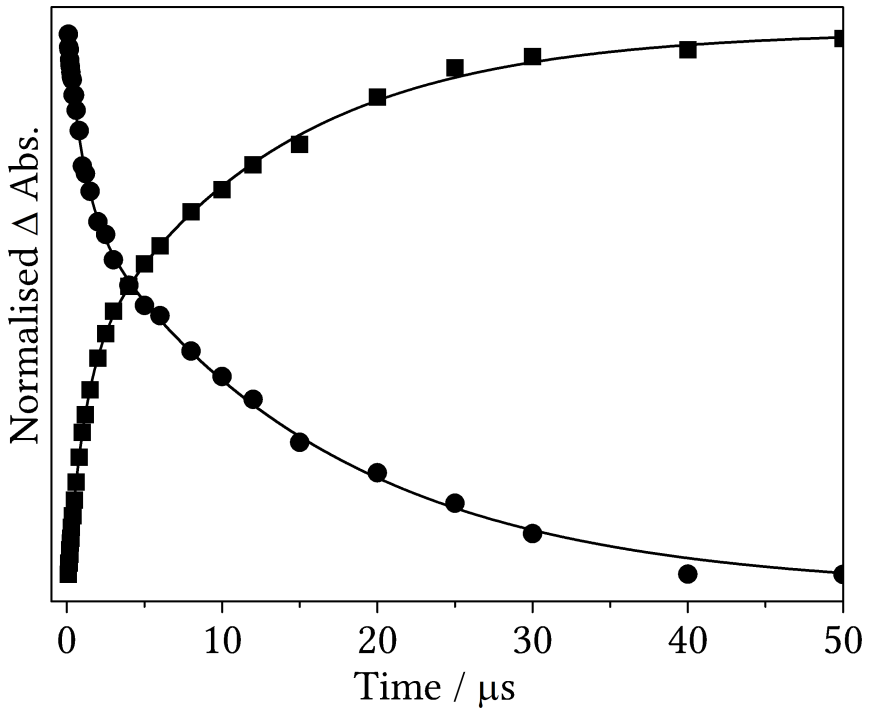
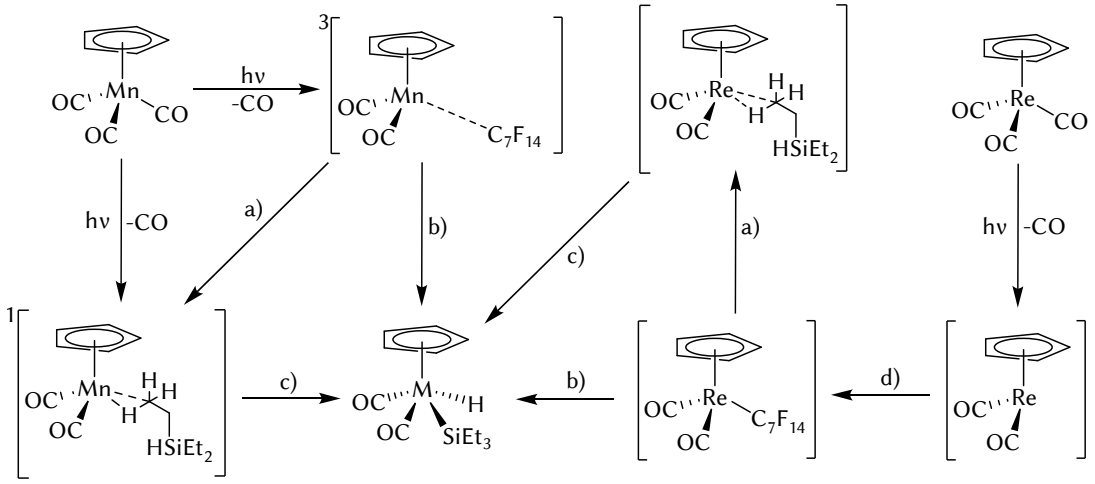


FIGURE 4.10: Single-point kinetic traces from TR^MPS difference spectra recorded on the nanosecond timescale following 266 nm photolysis of $CpRe(CO)_3$ in PFMCH doped with $HSiEt_3$ (0.5 M) under Ar, showing decay of $CpRe(CO)_2(EtSiHEt_2)$ (circles), and formation of $CpRe(CO)_2(SiEt_3)H$ (squares). Solid lines are bi-exponential fits.

As in pure $HSiEt_3$ solvent, Si-H activation is observed to occur on the microsecond timescale. Figure 4.10 shows kinetic traces from TR^MPS spectra showing the decay of the second dicarbonyl intermediate and the growth of the silyl hydride product $CpRe(CO)_2(SiEt_3)H$, which exhibits ν(CO) bands at 1999 and 1926 cm^{-1}. Unlike studies in pure $HSiEt_3$ however, both the growth and decay processes appear to consist of two components. The two components of the growth of the silyl hydride species (τ

= 1.1 (±0.1) and 13.5 (±1.5) μs) were observed to match those of the decay of the dicarbonyl species (τ = 1.0 (±0.1) and 15 (±1.5) μs).



SCHEME 4.5: Proposed reaction mechanism observed following 266 nm photolysis of $CpMn(CO)_3$ and $CpRe(CO)_3$ in $HSiEt_3$-doped PFMCH. a) Formation of ethyl-bound silane σ-complex. b) Direct, fast Si-H activation or partial activation. c) Slow Si-H activation or partial activation through rearrangement-activation of the ethyl-bound σ-complex. d) Formation of a PFMCH solvent complex. The structure of the final activated or partially activated species is shown with a formally broken Si-H bond for simplicity.

The presence of $CpRe(CO)_2(SiEt_3)H$ in solution suggests the presence of $CpRe(CO)_2(EtSiHEt_2)$, while the slowed rate of activation when compared with studies in neat $HSiEt_3$ [150,187] suggests possible formation of $CpRe(CO)_2(C_7F_{14})$ as an intermediate. Indeed, the ν(CO) bands of the second dicarbonyl intermediate match those reported in Chapter 3 of this Thesis for $CpRe(CO)_2(C_7F_{14})$. It is proposed that following initial formation of $CpRe(CO)_2$, the PFMCH solvent binds to form $CpRe(CO)_2(C_7F_{14})$. The initial fast component of the growth of $CpRe(CO)_2(SiEt_3)H$ is proposed to be due to direct activation of the Si-H bond from the PFMCH solvent complex. It is also possible that this fast component contains some contribution from silane σ-complexes which are formed directly from the coordinatively unsaturated intermediate. The slower

component may be due to Si-H activation through the ethyl-bound silane σ-complex $CpRe(CO)_2(EtSiHEt_2)$, which also forms from the solvent complex $CpRe(CO)_2(C_7F_{14})$. The experiment was repeated using *n*-heptane as the solvent, in place of PFMCH. In this case the spectra showed only formation of a dicarbonyl *n*-heptane complex with no evidence of Si-H activation, indicating that the alkane solvent is much more strongly binding than the silane. While the results exhibited here may resemble those reported in Chapter 3 following photolysis of $CpRe(CO)_3$ in cyclopentane-doped PFMCH in which no PFMCH complex is observed, the slowed rate of Si-H activation upon moving from neat $HSiEt_3$ to $HSiEt_3$-doped PFMCH is suggestive of some interaction with the solvent. Scheme 4.5 shows the proposed reaction mechanisms observed following photolysis of $CpRe(CO)_3$ and $CpMn(CO)_3$ in $HSiEt_3$-doped PFMCH. As above, while PFMCH may alter the chemistry observed following photolysis of $CpRe(CO)_3$ in the presence of triethylsilane, Re-mediated Si-H activation is still observed, indicating that this may be a useful test system for future TR-XAFS experiments.

TABLE 4.4: ν(CO) absorption band frequencies of $CpMn(CO)_3$, $CpRe(CO)_3$ and intermediates and photoproducts formed following photolysis in $HSiEt_3$ doped PFMCH under Ar. All experiments performed in solution phase at 298 K.

Compound	ν**(CO) (cm^{-1})**
$\mathbf{CpMn(CO)_3}$	2033, 1953
$\mathbf{^3CpMn(CO)_2}$	2007, 1849
$\mathbf{CpMn(CO)_2(EtSiHEt_2)}$	1966, 1897
$\mathbf{CpMn(CO)_2(H\text{-}SiEt_3)}$	1985, 1919
$\mathbf{CpRe(CO)_3}$	2036, 1948
$\mathbf{CpRe(CO)_2}$	1964, 1895
$\mathbf{CpRe(CO)_2(EtSiHEt_2)}$	1958, 1889
$\mathbf{CpRe(CO)_2(SiEt_3)H}$	1999, 1926

4.2.4 TR^{M}PS Studies of $W(CO)_6$ in Neat Triethylsilane

The high stability of tungsten alkane and noble gas complexes reported previously[34] makes $W(CO)_6$ an exciting prospect for future TR-XAFS studies of these species. In addition to this, $W(CO)_6$ exhibits relatively high solubility in perfluoroalkane solvents, allowing access to higher sample solution concentrations which are not possible for compounds such as $CpMn(CO)_3$ and $CpRe(CO)_3$.

$W(CO)_6$ does not exhibit Si-H activation chemistry, however photolysis of $W(CO)_6$ in $HSiEt_3$ may still present an interesting model system for future studies of alkane σ-complexes, as well as noble gas complexes. The large expected change in the XAFS difference spectra upon activation due to the change in oxidation state at the metal centre will not be observed, however finer differences in the EXAFS region of the spectrum due to removal of a carbonyl ligand and addition of the silane solvent will still be evident. It is with this in mind that the work of Kotz *et al.*, who undertook an extensive TRIR study on the 295 nm photolysis of $M(CO)_6$ (M = Cr, Mo, W) in triethylsilane,[314] is repeated herein.

Figure 4.11 shows a series of TR^{M}PS spectra recorded following 266 nm photolysis of $W(CO)_6$ in $HSiEt_3$ under an Ar atmosphere. The spectrum recorded 1 ps following photolysis shows bleaching of the parent ν(CO) band at 1983 cm^{-1}, and formation of a broad ν(CO) feature to lower wavenumber. This broad feature sharpened over the following 30 ps to yield two distinct ν(CO) bands at 1954 and 1940 cm^{-1}. With reference to the work of Kotz *et al.* [314] these ν(CO) bands are assigned to the ethyl-bound silane σ-complex $W(CO)_5(EtSiHEt_2)$. This species is not stable, however, decaying to yield

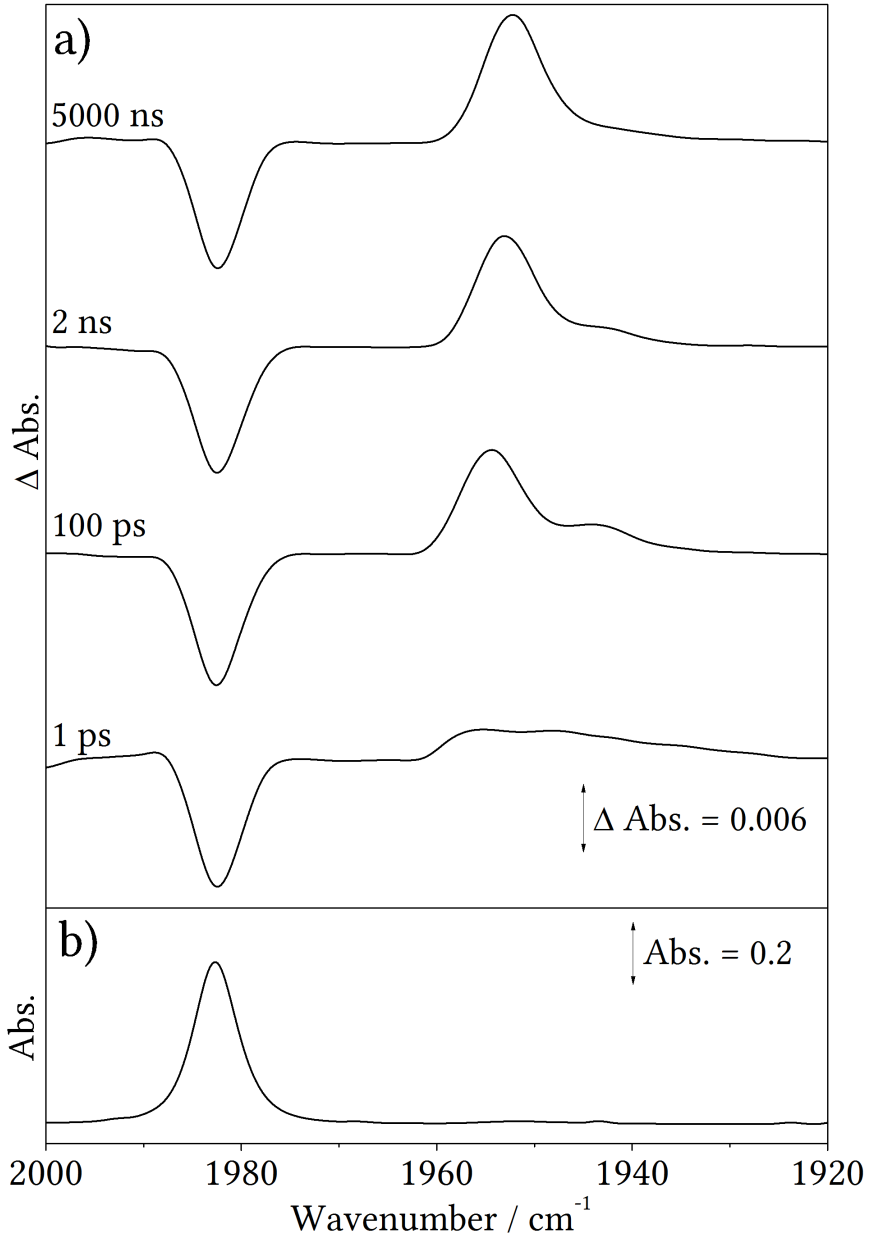


FIGURE 4.11: Selected ps and ns $TR^{M}PS$ difference spectra recorded at a series of time delays following 266 nm photolysis of a solution of $W(CO)_6$ in $HSiEt_3$ under an Ar atmosphere. Formation of the ethyl-bound $W(CO)_5(EtSiHEt_2)$, following by rearrangement of the $HSiEt_3$ ligand to form $W(CO)_5(H{-}SiEt_3)$ can be observed.

another pentacarbonyl species with a single resolvable ν(CO) feature at 1950 cm^{-1}. This shift to lower wavenumber is consistent with increased donation of electron density from ligand to metal, consistent with binding of an Si-H compares to a C-H moiety in an η^2

fashion. This species is assigned to the Si-H bound silane σ-complex $W(CO)_5(H{-}SiEt_3)$. An additional ν(CO) band is expected at lower wavenumber, however this feature is expected to be weak and is therefore not observed. This is in agreement with previous studies.[314]

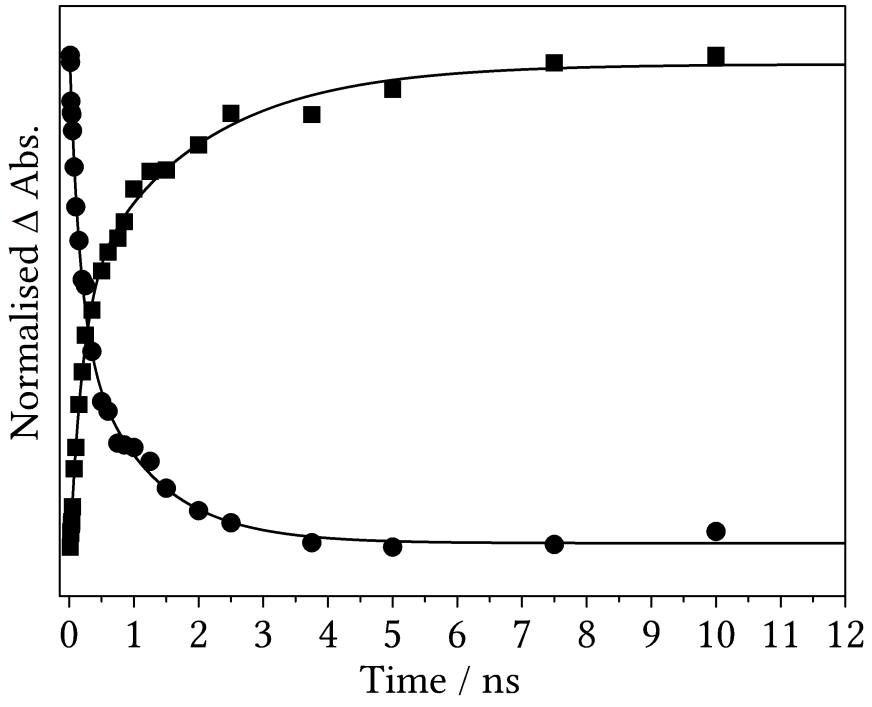


FIGURE 4.12: Single-point kinetic traces from picosecond and nanosecond TR^MPS difference spectra recorded following 266 nm photolysis of $W(CO)_6$ in $HSiEt_3$ under Ar, showing decay of $W(CO)_5(EtSiHEt_2)$ (circles) and formation of $W(CO)_5(H{-}SiEt_3)$ (squares). Solid lines are bi-exponential fits.

The rates of growth of $W(CO)_5(H{-}SiEt_3)$ and the decay of $W(CO)_5(EtSiHEt_2)$ were observed to match, indicating direct formation of the former from the latter. Figure 4.12 shows kinetic traces from TR^MPS spectra showing this process. Both the growth and decay processes shown in Figure 4.12 appear to be composed of a fast component and a slow component. The fast component of this process (τ = *ca.* 70 ps) occurs on approximately the same timescale as vibrational cooling of the initially formed species,

which may have some bearing on the observed kinetics. The slower component is observed to occur on the fast nanosecond timescale, and shows a clear link between the decay of $W(CO)_5(EtSiHEt_2)$ (τ = 2.0 ($\pm$0.3) ns) and the growth of $W(CO)_5(H{-}SiEt_3)$ (τ = 2.5 ($\pm$0.4) ns). In general, the kinetics of these process are in good agreement with previous studies, in which the authors cite the formation of vibrationally hot species, the ν(CO) bands of which overlap with the species of interest, as a possible reason for the observed bi-exponential behaviour for this solvent rearrangement process. Kotz *et al.* conclude that the rearrangement of the solvent occurs *via* the Dobson mechanism of dissociative rearrangement.[314] The results presented herein are not inconsistent with this conclusion. A comparison of the observed rate constants and ν(CO) band positions presented in this work with those presented by Kotz *et al.* is shown in Table 4.5.

TABLE 4.5: ν(CO) absorption band frequencies of $W(CO)_6$, $W(CO)_5(EtSiHEt_2)$ and $W(CO)_5(H{-}SiEt_3)$ formed following photolysis in $HSiEt_3$ under Ar. Observed rate constants (k_{obs}) for are also given, taken from the most intense ν(CO) band in each case. All experiments performed in solution phase at 298 K. Literature values are provided for comparison.

Compound	ν**(CO)** (cm^{-1})	k_{obs} (s^{-1}) **Fast**	**Slow**	**Reference**
$\mathbf{W(CO)_6}$	1983			This work
$\mathbf{W(CO)_5(EtSiHEt_2)}$	1953, 1940	1.4 ($\pm$0.2) x 10^{10}	5.0 ($\pm$0.5) x 10^8	This work
$\mathbf{W(CO)_5(H{-}SiEt_3)}$	1950	1.6 ($\pm$0.2) x 10^{10}	4.0 ($\pm$0.5) x 10^8	This work
$\mathbf{W(CO)_6}$	1983			314
$\mathbf{W(CO)_5(EtSiHEt_2)}$	1953, 1935	2.1 ($\pm$0.2) x 10^{10}	4.2 ($\pm$0.6) x 10^8	314
$\mathbf{W(CO)_5(H{-}SiEt_3)}$	1950	4.5 ($\pm$1.9) x 10^{10}	5.0 ($\pm$4.0) x 10^8	314

4.2.5 Preliminary TR-XAFS Studies of $CpRe(CO)_3$ and $W(CO)_6$ in Neat $HSiEt_3$

Following TRIR and TR^MPS studies described above, preliminary TR-XAFS spectroscopic studies of both $CpRe(CO)_3$ and $W(CO)_6$ in triethylsilane were undertaken, to determine the viability of future studies of organometallic and alkane complexes.

4.2.5.1 TR-XAFS Spectroscopy of $CpRe(CO)_3$ in Neat $HSiEt_3$

XAFS studies of $CpRe(CO)_3$ in neat $HSiEt_3$ were performed at the Advanced Photon Source (APS), Argonne National Laboratory, Illinois, USA. Studies were undertaken in collaboration with Drs. Xiaoyi Zhang and Qingyu Kong of the APS, Dr. Andrew Dent of the Diamond Light Source, Drs. Stuart Bartlett and Michelle Hamilton of the Rutherford Appleton Laboratory, Dr. Raphael Horvath of the University of Nottingham and Prof. John Evans of the University of Southampton.

Figure 4.13 shows the ground state x-ray absorption spectrum of $CpRe(CO)_3$ in neat triethylsilane, along with XAFS difference spectra recorded at two different time delays following 266 nm photolysis of $CpRe(CO)_3$ in $HSiEt_3$ under Ar. The ground state spectrum shows a large absorption edge at 10.539 keV, with no resolvable pre-edge features. The higher energy region of the spectrum shows small oscillations in absorbance indicative of the coordination geometry and nature of the coordinated ligands. The difference spectrum recorded 150 ns following 266 nm photolysis of $CpRe(CO)_3$ in $HSiEt_3$, shows significant noise. This is likely due to the low concentration of any transient species produced in solution. However, despite this the spectrum does show

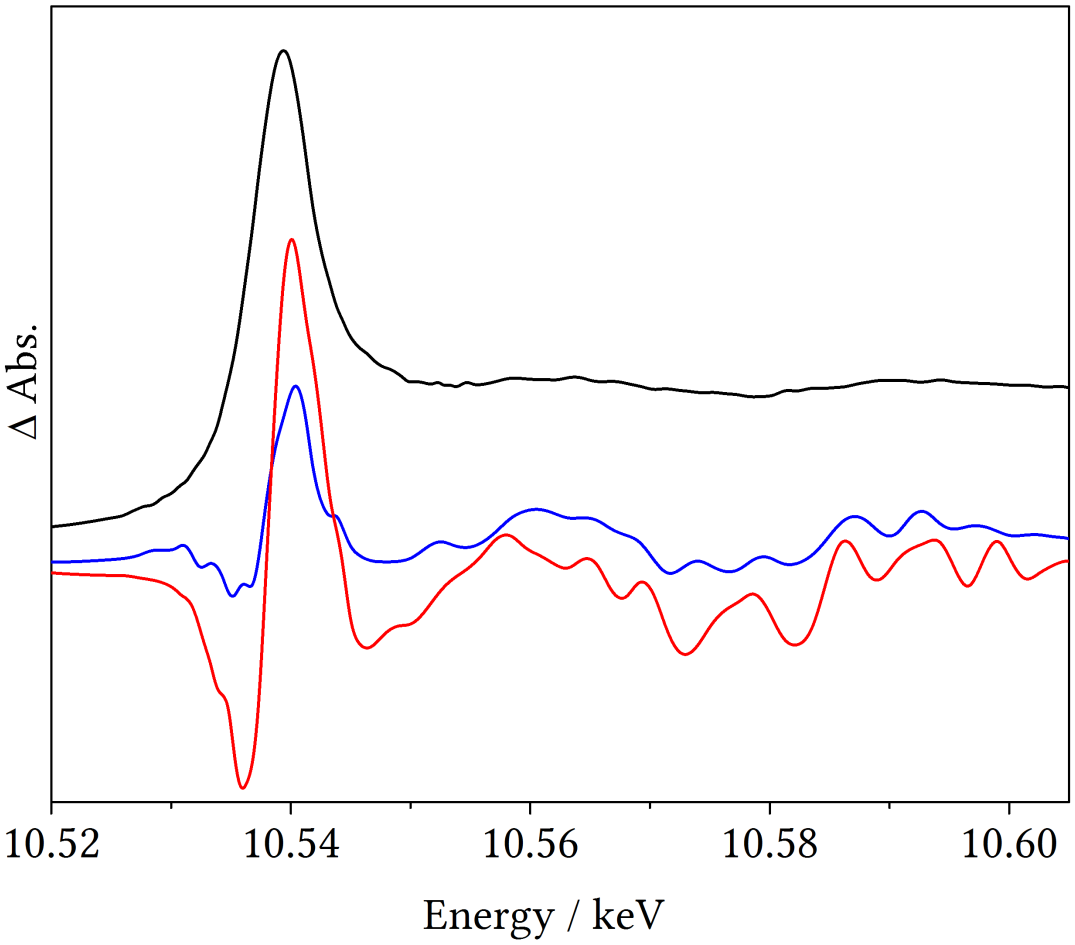


FIGURE 4.13: Ground state Re L_3-edge XAFS spectrum of $CpRe(CO)_3$ in neat $HSiEt_3$ (black), and XAFS difference spectra recorded 150 ns (red) and 1500 ns (blue) following 266 nm photolysis of a solution of $CpRe(CO)_3$ in $HSiEt_3$ under an Ar atmosphere. A small shift in the absorption edge following photolysis can be seen, as well as decay of a transient on the microsecond timescale.

some changes compared to the ground state spectrum. A negative feature at 10.536 keV and positive feature at 10.540 keV can be observed, indicating a small shift in the absorption edge following photolysis. This change is possibly indicative of a change in the electron density at the metal centre.

Examination of the higher energy region of the spectrum shows similar oscillations to those observed in the ground state spectrum. From the TR^MPS data reported above, we would expect to observe $CpRe(CO)_2(EtSiHEt_2)$ in solution following 266 nm

photolysis, along with a small amount of the Si-H activated species $CpRe(CO)_2(SiEt_3)H$. It is not clear from these spectra alone which of these species, if any, are observed during the XAFS studies presented here. There is, however, a clear change in the intensity of the observed features upon comparison of spectra record 150 ns and 1500 ns following photolysis. Both the negative and positive features observed in the 150 ns spectrum appear to have decreased in intensity after 1500 ns, indicating the decay of a transient species. The timescale of this decay is similar to the observed decay of $CpRe(CO)_2(EtSiHEt_2)$ to form $CpRe(CO)_2(SiEt_3)H$, as reported above. However, no additional positive features are observed to form concurrently with this decay process, which would be expected for the chemistry observed during TR^MPS studies. Computational modelling and DFT studies are currently underway to aid in our assignment of these XAFS spectra.

4.2.5.2 TR-XAFS Spectroscopy of $W(CO)_6$ in Neat $HSiEt_3$

XAFS studies of $W(CO)_6$ in neat $HSiEt_3$ were performed at the Swiss Light Source (SLS), Paul Scherrer Institut, Villigen, Switzerland. Studies were undertaken in collaboration with Drs. Grigori Smolentsev and Maarten Nachtegaal of the SLS, Drs. Andrew Dent and Sofia Diaz-Moreno of the Diamond Light Source, Dr. Stuart Bartlett of the Rutherford Appleton Laboratory, Dr. Raphael Horvath of the University of Nottingham and Prof. John Evans of the University of Southampton.

As above for $CpRe(CO)_3$, the ground state XAFS spectrum of $W(CO)_6$ in $HSiEt_3$ shows a large absorption edge (10.208 keV), as well as some smaller oscillations to higher energy of the absorption edge, indicating the nature of the coordination environment

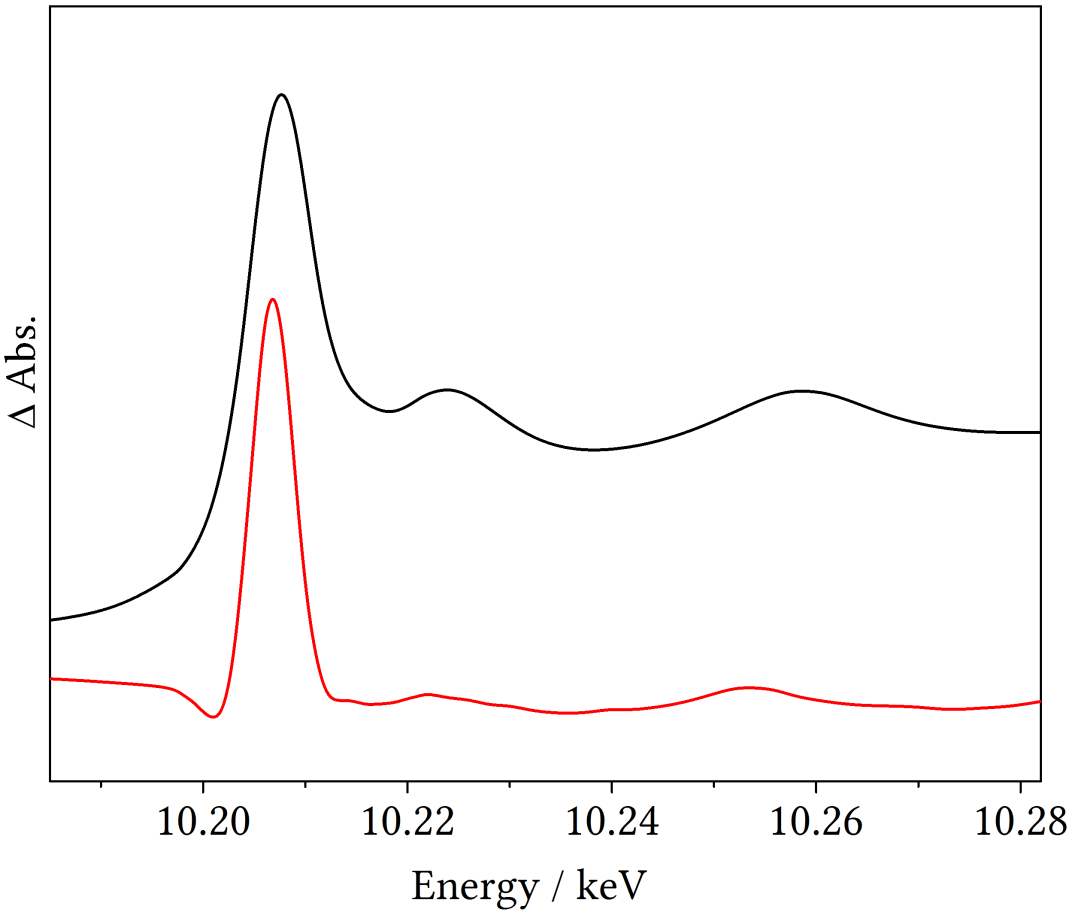


FIGURE 4.14: Ground state W L_3-edge XAFS spectrum of $W(CO)_6$ in neat $HSiEt_3$ (black), and XAFS difference spectrum recorded 10 μs (red) following 266 nm photolysis of a solution of $W(CO)_6$ in $HSiEt_3$ under a He atmosphere. A small shift in the absorption edge, as well as subtle changes in the higher energy region of the spectrum can be observed following photolysis.

around the metal centre. The XAFS difference spectrum recorded 10 μs following 266 nm photolysis of $W(CO)_6$ in neat $HSiEt_3$ under a He atmosphere shows a small shift in the absorption edge to 10.207 keV. The direction of this shift following photolysis is in contrast to that observed for $CpRe(CO)_3$ above. In addition to this edge-shift, the smaller features to higher energy of the edge also appear to shift to lower energy compared to the ground state spectrum. Both of these features are potentially indicative of a change in the coordination environment around the W metal. From TR^MPS studies

presented above, as well as those reported previously,[314] we would expect to observe a single transient species $W(CO)_5(H{-}SiEt_3)$ 10 μs following photolysis. However, as above, these spectra cannot be conclusively assigned without computational modelling and DFT studies, which are currently underway.

4.3 Conclusions and Future Outlook

In this Chapter, TR^MPS has been utilised to examine the photochemistry of a series of model transition metal carbonyl complexes in neat triethylsilane, as well as the perfluorinated alkane perfluoro(methylcyclohexane) doped with $HSiEt_3$.

266 nm photolysis of $CpMn(CO)_3$ in pure $HSiEt_3$ was shown to produce a variety of transient species. Initially, formation of both the 16-electron complex $^3CpMn(CO)_2$ and the ethyl-bound silane complex $CpMn(CO)_2(EtSiHEt_2)$ were observed. Direct Si-H activation on the picosecond timescale through a spin-forbidden reaction of $HSiEt_3$ with $^3CpMn(CO)_2$, is accompanied by a further spin-forbidden interaction which results in additional formation of $CpMn(CO)_2(EtSiHEt_2)$. Further Si-H activation on the nanosecond timescale was then observed through a concerted rearrangement-activation step to form $CpMn(CO)_2(H{\cdots}SiEt_3)$ from the ethyl-bound complex $CpMn(CO)_2(EtSiHEt_2)$. Studies of $CpRe(CO)_3$ and its derivative, $Cp^*Re(CO)_3$ exhibited a simpler reaction mechanism, with initial formation of both the Si-H activated species ($CpRe(CO)_2(SiEt_3)H$ or $Cp^*Re(CO)_2(SiEt_3)H$) and the ethyl-bound silane σ-complexes $CpRe(CO)_2(EtSiHEt_2)$ and $Cp^*Re(CO)_2(EtSiHEt_2)$.

Additional formation of the Si-H activated species is then observed on the microsecond timescale. These observations are in good agreement with previously published studies.[150,186,187]

Addition of triethylsilane to a solution of $CpMn(CO)_3$ in PFMCH was also undertaken, to examine what changes, if any, the perfluoroalkane makes to the Si-H activation chemistry observed in pure $HSiEt_3$. 266 nm photolysis of $CpMn(CO)_3$ in PFMCH doped with triethylsilane resulted in initial formation of $^3CpMn(CO)_2$ and $CpMn(CO)_2(EtSiHEt_2)$, with $^3CpMn(CO)_2$ undergoing spin-forbidden reactions with $HSiEt_3$ to form both the Si-H activation product $CpMn(CO)_2(H\text{---}SiEt_3)$ and the ethyl-bound silane σ-complex $CpMn(CO)_2(EtSiHEt_2)$ on the nanosecond timescale (τ = *ca.* 4.5 ns). Further Si-H activation through the ethyl-bound silane complex was subsequently observed to occur with a lifetime of *ca.* 140 ns, matching observations in pure $HSiEt_3$, indicating that PFMCH has little effect on the Si-H activation chemistry of $CpMn(CO)_3$, while changes in the rate of the initial spin-forbidden reaction with $HSiEt_3$ are slowed due to lowering the concentration of $HSiEt_3$ in solution. Additional of $HSiEt_3$ to a solution of $CpRe(CO)_3$ in PFMCH was shown to slow the Si-H activation chemistry observed following 266 nm photolysis. This slowed rate of activation was attributed to formation of $CpRe(CO)_2(C_7F_{14})$ in solution, which was proposed to undergo reaction with $HSiEt_3$ to produce $CpRe(CO)_2(SiEt_3)H$, as well as $CpRe(CO)_2(EtSiHEt_2)$, which was observed to undergo Si-H activation itself. While PFMCH appears to slow the formation of $CpRe(CO)_2(SiEt_3)H$ in solution, Si-H activation was still observed.

266 nm photolysis of $W(CO)_6$ in neat $HSiEt_3$ was found to result in the initial formation of a single pentacarbonyl species, assigned to the ethyl-bound silane σ-complex

$W(CO)_5(EtSiHEt_2)$, which was observed to decay on the nanosecond timescale to form the Si-H bound complex $W(CO)_5(H{-}SiEt_3)$. These results appear in good agreement with previously published work.[314]

Finally, preliminary TR-XAFS results were presented, recorded following the 266 nm photolysis of $CpRe(CO)_3$ and $W(CO)_6$ in neat triethylsilane under an inert atmosphere. XAFS difference spectra recorded following photolysis of $CpRe(CO)_3$ shows a small shift in the absorption edge compared to the ground state spectrum, indicating the possible formation of a transient species. This possible transient species was observed to decay on the microsecond timescale, possibly indicating decay of $CpRe(CO)_2(EtSiHEt_2)$ as observed in TR^MPS studies. XAFS difference spectra recorded following photolysis of $W(CO)_6$ in $HSiEt_3$ also showed a small shift in absorption edge, as well as changes in small features at higher energy, possibly indicative of changes in the coordination environment around the W centre. The XAFS spectra presented could not be conclusively assigned, and it is hoped that ongoing computational studies will allow us to gain more insight into the reasons for the observed spectral changes.

While the TR-XAFS spectra presented in this Chapter are by no means conclusive, future outlook for these studies remains positive. These preliminary results show that it is possible to record XAFS spectra at the low (1-2 mM) solution concentrations obtainable for metal carbonyl species in perfluoroalkane solvents, and that the low conversion from ground state to the species of interest (1-10 %) does not prevent us from observing spectral changes following photolysis. Future XAFS studies will likely involve the use of a bespoke enclosed flow setup, currently being developed, rather than the open jet system used in the investigations presented above. Use of an

enclosed system with allow the addition of gases to the solution (e.g., Xe, methane etc.) and decrease the likelihood of the sample solution being exposed to air or moisture. It is hoped that computer modelling of the TR-XAFS spectra reported above will allow us to determine whether the chemistry we have observed is in agreement with previous $TR^{M}PS$ studies. From the studies performed so far there is no indication that observation of organometallic alkane and noble gas complexes using the methodology discussed in Chapter 2 and 3 is an impossible task, however it is clear from the studies performed so far that some changes to the experimental setup will be required in order to achieve this ultimate goal.

Chapter 5

Experimental

All of the instrumentation used to perform the experiments outlined in this Thesis has been described in detail elsewhere.[24,38,39,315] This Chapter will present an overview of the various time-resolved spectroscopy facilities that have been utilised throughout the course of this PhD, including apparatus both at the University of Nottingham and the Rutherford Appleton Laboratory, Harwell Oxford. The remaining sections of this Chapter will detail the other apparatus and materials used during the work described in this Thesis.

5.1 Time-Resolved Spectroscopic Measurements

Time-resolved spectroscopic measurements on the picosecond to microsecond timescale were performed on apparatus at the University of Nottingham and the Rutherford Appleton Laboratory. Time-resolved infrared experiments at Nottingham were performed in collaboration with Dr. Xue-Zhong Sun. A description of each of the instruments

used in this Thesis is given below, including a description of how the spectroscopic data were recorded and analysed in each case.

5.1.1 Nottingham TRIR Apparatus

The University of Nottingham ultrafast TRIR (time-resolved infrared) apparatus is based on the PIRATE ultrafast infrared apparatus, previously located at the Rutherford Appleton Laboratory, which is described in detail elsewhere.[24] Laser pulses at 800 nm (2.3 mJ, 1 kHz, 140 fs) are produced by a Ti:sapphire oscillator (MaiTai, Spectra Physics) in combination with a regenerative amplifier (Spitfire Pro, Spectra Physics). These pulses are split into two beams. The first is used to pump a TOPAS-C optical parametric amplifier (Light Conversion), followed by a difference frequency generator to produce tunable mid-IR pulses (180 cm^{-1} fwhm, *ca.* 2 μJ at 2000 cm^{-1}). These pulses are split by a Germanium beam splitter, with a portion of the pulse aligned to a single element MCT (mercury cadmium telluride) detector (Kolmar Technology) and acting as a reference beam. The other half of the IR pulse is used as the probe beam, and is directed to the sample area. The second part of the initial 800 nm pulse is used to generate a pump pulse of 267 or 400 nm by harmonic generation (TimePlate Tripler, Minioptic Technology Inc.). In order to study a specific time delay, the pump beam is delayed using a translation stage (LMA Actuator, Aerotech). Using this technique, time delays of up to *ca.* 2 ns become accessible.

For TRIR spectra on the nanosecond to microsecond timescale, the output of a Q-switched Nd:YVO laser (1064 nm, 600 ps, Advanced Optical Technology) is frequency quadrupled to produce a pump pulse at 266 nm. The pump and probe pulses are

synchronised and the delay is set by a pulse generator (DG535, Stanford Research Systems). This method allows time delays between pump and probe of 0.5 ns to 100 μs to be obtained.

After passing through the sample, the transmitted portion of the IR probe beam is dispersed by a 250 nm IR monochromator (DK240, Spectra Physics) with a 150 L/mm grating, onto a 128-element MCT detector (Infrared Associates Inc.), giving *ca.* 4 cm^{-1} resolution. For both picosecond and nanosecond timescale experiments, the diameter of the pump beam (*ca.* 500 μm) is larger than that of the probe beam (*ca.* 200 μm). The signal is amplified by a 144-channel amplifier (Infrared Associates Inc.), then digitised by a 16-bit analog to digital converter (IR0144, Infrared Systems Development Corp.).

The ratio between pump-on and pump-off IR intensity measurements is used to determine the change in absorbance (ΔAbs). Pump-off measurements are generated using an optical chopper (500 Hz) which blocks every second pump pulse. In order to avoid sample degradation and overheating, and to ensure that fresh sample is probed with each laser pulse, the sample is rastered in the x and y planes, relative to the incident probe pulse.

5.1.2 TRIR Apparatus at the Rutherford Appleton Laboratory

Picosecond and nanosecond TRIR measurements were performed at the ULTRA ultrafast infrared absorption facility at the Rutherford Appleton Laboratory, Harwell Oxford. The ULTRA system has been described in detail elsewhere,[38] so only a brief summary is given. A pulse of 50 fs duration and 0.8 mJ output is produced by a Ti:sapphire

dual output amplifier (Thales Laser) with a repetition rate of 10 kHz, at 800 nm. This 800 nm beam is then split into two. The first section is used to generate a 266 nm UV pump pulse by third harmonic generation. The second is passed through optical parametric amplifiers (TOPAS, Light Conversion) to produce the tunable mid-IR probe beam. The IR probe beam is split into two to form probe and reference beams. After passing through the sample, the IR probe is dispersed onto two linear 128-element MCT array detectors (Infrared Associates). The 267 nm pump beam is focussed to a spot size of *ca.* 100 μm, and overlapped at the sample position with the mid-IR probe beam, which is focussed to *ca.* 80 μm. A small portion of the IR probe beam is dispersed onto a 64-element MCT array detector (Infrared Associates), acting as a reference.

Pump-on pump-off infrared absorption difference spectra were recorded at high speed (10 kHz). The two spectral windows were calibrated separately using the characteristic absorption lines of cis-stilbene. The overlapping spectral windows were interleaved using overlapping parent bleach signals recorded at the same delay time. The sample was rastered in the x and y directions during data acquisition.

5.1.3 TR^{M}PS Apparatus at the Rutherford Appleton Laboratory

Time-resolved multiple probe spectroscopy (TR^{M}PS) was utilised for some of the experiments outlined in this thesis. The TR^{M}PS apparatus at the Rutherford Appleton Laboratory is described in detail elsewhere.[39] In brief, two laser amplifiers (Thales Laser and Spectra Physics) are used as the pump and probe, operating at 1 and 10 kHz respectively. These two amplifiers are then synchronised to afford a data recording

scheme which incorporates multiple probe pulses per pump pulse, as outlined in Chapter 1 of this Thesis.

5.1.4 Transient Absorption Apparatus at the Rutherford Appleton Laboratory

For transient absorption (TA) spectroscopic measurements, the UV pump beam is generated in the same way as for TRIR and TR^{M}PS experiments described above. Additional details of the TA spectroscopy apparatus are described in the literature.[315] In the case of TA measurements the probe pulse is a white light continuum (WLC) which is generated by focussing pulses of 800 nm light into CaF_2. As above, the pump-probe delay time was controlled through use of an optical delay line and electronic delay generator, for picosecond and nanosecond timescales respectively. For TA measurements, the probe beam was *ca.* 50 μm in diameter. Probe wavelengths were calibrated against a variety of optical band-pass filters.

5.1.5 TRIR, TR^{M}PS and TA Data Analysis

Time delays recorded for each time-resolved experiment were selected to be appropriate to the process of interest. For each single-probe experiment *ca.* 40 time delays were selected. TR^{M}PS allows picosecond, nanosecond and microsecond timescales to be studied in the same experiment, so in this case *ca.* 80 time delays were selected. Signal-to-noise was improved through the use of averaging, with *ca.* 5 seconds of averaging on each time delay producing good signal-to-noise. In addition to averaging, the time delay cycle was repeated up to 5 times, and all cycles averaged together to further improve

signal-to-noise. Owing to the faster repetition rate of the ULTRA system, experiments performed on that apparatus usually required only *ca.* 3 seconds of averaging per time delay.

Data processing on all TRIR, TR^{M}PS and TA data was performed using custom software designed by M. R. Pollard and G. M. Greetham. Decay fitting was performed using OriginPro version 9.0. Monoexponential or biexponential fitting models were applied to single wavenumber points at band maxima to produce kinetic traces, or to fitted band area where applicable. Reported errors were obtained from the deviation of experimental data from the exponential fit function.

5.1.6 Time-Resolved XAFS Spectroscopy at the Swiss Light Source

Tungsten L_3-edge XAFS spectroscopic measurements were performed at the Swiss Light Source, Paul Scherrer Institut (PSI), Villigen, Switzerland. Data were obtained using a Si(111) crystal monochromator on the SuperXAS beamline. Avalanche photodiode (APD) detectors were used for fast detection in fluorescence mode, on an open jet sample system under a He atmosphere. Pump-probe measurements were collected using synchrotron radiation in multi-bunch mode giving *ca.* 200 ns per photon bunch. Each data point was averaged over 30 seconds. The reported data are an average of 40 individual scans over 10 μs, which is then normalised to I_0 and smoothed using a moving average smoothing function. Liquid samples were prepared under standard Schlenk conditions, using dry, degassed solvents. Sample solutions were flowed through an open jet sample system with an aperture of *ca.* 300 μm at a flow rate of 1 mL/s.

5.1.7 Time-Resolved XAFS Spectroscopy at the Advanced Photon Source

Rhenium L_3-edge XAFS spectroscopic measurements were conducted at the Advanced Photon Source, Argonne National Laboratory (ANL), Argonne, IL, USA. Data were recorded using a Si(111) monochromator on the 11-ID-D x-ray beamline. APD detectors were used for fast detection in fluorescence mode on an open jet liquid sample system under an Ar atmosphere. Pump-probe measurements were collected using synchrotron radiation in 24-bunch mode giving 153 ns between photon bunches. Each data point is averaged over 10 seconds, and the final presented data is an average of 50 individual scans for each 153 ns time slice, normalised to I_0 and smoothed using a moving average smoothing function. Liquid samples were prepared under standard Schlenk conditions, using dry, degassed solvents. Sample solutions were flowed through an open jet sample system with an aperture of *ca.* 200 μm at a flow rate of 0.5 mL/s.

5.2 Other Spectroscopic Measurements

5.2.1 FTIR and UV-visible Spectroscopy

FTIR (Fourier Transform Infrared) spectra were recorded on a variety of Nicolet FTIR spectrometers, with a resolution of 2 cm^{-1}. UV-Visible spectra were recorded on various Perkin-Elmer UV spectrophotometers, with a data spacing of 1 nm, and a dwell time of 0.5 secs. IR solution cells (Harrick Corp.), fitted with 2 CaF_2 windows (25 x 2 mm) were used during collection of both FTIR and UV-Visible spectra.

5.3 Sample Preparation

5.3.1 Solution Phase Sample Preparation

All solution phase samples were prepared under an Ar atmosphere using standard Schlenk line techniques. Sample solutions were made up to *ca.* 20 ml and degassed before use. Solutions were stored under an Ar atmosphere when not in use. All solution phase spectra were recording using Harrick transmission cells fitted with two CaF_2 windows of 2 mm thickness and 25 mm diameter. The path length of the transmission cell was varied through the use of a Teflon spacer, the thickness of which was varied between 0.1-0.8 mm depending on the required concentration of the sample solution. Solution concentrations were selected such that the IR absorbance of the ν(CO) bands of the species of interest was between 0.1-0.8. Due to the high repetition rate of the lasers used to record time-resolved spectra, sample solutions were refreshed constantly using a flow system consisting of a glass sample reservoir connected to the Harrick transmission cell by two Teflon tubes. Solutions were flowed through the system using a peristaltic pump.

In the case of experiments involving a dissolved gas, the solution was first prepared under Ar atmosphere using standard Schlenk line techniques. The solution was then degassed, and the flow system evacuated. A pressure of 1.5 bar of the gas of interest was then introduced to the flow system using a custom gas filling station constructed by Dr. Ian Clark (Central Laser Facility, Rutherford Appleton Laboratory) which had itself been evacuated prior to use, and the solution agitated to facilitate dissolution of the gas. Sample solutions were held under pressure of the gas of interest while spectra

were recorded. As above, these samples were constantly refreshed using a peristaltic pump.

5.4 Materials

5.4.1 Materials Used in Chapter 2

$Fe(CO)_5$ (Aldrich), $CpMn(CO)_3$ (Strem), $(MeCp)Mn(CO)_3$ (Aldrich), $CpV(CO)_4$ (Strem) and $CpCo(CO)_2$ (Strem) were all used as received, without further purification. Perfluoro(methylcyclohexane) (94 %, Alfa Aesar), perfluoro(hexanes) (98 %, Aldrich), perfluoro(triethylamine) (98 %, Acros Organics), cyclopentane (ReagentPlus grade, Aldrich) and *n*-heptane (spectrophotometric grade, Aldrich) were refluxed over CaH_2 under an inert argon atmosphere for 48 hours before use. Solvents were also stored under a slight pressure of argon, and subsequently degassed prior to use. Xenon ($>$ 99.99 %, Aldrich), methane (analytical grade, Aldrich), ethane (analytical grade, Aldrich), CO_2 ($>$ 99.8 %, Aldrich) were used without further purification.

5.4.2 Materials Used in Chapter 3

$CpRe(CO)_3$ (Strem), $Cp^*Re(CO)_3$ (Strem), $Cp^*Rh(CO)_2$ (Aldrich), $Cr(CO)_6$ (Aldrich), $Mo(CO)_6$ (Aldrich) and $W(CO)_6$ (Aldrich) were used as purchased, without further purification. $CpRh(CO)_2$ was synthesised by Dr. Alisdair Wriglesworth at the University of Nottingham, and was used as received. $CpRe(CO)_2(N_2)$ was synthesised by Dr. Stuart Bartlett of the Dynamic Structural Science Consortium at the Rutherford

Appleton Laboratory. Perfluoro(methylcyclohexane) (94 %, Alfa Aesar), perfluoro-(hexanes) (98 %, Aldrich), cyclopentane (ReagentPlus grade, Aldrich) and *n*-heptane (spectrophotometric grade, Aldrich) were refluxed over CaH_2 under an inert argon atmosphere for 48 hours before use. Solvents were also stored under a slight pressure of argon, and subsequently degassed prior to use. Xenon (> 99.99 %, Aldrich), methane (analytical grade, Aldrich) and ethane (analytical grade, Aldrich) were used without further purification.

5.4.3 Materials Used in Chapter 4

$CpRe(CO)_3$ (Strem), $Cp^*Re(CO)_3$ (Strem), $CpMn(CO)_3$ (Strem) and $W(CO)_6$ (Aldrich) were used as received, without further purification. Perfluoro(methylcyclohexane) (94 %, Alfa Aesar) and triethylsilane (99 %, Aldrich) were refluxed over CaH_2 under an inert argon atmosphere for 48 hours before use. Solvents were also stored under a slight pressure of argon, and subsequently degassed prior to use.

References

[1] K. C. Nicolaou, P. G. Bulger and D. Sarlah, *Angew. Chem., Int. Ed.*, 2005, **44**, 4442–4489.

[2] E. Iglesia, *Appl. Catal., A*, 1997, **161**, 59–78.

[3] G. J. P. Britovsek, V. C. Gibson and D. F. Wass, *Angew. Chem., Int. Ed.*, 1999, **38**, 428–447.

[4] V. C. Gibson and S. K. Spitzmesser, *Chem. Rev.*, 2003, **103**, 283–315.

[5] D. Alberico, M. E. Scott and M. Lautens, *Chem. Rev.*, 2007, **107**, 174–238.

[6] W. A. Herrmann, *Angew. Chem., Int. Ed.*, 2002, **41**, 1290–1309.

[7] M. K. Nazeeruddin, A. Kay, I. Rodicio, R. Humphry-Baker, E. Müller, P. Liska, N. Vlachopoulos and M. Gratzel, *J. Am. Chem. Soc.*, 1993, **115**, 6382–6390.

[8] A. Hagfeldt and M. Grätzel, *Acc. Chem. Res.*, 2000, **33**, 269–277.

[9] A. Kudo and Y. Miseki, *Chem. Soc. Rev.*, 2009, **38**, 253–278.

[10] S. Linic, P. Christopher and D. B. Ingram, *Nat. Mater.*, 2011, **10**, 911–921.

[11] K. Sumida, D. L. Rogow, J. A. Mason, T. M. McDonald, E. D. Bloch, Z. R. Herm, T. H. Bae and J. R. Long, *Chem. Rev.*, 2012, **112**, 724–781.

[12] D. M. D'Alessandro, B. Smit and J. R. Long, *Angew. Chem., Int. Ed.*, 2010, **49**, 6058–6082.

[13] M. Mikkelsen, M. Jorgensen and F. C. Krebs, *Energ. Environ. Sci.*, 2010, **3**, 43–81.

[14] G. Ferey, C. Serre, T. Devic, G. Maurin, H. Jobic, P. L. Llewellyn, G. De Weireld, A. Vimont, M. Daturi and J. S. Chang, *Chem. Soc. Rev.*, 2011, **40**, 550–562.

[15] G. Gasser, I. Ott and N. Metzler-Nolte, *J. Med. Chem.*, 2011, **54**, 3–25.

[16] M. J. Clarke, *Coord. Chem. Rev.*, 2002, **232**, 69–93.

[17] T. J. Wadas, E. H. Wong, G. R. Weisman and C. J. Anderson, *Curr. Pharm. Des.*, 2007, **13**, 3–16.

[18] M. J. Clarke, F. C. Zhu and D. R. Frasca, *Chem. Rev.*, 1999, **99**, 2511–2533.

[19] J. D. Simon and X. L. Xie, *J. Phys. Chem.*, 1986, **90**, 6751–6753.

[20] J. D. Simon and X. L. Xie, *J. Phys. Chem.*, 1987, **91**, 5538–5540.

[21] B. A. Thrush, *Photochem. Photobiol. Sci.*, 2003, **2**, 453–454.

[22] R. G. W. Norrish and G. Porter, *Nature*, 1949, **164**, 658–658.

[23] R. G. W. Norrish and G. Porter, *Proc. R. Soc. London, Ser. A*, 1952, **210**, 439.

[24] M. Towrie, D. C. Grills, J. Dyer, J. A. Weinstein, P. Matousek, R. Barton, P. D. Bailey, N. Subramaniam, W. M. Kwok, C. S. Ma, D. Phillips, A. W. Parker and M. W. George, *Appl. Spectrosc.*, 2003, **57**, 367–380.

[25] O. Einarsdóttir, R. B. Dyer, D. D. Lemon, P. M. Killough, S. M. Hubig, S. J. Atherton, J. J. López-Garriga, G. Palmer and W. H. Woodruff, *Biochemistry*, 1993, **32**, 12013–12024.

[26] A. Barth, *Biochim. Biophys. Acta, Bioenerg.*, 2007, **1767**, 1073–1101.

[27] A. Ostermann, R. Waschipky, F. G. Parak and G. U. Nienhaus, *Nature*, 2000, **404**, 205–208.

[28] A. J. Dixon, P. Glyn, M. A. Healy, P. M. Hodges, T. Jenkins, M. Poliakoff and J. J. Turner, *Spectrochim. Acta A*, 1988, **44**, 1309–1314.

[29] M. W. D. Hanson-Heine, A. Wriglesworth, M. Uroos, J. A. Calladine, T. S. Murphy, M. Hamilton, I. P. Clark, M. Towrie, J. Dowden, N. A. Besley and M. W. George, *J. Chem. Phys.*, 2015, **142**, 154119.

[30] K. N. Tanner and R. L. King, *Nature*, 1958, **181**, 963–965.

[31] X.-Z. Sun, S. M. Nikiforov, J. X. Yang, C. S. Colley and M. W. George, *Appl. Spectrosc.*, 2002, **56**, 31–39.

[32] M. W. George, M. Poliakoff and J. J. Turner, *Analyst*, 1994, **119**, 551–560.

[33] D. C. Grills and M. W. George, *Handbook of Vibrational Spectroscopy*, Wiley Interscience, New York, 2002.

[34] J. A. Calladine, K. Q. Vuong, X.-Z. Sun and M. W. George, *Pure Appl. Chem.*, 2009, **81**, 1667–1675.

[35] J. A. Calladine, R. Horvath, A. J. Davies, A. Wriglesworth, X.-Z. Sun and M. W. George, *Appl. Spectrosc.*, 2015, **69**, 519–524.

[36] H. van der Salm, M. G. Fraser, R. Horvath, S. A. Cameron, J. E. Barnsley, X.-Z. Sun, M. W. George and K. C. Gordon, *Inorg. Chem.*, 2014, **53**, 3126–3140.

[37] A. J. Cowan, P. Portius, H. K. Kawanami, O. S. Jina, D. C. Grills, X.-Z. Sun, J. McMaster and M. W. George, *Proc. Natl. Acad. Sci. U.S.A.*, 2007, **104**, 6933–6938.

[38] G. M. Greetham, P. Burgos, Q. Cao, I. P. Clark, P. S. Codd, R. C. Farrow, M. W. George, M. Kogimtzis, P. Matousek, A. W. Parker, M. R. Pollard, D. A. Robinson, Z.-J. Xin and M. Towrie, *Appl. Spectrosc.*, 2010, **64**, 1311–1319.

[39] G. M. Greetham, D. Sole, I. P. Clark, A. W. Parker, M. R. Pollard and M. Towrie, *Rev. Sci. Instrum.*, 2012, **83**, 103107.

[40] S. Geftakis and G. E. Ball, *J. Am. Chem. Soc.*, 1998, **120**, 9953–9954.

[41] G. E. Ball, C. M. Brookes, A. J. Cowan, T. A. Darwish, M. W. George, H. K. Kawanami, P. Portius and J. P. Rourke, *Proc. Natl. Acad. Sci. U.S.A.*, 2007, **104**, 6927–6932.

[42] G. E. Ball, T. A. Darwish, S. Geftakis, M. W. George, D. J. Lawes, P. Portius and J. P. Rourke, *Proc. Natl. Acad. Sci. U.S.A.*, 2005, **102**, 1853–1858.

[43] J. A. Calladine, O. Torres, M. Anstey, G. E. Ball, R. G. Bergman, J. Curley, S. B. Duckett, M. W. George, A. I. Gilson, D. J. Lawes, R. N. Perutz, X.-Z. Sun and K. P. C. Vollhardt, *Chem. Sci.*, 2010, **1**, 622–630.

[44] D. J. Lawes, S. Geftakis and G. E. Ball, *J. Am. Chem. Soc.*, 2005, **127**, 4134–4135.

[45] R. D. Young, D. J. Lawes, A. F. Hill and G. E. Ball, *J. Am. Chem. Soc.*, 2012, **134**, 8294–8297.

[46] J. A. Calladine, S. B. Duckett, M. W. George, S. L. Matthews, R. N. Perutz, O. Torres and Q. V. Khuong, *J. Am. Chem. Soc.*, 2011, **133**, 2303–2310.

[47] O. Torres, J. A. Calladine, S. B. Duckett, M. W. George and R. N. Perutz, *Chem. Sci.*, 2015, **6**, 418–424.

[48] G. I. Childs, C. S. Colley, J. Dyer, D. C. Grills, X.-Z. Sun, J. X. Yang and M. W. George, *J. Chem. Soc., Dalton Trans.*, 2000, 1901–1906.

[49] B. H. Weiller, *J. Am. Chem. Soc.*, 1992, **114**, 10910–10915.

[50] J. J. Turner, M. B. Simpson, M. Poliakoff and W. B. Maier, *J. Am. Chem. Soc.*, 1983, **105**, 3898–3904.

[51] A. J. Rest, *J. Mol. Struct.*, 1990, **222**, 87–93.

[52] R. N. Perutz, *Chem. Rev.*, 1985, **85**, 97–127.

[53] C. R. Kemnitz, E. S. Ball and R. J. McMahon, *Organometallics*, 2012, **31**, 70–84.

[54] R. B. Hitam and A. J. Rest, *Organometallics*, 1989, **8**, 1598–1604.

[55] R. H. Hill and M. S. Wrighton, *Organometallics*, 1987, **6**, 632–638.

[56] S. T. Belt, F. W. Grevels, W. E. Klotzbucher, A. McCamley and R. N. Perutz, *J. Am. Chem. Soc.*, 1989, **111**, 8373–8382.

[57] R. B. Hitam, K. A. Mahmoud and A. J. Rest, *Coord. Chem. Rev.*, 1984, **55**, 1–29.

[58] A. I. Cooper and M. Poliakoff, *Chem. Phys. Lett.*, 1993, **212**, 611–616.

[59] M. A. Graham, M. Poliakoff and J. J. Turner, *J. Chem. Soc. A*, 1971, 2939–2948.

[60] *Fluorine: The First 100 Years*, ed. R. E. Banks, D. W. A. Sharp and J. C. Tatlow, Elsevier: New York, 1986.

[61] S. W. Green, D. S. L. Slinn, R. N. F. Simpson and A. J. Woytek, *Organofluorine Chemistry, Principles and Commercial Applications*, Plenum: New York, 1994.

[62] K. C. Lowe, *Organofluorine Chemistry, Principles and Commercial Applications*, Plenum: New York, 1994.

[63] A. R. Ravishankara, S. Solomon, A. A. Turnipseed and R. F. Warren, *Science*, 1993, **259**, 194–199.

[64] R. K. Chowdhary, R. B. Cundall and C. G. Morgan, *Photochem. Photobiol.*, 1990, **51**, 395–399.

[65] R. D. Chambers, G. Sandford and A. Shah, *Synth. Commun.*, 1996, **26**, 1861–1866.

[66] G. Pozzi, F. Montanari and M. T. Rispens, *Synth. Commun.*, 1997, **27**, 447–452.

[67] M. J. Earle and K. R. Seddon, *Pure Appl. Chem.*, 2000, **72**, 1391.

[68] M. Poliakoff, N. J. Meehan and S. K. Ross, *Chem. Ind.*, 1999, 750–752.

[69] D. W. Zhu, *Synthesis*, 1993, 953–954.

[70] H. Nakano and T. Kitazume, *Green Chem.*, 1999, **1**, 179–181.

[71] I. T. Horvath, *Acc. Chem. Res.*, 1998, **31**, 641–650.

[72] J. L. Kiplinger, T. G. Richmond and C. E. Osterberg, *Chem. Rev.*, 1994, **94**, 373–431.

[73] T. Braun and F. Wehmeier, *Eur. J. Inorg. Chem.*, 2011, 613–625.

[74] T. A. Unzner and T. Magauer, *Tetrahedron Lett.*, 2015, **56**, 877–883.

[75] V. V. Grushin, *Acc. Chem. Res.*, 2010, **43**, 160–171.

[76] S. Burling, P. I. P. Elliott, N. A. Jasim, R. J. Lindup, J. McKenna, R. N. Perutz, S. J. Archibald and A. C. Whitwood, *Dalton Trans.*, 2005, 3686–3695.

[77] B. Rábay, T. Braun and J. P. Falkenhagen, *Dalton Trans.*, 2013, **42**, 8058–8065.

[78] J. M. Kelly, C. Long and R. Bonneau, *J. Phys. Chem.*, 1983, **87**, 3344–3349.

[79] R. Bonneau and J. M. Kelly, *J. Am. Chem. Soc.*, 1980, **102**, 1220–1221.

[80] R. N. Perutz and J. J. Turner, *J. Am. Chem. Soc.*, 1975, **97**, 4791–4800.

[81] J. M. Kelly and E. K. V. Gustorf, *J. Chem. Soc. Chem. Comm.*, 1973, 105–106.

[82] N. Leadbeater, *Coord. Chem. Rev.*, 1999, **188**, 35–70.

[83] J. N. Harvey and M. Aschi, *Faraday Discuss.*, 2003, **124**, 129–143.

[84] M. A. Schroeder and M. S. Wrighton, *J. Am. Chem. Soc.*, 1976, **98**, 551–558.

[85] D. M. Hayes and E. Weitz, *J. Phys. Chem.*, 1991, **95**, 2723–2727.

[86] G. T. Long and E. Weitz, *J. Am. Chem. Soc.*, 2000, **122**, 1431–1442.

[87] M. A. Schroeder and M. S. Wrighton, *J. Organomet. Chem.*, 1977, **128**, 345–358.

[88] M. Poliakoff and E. Weitz, *Acc. Chem. Res.*, 1987, **20**, 408–414.

[89] M. Poliakoff and J. J. Turner, *Angew. Chem., Int. Ed.*, 2001, **40**, 2809–2812.

[90] M. Poliakoff, *Chem. Soc. Rev.*, 1978, **7**, 527–540.

[91] I. W. Stolz, G. R. Dobson and R. K. Sheline, *J. Am. Chem. Soc.*, 1963, **85**, 1013–1014.

[92] A. J. Rest and J. J. Turner, *J. Chem. Soc. Chem. Comm.*, 1969, 1026.

[93] M. J. Newlands and J. F. Ogilvie, *Can. J. Chem.*, 1971, **49**, 343.

[94] M. Poliakoff and J. J. Turner, *J. Chem. Soc., Dalton Trans.*, 1973, 1351–1357.

[95] M. Poliakoff and J. J. Turner, *J. Chem. Soc., Dalton Trans.*, 1974, 2276–2285.

[96] J. K. Burdett, *J. Chem. Soc. Farad. T. 2*, 1974, **70**, 1599–1613.

[97] T. J. Barton, R. Grinter, J. Thomson, B. Davies and M. Poliakoff, *J. Chem. Soc. Chem. Comm.*, 1977, 841–842.

[98] C. Daniel, M. Benard, A. Dedieu, R. Wiest and A. Veillard, *J. Phys. Chem.*, 1984, **88**, 4805–4811.

[99] M. Poliakoff, *J. Chem. Soc., Dalton Trans.*, 1974, 210–212.

[100] L. A. Barnes, M. Rosi and C. W. Bauschlicher, *J. Chem. Phys.*, 1991, **94**, 2031–2039.

[101] S. C. Fletcher, M. Poliakoff and J. J. Turner, *Inorg. Chem.*, 1986, **25**, 3597–3604.

[102] M. Poliakoff and J. J. Turner, *J. Chem. Soc. A*, 1971, 2403–2410.

[103] P. Portius, J. X. Yang, X.-Z. Sun, D. C. Grills, P. Matousek, A. W. Parker, M. Towrie and M. W. George, *J. Am. Chem. Soc.*, 2004, **126**, 10713–10720.

[104] M. Poliakoff and E. Weitz, *Adv. Organomet. Chem.*, 1986, **25**, 277–316.

[105] A. J. Ouderkirk, P. Wermer, N. L. Schultz and E. Weitz, *J. Am. Chem. Soc.*, 1983, **105**, 3354–3355.

[106] A. J. Ouderkirk and E. Weitz, *J. Chem. Phys.*, 1983, **79**, 1089–1091.

[107] T. A. Seder, A. J. Ouderkirk and E. Weitz, *J. Chem. Phys.*, 1986, **85**, 1977–1986.

[108] R. J. Ryther and E. Weitz, *J. Phys. Chem.*, 1991, **95**, 9841–9852.

[109] R. J. Ryther and E. Weitz, *J. Phys. Chem.*, 1992, **96**, 2561–2567.

[110] P. C. Engelking and W. C. Lineberger, *J. Am. Chem. Soc.*, 1979, **101**, 5569–5573.

[111] G. Nathanson, B. Gitlin, A. M. Rosan and J. T. Yardley, *J. Chem. Phys.*, 1981, **74**, 361–369.

[112] J. T. Yardley, B. Gitlin, G. Nathanson and A. M. Rosan, *J. Chem. Phys.*, 1981, **74**, 370–378.

[113] S. A. Trushin, W. Fuss, K. L. Kompa and W. E. Schmid, *J. Phys. Chem. A*, 2000, **104**, 1997–2006.

[114] I. M. Waller and J. W. Hepburn, *J. Chem. Phys.*, 1988, **88**, 6658–6669.

[115] H. Ihee, J. M. Cao and A. H. Zewail, *Angew. Chem., Int. Ed.*, 2001, **40**, 1580–1584.

[116] S. P. Church, F. W. Grevels, H. Hermann, J. M. Kelly, W. E. Klotzbucher and K. Schaffner, *J. Chem. Soc. Chem. Comm.*, 1985, 594–596.

[117] F. W. Grevels, *Photoprocesses in Transition Metal Complexes, Biosystems and Other Molecules*, Kluwer, Amsterdam, 1992.

[118] P. T. Snee, C. K. Payne, K. T. Kotz, H. Yang and C. B. Harris, *J. Am. Chem. Soc.*, 2001, **123**, 2255–2264.

[119] S. K. Nayak and T. J. Burkey, *Inorg. Chem.*, 1992, **31**, 1125–1127.

[120] S. K. Nayak, G. J. Farrell and T. J. Burkey, *Inorg. Chem.*, 1994, **33**, 2236–2242.

[121] H. Angermund, A. K. Bandyopadhyay, F. W. Grevels and F. Mark, *J. Am. Chem. Soc.*, 1989, **111**, 4656–4661.

[122] P. T. Snee, C. K. Payne, S. D. Mebane, K. T. Kotz and C. B. Harris, *J. Am. Chem. Soc.*, 2001, **123**, 6909–6915.

[123] V. Bachler, F. W. Grevels, K. Kerpen, G. Olbrich and K. Schaffner, *Organometallics*, 2003, **22**, 1696–1711.

[124] S. C. Nguyen, J. P. Lomont, M. C. Zoerb, A. D. Hill, J. P. Schlegel and C. B. Harris, *Organometallics*, 2012, **31**, 3980–3984.

[125] M. Besora, J.-L. Carreon-Macedo, A. J. Cowan, M. W. George, J. N. Harvey, P. Portius, K. L. Ronayne, X.-Z. Sun and M. Towrie, *J. Am. Chem. Soc.*, 2009, **131**, 3583–3592.

[126] D. R. Yarkony, *J. Am. Chem. Soc.*, 1992, **114**, 5406–5411.

[127] M. Ohsaku, N. Koga and K. Morokuma, *J. Chem. Soc., [Perkin 2]*, 1993, 71–74.

[128] Q. Cui and K. Morokuma, *J. Chem. Phys.*, 1997, **107**, 4951–4959.

[129] Q. Cui, K. Morokuma, J. M. Bowman and S. J. Klippenstein, *J. Chem. Phys.*, 1999, **110**, 9469–9482.

[130] M. Aschi and F. Grandinetti, *J. Chem. Phys.*, 1999, **111**, 6759–6768.

[131] J. N. Harvey, *Phys. Chem. Chem. Phys.*, 2007, **9**, 331–343.

[132] N. Koga and K. Morokuma, *Chem. Phys. Lett.*, 1985, **119**, 371–374.

[133] M. J. Bearpark, M. A. Robb and H. B. Schlegel, *Chem. Phys. Lett.*, 1994, **223**, 269–274.

[134] D. R. Yarkony, *J. Phys. Chem.*, 1993, **97**, 4407–4412.

[135] K. M. Smith, R. Poli and J. N. Harvey, *New J. Chem.*, 2000, **24**, 77–80.

[136] R. Poli and J. N. Harvey, *Chem. Soc. Rev.*, 2003, **32**, 1–8.

[137] J.-L. Carreon-Macedo and J. N. Harvey, *Phys. Chem. Chem. Phys.*, 2006, **8**, 93–100.

[138] J. N. Harvey and M. Aschi, *Phys. Chem. Chem. Phys.*, 1999, **1**, 5555–5563.

[139] M. Besora, J.-L. Carreon-Macedo, A. Cimas and J. N. Harvey, *Adv. Inorg. Chem.*, 2009, **61**, 573–623.

[140] P. Wernet, K. Kunnus, I. Josefsson, I. Rajkovic, W. Quevedo, M. Beye, S. Schreck, S. Grübel, M. Scholz, D. Nordlund, W. Zhang, R. W. Hartsock, W. F. Schlotter, J. J. Turner, B. Kennedy, F. Hennies, F. M. F. de Groot, K. J. Gaffney, S. Techert, M. Odelius and A. Foehlisch, *Nature*, 2015, **520**, 78–81.

[141] S. A. Trushin, W. Fuss, K. L. Kompa and W. E. Schmid, *J. Phys. Chem. A*, 2000, **104**, 1997–2006.

[142] A. A. Bengali, R. G. Bergman and C. B. Moore, *J. Am. Chem. Soc.*, 1995, **117**, 3879–3880.

[143] J. P. Lomont, S. C. Nguyen and C. B. Harris, *J. Am. Chem. Soc.*, 2013, **135**, 11266–11273.

[144] J. P. Lomont, S. C. Nguyen and C. B. Harris, *Organometallics*, 2012, **31**, 3947–3957.

[145] J. P. Lomont, S. C. Nguyen, J. P. Schlegel, M. C. Zoerb, A. D. Hill and C. B. Harris, *J. Am. Chem. Soc.*, 2012, **134**, 3120–3126.

[146] J. P. Lomont, S. C. Nguyen, M. C. Zoerb, A. D. Hill, J. P. Schlegel and C. B. Harris, *Organometallics*, 2012, **31**, 3582–3587.

[147] P. T. Snee, H. Yang, K. T. Kotz, C. K. Payne and C. B. Harris, *J. Phys. Chem. A*, 1999, **103**, 10426–10432.

[148] J. R. Wells and E. Weitz, *J. Am. Chem. Soc.*, 1992, **114**, 2783–2787.

[149] J. K. Klassen, M. Selke, A. A. Sorensen and G. K. Yang, *J. Am. Chem. Soc.*, 1990, **112**, 1267–1268.

[150] H. Yang, M. C. Asplund, K. T. Kotz, M. J. Wilkens, H. Frei and C. B. Harris, *J. Am. Chem. Soc.*, 1998, **120**, 10154–10165.

[151] Y. F. Zheng, W. H. Wang, J. G. Lin, Y. B. She and K. J. Fu, *J. Phys. Chem.*, 1992, **96**, 9821–9827.

[152] Y. F. Zheng, W. H. Wang, J. G. Lin, Y. B. She and K. J. Fu, *J. Phys. Chem.*, 1992, **96**, 7650–7656.

[153] C. Hall, W. D. Jones, R. J. Mawby, R. Osman, R. N. Perutz and M. K. Whittlesey, *J. Am. Chem. Soc.*, 1992, **114**, 7425–7435.

[154] S. A. Macgregor, O. Eisenstein, M. K. Whittlesey and R. N. Perutz, *J. Chem. Soc., Dalton Trans.*, 1998, 291–300.

[155] R. D. Rimmer, D. C. Grills, H. Fan, P. C. Ford and K. G. Caulton, *J. Am. Chem. Soc.*, 2007, **129**, 15430–15431.

[156] M. J. Ingleson, M. Pink, H. Fan and K. G. Caulton, *J. Am. Chem. Soc.*, 2008, **130**, 4262–4276.

[157] D. Benito-Garagorri, L. G. Alves, L. F. Veiros, C. M. Standfest-Hauser, S. Tanaka, K. Mereiter and K. Kirchner, *Organometallics*, 2010, **29**, 4932–4942.

[158] A. J. Rest, J. R. Sodeau and D. J. Taylor, *J. Chem. Soc., Dalton Trans.*, 1978, 651–656.

[159] M. Herberhold, W. Kremnitz, H. Trampisch, R. B. Hitam, A. J. Rest and D. J. Taylor, *J. Chem. Soc., Dalton Trans.*, 1982, 1261–1273.

[160] P. S. Braterman and J. D. Black, *J. Organomet. Chem.*, 1972, **39**, C3.

[161] J. D. Black, M. J. Boylan and P. S. Braterman, *J. Chem. Soc., Dalton Trans.*, 1981, 673–677.

[162] B. S. Creaven, A. J. Dixon, J. M. Kelly, C. Long and M. Poliakoff, *Organometallics*, 1987, **6**, 2600–2605.

[163] F. P. A. Johnson, M. W. George, V. N. Bagratashvili, L. N. Vereshchagina and M. Poliakoff, *Mendeleev Commun.*, 1991, **1**, 26–28.

[164] P. Hofmann, *Angew. Chem., Int. Ed.*, 1977, **16**, 536–537.

[165] N. J. Fitzpatrick, A. J. Rest and D. J. Taylor, *J. Chem. Soc., Dalton Trans.*, 1979, 351–354.

[166] H. Brunner and T. Tsuno, *Acc. Chem. Res.*, 2009, **42**, 1501–1510.

[167] T. E. Bitterwolf, K. A. Lott, A. J. Rest and J. Mascetti, *J. Organomet. Chem.*, 1991, **419**, 113–126.

[168] M. J. Clarke, S. M. Howdle, M. Jobling and M. Poliakoff, *J. Am. Chem. Soc.*, 1994, **116**, 8621–8628.

[169] J. Full, L. González and C. Daniel, *J. Phys. Chem. A*, 2001, **105**, 184–189.

[170] C. Daniel, J. Full, L. González, C. Lupulescu, J. Manz, A. Merli, S. Vajda and L. Woeste, *Science*, 2003, **299**, 536–539.

[171] J. Full, L. González and J. Manz, *Chem. Phys.*, 2006, **329**, 126–138.

[172] L. González and J. Full, *Theor. Chem. Acc.*, 2006, **116**, 148–159.

[173] J. X. Yang, B. R. N'Guessan, A. Dedieu, D. C. Grills, X.-Z. Sun and M. W. George, *Organometallics*, 2009, **28**, 3113–3122.

[174] X.-Z. Sun, D. C. Grills, S. M. Nikiforov, M. Poliakoff and M. W. George, *J. Am. Chem. Soc.*, 1997, **119**, 7521–7525.

[175] S. Lugovskoy, J. Lin and R. H. Schultz, *Dalton Trans.*, 2003, 3103–3110.

[176] S. M. Howdle, M. A. Healy and M. Poliakoff, *J. Am. Chem. Soc.*, 1990, **112**, 4804–4813.

[177] S. M. Howdle and M. Poliakoff, *J. Chem. Soc. Chem. Comm.*, 1989, 1099–1101.

[178] T. J. Burkey, *J. Am. Chem. Soc.*, 1990, **112**, 8329–8333.

[179] M. J. Almond, R. W. Atkins and R. H. Orrin, *J. Chem. Soc., Dalton Trans.*, 1994, 311–313.

[180] S. N. Hu, G. J. Farrell, C. Cook, R. Johnston and T. J. Burkey, *Organometallics*, 1994, **13**, 4127–4128.

[181] D. M. Hester, J. M. Sun, A. W. Harper and G. K. Yang, *J. Am. Chem. Soc.*, 1992, **114**, 5234–5240.

[182] P. A. Hamley, S. G. Kazarian and M. Poliakoff, *Organometallics*, 1994, **13**, 1767–1774.

[183] D. C. Grills, X.-Z. Sun, G. I. Childs and M. W. George, *J. Phys. Chem. A*, 2000, **104**, 4300–4307.

[184] D. C. Grills and M. W. George, *Adv. Inorg. Chem.*, 2001, **52**, 113–150.

[185] G. I. Childs, D. C. Grills, X.-Z. Sun and M. W. George, *Pure Appl. Chem.*, 2001, **73**, 443–447.

[186] H. Yang, K. T. Kotz, M. Asplund, S. E. Bromberg, H. Frei and C. B. Harris, *J. Am. Chem. Soc.*, 1997, **213**, 115–116.

[187] H. Yang, K. T. Kotz, M. C. Asplund, M. J. Wilkens and C. B. Harris, *Acc. Chem. Res.*, 1999, **32**, 551–560.

[188] V. Jonas and W. Thiel, *J. Chem. Phys.*, 1995, **102**, 8474–8484.

[189] B. Yan, Y. Xie, R. B. King and H. F. Schaefer, *Eur. J. Inorg. Chem.*, 2009, 3982–3992.

[190] J. P. Lomont, S. C. Nguyen and C. B. Harris, *Acc. Chem. Res.*, 2014, **47**, 1634–1642.

[191] E. P. Wasserman, R. G. Bergman and C. B. Moore, *J. Am. Chem. Soc.*, 1988, **110**, 6076–6084.

[192] V. Gandon, N. Agenet, K. P. C. Vollhardt, M. Malacria and C. Aubert, *J. Am. Chem. Soc.*, 2009, **131**, 3007–3015.

[193] A. J. Rest, M. Herberhold and M. Schrepfermann, *Organometallics*, 1992, **11**, 3646–3658.

[194] G. C. Faber and R. J. Angelici, *Inorg. Chem.*, 1970, **9**, 1586–1587.

[195] D. G. Alway and K. W. Barnett, *Inorg. Chem.*, 1980, **19**, 779–781.

[196] R. M. Kowaleski, D. O. Kipp, K. J. Stauffer, P. N. Swepston and F. Basolo, *Inorg. Chem.*, 1985, **24**, 3750–3752.

[197] J. W. Freeman and F. Basolo, *Organometallics*, 1991, **10**, 256–263.

[198] A. Cowan, *Ph.D. thesis*, University of Nottingham, 2007.

[199] R. H. Hooker and A. J. Rest, *Appl. Organomet. Chem.*, 1990, **4**, 141–156.

[200] J. J. Turner, J. K. Burdett, R. N. Perutz and M. Poliakoff, *Pure Appl. Chem.*, 1977, **49**, 271–285.

[201] M. Poliakoff, B. Davies, A. McNeish, M. Tranquille and J. J. Turner, *Phys. Chem. Chem. Phys.*, 1978, **82**, 121–124.

[202] X.-Z. Sun, P. Portius, D. C. Grills, A. J. Cowan and M. W. George, *Appl. Spectrosc.*, 2008, **62**, 24–29.

[203] M. W. George, T. P. Dougherty and E. J. Heilweil, *J. Phys. Chem.*, 1996, **100**, 201–206.

[204] W. T. Grubbs, T. P. Dougherty and E. J. Heilweil, *Chem. Phys. Lett.*, 1994, **227**, 480–484.

[205] T. P. Dougherty, W. T. Grubbs and E. J. Heilweil, *J. Phys. Chem.*, 1994, **98**, 9396–9399.

[206] C. J. Breheny, J. M. Kelly, C. Long, S. O'Keefe, M. T. Pryce, G. Russell and M. M. Walsh, *Organometallics*, 1998, **17**, 3690–3695.

[207] B. S. Creaven, M. W. George, A. G. Ginzburg, C. Hughes, J. M. Kelly, C. Long, I. M. McGrath and M. T. Pryce, *Organometallics*, 1993, **12**, 3127–3131.

[208] A. Maciejewski, *J. Photochem. Photobiol., A*, 1990, **51**, 87–131.

[209] Y. Zhao and D. G. Truhlar, *Theor. Chem. Acc.*, 2008, **120**, 215–241.

[210] Y. Shao, Z. Gan, E. Epifanovsky, A. T. B. Gilbert, M. Wormit, J. Kussmann, A. W. Lange, A. Behn, J. Deng, X. Feng, D. Ghosh, M. Goldey, P. R. Horn, L. D. Jacobson, I. Kaliman, R. Z. Khaliullin, T. Kus, A. Landau, J. Liu, E. I. Proynov, Y. M. Rhee, R. M. Richard, M. A. Rohrdanz, R. P. Steele, E. J. Sundstrom, H. L. Woodcock, P. M. Zimmerman, D. Zuev, B. Albrecht, E. Alguire, B. Austin, G. J. O. Beran, Y. A. Bernard, E. Berquist, K. Brandhorst, K. B. Bravaya, S. T. Brown, D. Casanova, C.-M. Chang, Y. Chen, S. H. Chien, K. D. Closser, D. L. Crittenden, M. Diedenhofen, J. DiStasio, R. A., H. Do, A. D. Dutoi, R. G. Edgar, S. Fatehi, L. Fusti-Molnar, A. Ghysels, A. Golubeva-Zadorozhnaya, J. Gomes, M. W. D. Hanson-Heine, P. H. P. Harbach, A. W. Hauser, E. G. Hohenstein, Z. C. Holden, T.-C. Jagau, H. Ji, B. Kaduk, K. Khistyaev, J. H. Kim, J. Kim, R. A. King, P. Klunzinger, D. Kosenkov, T. Kowalczyk, C. M. Krauter, K. U. Lao, A. D. Laurent, K. V. Lawler, S. V. Levchenko, C. Y. Lin, F. Liu, E. Livshits, R. C. Lochan, A. Luenser, P. Manohar, S. F. Manzer, S.-P. Mao, N. Mardirossian, A. V. Marenich, S. A. Maurer, N. J. Mayhall, E. Neuscamman, C. M. Oana, R. Olivares-Amaya, D. P. O'Neill, J. A. Parkhill, T. M. Perrine, R. Peverati, A. Prociuk, D. R. Rehn, E. Rosta, N. J. Russ, S. M. Sharada, S. Sharma, D. W. Small, A. Sodt, T. Stein, D. Stueck, Y.-C. Su, A. J. W. Thom, T. Tsuchimochi, V. Vanovschi, L. Vogt, O. Vydrov, T. Wang, M. A. Watson, J. Wenzel, A. White, C. F. Williams, J. Yang, S. Yeganeh, S. R. Yost, Z.-Q. You, I. Y. Zhang, X. Zhang, Y. Zhao, B. R. Brooks, G. K. L. Chan, D. M. Chipman, C. J. Cramer, W. A. Goddard, M. S. Gordon, W. J. Hehre, A. Klamt, H. F. Schaefer, M. W. Schmidt, C. D. Sherrill, D. G. Truhlar, A. Warshel, X. Xu, A. Aspuru-Guzik, R. Baer, A. T. Bell, N. A. Besley, J.-D. Chai, A. Dreuw, B. D. Dunietz, T. R. Furlani, S. R. Gwaltney, C.-P. Hsu, Y. Jung, J. Kong, D. S. Lambrecht, W. Z. Liang, C. Ochsenfeld, V. A. Rassolov, L. V. Slipchenko, J. E. Subotnik, T. Van Voorhis, J. M. Herbert, A. I. Krylov, P. M. W. Gill and M. Head-Gordon, *Mol. Phys.*, 2015, **113**, 184–215.

[211] M. Dolg, U. Wedig, H. Stoll and H. Preuß, *J. Chem. Phys.*, 1987, **86**, 866–872.

[212] J. P. Merrick, D. Moran and L. Radom, *J. Phys. Chem. A*, 2007, **111**, 11683–11700.

[213] S. T. Astley, M. P. V. Churton, R. B. Hitam and A. J. Rest, *J. Chem. Soc., Dalton Trans.*, 1990, 3243–3253.

[214] B. Klingert, A. Roloff, B. Urwyler and J. Wirz, *Helv. Chim. Acta*, 1988, **71**, 1858–1867.

[215] G. Ellerhorst, W. Gerhartz and F. W. Grevels, *Inorg. Chem.*, 1980, **19**, 67–71.

[216] D. C. Grills, *Ph.D. thesis*, University of Nottingham, 1999.

[217] M. Gaensslen, U. Gross, H. Oberhammer and S. Rüdiger, *Angew. Chem., Int. Ed. Engl.*, 1992, **31**, 1467–1468.

[218] B. J. Palmer and R. H. Hill, *Can. J. Chem.*, 1996, **74**, 1959–1967.

[219] J. N. Harvey and R. Poli, *Dalton Trans.*, 2003, 4100–4106.

[220] P. E. M. Siegbahn and R. H. Crabtree, *J. Am. Chem. Soc.*, 1996, **118**, 4442–4450.

[221] T. Ziegler, V. Tschinke, L. Y. Fan and A. D. Becke, *J. Am. Chem. Soc.*, 1989, **111**, 9177–9185.

[222] M. R. A. Blomberg, P. E. M. Siegbahn and M. Svensson, *J. Am. Chem. Soc.*, 1992, **114**, 6095–6102.

[223] P. E. M. Siegbahn and M. Svensson, *J. Am. Chem. Soc.*, 1994, **116**, 10124–10128.

[224] M. W. George, M. T. Haward, P. A. Hamley, C. Hughes, F. P. A. Johnson, V. K. Popov and M. Poliakoff, *J. Am. Chem. Soc.*, 1993, **115**, 2286–2299.

[225] S. E. Bromberg, H. Yang, M. C. Asplund, T. Lian, B. K. McNamara, K. T. Kotz, J. S. Yeston, M. Wilkens, H. Frei, R. G. Bergman and C. B. Harris, *Science*, 1997, **278**, 260–263.

[226] A. A. Bengali, R. H. Schultz, C. B. Moore and R. G. Bergman, *J. Am. Chem. Soc.*, 1994, **116**, 9585–9589.

[227] R. H. Crabtree, *J. Organomet. Chem.*, 2004, **689**, 4083–4091.

[228] T. Lian, S. E. Bromberg, H. Yang, G. Proulx, R. G. Bergman and C. B. Harris, *J. Am. Chem. Soc.*, 1996, **118**, 3769–3770.

[229] J. A. Labinger and J. E. Bercaw, *Nature*, 2002, **417**, 507–514.

[230] R. N. Perutz and S. Sabo-Etienne, *Angew. Chem., Int. Ed.*, 2007, **46**, 2578–2592.

[231] A. J. Cowan and M. W. George, *Coord. Chem. Rev.*, 2008, **252**, 2504–2511.

[232] R. G. Bergman, T. R. Cundari, A. M. Gillespie, T. B. Gunnoe, W. D. Harman, T. R. Klinckman, M. D. Temple and D. P. White, *Organometallics*, 2003, **22**, 2331–2337.

[233] M. W. George, M. B. Hall, O. S. Jina, P. Portius, X.-Z. Sun, M. Towrie, H. Wu, X. Yang and S. D. Zarić, *Proc. Natl. Acad. Sci. U. S. A.*, 2010, **107**, 20178–20183.

[234] F. Godoy, C. L. Higgitt, A. H. Klahn, B. Oelckers, S. Parsons and R. N. Perutz, *J. Chem. Soc., Dalton Trans.*, 1999, 2039–2047.

[235] A. L. Pitts, A. Wriglesworth, X.-Z. Sun, J. A. Calladine, S. D. Zarić, M. W. George and M. B. Hall, *J. Am. Chem. Soc.*, 2014, **136**, 8614–8625.

[236] R. H. Crabtree, *J. Chem. Soc., Dalton Trans.*, 2001, 2437–2450.

[237] F. A. Cotton and G. Wilkinson, *Advanced Inorganic Chemistry, 5th Ed.*, Wiley Interscience, New York, 1988.

[238] E. G. Hope, *Coord. Chem. Rev.*, 2013, **257**, 902–909.

[239] M. A. Graham, J. J. Turner, M. Poliakoff and R. N. Perutz, *J. Organomet. Chem.*, 1972, **34**, C34–C36.

[240] C. Hall and R. N. Perutz, *Chem. Rev.*, 1996, **96**, 3125–3146.

[241] H. Hermann, F. W. Grevels, A. Henne and K. Schaffner, *J. Phys. Chem.*, 1982, **86**, 5151–5154.

[242] A. J. Lees and A. W. Adamson, *Inorg. Chem.*, 1981, **20**, 4381–4384.

[243] R. Paur-Afshari, J. Lin and R. H. Schultz, *Organometallics*, 2000, **19**, 1682–1691.

[244] A. Lugovskoy, R. Paur-Afshari and R. H. Schultz, *J. Phys. Chem. A*, 2000, **104**, 10587–10593.

[245] C. Kayran, M. Richards and P. C. Ford, *Inorg. Chim. Acta*, 2004, **357**, 143–148.

[246] J. M. Morse, G. H. Parker and T. J. Burkey, *Organometallics*, 1989, **8**, 2471–2474.

[247] S. Gittermann, T. J. Jiao and T. J. Burkey, *Photochem. Photobiol. Sci.*, 2003, **2**, 817–820.

[248] D. J. Lawes, T. A. Darwish, T. Clark, J. B. Harper and G. E. Ball, *Angew. Chem., Int. Ed.*, 2006, **45**, 4486–4490.

[249] C. E. Brown, Y. Ishikawa, P. A. Hackett and D. M. Rayner, *J. Am. Chem. Soc.*, 1990, **112**, 2530–2536.

[250] J. R. Wells, P. G. House and E. Weitz, *J. Phys. Chem.*, 1994, **98**, 8343–8351.

[251] R. H. Schultz, A. A. Bengali, M. J. Tauber, B. H. Weiller, E. P. Wasserman, K. R. Kyle, C. B. Moore and R. G. Bergman, *J. Am. Chem. Soc.*, 1994, **116**, 7369–7377.

[252] T. O. Northcutt, D. D. Wick, A. J. Vetter and W. D. Jones, *J. Am. Chem. Soc.*, 2001, **123**, 7257–7270.

[253] W. H. Bernskoetter, C. K. Schauer, K. I. Goldberg and M. Brookhart, *Science*, 2009, **326**, 553–556.

[254] M. D. Walter, P. S. White, C. K. Schauer and M. Brookhart, *J. Am. Chem. Soc.*, 2013, **135**, 15933–15947.

[255] D. R. Evans, T. Drovetskaya, R. Bau, C. A. Reed and P. D. W. Boyd, *J. Am. Chem. Soc.*, 1997, **119**, 3633–3634.

[256] R. H. Crabtree, E. M. Holt, M. Lavin and S. M. Morehouse, *Inorg. Chem.*, 1985, **24**, 1986–1992.

[257] S. D. Pike, A. L. Thompson, A. G. Algarra, D. C. Apperley, S. A. MacGregor and A. S. Weller, *Science*, 2012, **337**, 1648–1651.

[258] R. D. Young, A. F. Hill, W. Hillier and G. E. Ball, *J. Am. Chem. Soc.*, 2011, **133**, 13806–13809.

[259] J. L. Bennett and P. T. Wolczanski, *J. Am. Chem. Soc.*, 1997, **119**, 10696–10719.

[260] W. D. Jones and E. T. Hessell, *J. Am. Chem. Soc.*, 1993, **115**, 554–562.

[261] E. Clot, C. Mégret, O. Eisenstein and R. N. Perutz, *J. Am. Chem. Soc.*, 2006, **128**, 8350–8357.

[262] D. D. Wick and W. D. Jones, *Organometallics*, 1999, **18**, 495–505.

[263] S. D. Zarić and M. B. Hall, *J. Phys. Chem. A*, 1997, **101**, 4646–4652.

[264] A. J. Rest, I. Whitwell, W. A. G. Graham, J. K. Hoyano and A. D. McMaster, *J. Chem. Soc., Dalton Trans.*, 1987, 1181–1190.

[265] W. E. Billups, S. C. Chang, R. H. Hauge and J. L. Margrave, *J. Am. Chem. Soc.*, 1993, **115**, 2039–2041.

[266] C. E. C. A. Hop and T. B. McMahon, *J. Am. Chem. Soc.*, 1991, **113**, 355–357.

[267] P. E. M. Siegbahn, *J. Am. Chem. Soc.*, 1996, **118**, 1487–1496.

[268] H. Heiberg, O. Gropen and O. Swang, *Int. J. Quantum Chem.*, 2003, **92**, 391–399.

[269] K. J. de Almeida and A. Cesar, *Organometallics*, 2006, **25**, 3407–3416.

[270] M. Tramšek and B. Žemva, *J. Fluorine Chem.*, 2006, **127**, 1275–1284.

[271] T. Bunic, G. Tavčar, M. Tramšek and B. Žemva, *Inorg. Chem.*, 2006, **45**, 1038–1042.

[272] T. Bunic, M. Tramšek, E. Goreshnik, G. R. Tavčar and B. Žemva, *Inorg. Chem.*, 2007, **46**, 5276–5282.

[273] G. Tavčar and M. Tramšek, *J. Fluorine Chem.*, 2015, **174**, 14–21.

[274] S. Seidel and K. Seppelt, *Science*, 2000, **290**, 117–118.

[275] T. Drews, S. Seidel and K. Seppelt, *Angew. Chem., Int. Ed.*, 2002, **41**, 454–456.

[276] A. W. Ehlers, G. Frenking and E. J. Baerends, *Organometallics*, 1997, **16**, 4896–4902.

[277] R. J. Mawby, R. N. Perutz and M. K. Whittlesey, *Organometallics*, 1995, **14**, 3268–3274.

[278] S. A. Fairhurst, J. R. Morton, R. N. Perutz and K. F. Preston, *Organometallics*, 1984, **3**, 1389–1391.

[279] M. K. Whittlesey, R. N. Perutz, I. G. Virrels and M. W. George, *Organometallics*, 1997, **16**, 268–274.

[280] M. Brookhart, W. Chandler, R. J. Kessler, Y. M. Liu, N. J. Pienta, C. C. Santini, C. Hall, R. N. Perutz and J. A. Timney, *J. Am. Chem. Soc.*, 1992, **114**, 3802–3815.

[281] M. B. Simpson, M. Poliakoff, J. J. Turner, W. B. Maier and J. G. McLaughlin, *J. Chem. Soc., Chem. Commun.*, 1983, 1355–1357.

[282] D. P. Burney and T. J. Burkey, *Abstr. Pap. Am. Chem. S.*, 1994, **207**, 19.

[283] M. Jyo-O, H. Takeda, K. Omiya, Y. Ishikawa and S. Arai, *Bull. Chem. Soc. Jpn.*, 1993, **66**, 3618–3626.

[284] B. H. Weiller, E. P. Wasserman, R. G. Bergman, C. B. Moore and G. C. Pimentel, *J. Am. Chem. Soc.*, 1989, **111**, 8288–8290.

[285] B. H. Weiller, E. P. Wasserman, C. B. Moore and R. G. Bergman, *J. Am. Chem. Soc.*, 1993, **115**, 4326–4330.

[286] X.-Z. Sun, M. W. George, S. G. Kazarian, S. M. Nikiforov and M. Poliakoff, *J. Am. Chem. Soc.*, 1996, **118**, 10525–10532.

[287] D. C. Grills, G. I. Childs and M. W. George, *Chem. Commun.*, 2000, 1841–1842.

[288] O. S. Jina, X.-Z. Sun and M. W. George, *Dalton Trans.*, 2003, 1773–1778.

[289] J. S. Yeston, B. K. McNamara, R. G. Bergman and C. B. Moore, *Organometallics*, 2000, **19**, 3442–3446.

[290] R. G. Ball, A. K. Campen, W. A. G. Graham, P. A. Hamley, S. G. Kazarian, M. A. Ollino, M. Poliakoff, A. J. Rest, L. Sturgeoff and I. Whitwell, *Inorg. Chim. Acta*, 1997, **259**, 137–149.

[291] A. H. Klahnoliva, R. D. Singer and D. Sutton, *J. Am. Chem. Soc.*, 1986, **108**, 3107–3108.

[292] J. McMaster, P. Portius, G. E. Ball, J. P. Rourke and M. W. George, *Organometallics*, 2006, **25**, 5242–5248.

[293] M. J. Frisch, G. W. Trucks, H. B. Schlegel, G. E. Scuseria, M. A. Robb, J. Cheeseman, J. A. Montgomery, K. N. Vreven, J. C. Burant, K. N. Kudin, J. M. Millam, S. S. Iyengar, J. B. Tomasi, V. B. Mennucci and M. Cossi, *Gaussian03, Revision D.01*, 2004.

[294] R. Dennington II, T. Keith, J. Millam, K. Eppinnett, W. L. Hovell and R. Gilliland, *GaussView, Version 3.0*, 2003.

[295] B. K. McNamara, J. S. Yeston, R. G. Bergman and C. B. Moore, *J. Am. Chem. Soc.*, 1999, **121**, 6437–6443.

[296] S. T. Belt, S. B. Duckett, M. Helliwell and R. N. Perutz, *J. Chem. Soc., Chem. Commun.*, 1989, 928–930.

[297] S. T. Belt, M. Helliwell, W. D. Jones, M. G. Partridge and R. N. Perutz, *J. Am. Chem. Soc.*, 1993, **115**, 1429–1440.

[298] B. Procacci, Y. Jiao, M. E. Evans, W. D. Jones, R. N. Perutz and A. C. Whitwood, *J. Am. Chem. Soc.*, 2015, **137**, 1258–1272.

[299] G. J. Kubas, *Metal Dihydrogen and Sigma-Bond Complexes*, Kluwer Academic Publishers, New York, 2001.

[300] J. Y. Corey, *Chem. Rev.*, 2011, **111**, 863–1071.

[301] G. J. Kubas, *J. Organomet. Chem.*, 2001, **635**, 37–68.

[302] G. S. McGrady and G. Guilera, *Chem. Soc. Rev.*, 2003, **32**, 383–392.

[303] J. P. Collman, L. S. Hegedus, J. R. Norton and R. G. Finke, *Principles and Applications of Organotransition Metal Chemistry*, University Press Books, Mill Valley CA, 1987.

[304] G. I. Nikonov, *J. Organomet. Chem.*, 2001, **635**, 24–36.

[305] G. I. Nikonov, *Angew. Chem., Int. Ed.*, 2001, **40**, 3353–3355.

[306] G. I. Nikonov, *Adv. Organomet. Chem.*, 2005, **53**, 217–309.

[307] P. Braunstein and N. M. Boag, *Angew. Chem., Int. Ed.*, 2001, **40**, 2427–2433.

[308] G. S. McGrady, P. Sirsch, N. P. Chatterton, A. Ostermann, C. Gatti, S. Altmannshofer, V. Herz, G. Eickerling and W. Scherer, *Inorg. Chem.*, 2009, **48**, 1588–1598.

[309] J. K. Hoyano, M. Elder and W. A. G. Graham, *J. Am. Chem. Soc.*, 1969, **91**, 4568–4569.

[310] I. Atheaux, F. Delpech, B. Donnadieu, S. Sabo-Etienne, B. Chaudret, K. Hussein, J. C. Barthelat, T. Braun, S. B. Duckett and R. N. Perutz, *Organometallics*, 2002, **21**, 5347–5357.

[311] U. Schubert, K. Ackermann and B. Worle, *J. Am. Chem. Soc.*, 1982, **104**, 7378–7380.

[312] K. A. Smart, M. Grellier, Y. Coppel, L. Vendier, S. A. Mason, S. C. Capelli, A. Abinati, V. Montiel-Palma, M. A. Munoz-Hernandez and S. Sabo-Etienne, *Inorg. Chem.*, 2014, **53**, 1156–1165.

[313] M. Nagaoka, T. Shima, T. Takao and H. Suzuki, *Organometallics*, 2014, **33**, 7232–7240.

[314] K. T. Kotz, H. Yang, P. T. Snee, C. K. Payne and C. B. Harris, *J. Organomet. Chem.*, 2000, **596**, 183–192.

[315] C. J. Wood, M. Cheng, C. A. Clark, R. Horvath, I. P. Clark, M. L. Hamilton, M. Towrie, M. W. George, L. C. Sun, X. C. Yang and E. A. Gibson, *J. Phys. Chem. C*, 2014, **118**, 16536–16546.